Stony Brook University

Mechanistic and Structural Insight into Amyloid Formation by Islet Amyloid Polypeptide: Implications for Monitoring the Amylome

A Dissertation Presented

by

Amy Gar-lai Wong

to

The Graduate School

in Partial Fulfillment of the

Requirements

for the Degree of

Doctor of Philosophy

in

Chemistry

Stony Brook University

December 2016

Stony Brook University

The Graduate School

Amy Gar-lai Wong

We, the dissertation committee for the above candidate for the

Doctor of Philosophy degree, hereby recommend

acceptance of this dissertation.

Daniel P. Raleigh, Ph.D. – Dissertation Advisor
Professor and Vice Chair, Department of Chemistry

Carlos Simmerling, Ph.D. – Chairperson of Defense
Professor, Department of Chemistry

Elizabeth Boon, Ph.D. – Third Member
Associate Professor, Department of Chemistry

Brian Stockman, Ph.D. – Outside Member
Associate Professor and Department Chair, Department of Chemistry, Adelphi University

This dissertation is accepted by the Graduate School

Charles Taber

Dean of the Graduate School

Abstract of the Dissertation

Mechanistic and Structural Insight into Amyloid Formation by Islet Amyloid Polypeptide: Implications for Monitoring the Amylome

by

Amy Gar-lai Wong

Doctor of Philosophy

in

Chemistry

Stony Brook University

2016

Amyloid fibrils are insoluble peptide or protein aggregates that are fibrous, predominantly β-sheet, and highly ordered. Amyloid formation plays an important role in an array of human diseases including Alzheimer's, Parkinson's, and Huntington's disease. The proteins that form amyloid vary greatly in native structure and function however, the resultant amyloid plaques formed when these proteins misfold share many structural features. The work herein describes the recent research on islet amyloid polypeptide (IAPP, or amylin), a neuroendocrine hormone that is co-secreted with insulin and has been observed to form amyloid plaques in the pancreas, a process that has been shown to be toxic to β-cells and a ubiquitous feature in patients with type-2 diabetes. The structure and mechanism of IAPP is currently not known. Additionally, current methods of monitoring the formation of amyloid by IAPP have inherent weaknesses that can lead to misleading results. A clearer picture of the mechanism of amyloid formation by IAPP, the structure of the mature fibril, as well as the development of

more robust methods of monitoring amyloid formation in real time could lead to improved therapeutics and alluring candidates for xenobiotic transplantation.

In this dissertation, the role of helical intermediates in amyloid formation was explored by performing several replacements at position-17 in the IAPP sequence. The veracity of several amyloid prediction programs was also investigated and the ability of pufferfish IAPP to form amyloid was investigated which subsequently, revealed pitfalls in the commonly used thioflavin-T fluorescence assay. Several potential dyes were explored in order to provide alternative means of monitoring amyloid formation by IAPP in real time. In addition, baboon IAPP was examined, specifically it's toxicity to INS-1 β-cells and the distribution of oligomers populated during the lag phase. Finally, the role of the disulfide bond between Cys-2 and Cys-7 was explored by examining truncated variants of IAPP and reduced models of the peptide.

Table of Contents

List of Figures

List of Tables

List of Abbreviations

2DIR	Two-dimensional infrared spectroscopy
A25T	A Ala-25 to Thr variant of human islet amyloid polypeptide
AA	Amyloid A
Abu	2-aminobutyric acid
Ac8-37	IAPP8-37 variant containing an acetylated N-terminus
AL	Amyloid light-chain
ANS	anilinonapthalene-1-sulfonic acid
Aβ	The proteolytic fragment of the amyloid precursor protein which is the causative agent of Alzheimer's disease
b-IAPP	The baboon variant of human islet amyloid polypeptide
Bis-ANS	4,4'-dianilino-1,1'-binapthyl-5,5'-disulfonic acid
C2S, C7S	A Cys-2 to Ser and Cys-7 to Ser variant of human islet amyloid polypeptide
CD	circular dichroism
CPE	Carboxypeptidase E
DAPI	4',6-diamidino-2-phenylindole
DCVJ	9-(2,2-dicyanovinyl)julolidine
DFS	Differential fluorescence screening
DMSO	dimethyl sulfoxide
ER	Endoplasmic reticulum
Fmoc	9-fluorenylmethoxycarbonyl
Fmoc-PAL-PEG	5-(4'-Fmoc-aminomethyl-3',5-dimethoxyphenyl) valeric acid
FRET	Fluorescence resonance energy transfer
FTIR	Fourier transform infrared spectroscopy
H18R	A His-18 to Arg variant of human islet amyloid polypeptide
HFIP	Hexafluoroisopropanol
HPLC	High performance liquid chromatography
IAPP	Islet amyloid polypeptide
IAPP8-37	A peptide corresponding to residues 8-37 of human islet amyloid polypeptide

IAPPCAM	A variant of human islet amyloid polypeptide with the carboxyamidomethyl protecting group appended to each cysteine
IMS-MS	Ion mobility mass spectroscopy
K1I	A Lys-1 to Ile variant of human islet amyloid polypeptide
LC-MS	Liquid chromatography mass spectroscopy
MALDI-TOF MS	Matrix assisted laser desorption ionization-time of flight mass spectrometry
MBP	Maltose binding protein
MD	Molecular dynamics
NMR	Nuclear magnetic resonance
Nva	Norvaline
PAM	peptidyl amidating mono-oxygenase
PBS	Phosphate buffered saline
PC(1/3)	Subtilisin-like prohormone convertase enzyme 1/3
PC2	Subtilisin-like prohormone convertase enzyme 2
p-IAPP	The pufferfish variant of human islet amyloid polypeptide
r-IAPP	The rat variant of human islet amyloid polypeptide
t50	Time required to achieve half the maximum fluorescence change in a thioflavin-T assay
TEM	Transmission electron microscopy
TFA	Trifluoroacetic acid
TIPS	Triisopropyl silane
Tle	Ter-leucine
v/v	Volume to volume
V17A	A Val-17 to Ala variant of human islet amyloid polypeptide
V17Abu	A Val-17 to Abu variant of human islet amyloid polypeptide
V17I	A Val-17 to Ile variant of human islet amyloid polypeptide
V17Nva	A Val-17 to Nva variant of human islet amyloid polypeptide
V17Tle	A Val-17 to Tle variant of human islet amyloid polypeptide
YOYO-1	1,1'-(4,4,8,8-tetramethyl-4,8-diazaundecamethylene) bis[4-[(3-methylbenzo-1,3-oxazol-2-yl)methylidene]-l,4-dihydroquinolinium] tetraiodide

Acknowledgments

I would like to express my thanks to my advisor, Professor Daniel Raleigh for his continuous support during my time here. His guidance, expertise, and patience have been invaluable during the past five years.

I would also like to thank my thesis committee: Professor Carlos Simmerling and Professor Elizabeth Boon for their acuity and their ability to offer alternative perspectives on my work. I would also like to thank Professor Brian Stockman for kindly serving as an outside member.

Thanks to Dr. Cynthia Tu for mentoring me when I was an inexperienced neophyte in the lab. Additionally, thanks to all past and present members, Dr. Ping Cao, Dr. Hui Wang, Dr Vadim Patsalo, Dr. Shifeng Xiao, Dr. Wenli Meng, Harris Noor, Rehana Akter, Xiaoxue Zhang, Ivan Peran, Natalie Stenzoski, Yuan Chen, Matthew Watson, Zachary Ridgway, Junjie Zou, and Daeun Noh. All of them were a delight to work with over the years.

The faculty here was also a pleasure to work with especially Katherine Hughes, Dr. Bela Ruzsicska, and Susan Van Horn as well as the rest of the staff in the Department of Chemistry.

I also am thankful for the friends I made during my time here at Stony Brook. We had lots of fun during these five years. I would like to thank my family for their encouragement and support. Last of all but certainly not the least; I would like to thank Matthew Freitag for his endless support, both inside and outside the lab, and love. I could not have accomplished what I did without his help, and his endless jokes that never failed to make me laugh even on the worst days.

List of Publications

1. Tu, L. H., Young, L. M., **Wong, A. G.**, Ashcroft, A. E., Radford, S. E., and Raleigh, D. P. Mutational Analysis of the Ability of Resveratrol to Inhibit Amyloid Formation by Islet Amyloid Polypeptide: Critical Evaluation of the Importance of Aromatic-Inhibitor and Histidine-Inhibitor Interactions, *Biochemistry*, **2015,** *54*, 666-676

2. Akter, R., Cao, P., Noor, H., Ridgway, Z., Tu, L. H., Wang, H., **Wong, A.G.,** Zhang, X., Abedini, A., Schmidt, A. M., and Raleigh, D. P. Islet Amyloid Polypeptide: Structure, Function, and Pathophysiology, *J. Diabetes Res.*, **2016,** *2016*, 1-18

3. **Wong, A. G.,** Wu, C., Hannaberry, E., Watson, M. D., Shea, J. E., and Raleigh, D. P. Analysis of the Amyloidogenic Potential of Pufferfish (*Takifugu rubripes*) Islet Amyloid Polypeptide Highlights the Limitations of Thioflavin-T Assays and Difficulties in Defining Amyloidogenicity, *Biochemistry*, **2016**, *55*, 510-5183

4. Ilitchev, A. I., Giammona, M. J., Do, T. D., **Wong, A. G.,** Buratto, S. K., Shea, J. E., Raleigh, D. P., and Bowers, M. T. Human Islet Amyloid Polypeptide N-Terminus Fragment Self-Assembly: Effect of Conserved Disulfide Bond on Aggregation Propensity, *J. Am. Soc. Mass Spectrom.*, **2016**, *27*, 1010-1018

5. Abedini, A., Plesner, A., Cao, P., Ridgway, Z., Zhang, J., Tu, L. H., Middleton, C. T., Chao, B., Sartori, D. J., Meng, F., Wang, H., **Wong, A. G.,** Zanni, M. T., Verchere, C. B., Raleigh, D. P., and Schmidt, A. M. Time-Resolved Studies Define the Nature of Toxic IAPP Intermediates Providing Insight for Anti-Amyloidosis Therapeutics, *eLife*, **2016**, *5*, 1-28

6. **Wong, A. G.,** and Raleigh, D. P. The Dye SYPRO Orange Binds to Amylin Amyloid Fibrils But Not Pre-fibrillar Intermediates, *Protein Sci.*, **2016**, *25*, 1834-1840

Chapter 1. Introduction

Amyloids are insoluble peptide or protein aggregates that arrange themselves into long, highly ordered, unbranched fibrils. These amyloidogenic proteins and peptides vary greatly from each other in native structure and biological function. Amyloids are now associated with over 50 different conditions including Alzheimer's disease, Parkinson's disease, Huntington's disease, and type-2 diabetes (T2D). Additionally, functional amyloids play a beneficial role for their hosts in the animal kingdom indicating that amyloid may be more widespread than was initially perceived. This introduction summarizes current knowledge of the biophysical aspects of amyloid formation, the bioinformatics methods for predicting amyloidogenicity, and the current methodologies of observing amyloid formation, as well as other work in the field with emphasis on islet amyloid polypeptide (IAPP, amylin), a neuroendocrine hormone linked with the onset of type-2 diabetes.

1.1 General Features of Amyloid

1.1.1 Structural Characteristics of Amyloid

Though amyloid is formed from a wide array of proteins and peptides with a litany of different native structures and biological functions, the structures of the amyloid fibrils formed as a result of misfolding are remarkably similar. The fibrils tend to be predominantly β-sheet secondary structure, 5-10 nm in length, and are polymorphous (Figure 1-1A) [1]. The fibrils exhibit a distinct apple-green birefringence under polarized light when stained with Congo red [2, 3]. The individual proteins attach to each end of the growing fibril and align themselves perpendicular to the long axis of the fibril and the protofibrils then twist around each other in a

super helical fashion (Figure 1-1B) [4-6]. This structure is called the cross-β structure and has an easily identifiable pattern in X-ray fiber diffraction [7]. That being said, the mechanisms of formation and the intrinsic properties of each type of amyloid can vary greatly [8, 9].

1.1.2 Amyloid Formation in Human Pathology and in Nature

There are now more than 50 disorders associated with the conversion of biologically active proteins and peptides to amyloid fibrils. Amyloidosis can be divided into three general calibers based on the distribution of amyloid plaques [10, 11]. The first of which is neurodegenerative amyloidosis, in which amyloid plaques are deposited in the brain. Aβ, the causative agent of Alzheimer's disease and α-synuclein, the protein associated with Parkinson's disease are examples of neurodegenerative amyloidosis with the former being perhaps the most infamous of conditions associated with amyloid deposition [12, 13]. Systemic amyloidosis is characterized by the widespread deposition of amyloid plaques in several organs and tissues. Amyloid can spread to many organs by travelling through the bloodstream and these conditions can be especially pernicious if the heart or kidneys are affected. Amyloid light-chain (AL) amyloidosis and Amyloid A (AA) amyloidosis are examples of systemic amyloidosis. Localized amyloidosis involves the deposition of amyloid plaques in one targeted organ. Type-2 diabetes (T2D) has been linked to the presence of amyloid plaques in the islets of Langerhans and cataracts are caused by aggregation of γ-crystallins in the eyes [14]. Some types of amyloid such as the aforementioned AL amyloidosis are capable of both systemic and localized amyloid plaque deposition [15, 16]. Both the amyloid plaques and the prefibrillar intermediates have the potential to be toxic and can result in cell death and damage to tissue and vital organs. The different conditions associated with amyloidosis can be induced in a myriad of ways such as genetically or directly transmitted between hosts while others are considered sporadic and it is

unknown why amyloid formation occurs [11]. An abbreviated list of amyloidogenic proteins and peptides associated with disease is listed in Table 1-1.

The mechanism of cell death is not known. It was initially believed that amyloid fibrils were the primary cause of toxicity and cell death [17-19]. However, it is now believed that the prefibrillar intermediates are more toxic than the fibrils at least for some amyloid diseases [20-22]. Changes in morphology of the brain evident in *Drosophilae* expressing Aβ(1-42) and Aβ(1-40) prior to the appearance of amyloid plaques [23, 24]. Similarly, symptoms of early-onset Parkinson's can become apparent before the appearance of α-synuclein amyloid plaques known as Lewy bodies This also supports the theory that the prefibrillar intermediates are more toxic [25]. Transgenic mice that expressed α-synuclein, but had no fibrillar deposits in the brain showed neuronal degeneration [26].

The amyloid fibrils are stable once they have formed and so there are two obstacles in developing novel therapeutics for treating amyloidosis. The first is determining how to prevent fibril formation from occurring. The second is elucidating how to remove amyloid plaques that have already formed in order to prevent further damage to the patient.

The universe of amyloid forming proteins is considerably broader than those implicated in disease. A large number of proteins which are not known to form amyloid *in vivo* can be induced to do so *in vitro* [11, 27]. Not all amyloid formation is deleterious to their hosts and functional amyloids play a beneficial role in biology [28]. Many bacteria, mammals, and fungi are now being discovered to have the capability of assembling and disassembling amyloid fibrils at will [29]. Several members of the Enterobacteriaceae family such as *E. coli* are capable of producing curli fibrils as the primary proteinaceous component of biofilm [30]. Biofilms are groups of microorganisms that adhere to each other and to solid surfaces and which allow its

members to survive in adverse conditions for long periods of time [31, 32]. Spiders are capable of using amyloid to their advantage when producing their webs [33]. The resulting spider silk, composed of aggregated spidroin, is lightweight, incredibly strong and has potential applications in biomedicine [34]. The harnessing of amyloid forming machinery utilized by these living systems has applications in developing nanomaterials and nanomachines [35].

1.1.3 Methods for Predicting Amyloidogenicity

The ability to predict amyloid propensity based on an amino acid sequence has been of interest for some time. Several methods have been developed [36]. A list of the most commonly used methods is tabulated in table 1-2. The AGGRESCAN program locates amyloidogenic regions or "hotspots" based on the amyloid propensity of each individual amino acid. The method is capable of identifying at least one hotspot in 80 % of amyloidogenic sequences from a dataset of experimentally characterized peptide fragments derived from amyloidogenic proteins [37]. The aggregation propensity of each amino acid was determined from *in vivo* mutational analysis of the central hydrophobic cluster of Aβ. The program uses a five residue sliding window in order to locate these hotspots. FoldAmyloid is similar to AGGRESCAN. It also locates amyloidogenic regions by using a five residue sliding window. The amino acid propensities used in this method are derived from statistical analysis of structures of globular proteins. The aggregation propensity of each amino acid is based on several characteristics such as the capability to form hydrogen bonds and observed packing density. FoldAmyloid also has a similar rate of success compared to AGGRESCAN. The program was able to correctly classify 80 % of amyloidogenic proteins and 72 % nonamyloidogenic proteins. [38]. The Zyggregator method also uses a sliding window to determine amyloid propensity. Additionally, the program tries to locate regions with alternating polar and apolar residues since this is a common feature of

β-sheets and it takes into consideration the characteristics of each amino acid. The characteristics of each amino acid were derived from *in vitro* aggregation studies of unstructured peptides [39, 40].

The WALTZ program operates under the assumption that fragments of an amyloidogenic protein can also form amyloid and is based off of Eisenberg's method for obtaining the structure of full length proteins by crystallizing hexapeptide fragments. The program compares each hexapeptide in the submitted sequence to a template, the NNQQNY amyloidogenic hexapeptide from the sup35 prion protein. If the sequence is able to adopt the same cross-β spine structure as the template, the region is considered amyloidogenic. The method was found to have a sensitivity ranging from 58 % to 84 % depending on whether benchmarking was performed by cross-validation or not [41, 42]. ZipperDB is a program that is very similar to WALTZ. It compares short sequences to a template sequence but instead deduces if the sequence is capable of forming a steric zipper, a feature that is unique to amyloid fibrils rather than the β-sheet secondary structure. The program is capable of reaching an accuracy of 80 % when an appropriate energy threshold is used to separate peptides that form fibrils from those that do not [41, 43]. The TANGO program predicts the amyloidogenicity of a sequence by calculating its likelihood of forming β-sheets, how likely the residues of the β-sheet will bury themselves inside the protein and also if there are any charged residues which will increase the stability of the fibril with electrostatic interactions. If there are five residues that fit these criteria, the peptide is deemed likely to be amyloidogenic. When this program was performed on a dataset of 179 peptides, it yielded a success rate of 87 % [44].

The AmylPred program predicts amyloidogenicity by locating regions that are capable of switching from α-helix to β-sheet, or conformational switch. The program uses the SecStr

secondary structure tool which is a combination of six algorithms to analyze the sequence and to predict secondary structure information such as a region's ability to form α-helices, β-sheets, and which can switch between the two [45]. The PASTA program operates slightly differently than the aforementioned programs. Instead of locating potential β-sheets, the program determines pairwise contacts of amino acids with the rationale that the contacts between sidechains of two amino acids will increase the stability between the β-sheets. The program draws on the number of contacts between amino acid pairs and the relative abundance of the amino acids in both parallel and antiparallel β-sheets. Amino acid pairs that occur more frequently despite their relative abundance are deemed favorable to the β-sheet. This method for predicting aggregation propensity was found to have close to 80 % true positive predictions when performed on a dataset of 179 peptides [46, 47].

These programs suffer from many of the same drawbacks. First, these programs do not take into account post-translational modifications such as disulfide bonds between cysteines or modifications of the N or C-termini. With the exception of Zyggregator and TANGO, these programs also do not allow the user to select the pH, temperature, or ionic strength of the experimental conditions. The accuracy of each of these programs is still being determined and will be further discussed in Chapter 3.

1.2 Islet Amyloid Polypeptide (IAPP)

1.2.1 Synthesis and Processing of IAPP

Islet amyloid polypeptide (IAPP or amylin) is a 37 residue neuroendocrine hormone that is co-secreted with insulin [48]. The hormone is believe to play a role in gastric emptying,

hunger suppression, and appetite satiety [49]. Similar to insulin, IAPP originates as a longer pre-prohormone. It is initially synthesized as an 89 residue pre-prohormone on the ribosome (Figure 1-2)[50]. The 22 residue signal sequence is proteolytically cleaved to yield the prohormone. ProIAPP is further processed in the Golgi and the insulin secretory granule. The segment of proIAPP that includes mature IAPP and an additional C-terminal glycine is flanked on each side by two dibasic sites. These are proteolytically cleaved by the prohormone convertases PC(1/3) and PC2.[51] PC(1/3) is responsible for cleavage at the C-terminal dibasic site and PC2 cleaves the N-terminal dibasic site. These enzymes are both also responsible for the processing of insulin. The C-terminus is further processed by carboxypeptidase E (CPE) and peptidyl amidating mono-oxygenase complex (PAM) the latter of which produces the amidated C-terminus of IAPP. Prior to secretion, a disulfide bond is formed between Cys-2 and Cys-7 to yield mature IAPP. Both mature IAPP and insulin are stored in the insulin secretory granule until ready for use.

1.2.2 IAPP and Type-2 Diabetes

The deposition of amyloid plaques in the Islets of Langerhans was initially described in 1900 by Eugene L. Opie [52]. These plaques were not identified as being primarily composed of IAPP until 1987 by two separate groups. IAPP has since been under intense study [53, 54]. These plaques are a pathological feature of patients with T2D and they are found in up to 90% of patients with the disease post-mortem (Figure 1-3) [55]. Those with T2D suffer from a gradual loss of β-cells and decreased insulin secretion. There is a correlation between the amount of amyloid deposits and the severity of the disease. The process of islet amyloid formation contributes to β-cell dysfunction in T2D [56-58]. Model membranes have been interpreted to indicate IAPP causes cell death by inducing membrane leakage but other mechanisms have been

demonstrated as well [59]. Stress of the endoplasmic reticulum (ER) has been implicated in β-cell dysfunction and has been observed in transgenic mice models in the presence of excess IAPP though not in model β-cells [60]. Defects in autophagy have also been suggested as a possible cause of β-cell death and human IAPP has been shown to disrupt the lysosomal pathway in β-cells[61]. Yet another mechanism of β-cell death is that IAPP may be provoking an inflammatory response [62]. IAPP has been shown to stimulate the production of stimuli such as caspase 1 and cytokines such as IL-1β and IL-18. IL-1β may play a role in β-cell dysfunction [63]. Other mechanisms that have been proposed are disruption of mitochondria membranes, oxidative stress, and activation of signaling pathway. As model membranes become more refined, it will become possible to further understand how IAPP induces β-cell death in the disease.

IAPP is natively unfolded as a monomer but it can be induced to rapidly form amyloid fibrils. The only known mutation of IAPP is the S20G missense mutation that occurs in certain Asian populations [64]. The mutation is associated with a slightly higher risk of developing the disease [65]. IAPP amyloid formation likely plays a role in islet cell transplantation failure [66-68].

1.2.3 Models of the IAPP Fibril

The exact structure of IAPP amyloid is currently unknown, and there may be different polymeric structures. But several models have been proposed of which two are highly regarded. One model proposed, by the Eisenberg group is based on X-ray studies of small fragments of human IAPP. Fragments corresponding to the sequences of 21-27 and 28-33 were crystallized individually, these structures were solved, and a model was built around these crystal structures [69]. This model features two IAPP molecules that each fold into a β-sheet hairpin for a total of

four β-sheets per layer. The sidechains of each segment interdigitate to form a structure known as a steric zipper (Figure 1-4A). They then stack on top of each other with a 4.8 Å distance between layers. The basic structure is thus made up of two symmetrical U-shaped IAPP molecules (Figure 1-4B). The β-strands are between residues 8-20 and 23-37 and the backbone hydrogen bonds are formed between peptide chains and not within a single chain.

A model that is broadly similar to the Eisenberg model was also proposed by Tycko and coworkers. The Tycko model is derived from solid-state NMR and also features two IAPP molecules forming β-sheets hairpins (Figure 1-5B)[70]. This model contains some interdigitation between β-sheets but it is not as tightly packed as the model proposed by Eisenberg and differs in the length of the β-strands (Figure 1-5C). The segments 8-17 and 28-37 make up the core of this IAPP model. This model also features intermolecular hydrogen bonds between peptide chains rather than intrachain hydrogen bonds.

1.2.4 Mechanism of Amyloid Formation by IAPP

The pathway of IAPP amyloid formation is not yet known. But it is believed to be nucleation-dependent (Figure 1-6)[71, 72]. The formation of amyloid follows three phases, the first of which is a lag phase in which monomers slowly combine to form oligomers or "seeds" and is the slowest step of amyloid formation, this is followed by a rapid growth phase during which fibrils grow and new fibrils are formed by secondary nucleation. The final phase is a plateau phase where amyloid fibrils are in equilibrium with monomers. Amyloid formation can be vastly accelerated by the addition of seeds at the beginning of the reaction. A seed is a preformed oligomer of IAPP from which additional IAPP monomers can rapidly template off the ends to propagate more mature IAPP fibrils. The addition of seeds allows amyloid formation by IAPP to occur much more rapidly than if monomers were to form oligomers on their own and as

such results in an elimination of the lag phase. These seeding reactions are very specific and only catalyze aggregation if the two fibrils are similar enough in structure [73]. Thus, seeding studies are a useful test to determine similarity between wild-type IAPP and other variants.

1.2.5 Proposed Transient Intermediates of IAPP of Amyloid Formation

Little is known about the prefibrillar intermediates that may be formed during amyloid formation. Many techniques have been used to stabilize these transient intermediates in order to gain structural and mechanistic information on amyloid formation by IAPP. Rat IAPP (r-IAPP) has been used as a model because it does not form fibrils but it samples many of the same intermediates as human IAPP [74]. Fluorescence resonance energy transfer (FRET) studies with both human and rat IAPP showed transfer occurring between Phe-15 and Tyr-37 indicating the existence of a similar transient intermediate for both peptides [75]. Additionally, in the presence of membranes, human and rat IAPP were observed to adopt similar conformations when bound to the lipid bilayer as judged by CD spectroscopy [76]. In both cases, the intermediates for both human and rat IAPP were shown to be similar but only human IAPP continued to further fold into amyloid fibrils. Model membranes have also been used as a means of preventing aggregation and stabilizing the transient intermediate for a long enough period of time to allow structural data to be obtained[76, 77]. When analyzed by NMR spectroscopy, stabilization by r-IAPP and by model membranes showed a helical region from residues 5-20 [74]. It has been proposed that the formation of oligomers by IAPP and helical formation are linked. One way this may occur is after formation of the α-helix IAPP monomers would associate into oligomers by self-association of the helical intermediate which then would allow the amyloidogenic core region of different IAPP molecules to come into close contact with each other (Figure 1-7). The core region of IAPP then adopts a β-sheet structure which converts the rest of the peptide to β-

sheet, forming the oligomer seeds that allow templating of monomers onto each end generating the mature fibril [78]. Many small molecule inhibitors have also been designed to prevent aggregation and some have been designed to target this helical intermediate [79]. For example, an inhibitor may bind to the helix and disrupt helix-helix interactions preventing amyloid formation [73, 80, 81]. Replacement of Phe-15 with both natural and unnatural residues of varying helical propensity show a correlation with increasing helical propensity and the rate of amyloid formation by IAPP also lends credence to the helical model [82]. However, the structure of these helical intermediates is currently not known and other non-helical models for oligomers have also been proposed which are also consistent with experimental observations.

Ion-mobility mass spectroscopy (IMS-MS) in conjunction with MD simulations propose a β-hairpin dimer model of oligomers [83, 84]. However, these results were obtained when IAPP was in the gas phase and thus IAPP may not sample the same conformations in more physiological conditions. Another model using a variant of IAPP containing a free C-terminus proposes that oligomers adopt an antiparallel β-sheet dimer with His-18 and Tyr-37 forming interactions with each other [85]. However, since IAPP contains an amidated C-terminus and has a higher overall charge than the variant used in this study, Tyr-37 may be unable to make the same contacts with His-18 as it does in the model. Work from the Raleigh lab has shown that amidation of the C-terminus significantly affects IAPP aggregation and calls into question the model that relies on contacts between Tyr-37 and His-18. 2DIR analysis and MD simulations of isotopically labelled IAPP with the amidated C-terminus intact proposes that oligomers adopt a β-sheet hairpin [86]. What is most intriguing about this model is that the 23-27 region, a region that comprises the loop region of both the Eisenberg and Tycko models of the IAPP fibril, is located within one of the β-sheets of the transient intermediate. This model provides an

explanation for why amyloidogenicity of the full-length peptide is especially sensitive to substitutions in this region and also why fragments corresponding to the amyloidogenic core region are also amyloidogenic on their own [87, 88].

Each of these models suffers from similar limitations; they all use artificial means to stabilize the intermediate and may not be reflective of conditions *in vivo.* There is currently no structural data of the transient helical intermediate however; we can investigate the proposed helical region by introducing substitutions in this region and analyzing how this affects amyloid formation by IAPP. This is discussed further in Chapter 2.

1.2.6 The Disulfide Bond and First Seven Residues May Modulate Amyloidogenicity

Disulfide bonds are a common structural feature of proteins and are present in 15 % proteins in the human proteome, in 65 % of all secreted proteins, and over half of proteins associated with amyloidosis [89]. Removal of this bond can change the morphology of fibrils, the rate of aggregation, or change the toxicity of fibrils [90-92]. The disulfide bond between Cys-2 and Cys-7 is strictly conserved and it is found in all higher organisms regardless of the amyloidogenicity of the primary sequence of IAPP. The first seven residues of IAPP are also highly conserved with substitutions in this region found only in baboon, cow, pig, and horse [93]. The cyclical rigidity of the 1-7 segment of human IAPP led to the initial hypothesis that this region did not participate in amyloid formation. However removal of the first seven residues and the disulfide bond result in an elimination of the lag phase and an increased rate of aggregation [94, 95]. It is important to note that these studies were performed using a mixed hexafluoroisopropanol (HFIP) and H_2O solvent and this significantly affects amyloid formation. The role of the disulfide bond is currently not known but it appears to be necessary for

bioactivity and may play a protective role in preventing h-IAPP amyloid formation [39, 96-98]. Oxidized and reduced fragments corresponding to the first eight residues and a model variant with both cysteines replaced by Ser was analyzed by IMS-MS. Both the reduced peptide and the double serine peptide formed amyloid faster than the peptide with the disulfide bond. These findings agree that the disulfide bond is limiting the rate of aggregation of IAPP. Analysis of the oligomers formed by these peptides also revealed, the peptide aggregates via a different pathway when the disulfide bond is formed and samples different intermediates than when the cysteines are reduced or when they are both replaced by serines [99].

Alternative roles for the disulfide bond have been proposed. Fragments corresponding to the first eight residues and a variant with both cysteines replaced by serines showed that only the cyclical peptide was capable of forming amyloid and suggests that the disulfide loop may play a role in the mechanism of amyloid formation [100]. Triplet quenching reactions in which Tyr-37 was replaced by a Trp in order to determine when contacts occur between the Trp and disulfide bond suggest that human IAPP is less compact in its oxidized form and it samples an ensemble of conformational states in both cases. Quenching of the Trp was more rapid in h-IAPP than r-IAPP indicating that the sidechains in the different sequences also have a role in guiding the partial folding of IAPP [101]. These results are at odds with the previous findings that suggest the disulfide loop might prevent oligomerization and reduce the rate of amyloid formation by IAPP. The role of the disulfide bond and the first seven residues of IAPP are discussed further in Chapter 6.

1.2.7 Visualizing IAPP Amyloid Fibrils

The dye Congo red is often used to visualize amyloid fibrils in tissue samples. The dye shows a green birefringence under polarized light [2]. However, using Congo red to stain

amyloid fibrils has fallen out of use due to its propensity to bind to many types of fibrils such as cellulose and collagen and thus, does not show specificity to amyloid fibrils [102, 103]. Thioflavin-T is a dye commonly used to monitor the kinetics of amyloid. There are no high resolution structures of thioflavin-T bound to amyloid fibrils, but the dye is believed to bind to the surface of the cross-β structure of the amyloid fibrils (Figure 1-8). The parallel, in register β-sheet structures of typical amyloid fibrils create a series of grooves that run parallel to the long axis of the fibril and these are believed to form the thioflavin-T binding sites [104]. Binding of the dye fixes the position of the dimethylaminobenzyl and benzothiazole rings of thioflavin-T and reduces self-quenching, thereby leading to the enhancement in quantum yield [105]. As a result, thioflavin-T can be used to monitor amyloid formation in real time since it binds only to amyloid fibrils and not to monomers or oligomers. When bound to IAPP, Thioflavin-T features an excitation wavelength of 450 nm and emits at 482 nm [106].

Thioflavin-T assays are the most widely applied biophysical technique used to follow amyloid formation. But the dye provides an extrinsic probe of amyloid formation and the signal depends on the amount of dye bound and the quantum yield of the bound dye [104]. Thus, information this assay provides is more qualitative rather than quantitative in nature and the relationship between the intensity of thioflavin-T fluorescence and the amount of amyloid formed is not always clear and it is formally possible that the assay could give false positives and false negatives. Thioflavin-T assays are also used to identify potential inhibitors of amyloid formation. However, the signal from the dye can be compromised by inner filter effects due to absorbance from the putative inhibitor [107]. Additionally the compound of interest may displace thioflavin-T from the amyloid fibrils [108]. Inner filter effects depend on the

fluorescence properties of the compounds being screened. The potential limitations of the thioflavin-T assay are further discussed in Chapters 3, and 4.

Thioflavin-S, a dye with a chemical structure similar to thioflavin-T, is also used to visualize amyloid fibrils that are formed *in vivo* [109]. This dye also shows good selectivity to amyloid fibrils, however it does not have a shift in excitation and emission maxima when bound which results in very high background fluorescence signal. For this reason, the dye is used solely as a stain for *ex vivo* samples.

8-anilinonapthalene-1-sulfonic acid (ANS) is a polarity sensitive dye [110]. It is commonly used to study conformational changes in proteins because its fluorescence quantum yield increases when it is buried in the hydrophobic interior of a protein. Previous results show that the dye is able to bind to the prefibrillar intermediates of several amyloidogenic proteins such as Aβ, and human lysozyme [111, 112]. Due to this, the dye was initially believed to be unsuitable for monitoring amyloid formation. However, it was later shown that ANS does not bind to human IAPP monomers and oligomers, but it does bind to IAPP amyloid fibrils allowing it to be used to monitor amyloid formation by IAPP in real time [20, 113]. 4,4'-dianilino-1,1'-binapthyl-5,5'-disulfonic acid (Bis-ANS) is a homodimer of ANS [114]. The dye is also capable of binding to hydrophobic surfaces similar to ANS and is also used to monitor conformational changes in proteins but Bis-ANS also has the added advantage of a fluorescence quantum yield that is greater than ANS when bound.[114, 115] The versatility of these dyes and others will be discussed further in Chapter 4.

Unnatural amino acids can also be used to monitor amyloid formation. *p*-cyano-phenylalanine (*p*-cyanoPhe) has a high fluorescence when the residue is solvent exposed but is quenched when it is buried. *p*-cyanoPhe is also a FRET pair with Tyr which will also cause

fluorescence to be quenched after it donates its energy. Phe-15 and Phe-23 in human IAPP can be substituted for *p*-cyanoPhe in order to monitor amyloid formation in real time [116]. Incorporation of the residue does not perturb kinetics and results in a sigmodal curve that is a mirror image of the sigmoidal curve observed in a thioflavin-T fluorescence assay.

1.2.8 Sequence Variations of IAPP

Mature IAPP is a 37 residue polypeptide which has been found in all higher organisms examined and is highly conserved, but not all species form amyloid and the ability to do so correlates with the primary sequence of IAPP. A list of all known sequences of IAPP is shown in Figure 1-9. The cat and primate sequences are capable of forming amyloid whereas dogs and rats do not [117, 118]. Porcine and ferret IAPP have been reported to be significantly less amyloidogenic than human IAPP [83, 119]. The degu IAPP sequence is non-amyloidogenic, however degu islet amyloid is derived from insulin [120]. Only partial sequences are available for rabbit, hare, salmon, wolffish, and zebrafish. Rats and mice do not form islet amyloid *in vivo* and do not develop diabetes. R-IAPP polypeptide is non-amyloidogenic in solution although it can form low order oligomers.[96] The different behavior of the rat hormone is due to the six substitutions in the sequence relative to the human sequence. These include three prolines in the rat/mouse sequence and a His-18 to Arg replacement; collectively these substitutions reduce the ability of r-IAPP to form amyloid. Of the six substitutions in the rat sequence, five occur in the 20-29 putative amyloidogenic core region. There is a correlation between amyloidogenicity of fragments corresponding to the 20-29 region and amyloidogenicity of the full length peptide. A fragment corresponding to this 20-29 region in h-IAPP have been shown to be amyloidogenic while this same fragment corresponding to the sequence of r-IAPP was found to be nonamyloidogenic. Introducing substitutions in this region can greatly affect the overall

amyloidogenicity of the peptide [117, 121]. Though replacements in other parts of the sequence can also have an effect on the rate of amyloid formation by IAPP indicating that the 20-29 segment is not the sole determinant of amyloidogenicity [86, 117]. Previous results demonstrated that substituting Pro at position-17, 19, and 30 can also reduce the rate of amyloid formation and substitution of Asn-14 with Ala, Leu, and Ser has reportedly completely abolished amyloid formation [122, 123].

The sequence of several fish species of IAPP are currently known but it is not known whether fish are capable of developing diabetes. The sequences diverge significantly relative to h-IAPP and they contain a different sequence motif in the 20-29 core region than mammalian species. The amyloidogenic potential of any full-length fish IAPP has not been examined experimentally, although a ten residue fragment of salmon IAPP has been studied experimentally and larger fragments derived from different fish have been analyzed computationally. Recently, teleostean fish have been proposed as a source for xenobiotic transplantation in part because the pancreatic exocrine tissue is separated from the pancreatic endocrine cells [124, 125]. There is interest in finding organisms which do not form islet amyloid for potential use in transplanting for example, porcine islets have been considered a candidate for xenobiotic transplantation and there has been some success. Islet grafts derived from pigs demonstrated long-term graft survival in mouse models. Porcine IAPP is less amyloidogenic than human IAPP and is less toxic to INS-1 β-cells and so there may be a correlation between amyloidogenicity of the IAPP species and islet transplant viability [119]. For this reason, the amyloidogenicity of teleostean fish IAPP is of interest. The complete sequence of pufferfish IAPP (*Takifugu rubripes*) is known and is significantly different than the sequence of human IAPP [126]. The sequence differs at eleven

positions, seven of which are in the 20-29 amyloidogenic core region. The analysis of pufferfish IAPP is discussed further in Chapter 3.

Primate IAPP sequences are capable of forming amyloid, but baboon IAPP has not been studied. Baboon IAPP differs from human IAPP at three positions containing K1I, H18R, and A25T substitutions. The K1I substitution is a rare example of a replacement in the N-terminal region of IAPP. Its effects on amyloid formation have not been studied, but it reduces the net charge of the peptide. The K1I substitution is particularly interesting as it is the only IAPP sequence containing a substitution at position-1 and it is only one of four IAPP sequences that contain substitutions in the first seven residues. Due to the disulfide bond between Cys-2 and Cys-7, the first seven residues are believed to be unstructured in the fibril core and are not thought to play a significant role in amyloid formation [69, 70]. Additionally, the role of the residues within the disulfide loop is still unknown [122]. Analysis of the baboon IAPP sequence is further discussed in Chapter 5. Studying baboon IAPP could highlight the importance of this region. The A25T replacement involves a non-conservative substitution in a region of IAPP that is believed to be important in the early stages of aggregation. A model of the oligomeric state of IAPP derived from 2DIR predicts that a transient β-sheet is formed in this region and thus may be especially sensitive to substitutions and may have significant effects on the rate of aggregation of IAPP [86]. The H18R point mutant has been previously shown to reduce human IAPP toxicity in cell culture and to reduce aggregation [76, 127-130].

1.3 Figures

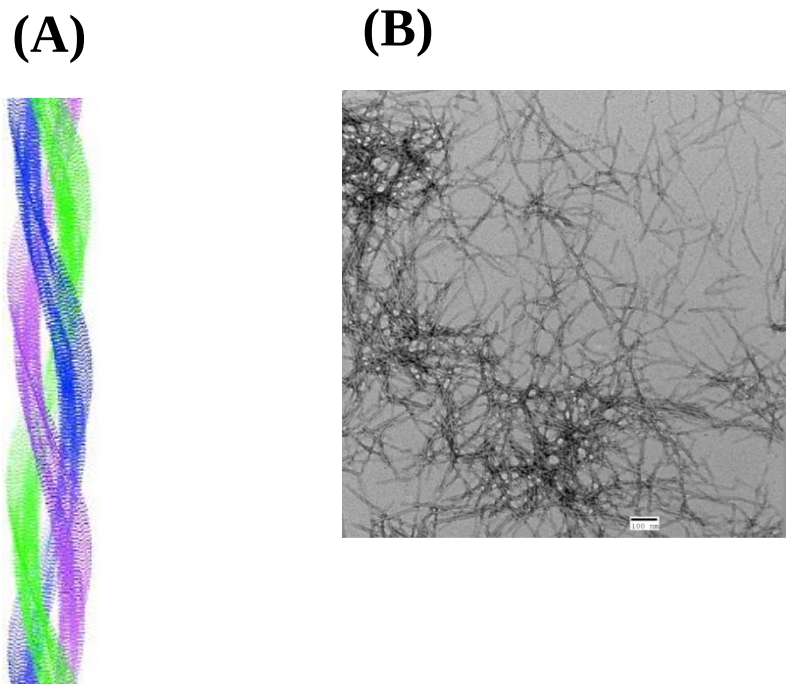

Figure 1-1: General features of the amyloid fibril. (A) Model of an individual fibril and its proposed structure showing three protofibrils in a cross-β structure. Image was taken from reference [1]. (B) A TEM image of human IAPP fibrils collected at Stony Brook. Scale bar is 100 nm.

Figure 1-2: ProIAPP is undergoes processing at several locations in order to yield mature IAPP. The peptide is synthesized as a pre-pro form which includes a leader sequence. Targeted cleavage of the leader sequence yields ProIAPP. The N and C-termini sequences are shown in red. The sites at which various enzymes process IAPP are indicated by arrows. Mature IAPP contains an amidated C-terminus and a disulfide bond between Cys-2 and Cys-7.

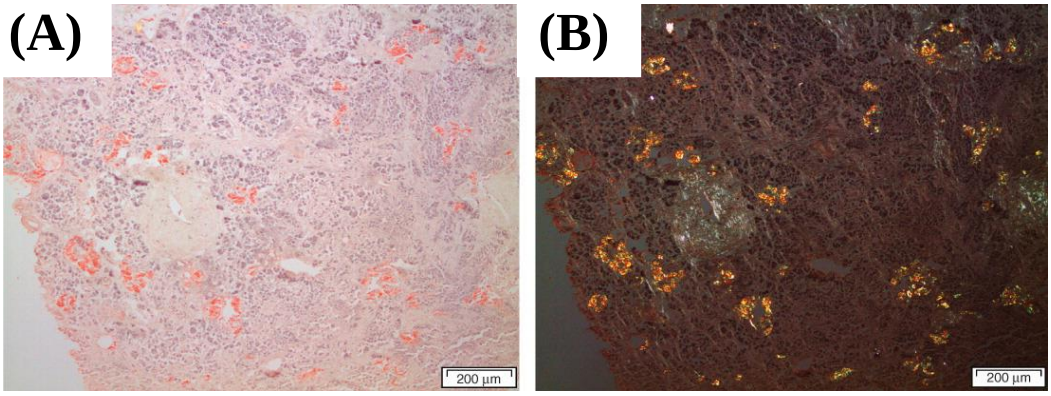

Figure 1-3: Section of a pancreas from a diabetic patient. (A) Sample has been stained with Congo red and is observed under normal light. (B) The same sample under polarized light shows amyloid fibrils with apple-green birefringence. Image taken from reference [3].

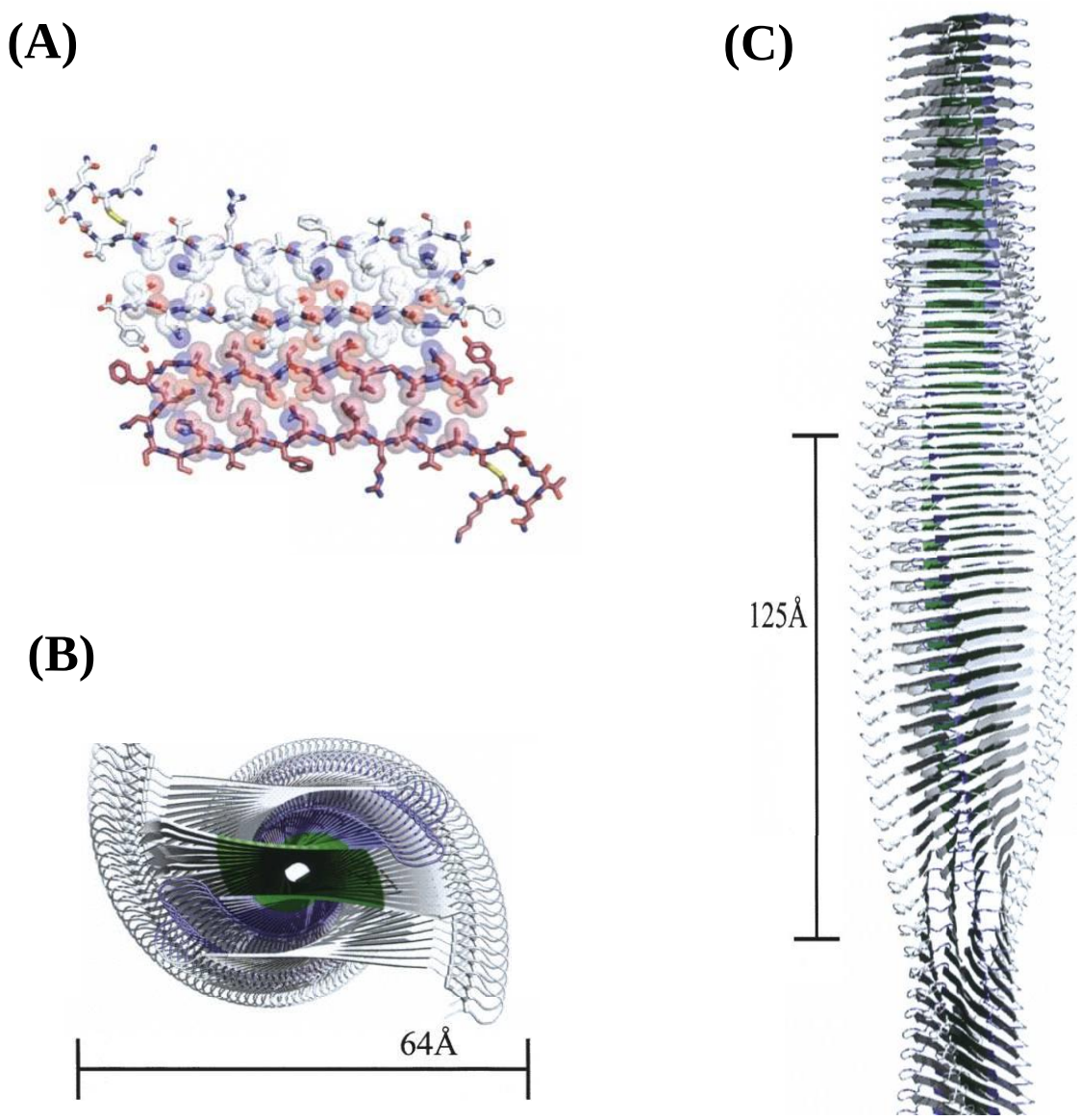

Figure 1-4: The Eisenberg model is derived from X-ray crystallography of small fragments of IAPP. (A) Proposed model based on crystal structures. The two IAPP molecules interdigitate to form a steric zipper between them. (B) View down the fibril axis showing the helical twist of the fibril. (C) View of the fibril perpendicular to the fibril axis. Images is taken from reference [69].

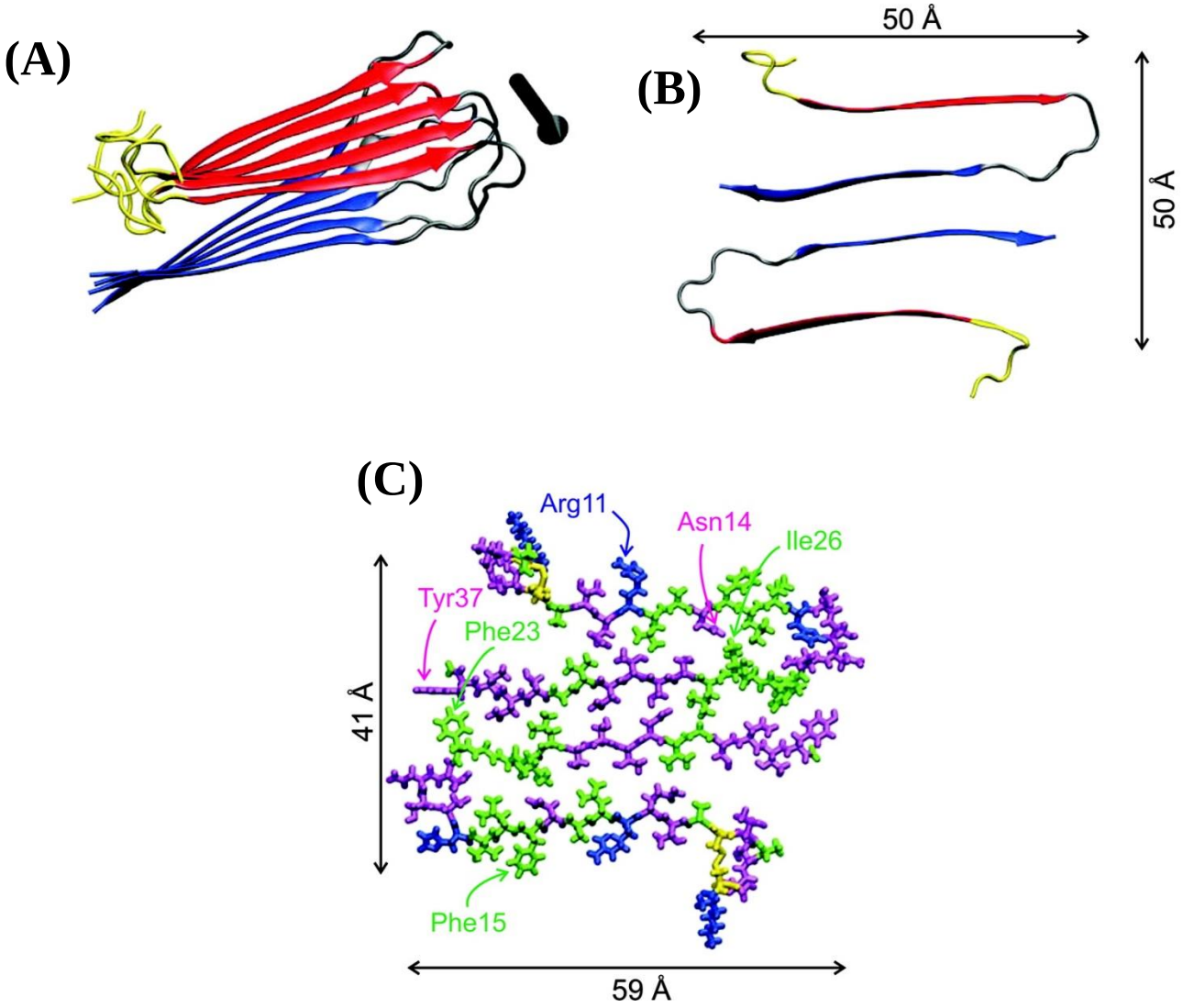

Figure 1-5: The Tycko model is derived from solid-state NMR. (A) Ribbon diagram of layers of one IAPP molecule. (B) View down the fibril axis showing the two IAPP molecules. (C) Proposed model of the IAPP fibril. This molecule does not contain the interdigitation that the Eisenberg model does and differs in the exact position of the loop which connects the two β-strands. Images taken from reference [70].

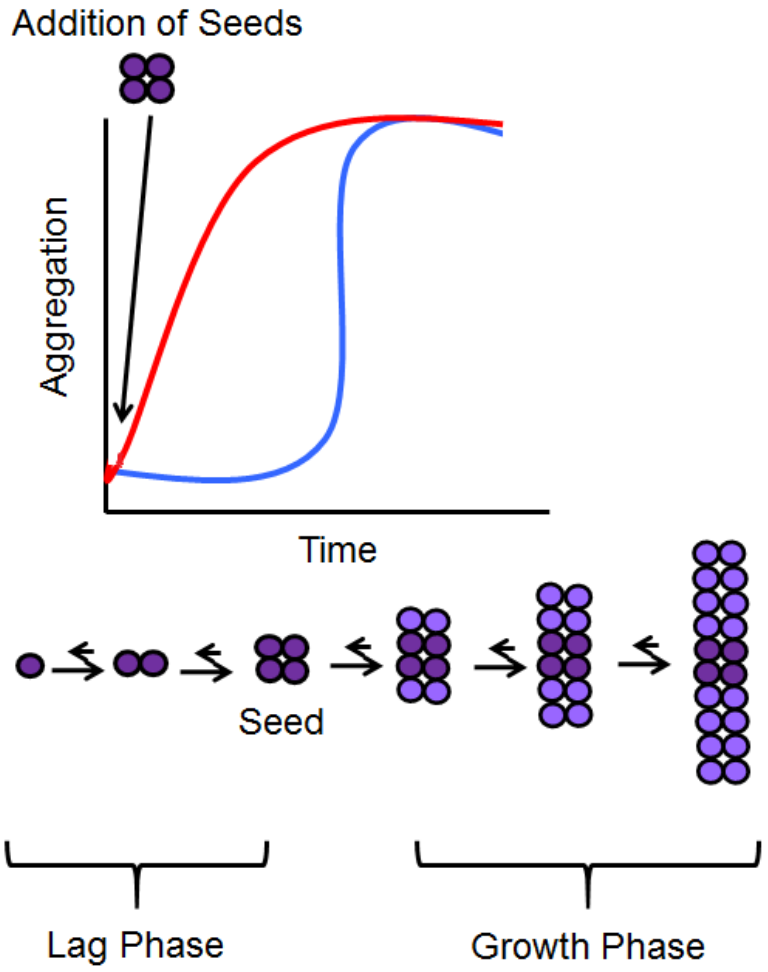

Figure 1-6: A nucleation dependent mechanism of amyloid formation. The blue curve is a depiction of a typical curve with a lag phase, growth phase, and final plateau. The red curve illustrates the elimination of the lag phase upon the addition of seeds.

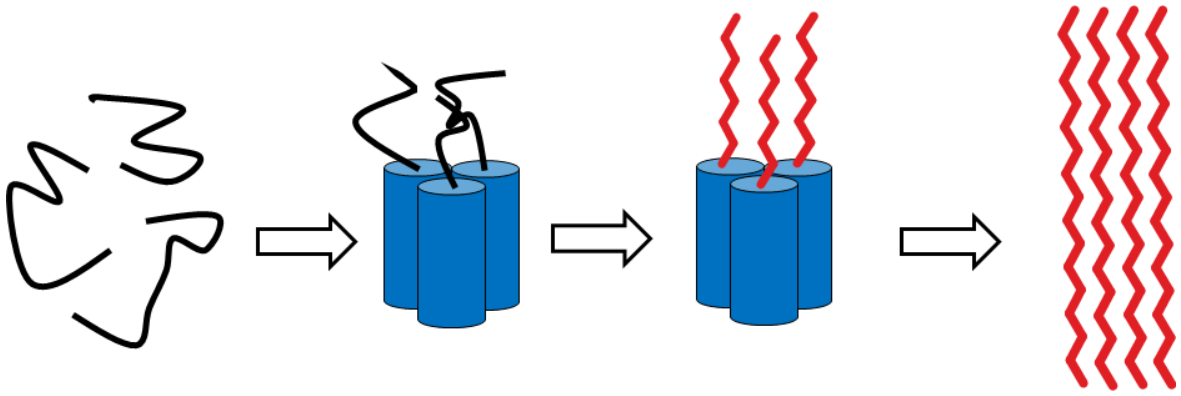

Figure 1-7: Schematic of how helical intermediates may induce amyloid formation by IAPP. α-helices are represented as cylinders and β-sheets by zigzags. IAPP is natively unstructured. It forms α-helices which self-associate via helix-helix interactions. This allows close proximity of the amyloidogenic region of IAPP which induces β-sheet formation. Finally, the peptide fully converts to β-sheet yielding a mature fibril. Image was adapted from reference [78].

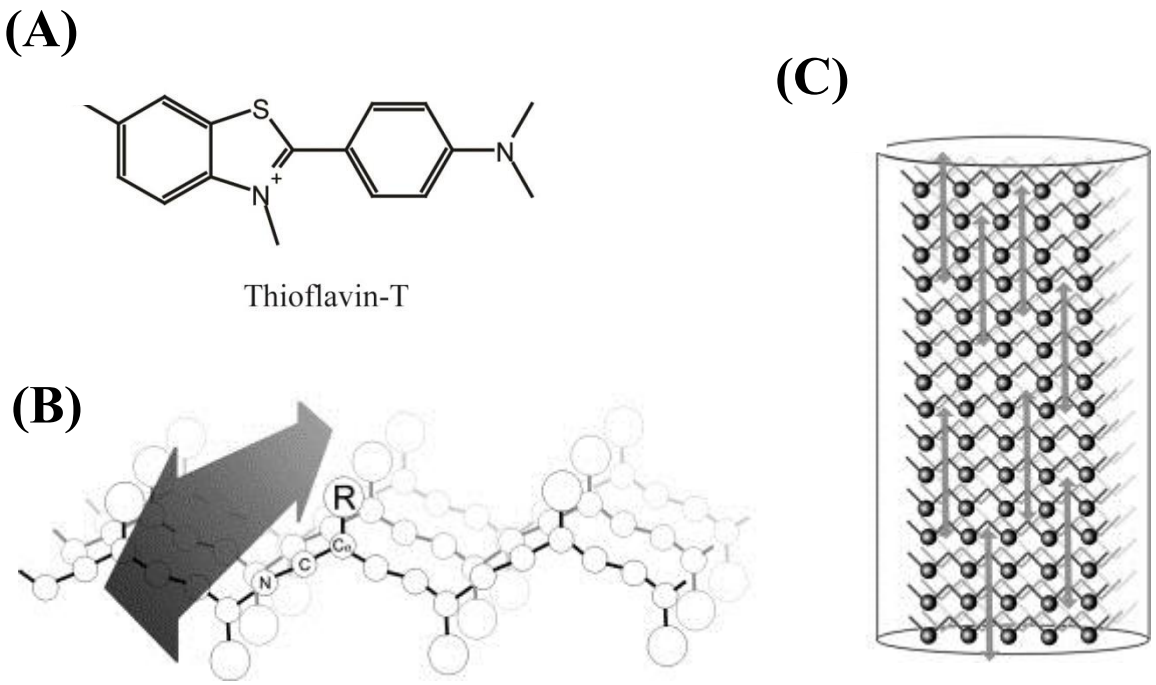

Figure 1-8: Proposed binding site of thioflavin-T. (A) Chemical structure of thioflavin-T. (B) A representation of β-sheets highlighting the grooves thioflavin-T is binding to. (C) A representation of an amyloid fibril. Black circles represent solvent-accessible sidechains. Thioflavin-T molecules are represented by double-headed arrows. Image was adapted from reference [104].

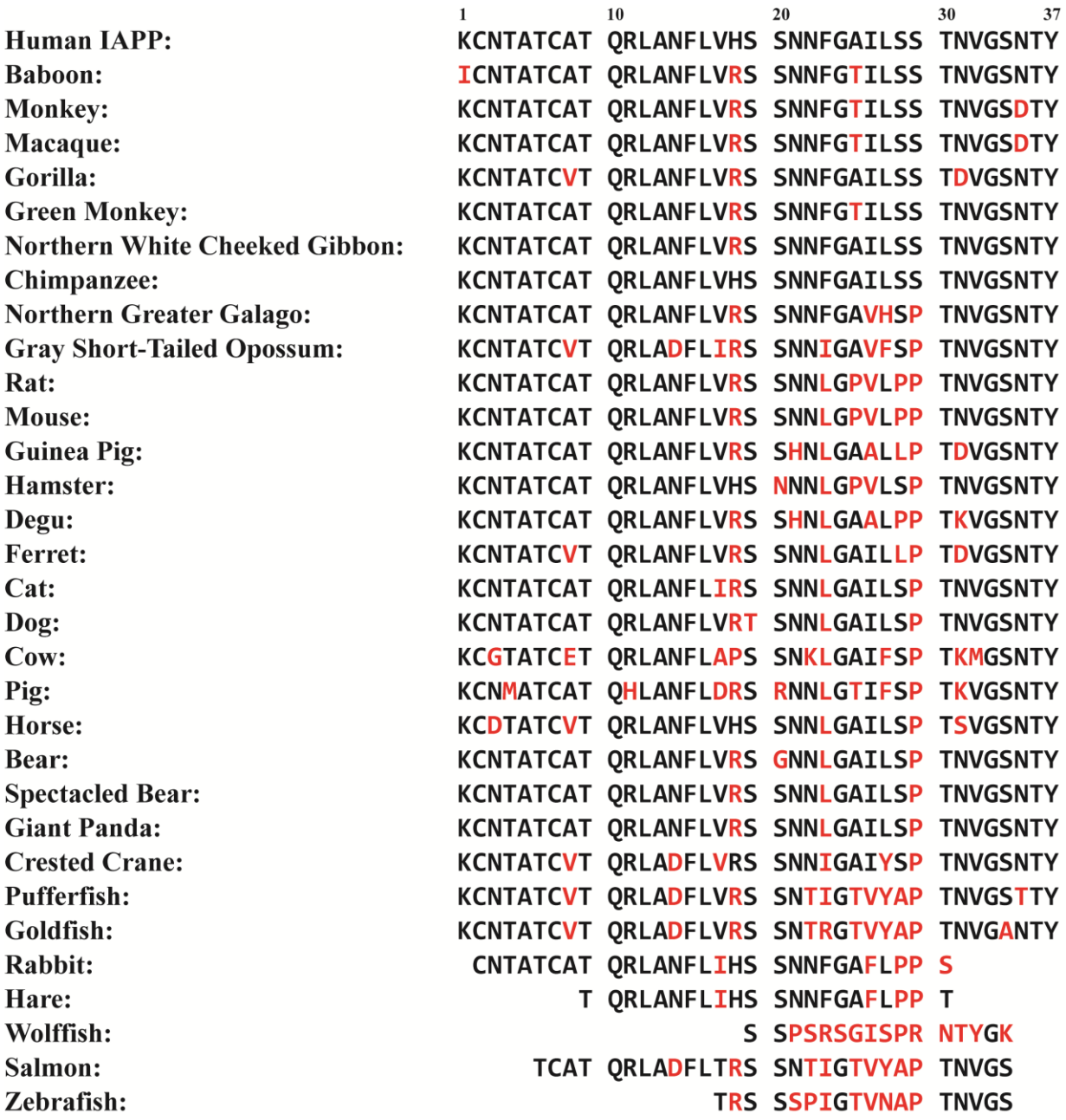

Figure 1-9: Comparison of the known sequences of IAPP from different species. Residues that differ from human IAPP are colored in red. Primate and cat variants have been reported to form islet amyloid whereas rodent and dog IAPP do not. Ferret, pig and bear IAPP has been reported to be significantly less amyloidogenic than human IAPP. The ability of, cow, and spectacled bear

variants has not been investigated although unpublished work from the Raleigh lab shows it is not amyloidogenic. Islet amyloid has been found in the degu, a rodent, but degu islet amyloid is derived from insulin. Only partial sequences are available for rabbit, hare, wolffish, zebrafish and Atlantic salmon IAPP.

1.4 Tables

Disease	Aggregating Protein or Peptide	Neurodegenerative, Systemic, or Localized
Alzheimer's Disease	Aβ	N
Amyloid A (AA) Amyoidosis	Serum amyloid A1 protein fragments	S
Amyloid light-chain (AL) amyloidosis	Immunoglobulin light-chain	S,L
Amyotrophic lateral sclerosis	Superoxide dismutase 1	N
Apolipoprotein A1 (Apo A-1)	Apo A-1 fragments	L
Familial amyloidotic polyneuropathy	Transthyretin mutants	N
Haemodialysis-related amyloidosis	β_2-microglobulin	S
Huntington's Disease	Huntingtin fragment	N
Injection-localized amyloidosis	Insulin	L
Lysozyme Amyloidosis	Lysozyme mutants	S
Parkinson's Disease	α-synuclein	N
Senile Systemic Amyloidosis	Wild-type transthyretin	S
Spongiform Encephalopathies	Prion protein or fragments	N
Type-2 Diabetes (T2D)	Amylin, IAPP	L

Table 1-1: Abbreviated list of diseases associated with amyloid deposits and the causative protein or peptide. Each disease is classified as either neurodegenerative (N), systemic (S), or localized (L). Table adapted from reference [10]

Name	Basic Approach	Server/Website
AGGRESCAN	Composition of amino acids	http://bioinf.uab.es/aggrescan/
FoldAmyloid	Composition of amino acids	http://bioinfo.protres.ru/fold-amyloid/oga.cgi
Zyggregator	Amino acid aggregation propensities and properties of β-structural conformation	http://www-vendruscolo.ch.cam.ac.uk/zyggregator.php
TANGO	Properties of β-structural conformation	http://tango.crg.es/
PASTA	Pairwise interactions within the β-sheets	http://protein.bio.unipd.it/pasta/
BetaScan	Pairwise interactions within the β-sheets	http://groups.csail.mit.edu/cb/betascan/betascan.html
ZipperDB	Amyloid-like structures of short peptides	http://services.mbi.ucla.edu/zipperdb/submit
Waltz	Amyloid-like structures of short peptides	http://waltz.switchlab.org/
NetCSSP	Conformational switches	http://cssp2.sookmyung.ac.kr/index.html
AmylPred	Conformational switches	http://biophysics.biol.uoa.gr/AMYLPRED/

Table 1-2: Common methods for predicting amyloidogenicity from inputted amino acid sequences and the methodology of each program. Table adapted from [36].

1.5 References

1. Kajava, A. V., Aebi, U., and Steven, A. C. The Parallel Superpleated Beta-Structure as a Model for Amyloid Fibrils of Human Amylin, *J. Mol. Biol.*, **2005**, *348*,247-252.

2. Westermark, G. T., Johnson, K. H., and Westermark, P. Staining Methods for Identification of Amyloid in Tissue, *Methods Enzymol.*, **1999**, *309*,3-25.

3. Westermark, P. Amyloid in the Islets of Langerhans: Thoughts and Some Historical Aspects, *Ups. J. Med. Sci.*, **2011**, *116*,81-89.

4. Sipe, J. D., Benson, M. D., Buxbaum, J. N., Ikeda, S., Merlini, G., Saraiva, M. J., Westermark, P., and Nomenclature Committee of the International Society of, A. Amyloid Fibril Protein Nomenclature: 2012 Recommendations from the Nomenclature Committee of the International Society of Amyloidosis, *Amyloid*, **2012**, *19*,167-170.

5. Serpell, L. C., Sunde, M., Benson, M. D., Tennent, G. A., Pepys, M. B., and Fraser, P. E. The Protofilament Substructure of Amyloid Fibrils, *J. Mol. Biol.*, **2000**, *300*,1033-1039.

6. Sunde, M., Serpell, L. C., Bartlam, M., Fraser, P. E., Pepys, M. B., and Blake, C. C. Common Core Structure of Amyloid Fibrils by Synchrotron X-ray Diffraction, *J. Mol. Biol.*, **1997**, *273*,729-739.

7. Makin, O. S., and Serpell, L. C. Structures for Amyloid Fibrils, *The FEBS journal*, **2005**, *272*,5950-5961.

8. Moreno-Gonzalez, I., and Soto, C. Misfolded Protein Aggregates: Mechanisms, Structures and Potential for Disease Transmission, *Semin. Cell. Dev. Biol.*, **2011**, *22*,482-487.

9. Eichner, T., and Radford, S. E. A Diversity of Assembly Mechanisms of a Generic Amyloid Fold, *Mol. Cell*, **2011**, *43*,8-18.

10. Abedini, A., Meng, F., and Raleigh, D. P. A Single-Point mutation Converts the Highly Amyloidogenic Human Islet Amyloid Polypeptide into a Potent Fibrillization Inhibitor, *J. Am. Chem. Soc.*, **2007**, *129*,11300-11301.

11. Chiti, F., and Dobson, C. M. Protein Misfolding, Functional Amyloid, and Human Disease, *Annu. Rev. Biochem*, **2006**, *75*,333-366.

12. Glenner, G. G. Reprint of "Alzheimer's Disease: Initial Report of the Purification and Characterization of a Novel Cerebrovascular Amyloid Protein", *Biochem. Biophys. Res. Commun.*, **2012**, *425*,534-539.

13. Invernizzi, G., Papaleo, E., Sabate, R., and Ventura, S. Protein Aggregation: Mechanisms and Functional Consequences, *Int. J. Bio. Cell Biol.*, **2012**, *44*,1541-1554.

14. Graw, J. The Crystallins: Genes, Proteins and Diseases, *Biol. Chem.*, **1997**, *378*,1331-1348.

15. Westermark, P., Benson, M. D., Buxbaum, J. N., Cohen, A. S., Frangione, B., Ikeda, S., Masters, C. L., Merlini, G., Saraiva, M. J., Sipe, J. D., and Nomenclature Committee of the International Society of, A. Amyloid: Toward Terminology Clarification. Report from the Nomenclature Committee of the International Society of Amyloidosis, *Amyloid*, **2005**, *12*,1-4.

16. Lundmark, K., Westermark, G. T., Olsen, A., and Westermark, P. Protein Fibrils in Nature Can Enhance Amyloid Protein A Amyloidosis in Mice: Cross-Seeding As a Disease Mechanism, *PNAS*, **2005**, *102*,6098-6102.

17. Glabe, C. G., and Kayed, R. Common Structure and Toxic Function of Amyloid Oligomers Implies a Common Mechanism of Pathogenesis, *Neurology*, **2006**, *66*,S74-78.

18. Stefani, M. Generic Cell Dysfunction in Neurodegenerative Disorders: Role of Surfaces in Early Protein Misfolding, Aggregation, and Aggregate Cytotoxicity, *Neuroscientist*, **2007**, *13*,519-531.

19. Lorenzo, A., Razzaboni, B., Weir, G. C., and Yankner, B. A. Pancreatic Islet Cell Toxicity of Amylin Associated with Type-2 Diabetes Mellitus, *Nature*, **1994**, *368*,756-760.

20. Abedini, A., Plesner, A., Cao, P., Ridgway, Z., Zhang, J., Tu, L. H., Middleton, C. T., Chao, B., Sartori, D. J., Meng, F., Wang, H., Wong, A. G., Zanni, M. T., Verchere, C. B., Raleigh, D. P., and Schmidt, A. M. Time-Resolved Studies Define the Nature of Toxic IAPP Intermediates, Providing Insight for Anti-Amyloidosis Therapeutics, *eLife*, **2016**, *5*.

21. Fandrich, M. Oligomeric Intermediates in Amyloid Formation: Structure Determination and Mechanisms of Toxicity, *J. Mol. Biol.*, **2012**, *421*,427-440.

22. Winner, B., Jappelli, R., Maji, S. K., Desplats, P. A., Boyer, L., Aigner, S., Hetzer, C., Loher, T., Vilar, M., Campioni, S., Tzitzilonis, C., Soragni, A., Jessberger, S., Mira, H., Consiglio, A., Pham, E., Masliah, E., Gage, F. H., and Riek, R. In vivo Demonstration That Alpha-Synuclein Oligomers Are Toxic, *PNAS*, **2011**, *108*,4194-4199.

23. Iijima-Ando, K., and Iijima, K. Transgenic Drosophila Models of Alzheimer's Disease and Tauopathies, *Brain. Struct. Funct.*, **2010**, *214*,245-262.

24. Crowther, D. C., Kinghorn, K. J., Miranda, E., Page, R., Curry, J. A., Duthie, F. A., Gubb, D. C., and Lomas, D. A. Intraneuronal Abeta, Non-Amyloid Aggregates and Neurodegeneration in a Drosophila Model of Alzheimer's Disease, *Neuroscience*, **2005**, *132*,123-135.

25. Kitada, T., Asakawa, S., Hattori, N., Matsumine, H., Yamamura, Y., Minoshima, S., Yokochi, M., Mizuno, Y., and Shimizu, N. Mutations in the Parkin Gene Cause Autosomal Recessive Juvenile Parkinsonism, *Nature*, **1998**, *392*,605-608.

26. Masliah, E., Rockenstein, E., Veinbergs, I., Mallory, M., Hashimoto, M., Takeda, A., Sagara, Y., Sisk, A., and Mucke, L. Dopaminergic Loss and Inclusion Body Formation in Alpha-Synuclein Mice: Implications for Neurodegenerative Disorders, *Science*, **2000**, *287*,1265-1269.

27. Selkoe, D. J. Cell Biology of Protein Misfolding: The Examples of Alzheimer's and Parkinson's Diseases, *Nat. Cell Biol.*, **2004**, *6*,1054-1061.

28. Tukel, C., Wilson, R. P., Nishimori, J. H., Pezeshki, M., Chromy, B. A., and Baumler, A. J. Responses to Amyloids of Microbial and Host Origin are Mediated Through Toll-Like Receptor 2, *Cell Host Microbe*, **2009**, *6*,45-53.

29. Wang, X., Smith, D. R., Jones, J. W., and Chapman, M. R. In vitro Polymerization of a Functional Escherichia coli Amyloid Protein, *J. Biol. Chem.*, **2007**, *282*,3713-3719.

30. Cabaleiro-Lago, C., Lynch, I., Dawson, K. A., and Linse, S. Inhibition of IAPP and IAPP(20-29) Fibrillation by Polymeric Nanoparticles, *Langmuir*, **2010**, *26*,3453-3461.

31. Chapman, M. R., Robinson, L. S., Pinkner, J. S., Roth, R., Heuser, J., Hammar, M., Normark, S., and Hultgren, S. J. Role of Escherichia coli Curli Operons in Directing Amyloid Fiber Formation, *Science*, **2002**, *295*,851-855.

32. Romero, D., Aguilar, C., Losick, R., and Kolter, R. Amyloid Fibers Provide Structural Integrity to Bacillus subtilis Biofilms, *PNAS*, **2010**, *107*,2230-2234.

33. Kenney, J. M., Knight, D., Wise, M. J., and Vollrath, F. Amyloidogenic Nature of Spider Silk, *Eur. J. Biochem.*, **2002**, *269*,4159-4163.

34. Rising, A., Widhe, M., Johansson, J., and Hedhammar, M. Spider Silk Proteins: Recent Advances in Recombinant Production, Structure-Function Relationships and Biomedical Applications, *Cell Mol. Life Sci.*, **2011**, *68*,169-184.

35. Chen, A. Y., Deng, Z., Billings, A. N., Seker, U. O., Lu, M. Y., Citorik, R. J., Zakeri, B., and Lu, T. K. Synthesis and Patterning of Tunable Multiscale Materials with Engineered Cells, *Nat. Mater.*, **2014**, *13*,515-523.

36. Ahmed, A. B., and Kajava, A. V. Breaking the Amyloidogenicity Code: Methods to Predict Amyloids from Amino Acid Sequence, *FEBS Lett.*, **2013**, *587*,1089-1095.

37. Conchillo-Sole, O., de Groot, N. S., Aviles, F. X., Vendrell, J., Daura, X., and Ventura, S. AGGRESCAN: a server for the prediction and evaluation of "hot spots" of aggregation in polypeptides, *BMC Bioinf.*, **2007**, *8*,65.

38. Garbuzynskiy, S. O., Lobanov, M. Y., and Galzitskaya, O. V. FoldAmyloid: A Method of Prediction of Amyloidogenic Regions From Protein Sequence, *Bioinformatics*, **2010**, *26*,326-332.

39. Tartaglia, G. G., Pawar, A. P., Campioni, S., Dobson, C. M., Chiti, F., and Vendruscolo, M. Prediction of Aggregation-Prone Regions in Structured Proteins, *J. Mol. Biol.*, **2008**, *380*,425-436.

40. Tartaglia, G. G., and Vendruscolo, M. The Zyggregator Method For Pedicting Potein Agregation Propensities, *Chem. Soc. Rev.*, **2008**, *37*,1395-1401.

41. Thompson, M. J., Sievers, S. A., Karanicolas, J., Ivanova, M. I., Baker, D., and Eisenberg, D. The 3D Profile Method for Identifying Fibril-Forming Segments of Proteins, *PNAS*, **2006**, *103*,4074-4078.

42. Maurer-Stroh, S., Debulpaep, M., Kuemmerer, N., Lopez de la Paz, M., Martins, I. C., Reumers, J., Morris, K. L., Copland, A., Serpell, L., Serrano, L., Schymkowitz, J. W., and Rousseau, F. Exploring the Sequence Determinants of Amyloid Structure Using Position-Specific Scoring Matrices, *Nat. Methods*, **2010**, *7*,237-242.

43. Sawaya, M. R., Sambashivan, S., Nelson, R., Ivanova, M. I., Sievers, S. A., Apostol, M. I., Thompson, M. J., Balbirnie, M., Wiltzius, J. J., McFarlane, H. T., Madsen, A. O., Riekel, C., and Eisenberg, D. Atomic Structures of Amyloid Cross-Beta Spines Reveal Varied Steric Zippers, *Nature*, **2007**, *447*,453-457.

44. Fernandez-Escamilla, A.-M., Rousseau, F., Schymkowitz, J., and Serrano, L. Prediction of Sequence-Dependent And Mutational Effects on the Aggregation of Peptides and Proteins, *Nat. Biotechnol.*, **2004**, *22*,1302-1306.

45. Hamodrakas, S. J., Liappa, C., and Iconomidou, V. A. Consensus Prediction of Amyloidogenic Determinants in Amyloid Fibril-Forming Proteins, *Int. J. Biol. Macromol.*, **2007**, *41*,295-300.

46. Trovato, A., Seno, F., and Tosatto, S. C. E. The PASTA Server For Protein Aggregation Prediction, *Protein Eng., Des. Sel.*, **2007**, *20*,521-523.

47. Trovato, A., Chiti, F., Maritan, A., and Seno, F. Insight into the Structure of Amyloid Fibrils from the Analysis of Globular Proteins, *PLoS Comput. Biol.*, **2006**, *2*,e170.

48. Gebre-Medhin, S., Mulder, H., Pekny, M., Westermark, G., Tornell, J., Westermark, P., Sundler, F., Ahren, B., and Betsholtz, C. Increased Insulin Secretion and Glucose Tolerance in Mice Lacking Islet Amyloid Polypeptide (Amylin), *Biochem. Biophys. Res. Commun.*, **1998**, *250*,271-277.

49. Wookey, P. J., Xuereb, L., Tikellis, C., and Cooper, M. E. Amylin in the Periphery, *Sci. World J.*, **2003**, *3*,163-175.

50. Sanke, T., Bell, G. I., Sample, C., Rubenstein, A. H., and Steiner, D. F. An Islet Amyloid Peptide Is Derived from an 89-Amino Acid Precursor by Proteolytic Processing, *J. Biol. Chem.*, **1988**, *263*,17243-17246.

51. Meng, F., Abedini, A., Song, B., and Raleigh, D. P. Amyloid Formation by Pro-Islet Amyloid Polypeptide Processing Intermediates: Examination of the Role of Protein Heparan Sulfate Interactions and Implications for Islet Amyloid Formation in Type 2 Diabetes, *Biochemistry*, **2007**, *46*,12091-12099.

52. Opie, E. L. Pathological Changes Affecting the Islands of Langerhans of the Pancreas, *J. Boston Soc. Med. Sci.*, **1900**, *4*,251-260.

53. Cooper, G. J. S., Willis, A. C., Clark, A., Turner, R. C., Sim, R. B., and Reid, K. B. M. Purification and Characterization of a Peptide from Amyloid-Rich Pancreases of Type 2 Diabetic Patients, *PNAS*, **1987**, *84*,8628-8632.

54. Westermark, P., Wernstedt, C., Wilander, E., Hayden, D. W., O'Brien, T. D., and Johnson, K. H. Amyloid Fibrils in Human Insulinoma and Islets of Langerhans of the Diabetic Cat Are Derived from a Neuropeptide-Like Protein Also Present in Normal Islet Cells, *PNAS*, **1987**, *84*,3881-3885.

55. Höppener, J. W. M., Ahrén, B., and Lips, C. J. M. Islet Amyloid and Type 2 Diabetes Mellitus, *N. Engl. J. Med.*, **2000**, *343*,411-419.

56. Poitout, V., and Robertson, R. P. Minireview: Secondary Beta-Cell Failure in Type 2 Diabetes--A Convergence of Glucotoxicity and Lipotoxicity, *Endocrinology*, **2002**, *143*,339-342.

57. Brunham, L. R., Kruit, J. K., Hayden, M. R., and Verchere, C. B. Cholesterol in Beta-Cell Dysfunction: The Emerging Connection Between HDL Cholesterol and Type 2 Diabetes, *Curr. Diab. Rep.*, **2010**, *10*,55-60.

58. Ehses, J. A., Perren, A., Eppler, E., Ribaux, P., Pospisilik, J. A., Maor-Cahn, R., Gueripel, X., Ellingsgaard, H., Schneider, M. K., Biollaz, G., Fontana, A., Reinecke, M., Homo-Delarche, F., and Donath, M. Y. Increased Number of Islet-Associated Macrophages in Type 2 Diabetes, *Diabetes*, **2007**, *56*,2356-2370.

59. Sparr, E., Engel, M. F. M., Sakharov, D. V., Sprong, M., Jacobs, J., de Kruijff, B., Höppener, J. W. M., and Antoinette Killian, J. Islet Amyloid Polypeptide-Induced Membrane Leakage Involves Uptake of Lipids by Forming Amyloid Fibers, *FEBS Lett.*, **2004**, *577*,117-120.

60. Matveyenko, A. V., and Butler, P. C. Beta-Cell Deficit Due to Increased Apoptosis in the Human Islet Amyloid Polypeptide Transgenic (HIP) Rat Recapitulates the Metabolic Defects Present in Type 2 Diabetes, *Diabetes*, **2006**, *55*,2106-2114.

61. Rivera, J. F., Gurlo, T., Daval, M., Huang, C. J., Matveyenko, A. V., Butler, P. C., and Costes, S. Human-IAPP disrupts the Autophagy/Lysosomal Pathway in Pancreatic Beta-Cells: Protective Role of p62-Positive Cytoplasmic Inclusions, *Cell Death Differ.*, **2011**, *18*,415-426.

62. Masters, S. L., Dunne, A., Subramanian, S. L., Hull, R. L., Tannahill, G. M., Sharp, F. A., Becker, C., Franchi, L., Yoshihara, E., Chen, Z., Mullooly, N., Mielke, L. A., Harris, J., Coll, R. C., Mills, K. H., Mok, K. H., Newsholme, P., Nunez, G., Yodoi, J., Kahn, S. E., Lavelle, E. C., and O'Neill, L. A. Activation of the NLRP3 Inflammasome by Islet Amyloid Polypeptide Provides a Mechanism for Enhanced IL-1Beta in Type 2 Diabetes, *Nat Immunol.*, **2010**, *11*,897-904.

63. Westwell-Roper, C., Dai, D. L., Soukhatcheva, G., Potter, K. J., van Rooijen, N., Ehses, J. A., and Verchere, C. B. IL-1 Blockade Attenuates Islet Amyloid Polypeptide-Induced Proinflammatory Cytokine Release and Pancreatic Islet Graft Dysfunction, *J. Immunol.*, **2011**, *187*,2755-2765.

64. Sanke, T., and Sakagashira, S. S20G Mutation of Amylin Gene--Amyloid Diabetes Due to S20G Amylin Gene Mutation, *Nihon Rinsho*, **2005**, *63 Suppl 2*,160-165.

65. Sakagashira, S., Sanke, T., Hanabusa, T., Shimomura, H., Ohagi, S., Kumagaye, K. Y., Nakajima, K., and Nanjo, K. Missense Mutation of Amylin Gene (S20G) in Japanese NIDDM Patients, *Diabetes*, **1996**, *45*,1279-1281.

66. Swift, S. M., Clayton, H. A., London, N. J., and James, R. F. The Potential Contribution of Rejection to Survival of Transplanted Human Islets, *Cell Transplant.*, **1998**, *7*,599-606.

67. Ryan, E. A., Paty, B. W., Senior, P. A., Bigam, D., Alfadhli, E., Kneteman, N. M., Lakey, J. R., and Shapiro, A. M. Five-Year Follow-Up After Clinical Islet Transplantation, *Diabetes*, **2005**, *54*,2060-2069.

68. Benoni, R., Pertinhez, T. A., Spyrakis, F., Davalli, S., Pellegrino, S., Paredi, G., Pezzotti, A., Bettati, S., Campanini, B., and Mozzarelli, A. Structural Insight into the Interaction of O-Acetylserine Sulfhydrylase with Competitive, Peptidic Inhibitors by Saturation Transfer Difference-NMR, *FEBS Lett.*, **2016**, *590*,943-953.

69. Wiltzius, J. J. W., Sievers, S. A., Sawaya, M. R., Cascio, D., Popov, D., Riekel, C., and Eisenberg, D. Atomic Structure of The Cross-Beta Spine of Islet Amyloid Polypeptide (Amylin), *Protein Sci.*, **2008**, *17*,1467-1474.

70. Luca, S., Yau, W. M., Leapman, R., and Tycko, R. Peptide Conformation and Supramolecular Organization in Amylin Fibrils: Constraints From Solid-State NMR, *Biochemistry*, **2007**, *46*,13505-13522.

71. Wetzel, R. Kinetics and Thermodynamics of Amyloid Fibril Assembly, *Acc. Chem. Res.*, **2006**, *39*,671-679.

72. Kumar, S., and Walter, J. Phosphorylation of Amyloid Beta (Abeta) Peptides - A Trigger for Formation of Toxic Aggregates in Alzheimer's Disease, *Aging*, **2011**, *3*,803-812.

73. Krebs, M. R., Morozova-Roche, L. A., Daniel, K., Robinson, C. V., and Dobson, C. M. Observation of sequence specificity in the seeding of protein amyloid fibrils, *Protein Sci.*, **2004**, *13*,1933-1938.

74. Williamson, J. A., and Miranker, A. D. Direct Detection of Transient Alpha-Helical States in Islet Amyloid Polypeptide, *Protein Sci.*, **2007**, *16*,110-117.

75. Padrick, S. B., and Miranker, A. D. Islet Amyloid Polypeptide: Identification of Long-Range Contacts and Local Order on the Fibrillogenesis Pathway, *J. Mol. Biol.*, **2001**, *308*,783-794.

76. Knight, J. D., Hebda, J. A., and Miranker, A. D. Conserved and Cooperative Assembly of Membrane-Bound Alpha-Helical States of Islet Amyloid Polypeptide, *Biochemistry*, **2006**, *45*,9496-9508.

77. Nanga, R. P., Brender, J. R., Xu, J., Veglia, G., and Ramamoorthy, A. Structures of Rat and Human Islet Amyloid Polypeptide IAPP(1-19) in Micelles by NMR Spectroscopy, *Biochemistry*, **2008**, *47*,12689-12697.

78. Abedini, A., and Raleigh, D. P. A Critical Assessment of the Role of Helical Intermediates in Amyloid Formation by Natively Unfolded Proteins and Polypeptides, *Protein Eng. Des. Sel.*, **2009**, *22*,453-459.

79. Hebda, J. A., Saraogi, I., Magzoub, M., Hamilton, A. D., and Miranker, A. D. A Peptidomimetic Approach to Targeting Pre-Amyloidogenic States in Type II Diabetes, *Chem. Biol.*, **2009**, *16*,943-950.

80. Meng, F., Raleigh, D. P., and Abedini, A. Combination of Kinetically Selected Inhibitors in trans Leads to Highly Effective Inhibition of Amyloid Formation, *J. Am. Chem. Soc.*, **2010**, *132*,14340-14342.

81. Cao, P., Meng, F., Abedini, A., and Raleigh, D. P. The Ability of Rodent Islet Amyloid Polypeptide to Inhibit Amyloid Formation by Human Islet Amyloid Polypeptide Has Important Implications for the Mechanism of Amyloid Formation and the Design of Inhibitors, *Biochemistry*, **2010**, *49*,872-881.

82. Tu, L.-H., and Raleigh, D. P. Role of Aromatic Interactions in Amyloid Formation by Islet Amyloid Polypeptide, *Biochemistry*, **2013**, *52*,333-342.

83. Dupuis, N. F., Wu, C., Shea, J. E., and Bowers, M. T. Human Islet Amyloid Polypeptide Monomers Form Ordered Beta-Hairpins: A Possible Direct Amyloidogenic Precursor, *J. Am. Chem. Soc.*, **2009**, *131*,18283-18292.

84. Dupuis, N. F., Wu, C., Shea, J. E., and Bowers, M. T. The Amyloid Formation Mechanism in Human IAPP: Dimers Have Beta-Strand Monomer-Monomer Interfaces, *J. Am. Chem. Soc.*, **2011**, *133*,7240-7243.

85. Wei, L., Jiang, P., Xu, W., Li, H., Zhang, H., Yan, L., Chan-Park, M. B., Liu, X. W., Tang, K., Mu, Y., and Pervushin, K. The Molecular Basis of Distinct Aggregation Pathways of Islet Amyloid Polypeptide, *J. Biol. Chem.*, **2011**, *286*,6291-6300.

86. Buchanan, L. E., Dunkelberger, E. B., Tran, H. Q., Cheng, P.-N., Chiu, C.-C., Cao, P., Raleigh, D. P., de Pablo, J. J., Nowick, J. S., and Zanni, M. T. Mechanism of IAPP Amyloid Fibril Formation Involves an Intermediate with a Transient Beta-Sheet, *PNAS*, **2013**, *110*,19285-19290.

87. Tenidis, K., Waldner, M., Bernhagen, J., Fischle, W., Bergmann, M., Weber, M., Merkle, M. L., Voelter, W., Brunner, H., and Kapurniotu, A. Identification of a Penta- and Hexapeptide of Islet Amyloid Polypeptide (IAPP) with Amyloidogenic and Cytotoxic Properties, *J. Mol. Biol.*, **2000**, *295*,1055-1071.

88. Ashburn, T. T., Auger, M., and Lansbury, P. T. The Structural Basis of Pancreatic Amyloid Formation: Isotope-Edited Spectroscopy in the Solid State, *J. Am. Chem. Soc.*, **1992**, *114*,790-791.

89. Li, Y., Yan, J., Zhang, X., and Huang, K. Disulfide Bonds in Amyloidogenesis Diseases Related Proteins, *Proteins*, **2013**, *81*,1862-1873.

90. Mossuto, M. F., Bolognesi, B., Guixer, B., Dhulesia, A., Agostini, F., Kumita, J. R., Tartaglia, G. G., Dumoulin, M., Dobson, C. M., and Salvatella, X. Disulfide Bonds Reduce the Toxicity of the Amyloid Fibrils Formed by an Extracellular Protein, *Angew. Chem. Int. Ed. Engl.*, **2011**, *50*,7048-7051.

91. Wang, S. S., Liu, K. N., and Wang, B. W. Effects of Dithiothreitol on the Amyloid Fibrillogenesis of Hen Egg-White Lysozyme, *Eur. Biophys. J.*, **2010**, *39*,1229-1242.

92. Sarkar, N., Kumar, M., and Dubey, V. K. Effect of Sodium Tetrathionate on Amyloid Fibril: Insight into the Role of Disulfide Bond in Amyloid Progression, *Biochimie*, **2011**, *93*,962-968.

93. Wu, C., and Shea, J. E. Structural Similarities and Differences Between Amyloidogenic and Non-Amyloidogenic Islet Amyloid Polypeptide (IAPP) Sequences and Implications for the Dual Physiological and Pathological Activities of These Peptides, *PLoS Comput. Biol.*, **2013**, *9*,e1003211.

94. Goldsbury, C., Goldie, K., Pellaud, J., Seelig, J., Frey, P., Muller, S. A., Kistler, J., Cooper, G. J., and Aebi, U. Amyloid Fibril Formation from Full-Length and Fragments of Amylin, *J. Struct. Biol.*, **2000**, *130*,352-362.

95. Tu, L. H., Young, L. M., Wong, A. G., Ashcroft, A. E., Radford, S. E., and Raleigh, D. P. Mutational Analysis of the Ability of Resveratrol to Inhibit Amyloid Formation by Islet Amyloid Polypeptide: Critical Evaluation of the Importance of Aromatic-Inhibitor and Histidine-Inhibitor Interactions, *Biochemistry*, **2015**, *54*,666-676.

96. Westermark, P., Andersson, A., and Westermark, G. T. Islet Amyloid Polypeptide, Islet Amyloid, and Diabetes Mellitus, *Physiol. Rev.*, **2011**, *91*,795-826.

97. Barwell, J., Gingell, J. J., Watkins, H. A., Archbold, J. K., Poyner, D. R., and Hay, D. L. Calcitonin and Calcitonin Receptor-Like Receptors: Common Themes with Family B GPCRs?, *Br. J. Pharmacol.*, **2012**, *166*,51-65.

98. Roberts, A. N., Leighton, B., Todd, J. A., Cockburn, D., Schofield, P. N., Sutton, R., Holt, S., Boyd, Y., Day, A. J., Foot, E. A., and et al. Molecular and Functional Characterization of Amylin, a Peptide Associated with Type 2 Diabetes Mellitus, *PNAS*, **1989**, *86*,9662-9666.

99. Ilitchev, A. I., Giammona, M. J., Do, T. D., Wong, A. G., Buratto, S. K., Shea, J. E., Raleigh, D. P., and Bowers, M. T. Human Islet Amyloid Polypeptide N-Terminus Fragment Self-Assembly: Effect of Conserved Disulfide Bond on Aggregation Propensity, *J. Am. Soc. Mass. Spectrom.*, **2016**, *27*,1010-1018.

100. Cope, S. M., Shinde, S., Best, R. B., Ghirlanda, G., and Vaiana, S. M. Cyclic N-terminal Loop of Amylin Forms Non Amyloid Fibers, *Biophys. J.*, **2013**, *105*,1661-1669.

101. Vaiana, S. M., Best, R. B., Yau, W. M., Eaton, W. A., and Hofrichter, J. Evidence for a Partially Structured State of the Amylin Monomer, *Biophys. J.*, **2009**, *97*,2948-2957.

102. Puchtler, H., Sweat, F., and Levine, M. On The Binding of Congo Red by Amyloid, *J. Histochem. Cytochem.*, **1962**, *10*,355-364.

103. Khurana, R., Uversky, V. N., Nielsen, L., and Fink, A. L. Is Congo Red an Amyloid-Specific Dye?, *J. Biol. Chem.*, **2001**, *276*,22715-22721.

104. Krebs, M. R., Bromley, E. H., and Donald, A. M. The Binding of Thioflavin-T to Amyloid Fibrils: Localisation and Implications, *J. Struct. Biol.*, **2005**, *149*,30-37.

105. Biancalana, M., and Koide, S. Molecular Mechanism of Thioflavin-T Binding to Amyloid Fibrils, *Biochim. Biophys. Acta, Proteins Proteomics*, **2010**, *1804*,1405-1412.

106. Levine, H. Thioflavine-T Interaction with Synthetic Alzheimers-Disease Beta-Amyloid Peptides - Detection of Amyloid Aggregation in Solution, *Protein Sci.*, **1993**, *2*,404-410.

107. Jameson, D. M., Croney, J. C., and Moens, P. D. Fluorescence: Basic Concepts, Practical Aspects, and Some Anecdotes, *Methods Enzymol.*, **2003**, *360*,1-43.

108. Meng, F. L., Marek, P., Potter, K. J., Verchere, C. B., and Raleigh, D. P. Rifampicin Does Not Prevent Amyloid Fibril Formation by Human Islet Amyloid Polypeptide But Does Inhibit Fibril Thioflavin-T Interactions: Implications For Mechanistic Studies Beta-Cell Death, *Biochemistry*, **2008**, *47*,6016-6024.

109. LeVine, H., 3rd. Quantification of Beta-Sheet Amyloid Fibril Structures with Thioflavin T, *Methods Enzymol.*, **1999**, *309*,274-284.

110. Stryer, L. The Interaction of a Naphthalene Dye with Apomyoglobin and Apohemoglobin. A Fluorescent Probe of Non-Polar Binding Sites, *J. Mol. Biol.*, **1965**, *13*,482-495.

111. Mannini, B., Mulvihill, E., Sgromo, C., Cascella, R., Khodarahmi, R., Ramazzotti, M., Dobson, C. M., Cecchi, C., and Chiti, F. Toxicity of Protein Oligomers is Rationalized by a Function Combining Size and Surface Hydrophobicity, *Acs Chemical Biology*, **2014**, *9*,2309-2317.

112. Pace, C. N., and Scholtz, J. M. A Helix Propensity Scale Based on Experimental Studies of Peptides and Proteins, *Biophys. J.*, **1998**, *75*,422-427.

113. Younan, N. D., and Viles, J. H. A Comparison of Three Fluorophores for the Detection of Amyloid Fibers and Prefibrillar Oligomeric Assemblies. ThT (Thioflavin T); ANS (1-Anilinonaphthalene-8-sulfonic Acid); and bisANS (4,4 '-Dianilino-1,1 '-binaphthyl-5,5 '-disulfonic Acid), *Biochemistry*, **2015**, *54*,4297-4306.

114. Rosen, C. G., and Weber, G. Dimer Formation from 1-Amino-8-Naphthalenesulfonate Catalyzed by Bovine Serum Albumin. A New Fluorescent Molecule with Exceptional Binding Properties, *Biochemistry*, **1969**, *8*,3915-3920.

115. Andersen, N. H., Dyer, R. B., Fesinmeyer, R. M., Gai, F., Liu, Z. H., Neidigh, J. W., and Tong, H. Effect of Hexafluoroisopropanol on the Thermodynamics of Peptide Secondary Structure Formation, *J. Am. Chem. Soc.*, **1999**, *121*,9879-9880.

116. Marek, P., Mukherjee, S., Zanni, M. T., and Raleigh, D. P. Residue-Specific, Real-Time Characterization of Lag-Phase Species and Fibril Growth During Amyloid Formation: A Combined Fluorescence and IR Study of p-Cyanophenylalanine Analogs of Islet Amyloid Polypeptide, *J. Mol. Biol.*, **2010**, *400*,878-888.

117. Betsholtz, C., Christmansson, L., Engstrom, U., Rorsman, F., Svensson, V., Johnson, K. H., and Westermark, P. Sequence Divergence in a Specific Region of Islet Amyloid Polypeptide (Iapp) Explains Differences in Islet Amyloid Formation between Species, *FEBS Lett.*, **1989**, *251*,261-264.

118. Westermark, P., Engstrom, U., Johnson, K. H., Westermark, G. T., and Betsholtz, C. Islet Amyloid Polypeptide Pinpointing Amino Acid Residues Linked to Amyloid Fibril Formation, *PNAS*, **1990**, *87*,5036-5040.

119. Potter, K. J., Abedini, A., Marek, P., Klimek, A. M., Butterworth, S., Driscoll, M., Baker, R., Nilsson, M. R., Warnock, G. L., Oberholzer, J., Bertera, S., Trucco, M., Korbutt, G. S., Fraser, P. E., Raleigh, D. P., and Verchere, C. B. Islet Amyloid Deposition Limits the Viability of Human Islet Grafts But Not Porcine Islet Grafts, *PNAS*, **2010**, *107*,4305-4310.

120. Obrien, T. D., Hellman, U., Westermark, P., Wernstedt, C., Rathbun, W. B., and Johnson, K. H. Pancreatic-Islet Amyloid in the Degu Is Derived from Insulin, *Amyloid and Amyloidosis 1990*, **1991**,462-465.

121. Moriarty, D. F., and Raleigh, D. P. Effects of Sequential Proline Substitutions on Amyloid Formation by Human Amylin 20-29, *Biochemistry*, **1999**, *38*,1811-1818.

122. Abedini, A., and Raleigh, D. P. Destabilization of Human IAPP Amyloid Fibrils By Proline Mutations Outside of The Putative Amyloidogenic Domain: Is There A Critical Amyloidogenic Domain in Human IAPP?, *J. Mol. Biol.*, **2006**, *355*,274-281.

123. Koo, B. W., Hebda, J. A., and Miranker, A. D. Amide Inequivalence in The Fibrillar Assembly of Islet Amyloid Polypeptide, *Protein Eng., Des. Sel.*, **2008**, *21*,147-154.

124. Nguyen, T. M., Wright, J. R., Jr., Nielsen, P. F., and Conlon, J. M. Characterization of the Pancreatic Hormones From The Brockmann Body of The Tilapia: Implications for Islet Xenograft Studies, *Comp. Biochem. Physiol. C: Pharmacol. Toxicol.*, **1995**, *111*,33-44.

125. Yang, H., Dickson, B. C., O'Hali, W., Kearns, H., and Wright, J. R., Jr. Functional Comparison of Mouse, Rat, and Fish Islet Grafts Transplanted Into Diabetic Nude Mice, *Gen. Comp. Endocrinol.*, **1997**, *106*,384-388.

126. Martinez-Alvarez, R. M., Volkoff, H., Cueto, J. A. M., and Delgado, M. J. Molecular Characterization of Calcitonin Gene-Related Peptide (CGRP) Related Peptides (CGRP, Amylin, Adrenomedullin And Adrenomedullin-2/Intermedin) in Goldfish (Carassius auratus): Cloning And Distribution, *Peptides*, **2008**, *29*,1534-1543.

127. Green, J., Goldsbury, C., Min, T., Sunderji, S., Frey, P., Kistler, J., Cooper, G., and Aebi, U. Full-Length Rat Amylin Forms Fibrils Following Substitution of Single Residues From Human Amylin, *J. Mol. Biol.*, **2003**, *326*,1147-1156.

128. Jha, S., Snell, J. M., Sheftic, S. R., Patil, S. M., Daniels, S. B., Kolling, F. W., and Alexandrescu, A. T. pH Dependence of Amylin Fibrillization, *Biochemistry*, **2014**, *53*,300-310.

129. Charge, S. B. P., De Koning, E. J. P., and Clark, A. Effect of pH and Insulin on Fibrillogenesis of Islet Amyloid Polypeptide In Vitro, *Biochemistry*, **1995**, *34*,14588-14593.

130. Abedini, A., and Raleigh, D. P. The Role of His-18 in Amyloid Formation By Human Islet Amyloid Polypeptide, *Biochemistry*, **2005**, *44*,16284-16291.

Chapter 2. The Role of Transient Helical Intermediates in Amyloid Formation by Islet Amyloid Polypeptide

Abstract

Islet amyloid polypeptide (IAPP, amylin) assembles from a random structure to the β-sheet amyloid fibril structure. It has been hypothesized that IAPP forms helical intermediates prior to folding into β-sheets. These helical intermediates have been proposed to be critical for IAPP amyloid formation. Molecular simulations suggest that the residues 15-17 in particular are important for the stability of the helical intermediate and structural studies of maltose binding protein (MBP) fused with h-IAPP suggest that the helical structure in this region can promote dimerization. A set of single residue substitutions at position-17 were synthesized to determine the role of helical intermediates in amyloid formation. Substitution of valine with 2-aminobutyric acid (Abu) and norvaline (Nva) showed a modest increase in the rate of aggregation. V17I had a similar rate of aggregation while alanine and tert-leucine (Tle) substitutions greatly increased the rate of aggregation. Tle is known to have a very high β-sheet propensity, but a very low α-helical propensity. There was a mild correlation between helical propensity and rate of aggregation. However, the kinetics were found to be sensitive to experimental conditions. The variants were capable of seeding amyloid formation by wild-type IAPP and CD spectroscopy revealed strong β-sheet character of the V17Abu and V17Nva variants.

2.1 Introduction

Islet amyloid polypeptide (h-IAPP) assembles from a random structure to the β-sheet amyloid structure. However, it has been theorized that IAPP forms helical intermediates prior to folding into β-sheets [1-4]. These helices are believed to form helix-helix interactions which in turn allow the association of the amyloidogenic core region of IAPP inducing the formation of fibrils. Many techniques have been used to stabilize this transient putative intermediate in order to gain structural and mechanistic information on amyloid formation by IAPP. Rat IAPP (r-IAPP) has been used as a model because it does not form fibrils but it samples many of the same intermediates as human IAPP [2, 5, 6] Model membranes have also been used as a means of stabilizing the helical intermediate and preventing aggregation [7-9]. When analyzed by NMR spectroscopy, both methods of stabilization showed low levels of helical structure from residues 5-20 but more helical structure was evident when bound to membranes [3, 10]. These results show h-IAPP adopts a helix from residues 5-17 and 20-27 on the surface of the model membranes. Studies have also been performed on fragments of both h-IAPP and r-IAPP. In the presence of detergent micelles, both h-$IAPP_{1-19}$ and r-$IAPP_{1-19}$ adopted persistent helical structures but adopted a different orientation when bound to membranes [9]. However, the problem with all of these techniques is that these experimental conditions may not accurately reflect IAPP behavior *in vivo.*

Inhibition studies lend credence to the helical model. r-IAPP, which contains six prolines in its sequence, and proline variants of h-IAPP can perhaps prevent aggregation by disrupting formation of the helical intermediate [11-13]. Small molecule inhibitors can also bind to the α-helix and disrupt helix-helix interactions preventing amyloid formation [14, 15]. However, these studies merely provide indirect information on the mechanism of inhibition of IAPP. These

inhibitors may be binding to the β-sheets of the amyloidogenic core region of the peptide and not to the proposed helical region. Alternative non-helical models for oligomers have also been proposed. Ion mobility mass spectroscopy experiments and MD simulations proposed oligomers that adopted a β-hairpin dimer [16, 17].

Crystal structures of the maltose binding protein (MBP) fused with h-IAPP suggest that helices can promote dimerization with key contacts being made in the 15-17 region of the peptide indicating these residues' potential importance in forming these intermediates [1]. Substitution of Leu-16 with glutamine, a residue that stabilizes α-helices, promoted greater stability to the helical intermediate [18]. Previous results revealed that substitutions of Phe-15 showed a correlation between α-helical propensity and the rate of amyloid formation [19]. Additionally, studies have been performed on position-17 with a truncated version of h-IAPP that is lacking the first seven residues [1]. This model lacks the disulfide bond contained in the N-terminal segment of IAPP. The truncated peptide has proven to be capable of forming amyloid fibrils but its behavior may not be representative of full length IAPP. There is little information about the effect of helical propensity at position-17 on amyloid formation of the full length peptide. Herein, we describe that increasing α-helical propensity at position-17 increases the rate of amyloid formation while increasing the β-sheet propensity at that position drastically decreases the rate of amyloid formation. Additionally, we show that structure of amyloid fibrils formed from each of the variants is similar enough to allow cross-seeding of amyloid formation by h-IAPP and that the fibrils are rich in β-sheet structure. Finally, we examine the implications of using organic solvents to accelerate amyloid formation.

2.2 Materials and Methods

2.2.1 Peptide Synthesis and Purification.

Peptides were synthesized with a CEM microwave peptide synthesizer on a 0.10 mmol scale utilizing 9-fluorenylmethoxycarbonyl (Fmoc) chemistry. 5-(4'-Fmoc-aminomethyl-3',5-dimethoxyphenol) valeric acid (PAL-PEG) resin was used to provide an amidated C-terminus. Fmoc-protected pseudoproline (oxazolidine) dipeptide derivatives were utilized as previously described [20, 21]. Solvents used were ACS-grade. β-branched residues, the first residue attached to the resin, pseudoproline dipeptide derivatives and the residues following the pseudoproline dipeptide derivatives were double-coupled. Peptides were cleaved from the resin via standard trifluoroacetic acid (TFA) methods. The cleaved crude peptides were dissolved into 20% (v/v) acetic acid and lyophilized. The disulfide bond was formed in 100% dimethyl sulfoxide at room temperature for three days. Peptides were purified via reverse-phase high-performance liquid chromatography (RP-HPLC) using a Higgins Analytical Proto 300 C18 preparative column (10 mm x 250 mm). A 20 – 70% buffer B gradient was used over 50 minutes where buffer A was 100 H_2O, 0.045 % HCl and buffer B was 80 % acetonitrile, 0.045 % HCl. The retention times of h-IAPP, V17Abu, V17Nva, V17A, V17I, and V17Tle were 32 minutes (52 % B), 32 minutes (52 % B), 33 minutes (53 % B), 19 minutes (39 % B), 34 minutes (54 % B), and 31 minutes (51 % B) respectively. The purity of the peptides was tested using analytical HPLC. The masses of the pure peptides were confirmed with MALDI time-of-flight mass spectrometry. h-IAPP, expected 3903.6, observed 3903.6; V17Abu, expected 3889.6, observed, 3889.9; V17Nva, expected 3903.6, observed, 3904.6; V17A, expected 3875.2, observed 3875.2; V17I expected 3917.3, observed 3918.0; V17Tle, expected 3917.3, observed 3918.0.

2.2.2 Sample Preparation and Fluorescence Assays.

Stock solutions were prepared by dissolving peptide into 100% hexafluoroisopropanol (HFIP) at 1.6 mM. Solutions were filtered with 0.45 μM Acrodisc syringe filters and stored at 4 °C. For experiments with HFIP, the stock solution was diluted into 20 mM tris buffer pH 7.4 containing thioflavin-T and additional HFIP. The final solution concentrations were 20 mM tris buffer pH 7.4, 16 μM peptide, 32 μM thioflavin-T, and 2% HFIP. For experiments without HFIP, the required amount of peptide stock was lyophilized overnight to remove HFIP. Dry peptide was then resuspended into tris buffer and thioflavin-T. The final solution concentrations were 20 mM tris buffer pH 7.4, 16 μM peptide and 32 μM thioflavin-T. For seeding experiments, samples were prepared similar to those for kinetic experiments as described previously. They were stirred for 120 minutes and then used to seed other solutions. These solutions were used within 8 hours to ensure reproducibility of seeding experiments. Seeds were added to the tris buffer, peptide, and thioflavin-T solution at a concentration of 1.6 μM corresponding to 10 % of the concentration of monomer peptide. Seed concentrations are given in monomer units.

The kinetics of amyloid formation were monitored using thioflavin-T binding assays conducted at 25 °C. Fluorescence measurements were performed using a Beckman Coulter DTX 880 plate reader with a multimode detector using an excitation wavelength of 430 nm and an emission wavelength of 485 nm.

2.2.3 Transmission Electron Microscopy.

TEM images were collected at the Life Science Microscopy Center at the State University of New York at Stony Brook. At the end of each experiment, 15 μL aliquots of the samples used for the kinetic studies were removed, blotted on a carbon-coated 300-mesh copper grid for 1 min and then negatively stained with saturated uranyl acetate for 1 min.

2.2.4 Circular Dichroism

Far UV CD experiments were performed on an Applied Photophysics Chirascan CD spectrophotometer. Samples were used at the end of a kinetic run. The spectrum was an average of three repeats recorded over a range of 190 – 260 nm, at 1 nm intervals. A 10 mm quartz cuvette was used and a background spectrum was subtracted from the collected data. Experiments were performed at 25 °C in 20 mM tris buffer at pH 7.4.

2.3 Results and Discussion

2.3.1 Helical Propensity at Position-17 Affects the Rate of Aggregation

In order to determine whether increasing the helical propensity at position-17 affected the rate of amyloid formation by IAPP, five different variants were synthesized three of which had the valine substituted by unnatural amino acids (Figure 2-1). 2-aminobutyric acid (Abu) and nor-Valine (Nva) both contain less sterically bulky sidechains than valine while maintaining only slightly changing hydrophobicity. Nva is a straight chain analogue of valine and is predicted to be more favorable in α-helices than valine. Abu is structurally similar to Nva with one less carbon on its side chain. A V17I replacement was also investigated. Isoleucine has a similar helical propensity as valine, and slightly larger hydrophobicity. An alanine replacement was also synthesized as it has the highest helical propensity though its hydrophobicity is also less than valine. Lastly, a tert-leucine (Tle) replacement was examined. The tert-leucine sidechain is extremely bulky. Due to the large size of the Tle sidechain, it is very unfavorable for the residue to lie in an α-helix without steric interactions from nearby residues and as a result, its conformation is restricted to β-sheets. A comparison of the characteristics of each of the sidechains is shown in Table 2-2. With these substitutions, a full spectrum of residues at

position-17 with high to low helical propensity can be examined. We compared the time course of amyloid formation of each of the variants using thioflavin-T fluorescence assays and transmission electron microscopy (TEM). We conducted experiments both in the presence and absence of 2 % hexafluoroisopropanol (HFIP) in 20 mM tris at pH 7.4 chosen because this buffer has been used extensively in studies of amyloid formation by IAPP. HFIP was used because it greatly accelerates amyloid formation by IAPP [22, 23]. The concentration of the peptide used was 16 μM, again chosen because it is typical of values used for biophysical studies with the polypeptide. A 2-fold excess of thioflavin-T relative to monomer concentration of h-IAPP was used for a final concentration of 32 μM. In the presence of each of the variants with HFIP used as an accelerant, a sigmoidal thioflavin-T fluorescence time course, consisting of a lag phase, an elongation phase, and a final plateau was observed which is indicative of amyloid fibril formation (Figure 2-2A). The t_{50} of each of the variants was ascertained and compared to wild-type h-IAPP (Table 2-1). The t_{50} is defined as the time required for each variant to reach half the maximum fluorescence.

The V17Nva variant had the shortest lag time in the presence of HFIP with a rate of aggregation that was nearly half that of h-IAPP. The t_{50} for V17Nva was found to be 755 ± 12 s. The V17Abu also formed amyloid faster than h-IAPP though slower than the V17Nva substitution. The V17I variant formed amyloid at a similar rate as h-IAPP. This is unsurprising since both valine and isoleucine are β-branched residues with a similar helical propensity. V17Tle was found to form amyloid much slower than the variants with a greater helical propensity residue at position-17 with a t_{50} that was 15-fold greater than h-IAPP (Figure 2-2B). Surprisingly, the V17A variant formed amyloid the slowest of all the variants with a t_{50} that was 22-fold greater than h-IAPP. This is surprising due to alanine having the highest helical

propensity of all the substitutions examined. Aliquots were removed at the end of each kinetic experiment and transmission electron microscopy (TEM) images were recorded (Figure 2-2C). Dense mats of fibrils were observed in the images of all of the peptides and each exhibited the typical morphology associated with *in vitro* h-IAPP amyloid fibrils.

2.3.2 Val-17 Substitutions are Sensitive to Experimental Conditions

Experiments were also performed at pH 7.4 in the absence of HFIP. Under these conditions, wild-type h-IAPP has a t_{50} of 25.3 ± 0.47 hours. The experiments without HFIP showed a slightly different relationship than experiments in the presence of the alcohol. V17Abu under these conditions formed amyloid the fastest of all with almost no lag phase (Figure 2-3A). It also exhibited a much lower thioflavin-T response (Figure 2-3B). V17Nva was found to form amyloid slower than V17Abu but faster than h-IAPP with a t_{50} of 18.3 ± 1.7 hrs. V17I variant had a t_{50} of 31.3 ± 2.9 hrs and ultimately performed the most consistently in both experimental conditions (Table 2-1). V17A and V17Tle were monitored for 1 week and did not form amyloid in that time period. TEM images were recorded at the end of each experiment. Dense mats of fibrils were again observed in the images of the peptides.

2.3.3 V17Abu Shows Low Fluorescence But Strong β-Sheet Character

V17Abu exhibited significantly less fluorescence than wild-type and V17Nva (Figure 2-4). In order to determine whether this was from a lack of fibrils for the thioflavin-T to bind to, we turned to circular dichroism (CD) to probe the secondary structure of wild-type h-IAPP, V17Abu, and V17Nva fibrils (Figure 2-5). Samples of each of the peptides were prepared at the end of a kinetic run and the CD spectrum was recorded. The three peptides displayed a strong minimum near 218 nm, consistent with β-sheet structure and the shape of the spectrum is very

similar to that reported for the h-IAPP amyloid fibrils. The CD and TEM images indicate that all the peptides formed amyloid fibrils. Differences in intensity at 218 nm are likely due to differences in concentration of the amyloid fibrils. We can conclude that V17Abu is forming fibrils and the low signal is not due to the dye binding to non-amyloid aggregates.

2.3.4 Val-17 Substitutions Produce Fibrils Similar in Structure to h-IAPP Amyloid Fibrils

Amyloid fibril formation can be seeded by addition of preformed amyloid fibrils or "seeds". These seeds when added to monomer solution can bypass the lag phase. Seeding is usually specific and can only catalyze amyloid fibril formation when the mechanisms of amyloid formation between monomer peptide and seeds are the same or if the fibril structure allows for templating off of the ends of the preformed fibril tips [24, 25]. Thus, seeding experiments are a convenient and easy way to deduce structural similarity between fibrils. As a control, in the presence of HFIP, wild-type h-IAPP when added to h-IAPP fibrils was able to seed itself and a complete elimination of the lag phase was observed (Figure 2-6A). We then tested the ability of each of the variants to seed h-IAPP amyloid fibril formation with the addition of preformed fibrils. When added as seeds to wild-type h-IAPP in the presence of HFIP, each of the Val-17 variants was able to catalyze amyloid fibril formation by h-IAPP and bypass the lag phase (Figure 2-6A). The resulting fibrils had a similar morphology to that of wild-type h-IAPP fibrils as judged by TEM (Figure 2-6B). Thus, the structures of the fibrils of each of the Val-17 fibrils examined were similar enough to allow seeding of h-IAPP.

Seeding experiments were also performed in the absence of HFIP (Figure 2-7A). A shortening of the lag phase is observed for each of the variants tested though the efficiencies varied. h-IAPP seeded by itself was able to form amyloid faster than when the peptide was

seeded by preformed V17Abu fibrils, and V17Nva fibrils. The V17I h-IAPP variant was less efficient at seeding h-IAPP in the absence of HFIP. The resulting lag phase was reduced by a factor of about ten relative to wild-type h-IAPP by itself. The fibrils produced from each of the seeding experiments produced fibrils sharing a similar morphology to h-IAPP amyloid fibrils (Figure 2-7B).

2.4 Conclusions

The data presented here showed a mild correlation with helical propensity at position-17 and the rate of amyloid formation. This adds to the mounting evidence that IAPP first forms helical intermediates before β-sheets and suggests that Val-17 is in the putative helical region of IAPP. These results are in agreement with previous work examining substitutions on Leu-15. Valine has a relatively low helical propensity. The valine at position-17 is highly conserved across species in both amyloidogenic and non-amyloidogenic variants of IAPP (Figure 1-9). The variants studied were also sensitive to experimental conditions though in both conditions, there was a mild correlation between helical propensity and the rate of amyloid fibril formation. The presence of organic solvent and stirring changed the behavior of these variants. The introduction of shear forces could be inducing aggregation in a way that is different than without stirring. HFIP accelerates amyloid formation and this organic solvent could be changing the electrostatic and hydrophobic interactions of these mutants as well as enhancing helical formation. HFIP has commonly been employed as an accelerant of amyloid fibril formation. The results here reveal the perils of relying on organic solvents to induce amyloid formation.

It is surprising that the V17A replacement formed amyloid much slower than h-IAPP though it has the highest helical propensity of the variants studied here. This observation is especially interesting because thioflavin-T fluorescence assays with a truncated version of the variant, V17A $IAPP_{8-37}$, showed it was able to form amyloid faster than $IAPP_{8-37}$ [1]. Generally, the truncated version of h-IAPP is able to form amyloid faster than the full length peptide indicating that the disulfide bond between Cys-2 and Cys-7 play a role in amyloid formation. This region may also have a role in stabilizing V17A by forming contacts that delay amyloid formation. Ala is also significantly smaller than Val and so it may not be able to make the contacts necessary to form the initial helix nor be able to form helix-helix interactions as effectively as a larger residue. The role of the disulfide bond will be discussed in more detail in Chapter 6.

V17Abu displayed low fluorescence during kinetic studies. It was investigated whether this could be caused by lack of β-sheet fibril formation. CD spectroscopy revealed that this was not the case. Another possibility is that during the lag phase there is lack of seeds forming. Thioflavin-T fluorescence assays are not quantitative and it is thus impossible to determine fibril concentration from them alone. There can be a correlation between thioflavin-T signal and fibril concentration, but other factors can influence the final intensities.

The Val-17 variants were all able to seed wild-type h-IAPP with varying efficiencies. The fibrils formed by these variants had a similar enough structure and to result in a near elimination of the lag phase of h-IAPP. It is possible that the fibril concentration of V17I was less than that of V17Abu, V17Nva, and h-IAPP fibrils. Though the monomer concentration is known at the beginning of each experiment, the final concentration of fibrils is not known. Differences in fibril concentration between samples can lead to fewer surfaces for h-IAPP to use for nucleation and a

lengthening of the lag phase. It is also possible that the structure of V17I fibrils is different in the absence of HFIP than in the presence of the organic solvent. This can also lead to a decreased seeding efficiency.

The mechanism of IAPP amyloid formation is not known, and the oligomers formed prior to fibril formation have not been fully characterized. Pre-amyloid IAPP oligomers have recently been found to be more toxic to β-cells than mature fibrils [26]. Thus, it is becoming more critical to elucidate the structure of these oligomers. Fully characterizing the helical region will allow the rational design of novel drugs in order to inhibit amyloid fibril formation and to treat β-cell death.

2.5 Figures

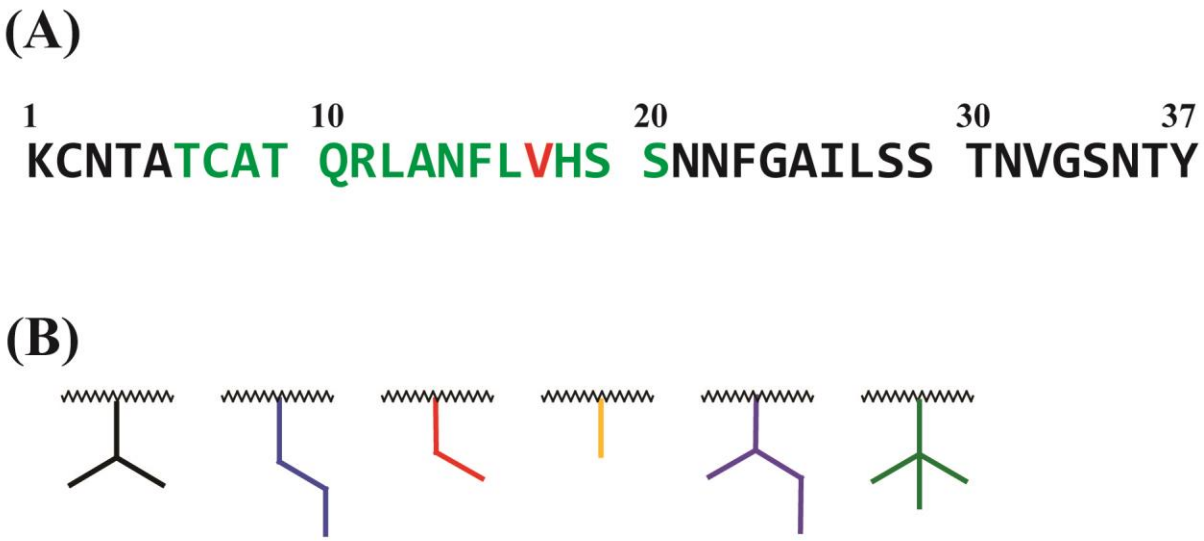

Figure 2-1: (A) Sequence of h-IAPP. Residues predicted to reside in the helical region are denoted in green. Val-17, the peptide of interest is highlighted in red. (B) Substitutions made at position-17. The residues used vary α-helical and β-sheet propensity while maintaining hydrophobicity. The residues used from left to right were Val for wild-type h-IAPP (black), Nva (blue), Abu (red), Ala (yellow), Ile (purple), and Tle (green).

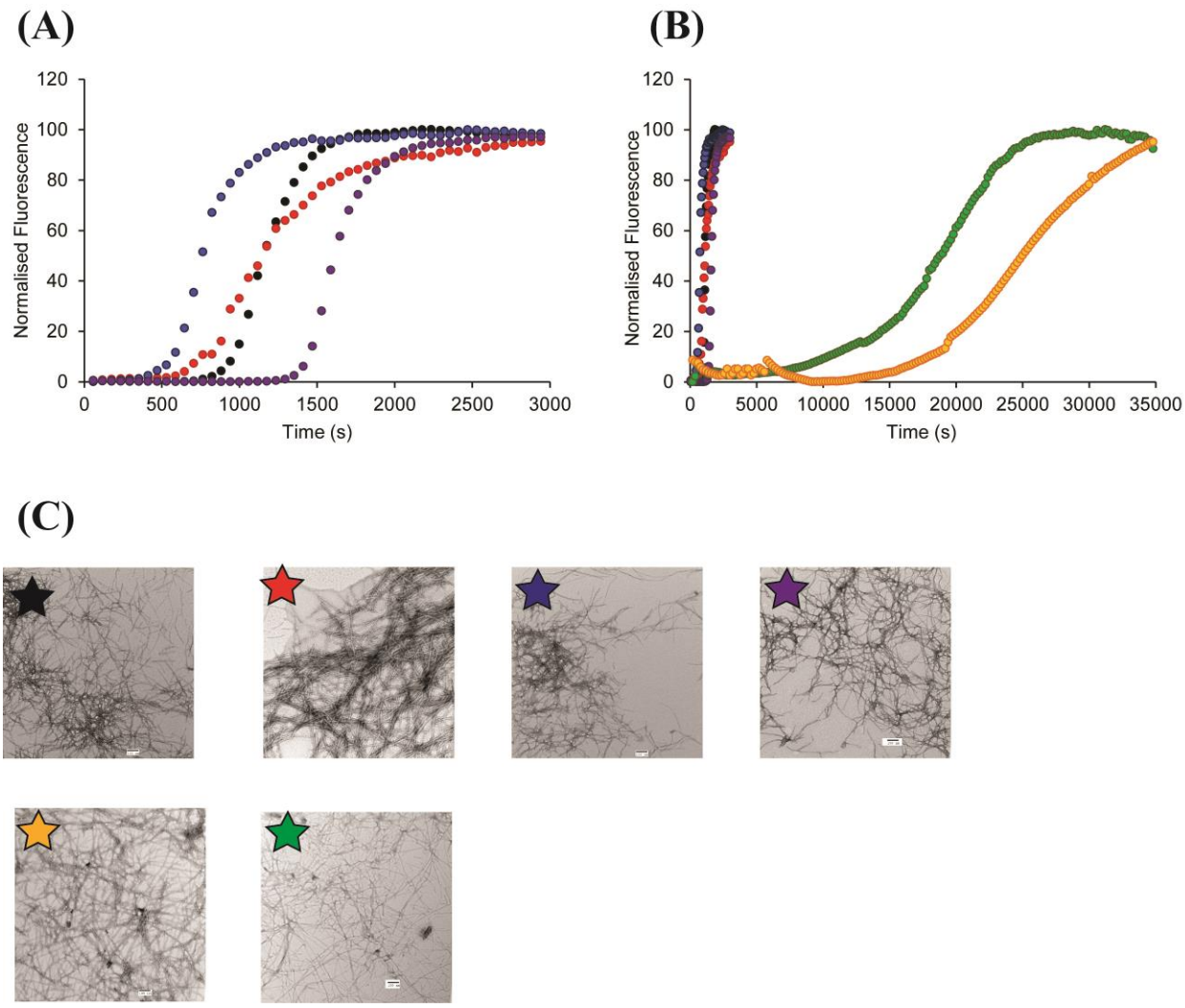

Figure 2-2: Analysis of amyloid formation of h-IAPP and Val-17 variants in the presence of 2 % HFIP and stirring. (A) Thioflavin-T fluorescence assays of h-IAPP (black), V17Abu (red), V17Nva (blue), and V17I (purple). (B) Thioflavin-T fluorescence assays of h-IAPP (black), V17Abu (red), V17Nva (blue), V17I (purple), V17A (yellow), and V17Tle (green). (C) TEM images of h-IAPP (black), V17Abu (red), V17Nva (blue), V17A (yellow), V17I (purple), and V17Tle (green) Aliquots were removed at the end of each kinetic experiment.

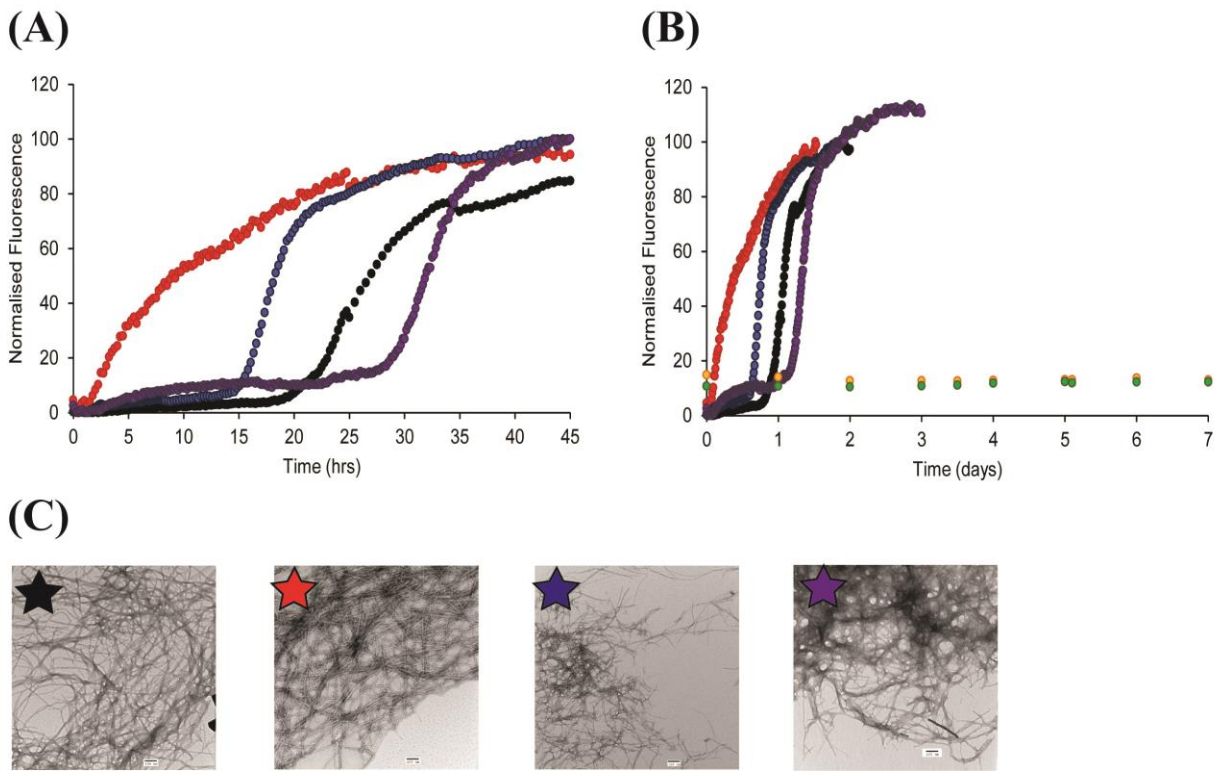

Figure 2-3: Fluorescence monitored thioflavin-T assays of amyloid formation with no HFIP and no stirring. (A) Analysis of h-IAPP (black), V17Abu (red), V17Nva (blue), and V17I (purple) (B) Analysis of h-IAPP (black), V17Abu (red), V17Nva (blue), V17I (purple), V17A (yellow) and V17Tle (green)substitutions. (C)TEM images of samples of h-IAPP (black), V17Abu (red), V17Nva (blue), and V17I (purple). Aliquots were taken at after 48 hours. Experiments were conducted with 16 µM IAPP.

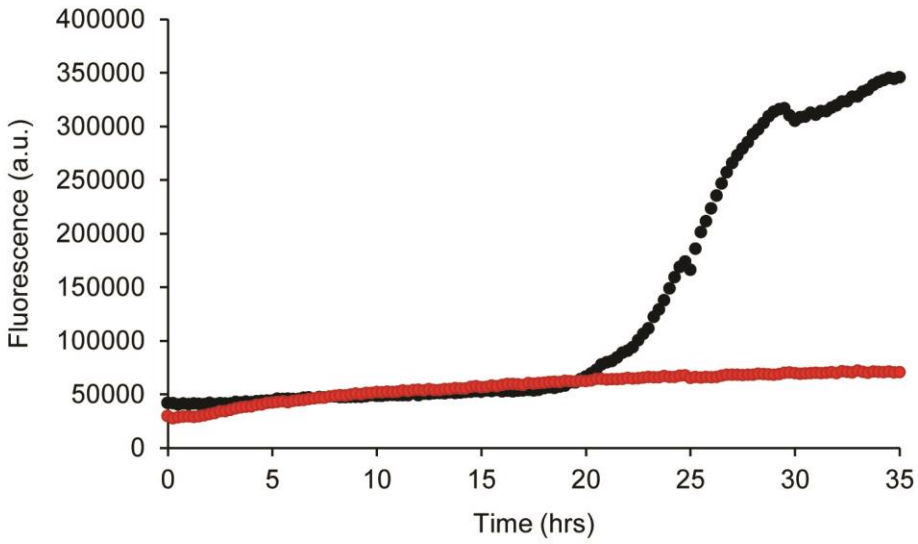

Figure 2-4: V17Abu h-IAPP exhibits low fluorescence. Fluorescence monitored thioflavin-T assays of amyloid formation of h-IAPP (black) and V17Abu h-IAPP (red). The time course shown here is a non-normalized version of Figure 2-3A.

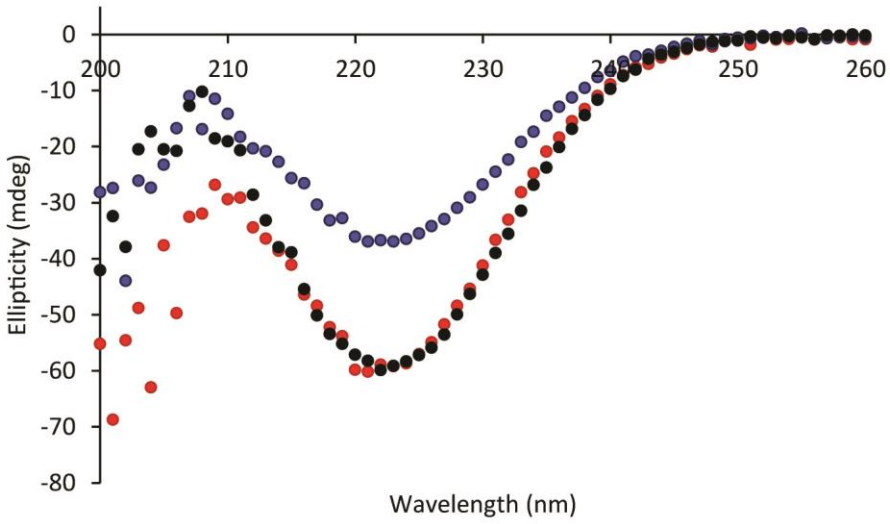

Figure 2-5: h-IAPP, V17Abu, and V17Nva form fibrils with significant β-sheet character. CD wavelength scans of h-IAPP (black), V17Abu (red), and V17Nva (blue) taken at the end of a kinetic experiment.

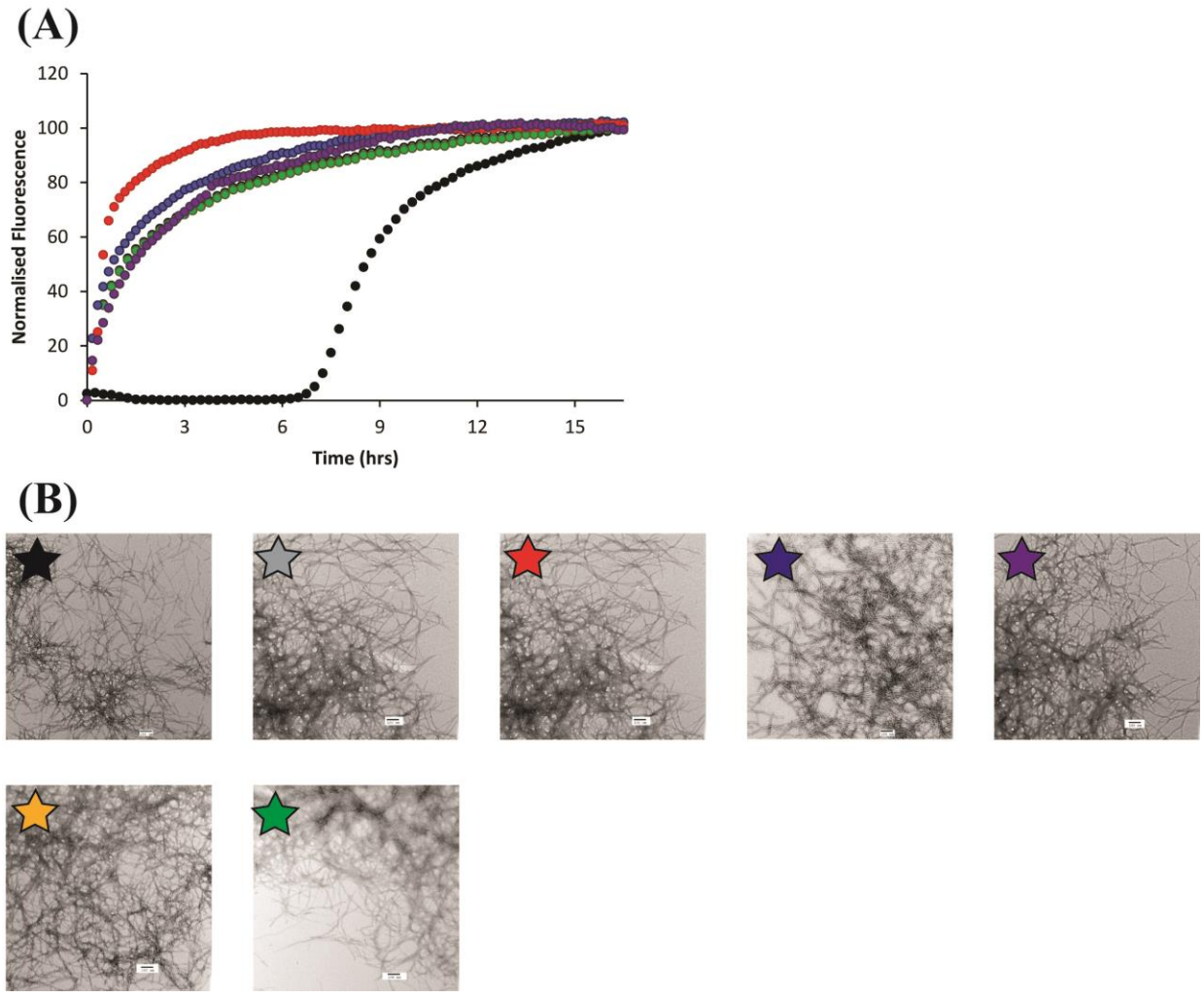

Figure 2-6: Seeding curves of h-IAPP. (A) The lag phase of amyloid formation by h-IAPP (black) can be bypassed by the addition of preformed fibrils corresponding to h-IAPP (grey), V17Abu (red), V17Nva (blue), V17A (yellow), V17I (purple) and V17Tle (green). Experiments were conducted at 14.4 µM peptide, 1.6 µM preformed fibrils, 32 µM thioflavin-T, 2 % HFIP, and 20 mM tris buffer at pH 7.4 25 °C. (B) TEM images of samples of h-IAPP by itself (black), h-IAPP seeded with h-IAPP (grey), V17Abu (red), V17Nva (blue), V17I (purple), V17A (yellow), and V17Tle (green). Aliquots were taken at after 24 hours. Experiments were conducted with 16 µM IAPP.

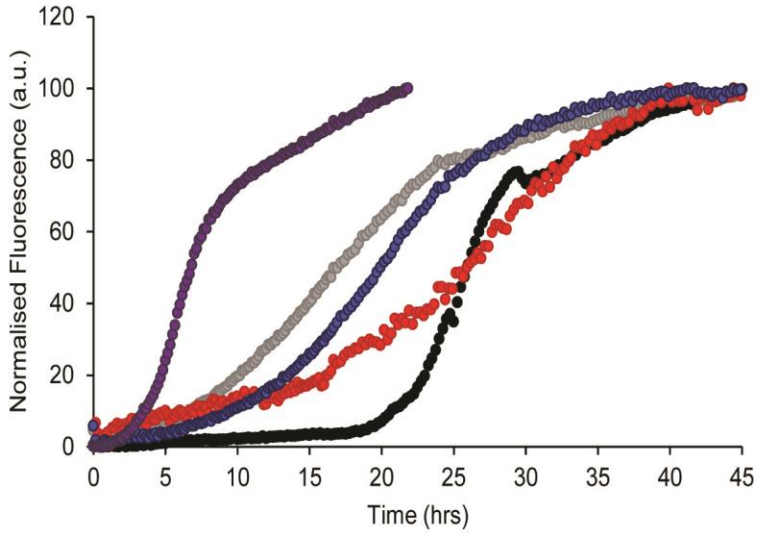

Figure 2-7: Seeding curves of h-IAPP. (A) The lag phase of amyloid formation by h-IAPP (black) can be bypassed by the addition of preformed fibrils corresponding to h-IAPP (grey), V17Abu (red), V17Nva (blue), and V17I (purple) Experiments were conducted at 14.4 µM peptide, 1.6 µM preformed fibrils, 32 µM thioflavin-T and 20 mM tris buffer at pH 7.4 25 °C.

2-6 Tables

	With HFIP and Stirring t_{50} (s)	No HFIP and No Stirring t_{50} (hrs)
h-IAPP	1159 ± 91	25.3 ± 0.47
V17Abu	1080 ± 164	3.03 ± 0.77
V17Nva	755 ± 12	18.3 ± 1.7
V17I	1567 ± 49	31.3 ± 2.9
V17A	25217	N/A
V17Tle	17467 ± 1354	N/A

Table 2-1: A comparison of the t_{50} of wild-type h-IAPP and Val-17 substitutions in both experimental conditions. The presence of stirring and HFIP greatly accelerates aggregation.

	Helical Propensity	β-Sheet Propensity	Π
Valine	-0.27	0.13	1.22
2-aminobutyric acid	-0.70	< Valine	0.82
Norvaline	-0.76	< Valine	1.37
Isoleucine	-0.32	0.10	1.8
Alanine	-0.74	0.47	.31
Tert-Leucine	0.22	> Valine	1.51

Table 2-2: A comparison of the helical propensity, β-sheet propensity and hydrophobicity (Π) of each of the residues substituted at position-17. Helical propensity values were derived from free energy for helix formation related to glycine [27]. More negative values correspond to higher helix stabilization while greater values correspond to less helix stabilitzation. β-sheet propensiy values were derived from [28]. Values were normalized from 0 to 1 with 0 corresponding to a high β-sheet propensity and 1 with a low β-sheet propensity. Π values were derived from [29]. Values are normalized with respect to glycine which has a value of 0.

2-7 References

1. Wiltzius, J. J. W., Sievers, S. A., Sawaya, M. R., and Eisenberg, D. Atomic Structures of IAPP (amylin) Fusions Suggest a Mechanism for Fibrillation and the Role of Insulin in the Process, *Protein Sci.*, **2009**, *18*,1521-1530.

2. Williamson, J. A., and Miranker, A. D. Direct Detection of Transient Alpha-Helical States in Islet Amyloid Polypeptide, *Protein Sci.*, **2007**, *16*,110-117.

3. Williamson, J. A., Loria, J. P., and Miranker, A. D. Helix Stabilization Precedes Aqueous And Bilayer-Catalyzed Fiber Formation in Islet Amyloid Polypeptide, *J. Mol. Biol.*, **2009**, *393*,383-396.

4. Abedini, A., and Raleigh, D. P. A Role for Helical Intermediates in Amyloid Formation by Natively Unfolded Polypeptides?, *Phys. Biol.*, **2009**, *6*,015005.

5. Westermark, P., Engstrom, U., Johnson, K. H., Westermark, G. T., and Betsholtz, C. Islet Amyloid Polypeptide Pinpointing Amino Acid Residues Linked to Amyloid Fibril Formation, *PNAS*, **1990**, *87*,5036-5040.

6. Romero, D., Aguilar, C., Losick, R., and Kolter, R. Amyloid Fibers Provide Structural Integrity to Bacillus subtilis Biofilms, *PNAS*, **2010**, *107*,2230-2234.

7. Knight, J. D., Hebda, J. A., and Miranker, A. D. Conserved and Cooperative Assembly of Membrane-Bound Alpha-Helical States of Islet Amyloid Polypeptide, *Biochemistry*, **2006**, *45*,9496-9508.

8. Nanga, R. P., Brender, J. R., Xu, J., Hartman, K., Subramanian, V., and Ramamoorthy, A. Three-Dimensional Structure and Orientation of Rat Islet Amyloid Polypeptide Protein in a Membrane Environment by Solution NMR Spectroscopy, *J. Am. Chem. Soc.*, **2009**, *131*,8252-8261.

9. Nanga, R. P., Brender, J. R., Xu, J., Veglia, G., and Ramamoorthy, A. Structures of Rat and Human Islet Amyloid Polypeptide IAPP(1-19) in Micelles by NMR Spectroscopy, *Biochemistry*, **2008**, *47*,12689-12697.

10. Nanga, R. P., Brender, J. R., Vivekanandan, S., and Ramamoorthy, A. Structure and Membrane Orientation of IAPP in Its Natively Amidated Form at Physiological pH in a Membrane Environment, *Biochim. Biophys. Acta*, **2011**, *1808*,2337-2342.

11. Cao, P., Meng, F., Abedini, A., and Raleigh, D. P. The Ability of Rodent Islet Amyloid Polypeptide to Inhibit Amyloid Formation by Human Islet Amyloid Polypeptide Has Important Implications for the Mechanism of Amyloid Formation and the Design of Inhibitors, *Biochemistry*, **2010**, *49*,872-881.

12. Abedini, A., Meng, F., and Raleigh, D. P. A Single-Point mutation Converts the Highly Amyloidogenic Human Islet Amyloid Polypeptide into a Potent Fibrillization Inhibitor, *J. Am. Chem. Soc.*, **2007**, *129*,11300-11301.

13. Meng, F., Raleigh, D. P., and Abedini, A. Combination of Kinetically Selected Inhibitors in trans Leads to Highly Effective Inhibition of Amyloid Formation, *J. Am. Chem. Soc.*, **2010**, *132*,14340-14342.

14. Sparks, S., Liu, G., Robbins, K. J., and Lazo, N. D. Curcumin Modulates the Self-Assembly of the Islet Amyloid Polypeptide by Disassembling Alpha-Helix, *Biochem. Biophys. Res. Commun.*, **2012**, *422*,551-555.

15. Hebda, J. A., Saraogi, I., Magzoub, M., Hamilton, A. D., and Miranker, A. D. A Peptidomimetic Approach to Targeting Pre-Amyloidogenic States in Type II Diabetes, *Chem. Biol.*, **2009**, *16*,943-950.

16. Dupuis, N. F., Wu, C., Shea, J. E., and Bowers, M. T. Human Islet Amyloid Polypeptide Monomers Form Ordered Beta-Hairpins: A Possible Direct Amyloidogenic Precursor, *J. Am. Chem. Soc.*, **2009**, *131*,18283-18292.

17. Dupuis, N. F., Wu, C., Shea, J. E., and Bowers, M. T. The Amyloid Formation Mechanism in Human IAPP: Dimers Have Beta-Strand Monomer-Monomer Interfaces, *J. Am. Chem. Soc.*, **2011**, *133*,7240-7243.

18. Wang, M., Yang, J. P., Wang, J. Y., and Wang, X. J. Structural Effects of L16Q, S20G, and L16Q-S20G Mutations on hIAPP: A Comparative Molecular Dynamics Study, *Chin. J. Chem* . **2012**, *30*,241-248.

19. Tu, L.-H., and Raleigh, D. P. Role of Aromatic Interactions in Amyloid Formation by Islet Amyloid Polypeptide, *Biochemistry*, **2013**, *52*,333-342.

20. Marek, P., Woys, A. M., Sutton, K., Zanni, M. T., and Raleigh, D. P. Efficient Microwave Assisted Synthesis of Human Islet Amyloid Polypeptide Designed to Facilitate The Specific Incorporation of Labeled Amino Acids, *Org. Lett.*, **2010**, *12*,4848-4851.

21. Abedini, A., and Raleigh, D. P. Incorporation of Pseudoproline Derivatives Allows the Facile Synthesis of Human IAPP, A Highly Amyloidogenic and Aggregation-Prone Polypeptide, *Org. Lett.*, **2005**, *7*,693-696.

22. Andersen, N. H., Dyer, R. B., Fesinmeyer, R. M., Gai, F., Liu, Z. H., Neidigh, J. W., and Tong, H. Effect of Hexafluoroisopropanol on the Thermodynamics of Peptide Secondary Structure Formation, *J. Am. Chem. Soc.*, **1999**, *121*,9879-9880.

23. Yanagi, K., Ashizaki, M., Yagi, H., Sakurai, K., Lee, Y. H., and Goto, Y. Hexafluoroisopropanol Induces Amyloid Fibrils of Islet Amyloid Polypeptide by Enhancing Both Hydrophobic and Electrostatic Interactions, *J. Biol. Chem.*, **2011**, *286*,23959-23966.

24. O'Nuallain, B., Williams, A. D., Westermark, P., and Wetzel, R. Seeding Specificity in Amyloid Growth Induced by Heterologous Fibrils, *J. Biol. Chem.*, **2004**, *279*,17490-17499.

25. Krebs, M. R., Morozova-Roche, L. A., Daniel, K., Robinson, C. V., and Dobson, C. M. Observation of Sequence Specificity in the Seeding of Protein Amyloid Fibrils, *Protein Sci.*, **2004**, *13*,1933-1938.

26. Abedini, A., Plesner, A., Cao, P., Ridgway, Z., Zhang, J., Tu, L. H., Middleton, C. T., Chao, B., Sartori, D. J., Meng, F., Wang, H., Wong, A. G., Zanni, M. T., Verchere, C. B., Raleigh, D. P., and Schmidt, A. M. Time-Resolved Studies Define the Nature of Toxic IAPP Intermediates, Providing Insight for Anti-Amyloidosis Therapeutics, *eLife*, **2016**, *5*.

27. Lyu, P. C., Sherman, J. C., Chen, A., and Kallenbach, N. R. Alpha-Helix Stabilization by Natural and Unnatural Amino Acids with Alkyl Side Chains, *PNAS*, **1991**, *88*,5317-5320.

28. Street, A. G., and Mayo, S. L. Intrinsic Beta-Sheet Propensities Result From Van der Waals Interactions Between Side Chains and the Local Backbone, *PNAS*, **1999**, *96*,9074-9076.

29. Fauchere, J. L., Charton, M., Kier, L. B., Verloop, A., and Pliska, V. Amino Acid Side Chain Parameters for Correlation Studies in Biology and Pharmacology, *Int. J. Pept. Protein Res.*, **1988**, *32*,269-278.

Chapter 3. Analysis of the Amyloidogenic Potential of Pufferfish (*Takifugu rubripes*) Islet Amyloid Polypeptide

Abstract

IAPP has been found in all higher organisms examined, but not all species form amyloid and the ability to do so correlates with the primary sequence. The amyloidogenic potential of fish IAPPs have not been examined, although fish have been proposed as a source for xenobiotic transplantation. The sequence of pufferfish IAPP (*Takifugu rubripes*) is known and is the most divergent from human IAPP of any reported IAPP sequence, differing at eleven positions including seven located within residues 20 to 29, a segment of the molecule that is important for controlling amyloidogenicity. Several of the substitutions found in pufferfish IAPP are non-conservative including Ser to Pro, Asn to Thr, Ala to Tyr and Leu to Tyr replacements and several of these have not been reported in mammalian IAPP sequences. Amyloid prediction programs give conflicting results for pufferfish IAPP. CD spectroscopy, FTIR, and transmission electron microscopy reveal that pufferfish IAPP forms amyloid and does so more rapidly than human IAPP in tris buffer at pH 7.4, but does so more slowly in phosphate buffered saline at pH 7.4. Molecular dynamics simulations indicate that the pufferfish sequence is compatible with models of IAPP amyloid. The fish polypeptide does not significantly bind to thioflavin-T in tris and does so only weakly in phosphate buffered saline. The results highlight difficulties with thioflavin-T assays and the ambiguity in defining amyloidogenicity.

NOTE: The material presented in this chapter has been published (Amy G. Wong, Chun Wu, Eleni Hannaberry, Matthew D. Watson, Joan-Emma Shea, and Daniel P. Raleigh "Analysis of the Amyloidogenic Potential of Pufferfish (*Takifugu rubripes*) Islet Amyloid Polypeptide Highlights the Limitations of Thioflavin-T Assays and the Difficulties in Defining Amyloidogenicity" *Biochemistry* **2016**, 55(3) 510-518). This chapter contains direct excerpts from the manuscript, which was written by me with suggestions and revisions from Professor Daniel P. Raleigh. The molecular dynamics simulations and modelling of pufferfish and human IAPP were performed by Dr, Chun Wu in the Joan-Emma Shea group in University of California and Santa Barbara.

3.1 Introduction

Mature IAPP has been found in all higher organisms examined and is highly conserved, but not all species form amyloid and the ability to do so correlates with the primary sequence of IAPP. Teleostean fish have been proposed as a source for xenobiotic transplantation and for studies of diabetes mellitus, in part because in teleostean fish the pancreatic exocrine tissue is separated from the pancreatic endocrine cells, facilitating the isolation of the endocrine cells [1-5]. However, the amyloidogenicity of fish IAPP is not well understood and this is an issue for islet transplantation [6, 7]. The amyloidogenic potential of any full-length fish IAPP has not been examined, although a ten residue fragment of salmon IAPP has been studied experimentally and larger fragments derived from different fish have been analyzed computationally [2, 3]. The complete sequence of pufferfish IAPP (*Takifugu rubripes*) is known and diverges the most from human IAPP (h-IAPP) of any reported IAPP sequence, differing at eleven positions, including multiple substitutions in regions believed to be important for amyloid formation (Figures 3-1,3-

2). The primary sequence of h-IAPP and pufferfish IAPP (p-IAPP) are compared in Figure 3-1A, the location of the residues in p-IAPP that differ from those in h-IAPP is also displayed within the context of a structural model of the h-IAPP amyloid fibril (Figure 3-1B)[8]. The structured core of the h-IAPP amyloid fibril is thought to be comprised of residues 8 to 37 [8-10]. All eleven of the changes in p-IAPP relative to h-IAPP are found within this 30 residue segment. Of the eleven differences in the sequence, seven are found between residues 22 and 29, a segment which has been proposed to be important for modulating amyloidogenicity [11-14]. p-IAPP also contains a His-18 to Arg substitution. This replacement is known to reduce the amyloidogenicity of h-IAPP and modulates IAPP toxicity in cell culture [15, 16]. The pufferfish polypeptide also includes an Asn-14 to Asp substitution relative to h-IAPP which has been reported in other fish IAPPs, but not in mammals. Other substitutions which have not been reported in mammals include a Leu-27 to Tyr replacement and the replacement of Phe-23 by Ile (Figure 3-1A).

Here we examine the ability of p-IAPP to form amyloid *in vitro*. The analysis reveals that the relative amyloidogenicity, as defined by the kinetics of amyloid formation, of human and pufferfish IAPP depend on solution conditions and thus amyloidogencity is context dependent. The analysis also highlights complications with the widely applied thioflavin-T assay of amyloid formation and provides more evidence that they can lead to false negatives.

Amyloid formation *in vitro* is commonly followed using fluorescence detected thioflavin-T binding assays.[17, 18] Thioflavin-T is a small dye whose quantum yield increases and whose emission maximum shifts upon binding to amyloid fibrils [19]. There are no high resolution structures of thioflavin-T bound to amyloid fibrils, but the dye is believed to bind to the surface of the cross-β structure of the amyloid fibrils [18-22]. The parallel, in register β-sheet structures of typical amyloid fibrils create a series of grooves that run parallel to the long axis of the fibril

and these are believed to form the thioflavin-T binding sites. Binding of the dye fixes the position of the dimethylaminobenzyl and benzothiazole rings of thioflavin-T and reduces self-quenching, thereby leading to the enhancement in quantum yield. Thioflavin-T assays are the most widely applied biophysical technique used to follow amyloid formation. They are simple, easy to apply and have proven to be very informative, but the dye provides an extrinsic probe of amyloid formation and the signal depends on the amount of dye bound and the quantum yield of the bound dye. Thus, the relationship between the intensity of thioflavin-T fluorescence and the amount of amyloid formed is not always clear and it is formally possible that the assay could give false positives and false negatives [23].

3.2 Materials and Methods

3.2.1 Peptide Synthesis and Purification.

Peptides were synthesized with a CEM microwave peptide synthesizer on a 0.10 mmol scale utilizing 9-fluorenylmethoxycarbonyl (Fmoc) chemistry. 5-(4'-Fmoc-aminomethyl-3',5-dimethoxyphenol) valeric acid (PAL-PEG) resin was used to provide an amidated C-terminus. Fmoc-protected pseudoproline (oxazolidine) dipeptide derivatives were utilized as previously described [24, 25]. Solvents used were ACS-grade. β-branched residues, the first residue attached to the resin, pseudoproline dipeptide derivatives and the residues following the pseudoproline dipeptide derivatives were double-coupled. Peptides were cleaved from the resin via standard trifluoroacetic acid (TFA) methods. The cleaved crude peptides were dissolved into 15% (v/v) acetic acid and lyophilized. The disulfide bond was formed in 100% dimethyl sulfoxide at room temperature. Peptides were purified via reverse-phase high-performance liquid

chromatography (RP-HPLC) using a Higgins Analytical Proto 300 C18 preparative column (10 mm x 250 mm). A 25 – 60 % gradient was used over 40 minutes where buffer A was 100 % H_2O, 0.045 % HCl and buffer B was 80 % acetonitrile, 0.045 % HCl. h-IAPP had a retention time of 31 minutes (51 % B). p-IAPP had a retention time of 22 minutes (47 % buffer B). The purity of the peptides was tested using analytical HPLC. The masses of the pure peptides were confirmed with MALDI time-of-flight mass spectrometry. h-IAPP, expected 3903.6, observed 3902.9; p-IAPP, expected 3948.9, observed 3949.4.

3.2.2 Sample Preparation and Fluorescence Assays.

Stock solutions were prepared by dissolving peptide into 100% hexafluoroisopropanol (HFIP) at 1.6 mM. Solutions were filtered with 0.45 μM Acrodisc syringe filters and the required amount was lyophilized overnight to remove HFIP. Dry peptide was then dissolved into tris buffer or PBS for the fluorescence assays. The kinetics of amyloid formation were monitored using thioflavin-T binding assays conducted at 25 °C. Fluorescence measurements were performed using a Beckman Coulter DTX 880 plate reader with a multimode detector using an excitation wavelength of 430 nm and an emission wavelength of 485 nm.

3.2.3 Transmission Electron Microscopy.

TEM images were collected at the Life Science Microscopy Center at the State University of New York at Stony Brook. At the end of each experiment, 15 μL aliquots of the samples used for the kinetic studies were removed, blotted on a carbon-coated 300-mesh copper grid for 1 min and then negatively stained with saturated uranyl acetate for 1 min.

3.2.4 Circular Dichroism

Far UV CD experiments were performed on an Applied Photophysics Chirascan CD spectrophotometer. The sample was incubated on the bench for two weeks and the spectrum was

recorded. The spectrum was an average of three repeats recorded over a range of 190 – 260 nm, at 1 nm intervals. A 10 mm quartz cuvette was used and a background spectrum was subtracted from the collected data. Experiments were performed at 25 °C in 20 mM tris buffer at pH 7.4. The sample concentration was 40 μM.

3.2.5 FTIR Spectroscopy

FTIR spectra were recorded on a Bruker Vertex 80 FTIR spectrometer equipped with a globar source, KBr beamsplitter and a liquid nitrogen-cooled mercury cadmium telluride (MCT) detector. Spectra were recorded as the result of 2048 scans at a resolution of 1 cm-1 using a Bruker BioATR II cell. The effective path length of the cell was approximately 6−8 μm. Experiments were performed at 20 °C and a protein concentration of 600 μM.

3.2.6 Molecular Dynamics Simulations and Modelling of Pufferfish and Human Amyloid Fibrils

NOTE: The molecular dynamics simulations and modelling of pufferfish and human amyloid fibrils were performed by the Joan-Emma Shea group at University of California at Santa Barbara. The methods have been included here for completeness.

The two initial fibril structures of human IAPP (two layers of 5 peptides) were taken from two sources: one derived from solid state NMR studies of full length human IAPP and the other from crystal structures of small "steric zipper" peptides derived from the human IAPP sequence. The two initial fibril structures of pufferfish IAPP were derived from the two experimental fibril structures of human IAPP by mutating the corresponding residues (Figure-1A). Each of the four initial fibril structures was immersed in a truncated octahedral box ($a = b = c$ = ~69 Å, $\alpha = \beta = \gamma$ = 109.47º) filled with water molecules. The all-atom point-charge force field

(AMBER ff03) was used to represent the peptides [26]. This force field has been successfully used to model the binding of Aβ(39–42) to Aβ40/ Aβ42 peptides, the binding among Aβ protofibrils and the binding of fluorescent dyes to Aβ protofibrils.[27-29] The water solvent was explicitly represented by the TIP3P model [30]. The AMBER 14 simulation suite was used in molecular dynamics simulations and data analysis [31]. After an initial energy minimization, a total of 4 simulations (one run for each fibril system) were performed with different initial random velocities. The random velocities of atoms were generated according to the Maxwell-Boltzmann distribution at 300 K. The production run (500 ns) was performed at 300 K and was comprised of 1 ns of molecular dynamics in the NPT ensemble mode (constant pressure and temperature) to equilibrate the solvent and 499 ns dynamics in the NVT ensemble mode (constant volume and temperature). Periodic boundary conditions were imposed on the system. The particle-mesh Ewald method was used to treat the long-range electrostatic interactions [32]. SHAKE was applied to constrain all bonds connecting hydrogen atoms, enabling a 2 fs time step used in the dynamics [33]. To reduce computation time, non-bonded forces were calculated using a two-stage RESPA approach where the short-range forces within a 10 Å radius were updated every step and the long range forces beyond 10 Å are updated every two steps [34]. Langevin dynamics were used to control the temperature (300 K) using a collision frequency of 1 ps-1. The center of mass translation and rotation was removed every 500 steps to remove the "block of ice" problem [35, 36]. The trajectories were saved at 50 ps intervals for analysis.

3.3 Results and discussion

3.3.1 Amyloid Prediction Algorithms Give Conflicting Results for the Relative Amyloidogenicity of Pufferfish IAPP

A range of amyloid prediction programs have been developed and most rely on physicochemical analysis of the properties of the primary sequence, although the ZipperDB algorithm uses a template approach based on steric zippers [37-42]. The different methods lead to different predictions for the relative amyloidogenicity of h-IAPP and p-IAPP (Table 3-1). AGGRESCAN and AmylPred predict h-IAPP is more amyloidogenic than p-IAPP, while TANGO and ZipperDB predict that it is less amyloidogenic and Zyggregator and PASTA predict that there is no change. Thus, existing methods to predict amyloidogenicity give ambiguous results when applied to p-IAPP. Amyloid prediction algorithms have also been shown to improperly predict the amyloidogenicity of scrambled peptide sequences derived from the N-terminal segment of the Huntingtin peptide [43]. The ability of any full-length fish IAPP to form amyloid has not yet been experimentally evaluated.

3.3.2 Pufferfish IAPP Forms Amyloid But Does Not Bind to Thioflavin-T in Tris Buffer

We compared the time course of amyloid formation by human and pufferfish IAPP using thioflavin-T fluorescence assays and by transmission electron microscopy (TEM). We conducted initial experiments in 20 mM tris at pH 7.4, chosen because this buffer has been used extensively in studies of amyloid formation by IAPP. The concentration of IAPP used was 16 μM, again chosen because it is typical of values used for biophysical studies with the polypeptide. A 2-fold excess of thioflavin-T was used. Most experiments with h-IAPP avoid a large excess of thioflavin-T to avoid any perturbation of the kinetics of amyloid formation. Thioflavin-T does not impact the kinetics of IAPP aggregation under these conditions [44]. A sigmoidal thioflavin-T fluorescence time course, consisting of a lag period, a growth phase and final plateau is

observed in the presence of h-IAPP which is characteristic of amyloid formation (Figure 3-2A). No change in thioflavin-T intensity is observed for the sample of p-IAPP, even for a time which is 6-fold longer than the lag time of human IAPP amyloid formation (Figure 3-2A). The standard interpretation of these results would be that pufferfish IAPP is not amyloidogenic under these conditions. However, time-dependent TEM studies show that this is not the case (Figure 3-3B). Aliquots were collected at five different time points, including two time points within the lag phase of h-IAPP amyloid formation. Samples were removed at t= 0, $0.25t_{50}$, $2t_{50}$, $3t_{50}$ and $5t_{50}$, where t_{50} refers to the time required for human IAPP to reach half maximum fluorescence intensity in a thioflavin-T assay. As expected, no amyloid fibrils are detected in the samples of h-IAPP removed at t = 0, and t = $0.25t_{50}$, In contrast, amyloid fibrils are clearly present in the p-IAPP sample at the $0.25t_{50}$ time point (Figure 3-2B). Mats of amyloid fibrils are observed for both h-IAPP and p-IAPP in samples removed at 24 hours and at subsequent time points even though no change in thioflavin-T fluorescence intensity is detected for the p-IAPP sample. These experiments clearly indicate that thioflavin-T based assays give a misleading view of p-IAPP amyloid formation. The thioflavin-T assays displayed in Figure 3-3A involved monitoring the fluorescence intensity at 485 nm. We confirmed that the lack of a change in the signal of the p-IAPP sample is not a consequence of the emission wavelength chosen by collecting complete fluorescence emission spectra of thioflavin-T in the absence of peptide and in the presence of either human or pufferfish IAPP amyloid fibrils. The spectra of thioflavin-T alone or in the presence of p-IAPP amyloid are essentially identical with a weak emission maximum near 520 nm (Figure 3-3). In contrast, the emission maximum is shifted to near 480 nm in the presence of h-IAPP amyloid fibrils and there is a significant enhancement in quantum yield. The lack of thioflavin-T signal could be due to changes in the surface structure of the amyloid fibrils that

lead to weaker dye binding, or be caused by changes in the quantum yield of the bound dye. A lower yield of fibrils will also lead to a weaker thioflavin-T signal. Another potential factor that can lead to lower thioflavin-T is changes in the association of fibrils. If the fibrils tightly associate, the dye binding surfacing could potentially be occluded, leading to fewer thioflavin-T binding sites.

The TEM images of h-IAPP and p-IAPP amyloid fibrils are very similar (Figure 3-2B), but it is difficult to detect molecular level changes in structure by TEM, given the resolution of the method and the negative stains employed. Thus, we turned to circular dichroism (CD) to probe the secondary structure of the p-IAPP fibrils. A sample of p-IAPP was prepared and incubated until amyloid fibrils were formed, as judged by TEM, and the CD spectrum recorded (Figure 3-4A). The CD spectrum of the pufferfish peptide exhibits a broad minimum near 218 nm, consistent with β-sheet structure, and the shape of the spectrum is very similar to that reported for the h-IAPP amyloid fibrils.

We also recorded the Fourier-transform infrared (FTIR) spectra of h-IAPP and p-IAPP (Figure 3-4B). The amide-I mode is sensitive to secondary structure, exhibiting characteristic shifts to lower energy, lower wavenumber, observed in β-sheets. There is considerable variability in the FTIR spectra of amyloid, but most amyloids exhibit a broad peak near the region of 1615 to 1630 cm-1 while random coil features are found at higher wavenumbers [45]. Monomeric h-IAPP has been reported to give an FTIR spectrum with a broad peak centered near 1645 to 1650 cm-1 [46]. Our experimental spectrum of h-IAPP exhibits a peak at 1627 cm-1 while p-IAPP displays a peak at 1635 cm-1. In both cases, the peak is shifted away from the random coil position. The relatively modest difference in band position for the two polypeptides suggests that

there could be differences in the structure of the aggregates. MD simulations, described in a subsequent section, provide a possible explanation for the difference.

3.3.3 The Relative Rates of Amyloid Formation by Human and Pufferfish IAPP are Dependent on the Choice of Buffer

We next examined the behavior of h-IAPP and p-IAPP in a more physiological buffer consisting of 20 mM sodium phosphate, 140 mM KCl at pH 7.4. A typical thioflavin-T curve is observed for h-IAPP in PBS with a shorter lag phase than observed in tris (Figure 3-5A). The shorter lag phase is consistent with the known effects of salts on IAPP amyloid formation [47]. A weak thioflavin-T signal is observed from the p-IAPP sample under these conditions, but the final thioflavin-T intensity is 15 to 20-fold weaker than observed for the h-IAPP sample. Somewhat surprisingly, the time required to reach the plateau of the thioflavin-T response is longer for the p-IAPP sample in phosphate buffer relative to the time required for h-IAPP to form amyloid even though p-IAPP forms amyloid more rapidly in tris buffer. A TEM time course confirms this observation. Amyloid fibrils are detected from the sample of h-IAPP before they are observed in the p-IAPP sample. Thus, the relative rate of amyloid formation by p-IAPP and h-IAPP depends upon the choice of buffer, an observation which indicates discussions of relative amyloidogenicity should be treated with caution.

3.3.4 Pufferfish IAPP is Compatible with Existing Models of Human IAPP Amyloid Fibrils

We next performed molecular dynamics simulations to test if the pufferfish sequence is compatible with existing models of the h-IAPP amyloid fibrils. There are two high resolution models of the h-IAPP fibrils: one derived from solid state NMR studies of full length h-IAPP and the other from crystal structures of small “steric zipper” peptides derived from the h-IAPP sequence [8, 9]. While the two models differ in their details, they have many common features

and their similarities outweigh their differences. In both structures, the fibril core is made up of two C2 symmetric stacks of monomers (Figure 3-1B). Each monomer adopts a U-shaped structure which includes two β-strands connected by a less structured linker. The N-terminal strand is on the exterior of the fibril and the C-terminal strand forms the interface between two peptide molecules in one layer. We threaded the pufferfish sequence onto each model structure, here using two stacks of five monomers as the model, and conducted all-atom molecular dynamics simulations of both with explicit solvent model. We also ran MD simulations of each model using the human peptide as a control. The 500 ns simulations indicate that the p-IAPP sequence is compatible with the proposed fibril models for h-IAPP, retaining the overall strand-loop-strand fold. The Cα-RMSD at the end of the simulations are shown in Figure 3-7 and the last snapshots of the four simulations are shown in Figure 3-8. The NMR-derived fibril model fits the p-IAPP sequence particularly well, with less than a 1 Å deviation in Cα-RMSD between the h-IAPP and the p-IAPP forms, suggesting that the backbone fold is very similar between human and pufferfish. However, as can be seen from the two representative structures shown in Figure 3-7, while the overall U-shape fold (β-strand-loop-β-strand) is maintained in p-IAPP, the region adjacent to the loop has more coil and less β-sheet structure than in the case of h-IAPP. This is an interesting observation in light of the FTIR results. The loop which connects the two β-strands also appears to be more flexible in p-IAPP. A notable feature is that the sidechains on the surface of the pufferfish fibrils are more disordered relative to the models of h-IAPP. Our early computational studies of the binding of thioflavin-T to a number of amyloid fibril models showed that the primary binding sites for thioflavin-T were regular grooves formed by ordered side-chains on the surface of amyloid fibrils, with minor sites located the ends of the fibril [20-

22]. The lack of ordered grooves on the surface of the p-IAPP fibrils may explain the weak thioflavin-T fluorescence signal, despite clear evidence of fibril formation from TEM.

3.3.5 Thioflavin-T Assays Do Not Accurately Report on Pufferfish IAPP Amyloid Formation Even if the Dye is in Excess

We also examined the effect of increasing the concentration of thioflavin-T to a 20-fold excess relative to IAPP in monomer units. Normally, these concentrations are avoided for fear that high dye concentrations might perturb the kinetics of amyloid formation. The dye has a small impact on the kinetics of h-IAPP amyloid formation, leading to a slightly more rapid time course (Figure 3-9). A weak thioflavin-T signal is detected when 20-fold excess of dye is added to pufferfish IAPP in tris buffer, but the signal is still weaker than observed for the sample of h-IAPP with a 10-fold lower concentration of dye. The small thioflavin-T signal for the pufferfish IAPP sample exhibits a time course with a longer apparent lag phase (Figure 3-9A) than h-IAPP. The normal interpretation would be that pufferfish IAPP forms amyloid more slowly than h-IAPP, but generates less amyloid fibers than h-IAPP. However, TEM reveals that this is not the case. Images recorded of samples removed during the lag phase of h-IAPP amyloid formation revealed no detectable fibrils in the h-IAPP samples, but mats of amyloid fibrils were evident in the pufferfish IAPP samples (Figure 3-9B). This clearly indicates that pufferfish IAPP forms amyloid more rapidly than does h-IAPP under these conditions and provides further evidence that thioflavin-T assays can give misleading results.

3.4 Conclusions

The data presented here demonstrates that p-IAPP is capable of forming amyloid, but shows that the relative rate of amyloid formation as compared to human IAPP depends upon the choice of buffer. This observation has clear implications for studies which attempt to define and compare the relative amyloidogenicity of different polypeptides. In the present case, the differential effects may reflect the different charge distributions of the two polypeptides. Analysis of the effects of anions on h-IAPP amyloid formation have shown that their effects follow the ion selectivity series at low to moderate concentrations, arguing for a contribution from ion binding [47]. p-IAPP has a lower net charge than h-IAPP due to the Asn to Asp substitution and this may reduce the affinity for phosphate. In this scenario, phosphate accelerates h-IAPP amyloid formation to a greater extent than it does amyloid formation by p-IAPP and this leads to a reversal in the relative rates of amyloid formation. Irrespective of the mechanistic details, the results indicate that solution conditions are important in evaluating relative amyloidogenicity. Our observation that different amyloid prediction programs give differing results for p-IAPP and h-IAPP, together with the context dependent effects described above, and earlier studies on the reliability of amyloidogenicity algorithms indicates that caution should be applied when interpreting the results of amyloidogenicity algorithms [43].

We believe that the observation of weak or non-existent thioflavin-T binding by p-IAPP is also important. Thioflavin-T is the most widely used probe of amyloid formation and the present study provides a clear cautionary example of the assay yielding a false negative. Thioflavin-T is believed to bind to surface grooves found on amyloid fibrils that are a consequence of their cross-β structure. The large number of substitutions in p-IAPP, 11 out of the 30 residues which are believed to form the core of the fibril, could change the structure and physicochemical nature of the surface grooves. Our all atom MD simulations show that the pufferfish sequence is

compatible with the solid state NMR model of the h-IAPP amyloid fibrils as well as with the model derived from crystal structures of small peptide fragments of h-IAPP. However, two significant differences are observed. First, the part of the region located adjacent to the loop in the U-shape motif adopts coil-like conformations rather than the extended β-sheet conformations seen in h-IAPP. Importantly, the sidechains of the pufferfish IAPP model are more disordered than in the case of the human fibrils and, as a result, do not form the well-ordered surface grooves on the face of the fibril that serve as binding sites for thioflavin-T. The differences in the FTIR spectra of human and pufferfish IAPP are consistent with some structural changes. These differences may contribute to the reduced binding of thioflavin-T to pufferfish IAPP. A reduced yield of amyloid fibrils by the pufferfish peptide could potentially contribute to the lower thioflavin-T signal. In this scenario, p-IAPP forms fewer fibrils and there would be a significant fraction of the polypeptide that remains unaggregated. This seems unlikely, especially given that the CD spectrum and FTIR spectrum indicate that the conformational ensemble is dominated by β-structure. Gravimetric data could formally rule out this possibility but is not available. It would be interesting to see if p-IAPP could seed amyloid formation by h-IAPP and if the resulting fibrils would be able to bind with thioflavin-T especially since models of the p-IAPP amyloid fibril are compatible with the solid state NMR model of the h-IAPP fibril. Again, the mechanistic details of the reduced thioflavin-T signal are not completely clear, but the key result is that thioflavin-T assays can give rise to false negatives and the final thioflavin-T intensity should not be interpreted as a quantitative measure of the amount of amyloid formed when comparing different peptides. Work on Aβ polymorphs and poly-Q peptides as well as a comparison of Aβ(1-40) and Aβ(1-42) also highlights the dangers of quantitative interpretation of thioflavin-T intensities [48-50].

Finally, we note that teleostean fish have been proposed to be a source of xenobiotic islet transplants. Encouraging success has been obtained using porcine islets for xenobiotic islet transplants, but porcine IAPP is much less amyloidogenic than h-IAPP under all conditions tested and its reduced amyloidogencity correlates with enhanced islet survival [7]. The comparable amyloidogenicity of pufferfish and human IAPP indicates that caution should be used if fish are employed for transplant studies [3-5]. However, it is also worth noting that the partial sequence of Atlantic wolffish (*Anarhichas lupus*) includes additional proline substitutions as well as additional charge substitutions which likely render the sequence less amyloidogenic and it may be a more attractive candidate for xenobiotic studies [3]. Of course, other factors also need to be addressed when considering candidates for xenobiotic studies. These include the activity relative to human IAPP and immunogenicity. Nonetheless, it will be interesting to examine the behavior of the full-length wolfish sequence once it becomes available.

3.5 Figures

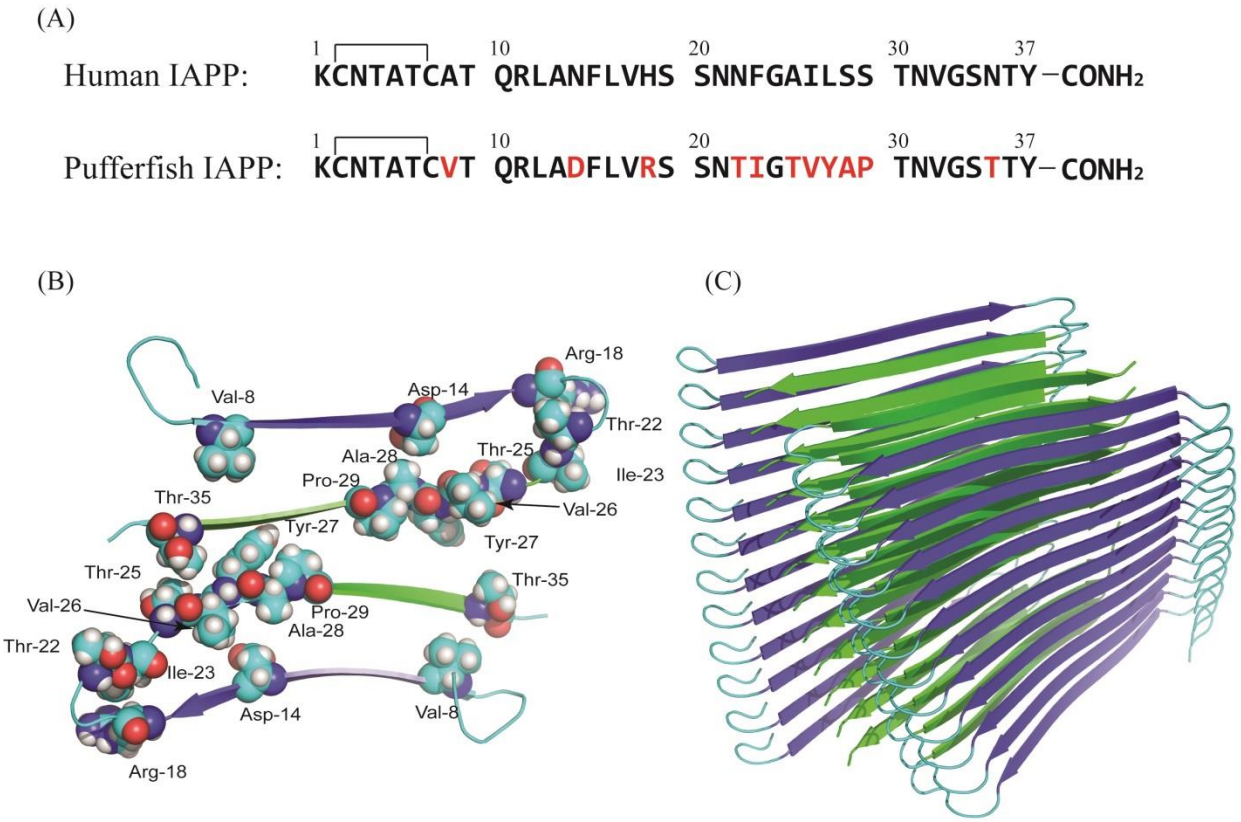

Figure 3-1: (A) Comparison of the primary sequence of human IAPP and pufferfish IAPP. Residues which differ from the human peptide are colored red. Both sequences have amidated C-termini and contain a disulfide bond between residues 2 and 7. (B) Cross-section of a model of the human IAPP amyloid fibril based on crystal structures of fragments of the molecule. Residues in pufferfish IAPP which differ from the human sequence are built into the model and are shown in space filling format. (C) Ribbon diagram of the fibril.

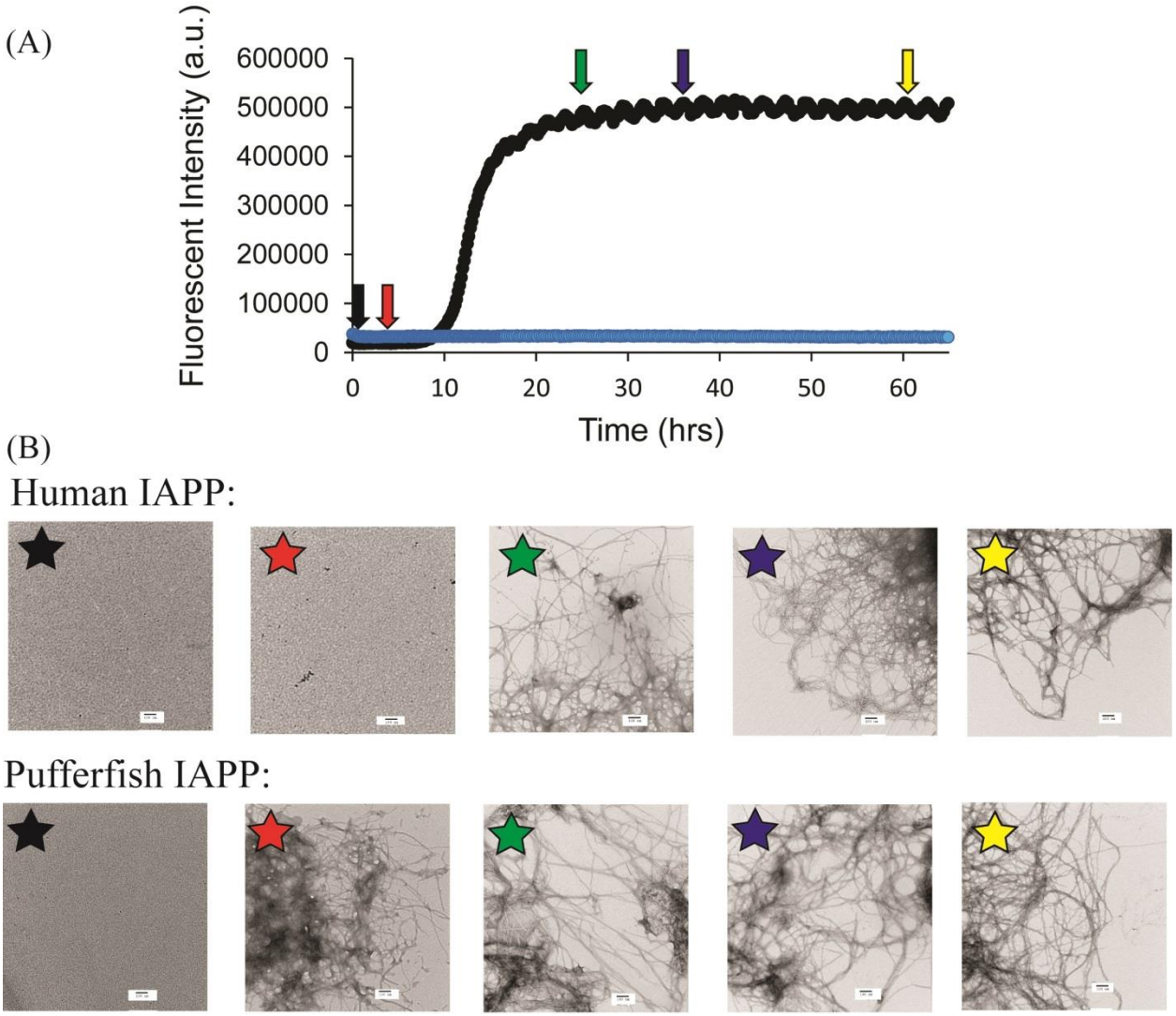

Figure 3-2: Analysis of amyloid formation by pufferfish IAPP (blue) and human IAPP (black) in 20 mM tris-HCl at pH 7.4. (A) Fluorescence monitored thioflavin-T assays of amyloid formation. No change in thioflavin-T fluorescence is detected for the pufferfish peptide over the entire time course of the experiment. Arrows indicate times, at which aliquots where collected for TEM analysis. (B) TEM images of samples of human IAPP (top) and pufferfish IAPP (bottom) collected at the different time points. Experiments were conducted with 16 μM IAPP,

32 μM thioflavin-T at 25 °C in 20 mM tris-HCl at pH 7.4. Scale bars in TEM images represent 100 nm.

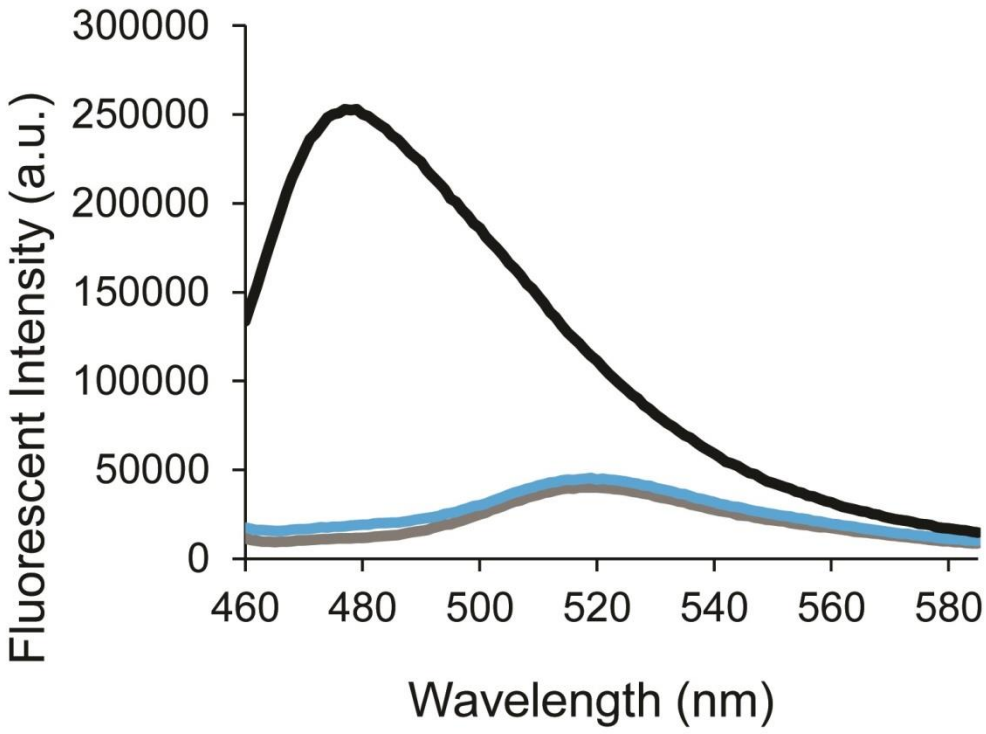

Figure 3-3: Thioflavin-T emission spectra of samples of 32 μM thioflavin-T, with human IAPP (black), pufferfish IAPP amyloid fibrils (blue), and thioflavin-T alone (grey). IAPP when present is at 16 μM in monomer concentration. Spectra were recorded at the end of the kinetic experiments depicted in Figure 2. Samples contained 20 mM tris-HCl at pH 7.4 and measurements were made at 25 °C. Excitation at 450 nm.

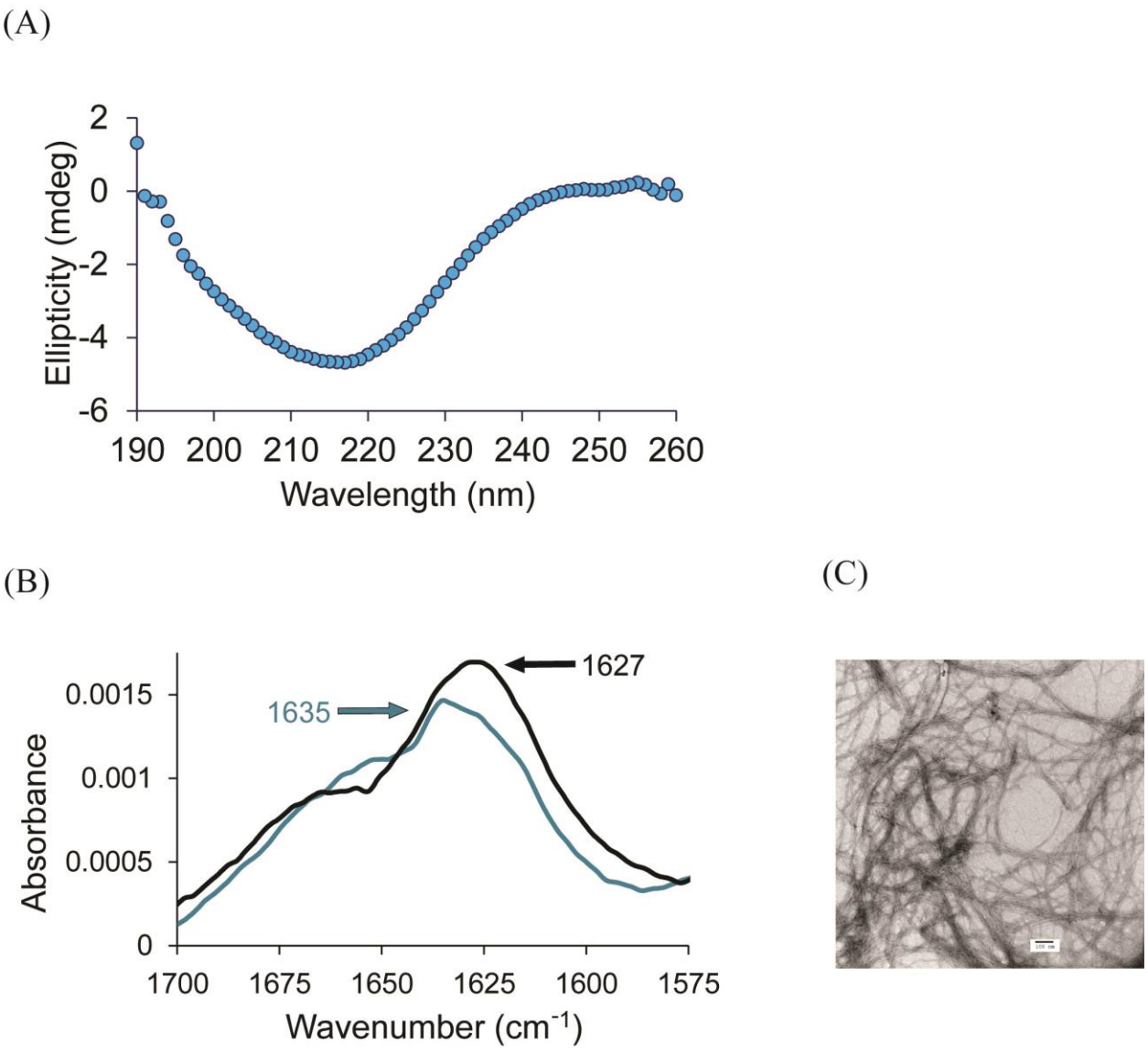

Figure 3-4: Pufferfish IAPP forms fibrils with significant β-sheet secondary structure. (A) CD spectrum of a sample of the fibril material formed by a 40 μM sample of pufferfish IAPP. The spectrum is the smoothed average of three scans. (B) FTIR spectra of p-IAPP (blue) and h-IAPP (black). (C) TEM image of the pufferfish IAPP sample collected at time of CD measurement. Samples were incubated at 25 °C. Scale bars in TEM images represent 100 nm.

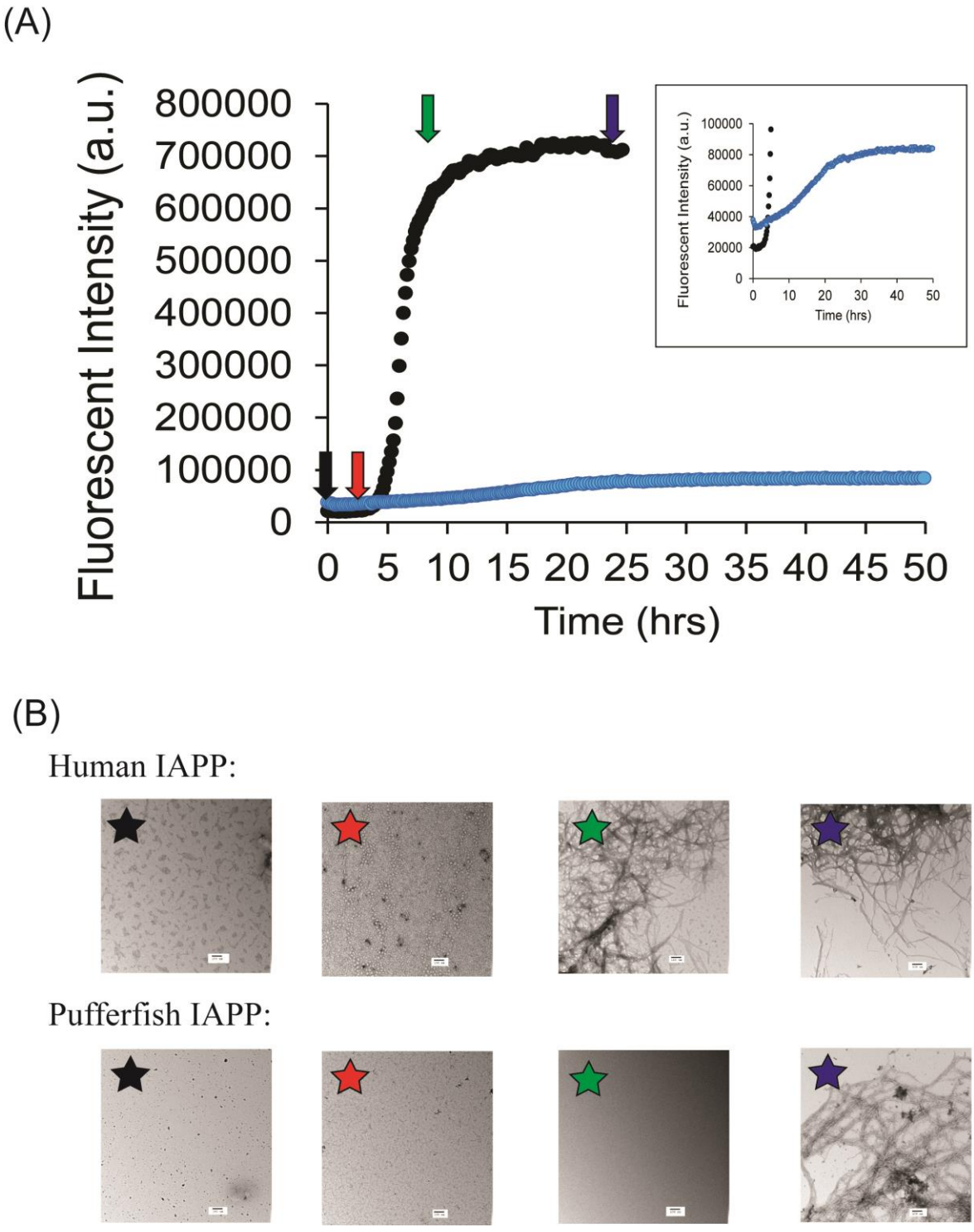

Figure 3-5: Analysis of the ability of pufferfish IAPP to form amyloid in phosphate buffered saline solution. (A) Fluorescence monitored thioflavin-T assays of human IAPP (black) and

pufferfish IAPP (blue) amyloid formation in phosphate buffer saline. Arrows indicate times at which aliquots where collected for TEM analysis. Aliquots were collected at t = 0 (black), 3 hrs (red), 7 hrs (green), and 24 hrs (blue) (B) TEM images of samples human IAPP (top) and pufferfish IAPP (bottom) collected at the different time points. Experiments were conducted with 16 μM IAPP, 32 μM thioflavin-T at 25 °C in 20 mM sodium phosphate, 140 mM potassium chloride at pH 7.4. Scale bars in TEM images represent 100 nm.

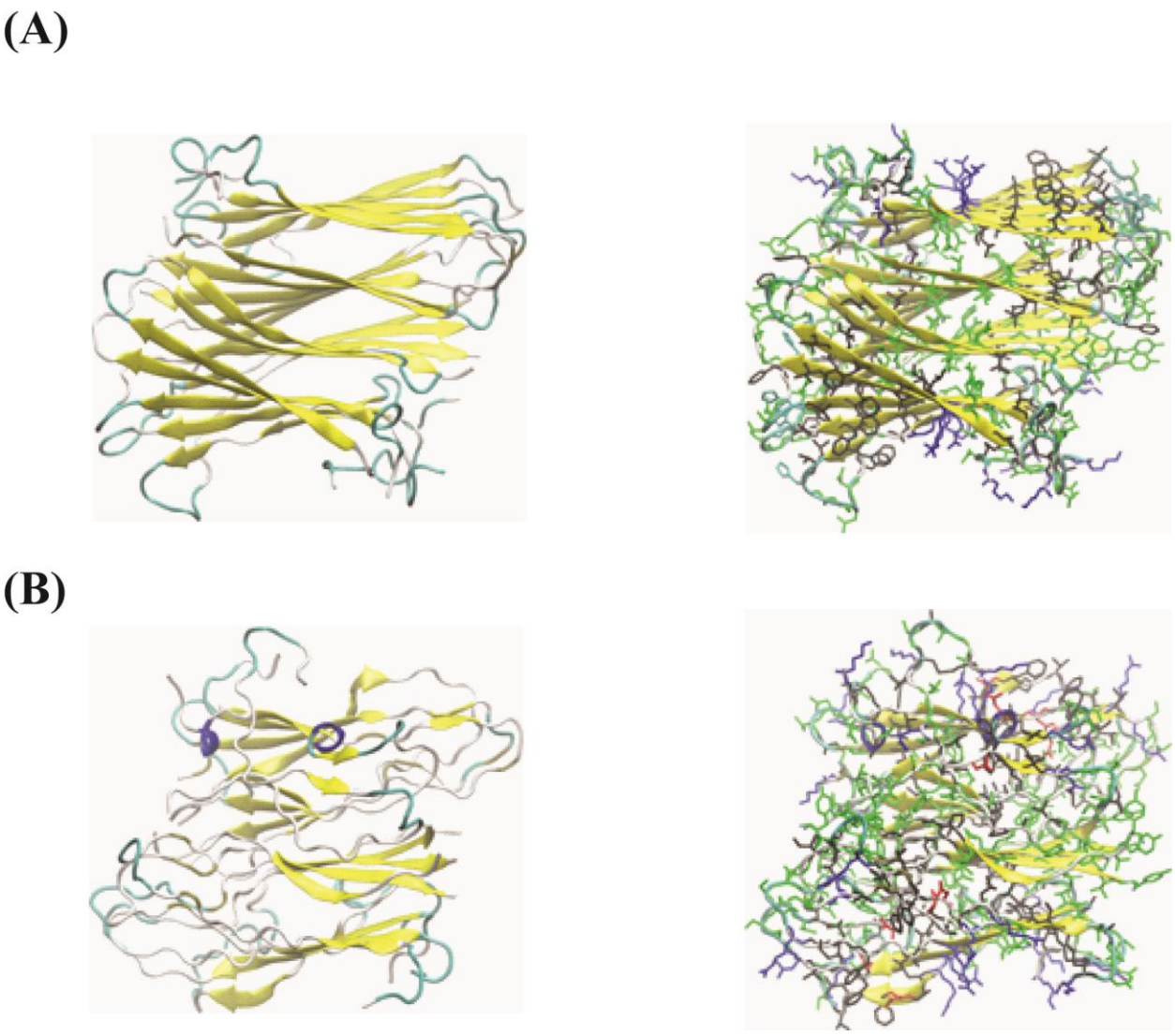

Figure 3-6: Last snapshots of two representative simulations. (A) Human IAPP fibril model from the solid state NMR study. (B) Pufferfish IAPP fibril model is derived from the NMR model by threading. 310, α-helical, β-strand, turn and coiled conformations are colored in blue, yellow, cyan and white respectively. Sidechains are color-coded as positively charged (blue), negatively charged (red), hydrophobic (black) and hydrophilic (green).

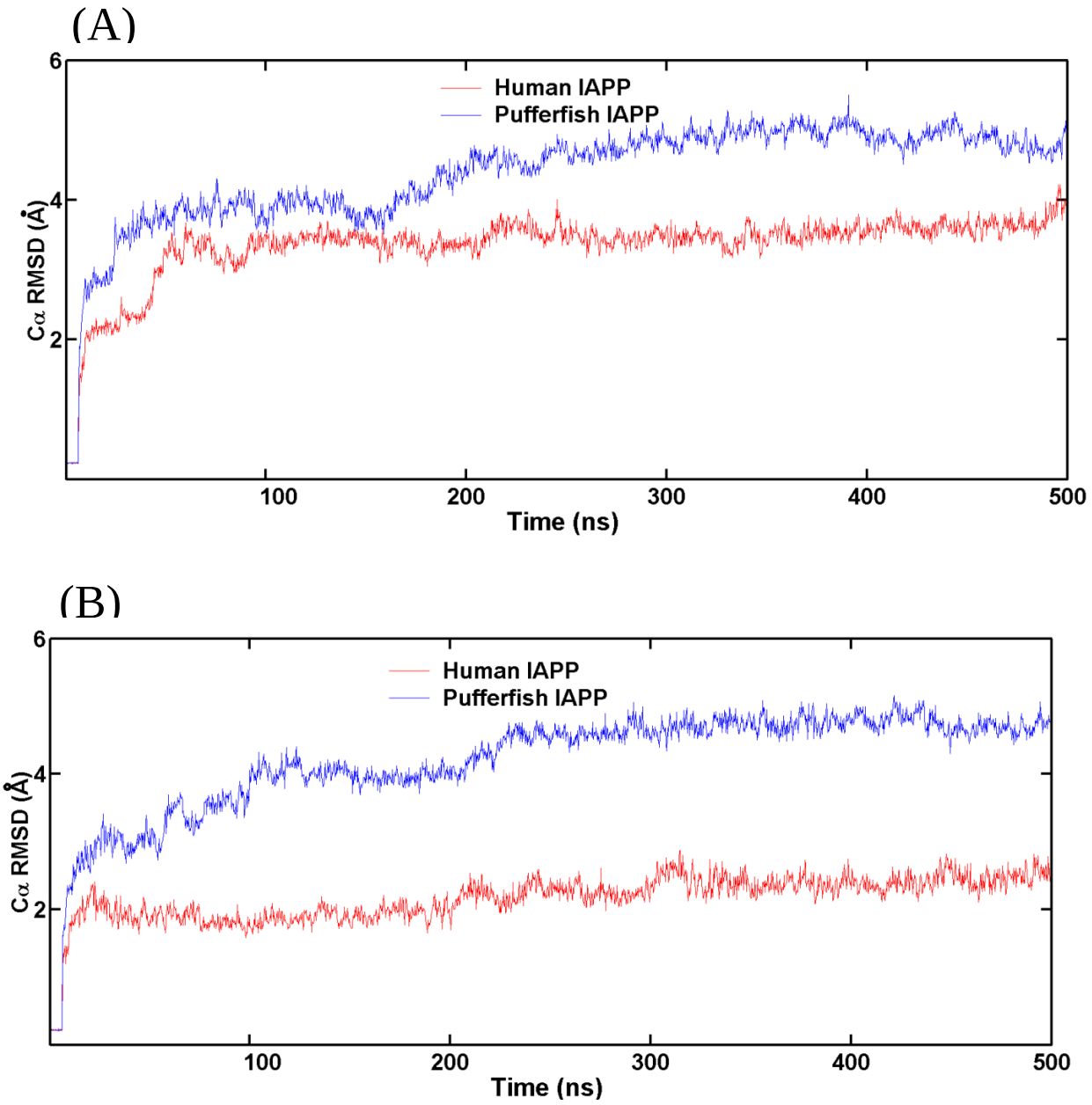

Figure 3-7: Cα RMSD of pufferfish IAPP (red) and human IAPP (blue) relative to the starting fibril structure. (A) Human IAPP fibril model from the solid state NMR study. The pufferfish IAPP fibril model is derived from the NMR model by threading. (B) Human IAPP fibril model from the crystal structure of small "steric zipper" peptides (red).The pufferfish IAPP fibril model is derived from the crystal model by threading (blue). Red curves are for the human peptide and blue is for the pufferfish peptide. The relevant comparison is the difference in the RMSD at the

ends of the simulation as this takes into account relaxation of both the human and pufferfish models. The peptide chains at the ends of the fibrils are not included in the Cα RMSD calculation.

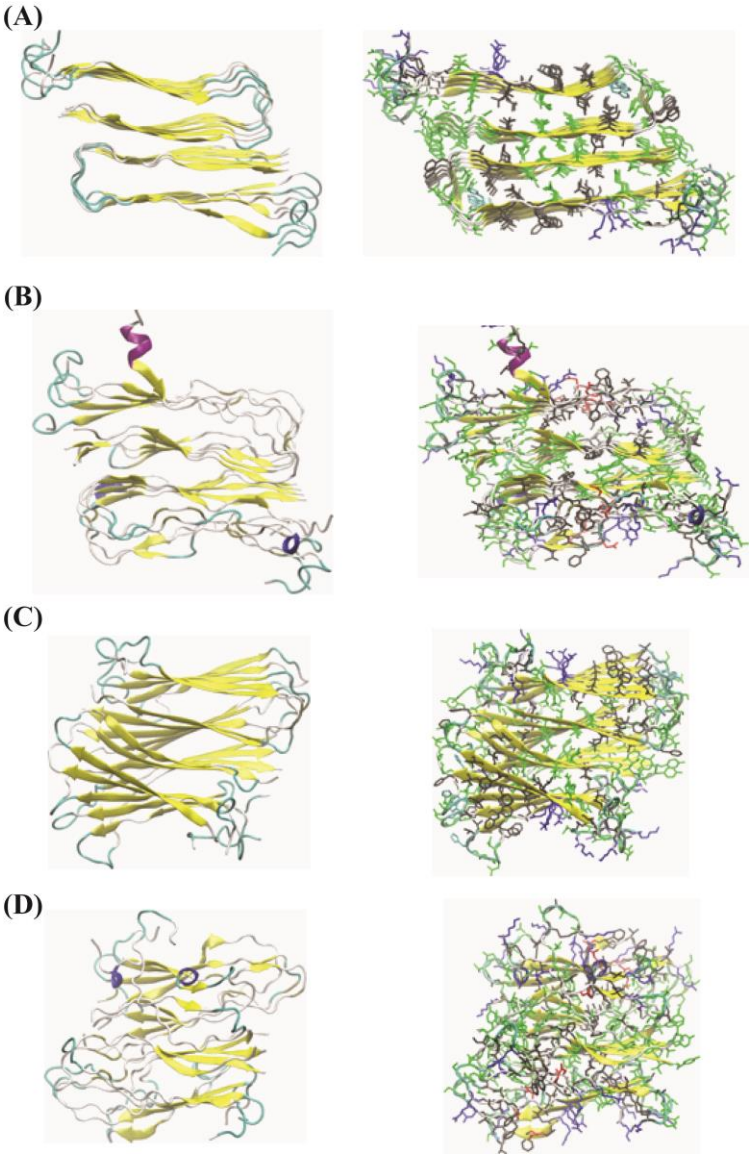

Figure 3-8: Final snapshots of four simulations. (A) Human IAPP fibril model from the crystal structure of small "steric zipper" peptides. (B) Pufferfish IAPP fibril model derived from the crystal model by threading. (C) Human IAPP fibril model from the solid state NMR study. (D) Pufferfish IAPP fibril model is derived from the NMR model by threading. 310 α-helical, β-extended, turn and coiled conformation are colored in blue, yellow, cyan and white. Sidechains

are color-coded as positively charged (blue), negatively charged (red), hydrophobic (black) and hydrophilic (green).

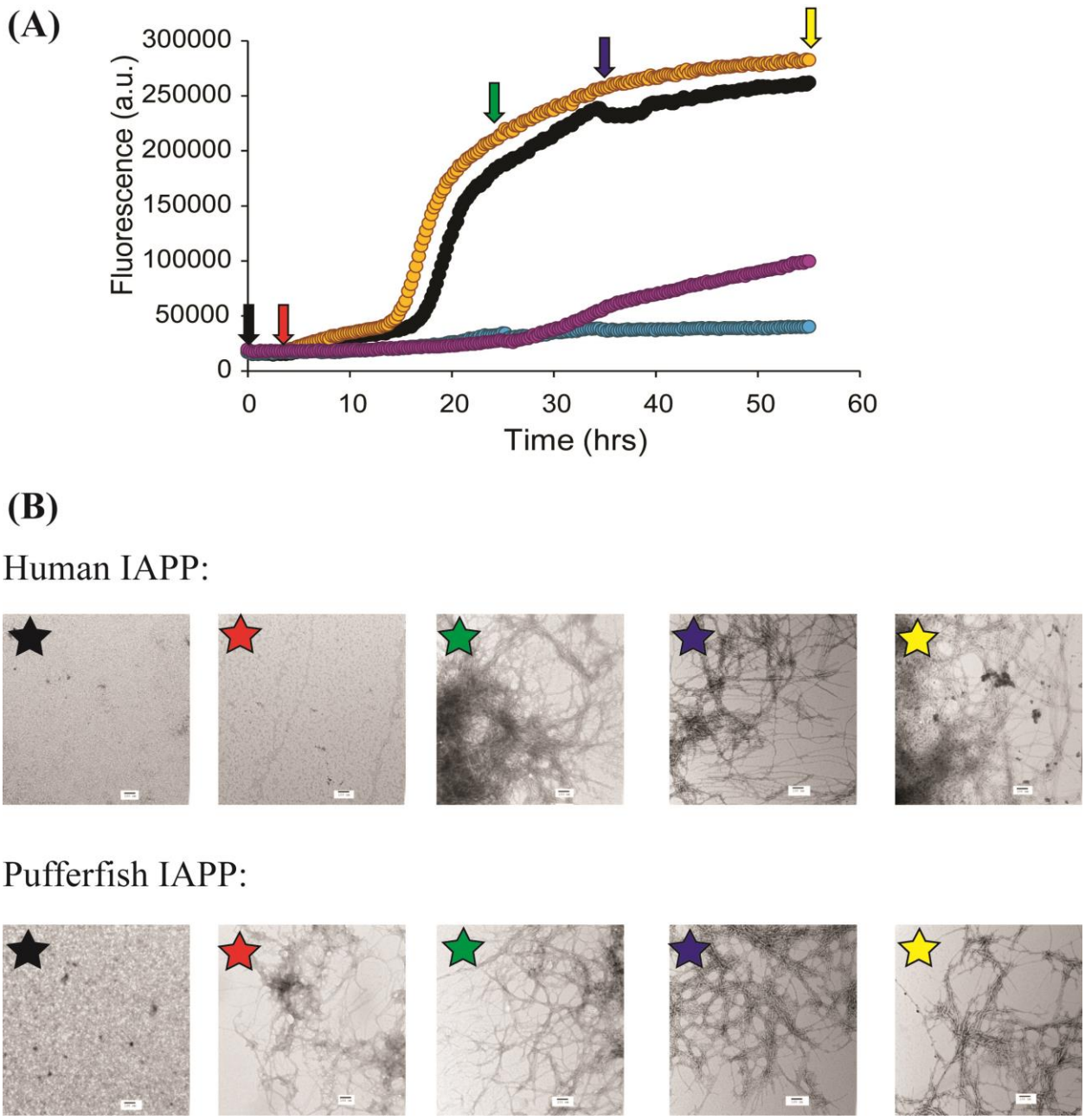

Figure 3-9: Analysis of amyloid formation by pufferfish IAPP and human IAPP in the presence of excess thioflavin-T in 20 mM tris-HCl at pH 7.4. (A) Fluorescence monitored thioflavin-T assays of human IAPP with 2-fold and 20-fold excess of thioflavin-T (black and orange respectively) and of pufferfish IAPP with 2-fold and 20-fold excess of the dye (blue and purple respectively). Arrows indicate times at which aliquots were collected for TEM analysis. Aliquots

were collected at t = 0 (black), 0.25t50 (red), 2t50 (green), 3t50 (blue), and 5t50 (yellow), where t50 refers to the time required for human IAPP to reach half maximum fluorescence intensity in a thioflavin-T assay. (B) TEM images of samples of human IAPP (top) and pufferfish IAPP (bottom) in the presence of 20-fold excess of thioflavin-T collected at different time points. Experiments were conducted with 16 μM IAPP, 32 μM or 320 μM thioflavin-T at 25 °C in 20 mM tris-HCl at pH 7.4. Scale bars in TEM images represent 100 nm.

3.6 Tables

Name of Program	Relative Amyloidogenicity of p-IAPP
AGGRESCAN	▲
FoldAmyloid	-
WALTZ	▼
AmylPred	▲
Zyggregator	-
TANGO	▼
Agadir	-
ZipperDB	▼
PASTA	-

Table 3-1: Summary of the results of amyloid prediction algorithms. The program name is given as well as the predicted effect on the relative amyloidogenicity of p-IAPP and h-IAPP. (▲) The program predicts higher amyloidogenicity for p-IAPP. (▼) The program predicts lower amyloidogenicity for p-IAPP. (-) The program predicts no change in amyloidogenicity.

3.7 References

1. Martinez-Alvarez, R. M., Volkoff, H., Cueto, J. A. M., and Delgado, M. J. Molecular Characterization of Calcitonin Gene-Related Peptide (CGRP) Related Peptides (CGRP, Amylin, Adrenomedullin And Adrenomedullin-2/Intermedin) in Goldfish (Carassius auratus): Cloning And Distribution, *Peptides*, **2008**, *29*,1534-1543.

2. Westermark, G. T., Falkmer, S., Steiner, D. F., Chan, S. J., Engstrom, U., and Westermark, P. Islet Amyloid Polypeptide is Expressed in The Pancreatic Islet Parenchyma of the Teleostean Fish, Myoxocephalus (Cottus) Scorpius, *Comp. Biochem. Physiol., Part B: Biochem. Mol. Biol.*, **2002**, *133*,119-125.

3. Fortin, J. S., Santamaria-Bouvier, A., Lair, S., Dallaire, A. D., and Benoit-Biancamano, M. O. Anatomic and Molecular Characterization of the Endocrine Pancreas of a Teleostean Fish: Atlantic Wolffish (Anarhichas lupus), *Zool. Stud.*, **2015**, *54*.

4. Nguyen, T. M., Wright, J. R., Jr., Nielsen, P. F., and Conlon, J. M. Characterization of the Pancreatic Hormones From The Brockmann Body of The Tilapia: Implications for Islet Xenograft Studies, *Comp. Biochem. Physiol. C: Pharmacol. Toxicol.*, **1995**, *111*,33-44.

5. Yang, H., Dickson, B. C., O'Hali, W., Kearns, H., and Wright, J. R., Jr. Functional Comparison of Mouse, Rat, and Fish Islet Grafts Transplanted Into Diabetic Nude Mice, *Gen. Comp. Endocrinol.*, **1997**, *106*,384-388.

6. Westermark, G. T., Westermark, P., Berne, C., and Korsgren, O. Widespread Amyloid Deposition in Transplanted Human Pancreatic Islets, *N. Engl. J. Med.*, **2008**, *359*,977-979.

7. Potter, K. J., Abedini, A., Marek, P., Klimek, A. M., Butterworth, S., Driscoll, M., Baker, R., Nilsson, M. R., Warnock, G. L., Oberholzer, J., Bertera, S., Trucco, M., Korbutt, G. S., Fraser, P. E., Raleigh, D. P., and Verchere, C. B. Islet Amyloid Deposition Limits the Viability of Human Islet Grafts But Not Porcine Islet Grafts, *PNAS*, **2010**, *107*,4305-4310.

8. Wiltzius, J. J. W., Sievers, S. A., Sawaya, M. R., Cascio, D., Popov, D., Riekel, C., and Eisenberg, D. Atomic Structure of The Cross-Beta Spine of Islet Amyloid Polypeptide (Amylin), *Protein Sci.*, **2008**, *17*,1467-1474.

9. Luca, S., Yau, W. M., Leapman, R., and Tycko, R. Peptide Conformation and Supramolecular Organization in Amylin Fibrils: Constraints From Solid-State NMR, *Biochemistry*, **2007**, *46*,13505-13522.

10. Bedrood, S., Li, Y., Isas, J. M., Hegde, B. G., Baxa, U., Haworth, I. S., and Langen, R. Fibril Structure of Human Islet Amyloid Polypeptide, *J. Biol. Chem.*, **2012**, *287*,5235-5241.

11. Westermark, P., Engstrom, U., Johnson, K. H., Westermark, G. T., and Betsholtz, C. Islet Amyloid Polypeptide Pinpointing Amino Acid Residues Linked to Amyloid Fibril Formation, *PNAS*, **1990**, *87*,5036-5040.

12. Ashburn, T. T., and Lansbury, P. T. Interspecies Sequence Variations Affect the Kinetics and Thermodynamics of Amyloid Formation - Peptide Models of Pancreatic Amyloid, *J. Am. Chem. Soc.*, **1993**, *115*,11012-11013.

13. Betsholtz, C., Christmansson, L., Engstrom, U., Rorsman, F., Svensson, V., Johnson, K. H., and Westermark, P. Sequence Divergence in a Specific Region of Islet Amyloid Polypeptide (Iapp) Explains Differences in Islet Amyloid Formation between Species, *FEBS Lett.*, **1989**, *251*,261-264.

14. Buchanan, L. E., Dunkelberger, E. B., Tran, H. Q., Cheng, P.-N., Chiu, C.-C., Cao, P., Raleigh, D. P., de Pablo, J. J., Nowick, J. S., and Zanni, M. T. Mechanism of IAPP Amyloid Fibril Formation Involves an Intermediate with a Transient Beta-Sheet, *PNAS*, **2013**, *110*,19285-19290.

15. Green, J., Goldsbury, C., Min, T., Sunderji, S., Frey, P., Kistler, J., Cooper, G., and Aebi, U. Full-Length Rat Amylin Forms Fibrils Following Substitution of Single Residues From Human Amylin, *J. Mol. Biol.*, **2003**, *326*,1147-1156.

16. Jha, S., Snell, J. M., Sheftic, S. R., Patil, S. M., Daniels, S. B., Kolling, F. W., and Alexandrescu, A. T. pH Dependence of Amylin Fibrillization, *Biochemistry*, **2014**, *53*,300-310.

17. Hobbs, J. R., and Morgan, A. D. Fluorescence Microscopy with Thioflavine-T in Diagnosis of Amyloid, *J. Pathol. Bacteriol.*, **1963**, *86*,437-&.

18. Levine, H. Thioflavine-T Interaction with Synthetic Alzheimers-Disease Beta-Amyloid Peptides - Detection of Amyloid Aggregation in Solution, *Protein Sci.*, **1993**, *2*,404-410.

19. Sulatskaya, A. I., Maskevich, A. A., Kuznetsova, I. M., Uversky, V. N., and Turoverov, K. K. Fluorescence Quantum Yield of Thioflavin T in Rigid Isotropic Solution and Incorporated Into The Amyloid Fibrils, *PLoS One*, **2010**, *5*,e15385.

20. Wu, C., Wang, Z., Lei, H., Duan, Y., Bowers, M. T., and Shea, J. E. The Binding of Thioflavin T and its Neutral Analog BTA-1 to Protofibrils of the Alzheimer's Disease Abeta(16-22) Peptide Probed by Molecular Dynamics Simulations, *J. Mol. Biol.*, **2008**, *384*,718-729.

21. Wu, C., Biancalana, M., Koide, S., and Shea, J.-E. Binding Modes of Thioflavin-T to the Single-Layer beta-Sheet of the Peptide Self-Assembly Mimics, *J. Mol. Biol.*, **2009**, *394*,627-633.

22. Wu, C., Bowers, M. T., and Shea, J.-E. On the Origin of the Stronger Binding of PIB over Thioflavin T to Protofibrils of the Alzheimer Amyloid-beta Peptide: A Molecular Dynamics Study, *Biophys. J.*, **2011**, *100*,1316-1324.

23. Cloe, A. L., Orgel, J. P. R. O., Sachleben, J. R., Tycko, R., and Meredith, S. C. The Japanese Mutant Abeta (DeltaE22-Abeta(1-39)) Forms Fibrils Instantaneously, with Low-Thioflavin T Fluorescence: Seeding of Wild-Type Abeta(1-40) Into Atypical Fibrils by DeltaE22-Abeta(1-39), *Biochemistry*, **2011**, *50*,2026-2039.

24. Marek, P., Woys, A. M., Sutton, K., Zanni, M. T., and Raleigh, D. P. Efficient Microwave Assisted Synthesis of Human Islet Amyloid Polypeptide Designed to Facilitate The Specific Incorporation of Labeled Amino Acids, *Org. Lett.*, **2010**, *12*,4848-4851.

25. Abedini, A., and Raleigh, D. P. Incorporation of Pseudoproline Derivatives Allows the Facile Synthesis of Human IAPP, A Highly Amyloidogenic and Aggregation-Prone Polypeptide, *Org. Lett.*, **2005**, *7*,693-696.

26. Duan, Y., Wu, C., Chowdhury, S., Lee, M. C., Xiong, G., Zhang, W., Yang, R., Cieplak, P., Luo, R., Lee, T., Caldwell, J., Wang, J., and Kollman, P. A Point-Charge Force Field for Molecular Mechanics Simulations of Proteins Based on Condensed-Phase Quantum Mechanical Calculations, *J. Comput. Chem.*, **2003**, *24*,1999-2012.

27. Gessel, M. M., Wu, C., Li, H., Bitan, G., Shea, J. E., and Bowers, M. T. Abeta(39-42) Modulates Abeta Oligomerization but not Fibril Formation, *Biochemistry*, **2012**, *51*,108-117.

28. Wu, C., Wang, Z., Lei, H., Zhang, W., and Duan, Y. Dual Binding Modes of Congo Red to Amyloid Protofibril Surface Observed in Molecular Dynamics Simulations, *J. Am. Chem. Soc.*, **2007**, *129*,1225-1232.

29. Wu, C., Bowers, M. T., and Shea, J. E. Molecular Structures of Quiescently Grown and Brain-Derived Polymorphic Fibrils of the Alzheimer Amyloid Abeta9-40 Peptide: A Comparison to Agitated Fibrils, *PLoS Comput. Biol.*, **2010**, *6*,e1000693.

30. Jorgensen, W. L., Chandrasekhar, J., Madura, J. D., Impey, R. W., and Klein, M. L. Comparison of Simple Potential Functions for Simulating Liquid Water, *J. Chem. Phys.*, **1983**, *79*,926-935.

31. Wang, J. M., Wolf, R. M., Caldwell, J. W., Kollman, P. A., and Case, D. A. Development and Testing of a General AMBER Force Field, *J. Comput. Chem.*, **2004**, *25*,1157-1174.

32. Essmann, U., Perera, L., Berkowitz, M. L., Darden, T., Lee, H., and Pedersen, L. G. A Smooth Particle Mesh Ewald Method, *J. Chem. Phys.*, **1995**, *103*,8577-8593.

33. Ryckaert, J. P., Ciccotti, G., and Berendsen, H. J. C. Numerical-Integration of Cartesian Equations of Motion of a System with Constraints - Molecular-Dynamics of N-Alkanes, *J. Comput. Phys.*, **1977**, *23*,327-341.

34. Procacci, P., and Berne, B. J. Multiple Time-Scale Methods for Constant-Pressure Molecular-Dynamics Simulations of Molecular-Systems, *Mol. Phys.*, **1994**, *83*,255-272.

35. Chiu, S. W., Clark, M., Subramaniam, S., and Jakobsson, E. Collective Motion Artifacts Arising in Long-Duration Molecular Dynamics Simulations, *J. Comput. Chem.*, **2000**, *21*,121-131.

36. Harvey, S. C., Tan, R. K. Z., and Cheatham, T. E. The Flying Ice Cube: Velocity Rescaling in Molecular Dynamics Leads to Violation of Energy Equipartition, *J. Comput. Chem.*, **1998**, *19*,726-740.

37. Thompson, M. J., Sievers, S. A., Karanicolas, J., Ivanova, M. I., Baker, D., and Eisenberg, D. The 3D Profile Method for Identifying Fibril-Forming Segments of Proteins, *PNAS*, **2006**, *103*,4074-4078.

38. Chakraborty, S., Chatterjee, B., and Basu, S. A Mechanistic Insight into the Amyloidogenic Structure of hIAPP Peptide Revealed From Sequence Analysis and Molecular Dynamics Simulation, *Biophys. Chem.*, **2012**, *168*,1-9.

39. Hamodrakas, S. J., Liappa, C., and Iconomidou, V. A. Consensus Prediction of Amyloidogenic Determinants in Amyloid Fibril-Forming Proteins, *Int. J. Biol. Macromol.*, **2007**, *41*,295-300.

40. Tartaglia, G. G., and Vendruscolo, M. The Zyggregator Method For Pedicting Potein Agregation Propensities, *Chem. Soc. Rev.*, **2008**, *37*,1395-1401.

41. Trovato, A., Seno, F., and Tosatto, S. C. E. The PASTA Server For Protein Aggregation Prediction, *Protein Eng., Des. Sel.*, **2007**, *20*,521-523.

42. Fernandez-Escamilla, A.-M., Rousseau, F., Schymkowitz, J., and Serrano, L. Prediction of Sequence-Dependent And Mutational Effects on the Aggregation of Peptides and Proteins, *Nat. Biotechnol.*, **2004**, *22*,1302-1306.

43. Roland, B. P., Kodali, R., Mishra, R., and Wetzel, R. A Serendipitous Survey of Prediction Algorithms for Amyloidogenicity, *Biopolymers*, **2013**, *100*,780-789.

44. Tu, L.-H., and Raleigh, D. P. Role of Aromatic Interactions in Amyloid Formation by Islet Amyloid Polypeptide, *Biochemistry*, **2013**, *52*,333-342.

45. Moran, S. D., and Zanni, M. T. How to Get Insight into Amyloid Structure and Formation from Infrared Spectroscopy, *J. Phys. Chem. Lett.*, **2014**, *5*,1984-1993.

46. Reddy, A. S., Wang, L., Singh, S., Ling, Y. L., Buchanan, L., Zanni, M. T., Skinner, J. L., and de Pablo, J. J. Stable and Metastable States of Human Amylin in Solution, *Biophys. J.*, **2010**, *99*,2208-2216.

47. Marek, P. J., Patsalo, V., Green, D. F., and Raleigh, D. P. Ionic Strength Effects on Amyloid Formation by Amylin Are a Complicated Interplay among Debye Screening, Ion Selectivity, and Hofmeister Effects, *Biochemistry*, **2012**, *51*,8478-8490.

48. Kodali, R., Williams, A. D., Chemuru, S., and Wetzel, R. A Beta(1-40) Forms Five Distinct Amyloid Structures Whose Beta-Sheet Contents and Fibril Stabilities Are Correlated, *J. Mol. Biol.*, **2010**, *401*,503-517.

49. Lindberg, D. J., Wranne, M. S., Gatty, M. G., Westerlund, F., and Esbjorner, E. K. Steady-State and Time-Resolved Thioflavin-T Fluorescence Can Report on Morphological Differences in Amyloid Fibrils Formed by A Beta(1-40) and A Beta(1-42), *Biochem. Biophys. Res. Commun.*, **2015**, *458*,418-423.

50. Chen, S., Berthelier, V., Hamilton, J. B., O'Nuallain, B., and Wetzel, R. Amyloid-Like Features of Polyglutamine Aggregates and Their Assembly Kinetics, *Biochemistry*, **2002**, *41*,7391-7399.

Chapter 4. Analysis of the Amyloid Sensitivity of Dyes Offer Several Alternatives to the Thioflavin-T Assay For Detecting Amyloid Formation by Islet Amyloid Polypeptide

Abstract

Amyloid deposition underlies a broad range of diseases including multiple neurodegenerative diseases, systemic amyloidosis and type-2 diabetes. Amyloid sensitive dyes, particularly thioflavin-T, are widely used to detect *ex-vivo* amyloid deposits, to monitor amyloid formation *in vitro* and to follow the kinetics of amyloid self-assembly. We show that the dyes SYPRO-orange, 8-anilinonapthalene-1-sulfonic acid (ANS), and 4,4'-dianilino-1,1'-binapthyl-5,5'-disulfonic acid (Bis-ANS) bind to amyloid fibrils formed by human islet amyloid polypeptide (h-IAPP), the polypeptide responsible for islet amyloid formation in type-2 diabetes, while Nile Red, 9-(2,2-dicyanovinyl)julolidine (DCVJ), 4',6-diamidino-2-phenylindole (DAPI), and 1,1'-(4,4,8,8-tetramethyl-4,8-diazaundecamethylene)bis[4-[(3-methylbenzo-1,3-oxazol-2-yl)methylidene]-l,4-dihydroquinolinium] tetraiodide (YOYO-1) do not. No fluorescence enhancement is observed in the presence of pre-fibrillar species for any of the dyes. The kinetics of human IAPP amyloid formation can be monitored by SYPRO-orange, ANS, and Bis-ANS fluorescence assays and match the time course determined with thioflavin-T assays. The dye SYPRO-orange shows specificity to amyloid fibrils of islet amyloid polypeptide and shows no fluorescence enhancement in the presence of non-amyloidogenic rat IAPP. Thus, SYPRO-orange, ANS, and Bis-ANS offer an alternative to the thioflavin-T assay. The implications for the interpretation of SYPRO-orange, ANS, and Bis-ANS assays are discussed.

NOTE: Part of the material presented in this chapter has been published (Amy. G Wong and Daniel P. Raleigh "The Dye SYPRO Orange Binds to IAPP Amyloid Fibrils but Not Pre-fibrillar Intermediates" *Protein Science* **2016,** *25* 1834-1840). This chapter contains direct excerpts from the manuscript, which was written by me with suggestions and revisions from Professor Daniel P. Raleigh.

4.1 Introduction

Amyloid is typically identified via dye binding assays; the classic reagents Congo-red and thioflavin-S are widely used to detect amyloid deposits in tissue. The dye thioflavin-T is the standard probe to follow amyloid formation *in vitro*. Thioflavin-T assays are widely applied, although they can yield false positives in amyloid inhibition assays and there are examples of proteins which form amyloid, but which do not lead to an enhancement of thioflavin-T fluorescence in the fibril state or exhibit very weak fluorescence enhancement [1-4]. Here we demonstrate that the commercially available dye SYPRO-orange, which is widely used in thermal shift assays of stability, is an amyloid sensitive dye.[5] Additionally, we show that 8-anilinonapthalene-1-sulfonic acid (ANS), a dye previously believed to be unsuitable for monitoring formation of amyloid fibrils, and 4,4'-dianilino-1,1'-binapthyl-5,5'-disulfonic acid (Bis-ANS), a dimer analog of ANS, are also amyloid sensitive dyes, at least for amyloid formation by islet amyloid polypeptide (IAPP, amylin). The dyes Nile Red, 9-(2,2-dicyanovinyl)julolidine (DCVJ), 4',6-diamidino-2-phenylindole (DAPI), and YOYO-1 were also examined to determine possible specificity to amyloid fibrils.

SYPRO-orange is a polarity sensitive dye and was first used for post-electrophoretic fluorescence staining of proteins [6, 7]. SYPRO-orange has been used in differential

fluorescence screening (DFS) assays for high throughput thermal shift studies of protein stability and for studies of protein ligand interactions, but there are no reports of the dye binding to amyloids [5, 8-10]. ANS is another polarity sensitive probe that is commonly used to study conformational changes in proteins. The dye was previously believed to not be suitable for amyloid detection assays as it was shown to bind to several pre-amyloid oligomers [11]. However, this dye was later shown to not bind to human islet amyloid polypeptide (h-IAPP) oligomers but instead to mature IAPP amyloid fibrils [12]. Bis-ANS is also a polarity sensitive dye. It is composed of two ANS molecules bonded together. This dye is capable of binding to hydrophobic surfaces of proteins similar to ANS with the advantage of a fluorescence quantum yield that is greater than ANS [13, 14]. Nile Red is a lipophilic dye commonly used for membrane studies [15, 16]. The dye is sensitive to polarity and has a varying fluorescence emission maximum depending on the composition of the lipid membranes being stained [17]. The dye has also previously been shown to bind to the hydrophobic surfaces of proteins and has more recently been shown to bind to several types of amyloid fibrils including transthyretin, Aβ(1-42), and lysozyme amyloid [18-20]. DCVJ is a molecular rotor similar to thioflavin-T and unlike the previously described dyes is sensitive to viscosity rather than polarity [21]. The dye contains a bond between the dicyanovinyl and the julolidine groups and when this bond becomes rigid the fluorescence quantum yield increases (Figure 4-2). DCVJ will also exhibit increased fluorescence intensity when bound in an environment that restricts it motion and this characteristic has been used to monitor the polymerization of tubulin [22]. DCVJ has also been shown to be sensitive to prefibrillar transthyretin oligomers [23]. DAPI is a dye commonly used to stain DNA with affinity specifically towards the adenine and guanine base pairs for the detection of cell apoptosis [24, 25]. Its structure and size allow the dye to fit in the minor groove

of the DNA strand [26]. The structure of DAPI is similar to thioflavin-T and thioflavin-S and thus may also be sensitive to amyloid (Figure 4-2). Lastly, YOYO-1 is also used to stain double-stranded DNA and is used to determine cell viability similar to DAPI [27]. The dye has a low fluorescence quantum yield in solution but the intensity of fluorescence increases upon intercalation to the double-stranded DNA. There are reports that indicate YOYO-1 may be sensitive to amyloid, it has been shown to have the ability to bind to Aβ(1-42) fibrils [28].

Here we show that SYPRO-orange, ANS, and Bis-ANS selectively bind to amyloid fibrils formed by h-IAPP, but not to prefibrillar species. We show SYPRO-orange is unable to bind to non-amyloidogenic rat IAPP (r-IAPP). We also examine Nile Red, DCVJ, DAPI, and YOYO-1 and show that they are not able to bind to any forms of h-IAPP under the conditions of our assays.

4.2 Materials and Methods

4.2.1 Peptide Synthesis and Purification

Peptides were synthesized with a CEM microwave peptide synthesizer on a 0.10 mmol scale utilizing 9-fluorenylmethoxycarbonyl (Fmoc) chemistry. 5-(4'-Fmoc-aminomethyl-3',5-dimethoxyphenol) valeric acid (PAL-PEG) resin was used to provide an amidated C-terminus. Fmoc-protected pseudoproline (oxazolidine) dipeptide derivatives were utilized as previously described [29, 30]. Solvents used were ACS-grade. β-branched residues, the first residue attached to the resin, pseudoproline dipeptide derivatives and the residues following the pseudoproline dipeptide derivatives were double-coupled. Peptides were cleaved from the resin via standard trifluoroacetic acid (TFA) methods. The cleaved crude peptides were dissolved into 15% (v/v) acetic acid and lyophilized. The disulfide bond was formed in 100% dimethyl

sulfoxide at room temperature over a period of three days. Peptides were purified via reverse-phase high-performance liquid chromatography (RP-HPLC) using a Higgins Analytical Proto 300 C18 preparative column (10 mm x 250 mm). A 25 – 65% B gradient was used over a period of 40 minutes where Bufer A was 100% H_2O, 0.045 % HCl and Buffer B was 80% acetonitrile, 0.045% HCl. h-IAPP had a retention time of 25 minutes (50% B) and r-IAPP had a retention time of 21 minutes (46% B). The purity of the peptides was tested using analytical HPLC. The masses of the pure peptides were confirmed with MALDI time-of-flight mass spectrometry. h-IAPP, expected 3903.6, observed 3902.9; r-IAPP, expected 3918.0, observed 3918.4.

4.2.2 Sample Preparation and Fluorescence Emission Scans

Stock solutions were prepared by dissolving peptide into 100% hexafluoroisopropanol (HFIP) at 1.6 mM. Solutions were filtered with 0.45 μM Acrodisc syringe filters and the required amount was lyophilized overnight to remove HFIP. Dry peptide was then dissolved into tris buffer for the fluorescence assays. Fluorescence measurements were performed using an Applied Photon Technology fluorescence spectrophotometer. SYPRO-orange emission scans were collected using an excitation wavelength of 490 nm and emission wavelengths from 520 – 695 nm with a slit width of 15 nm. ANS emission scans were collected using an excitation of 370 nm and emission wavelengths from 400-600 nm with a slit width of 10 nm. Bis-ANS emission scans were collected using an excitation wavelength of 385 nm and emission wavelengths from 425-600 nm with a slit width of 10 nm. Nile Red emission scans were collected using an excitation wavelength of 552 nm and emission wavelengths from 580 – 750 nm with a slit width of 10 nm. DCVJ emission scans were collected using an excitation wavelength of 450 nm and emission wavelengths from 500 – 650 nm with an 8 nm slit width. DAPI emission scans were collected using an excitation wavelength of 350 nm and emission wavelengths from 420 – 510 nm with a 4

nm slit width. YOYO-1 emission scans were collected using an excitation wavelength of 400 nm and emission wavelengths from 500 – 600 nm with an 8 nm slit width. Monomers, oligomers, and fibrils were produced by incubating human IAPP. Measurements were made at several time points; immediately after dissolving the peptides, in the middle of the lag phase (as defined by thioflavin-T assays), and after amyloid formation was complete.

4.2.3 Fluorescence Assays

The kinetics of amyloid formation was monitored using thioflavin-T, SYPRO-orange, ANS, Bis-ANS, and Nile Red assays conducted at 25 °C. The final concentration of the fluorescence assays was 16 μM peptide, 32 μM thioflavin-T, or SYPRO-orange diluted 4000-fold from the supplied stock solution, or 4 μM ANS, or 4 μM Bis ANS, or 4 μM Nile Red in 20 mM tris buffer at pH 7.4. The concentration of commercially supplied SYPRO-orange is not given in the product literature, but is supplied as a 5000x solution in DMSO. Thioflavin-T experiments were monitored using an excitation wavelength of 450 nm and an emission wavelength of 485 nm. SYPRO-orange experiments were recorded using an excitation wavelength of 490 nm and emission wavelength of 594 nm. ANS experiments were monitored using an excitation wavelength of 370 nm and an emission wavelength of 500 nm. Bis-ANS experiments were monitored using an excitation wavelength of 385 nm and an emission wavelength of 495 nm. Nile Red experiments were monitored using an excitation wavelength of 552 nm and an emission wavelength of 650 nm. A slit width of 8 nm was used for the thioflavin-T and Bis-ANS assays and 10 nm was used for and SYPRO-orange, ANS, and Nile Red experiments. A 3 mm cuvette was used for all assays. Each point was averaged over a period of 2 minutes.

4.2.4 Transmission Electron Microscopy

TEM images were collected at the Life Science Microscopy Center at the State University of New York at Stony Brook. At the end of each experiment, 15 μL aliquots of the samples used for the kinetic studies were removed, blotted on a carbon-coated 300-mesh copper grid for 1 min and then negatively stained with saturated uranyl acetate for 1 min.

4.3 Results and Discussions

4.3.1 LC-MS Analysis Reveal the Purity and Structure of the SYPRO Orange Dye

The molecular structure of SYPRO-orange has not been reported in the literature, but it is a merocyanine based dye and the patent literature lists a variety of structures in this class of dye [7]. We first conducted LC-MS analysis of the commercially available dye to test its purity and to examine which members of this class of compounds might make up the marketed form of the dye (Figure 4-3). Analysis of the LC trace suggests the dye is on the order of 95 % pure. The observed m/z (486.3) is consistent with the structure shown in Figure-1.

4.3.2 Emission Spectra of the Dyes in the Presence of Human IAPP Fibrils Reveal if Binding is Taking Place

We recorded fluorescence emission spectra of each of the dyes in the presence of freshly resuspended h-IAPP amyloid monomers as well as prefibrillar intermediates and fibrils (Figure 4-4A – 4-4F). Emission scans containing h-IAPP in its monomer form were collected in the presence of each at t = 0. Emission scans containing h-IAPP in oligomer form were collected in the presence of each dye after h-IAPP had incubated on the bench for 24 hours which corresponds to the middle of the lag phase. Emission scans containing h-IAPP amyloid fibrils were collected in the presence of each dye after h-IAPP had incubated on the bench for at least 90 hours corresponding to the final plateau of amyloid formation by h-IAPP. A significant

increase in fluorescence intensity of the SYPRO-orange, 6-fold, is observed when h-IAPP amyloid fibrils are present. There is a shift in emission maxima of the dye in the presence of h-IAPP relative to the dye by itself going from 610 nm to 590 nm when bound to h-IAPP fibrils. These studies were conducted using 16 μM h-IAPP, in monomer units. The concentration of commercially supplied SYPRO-orange is not given in the product literature, but is supplied as a 5000x solution in pure DMSO. This solution was diluted 4000-fold for the studies that collected the data displayed in Figure 4-4A.

We performed additional experiments in the presence of h-IAPP fibrils (16 μm in monomer units) using a range of different dye concentrations (Figure 4-5). A net 8,000 fold dilution of the commercially supplied dye solution was examined. When the solution was diluted 8,000-fold it showed a 3-fold higher fluorescence in the presence of h-IAPP amyloid fibrils relative to h-IAPP monomers. When the solution was diluted 1000-fold, the dye only showed a 2-fold increase in fluorescence in the presence of fibrils relative to h-IAPP monomers. A 4000-fold dilution showed the greatest fluorescence gain with a 4-fold increase in fluorescence in the presence of fibrils relative to h-IAPP monomers. The concentration of dye molecules present in the solution is unknown, thus it is not possible to determine the ratio of fibrils to SYPRO-orange. The origin of the modest decrease in dye fluorescence at higher concentration is unknown, but there may be contributions from self-quenching at higher concentrations. Additionally, the dye may be aggregating when it is present in solution in higher concentrations. From a purely practical perspective, the experiment provides guidance on appropriate dilutions of the commercially supplied dye to use in h-IAPP amyloid assays.

We repeated this experiment with the other dyes. A significant fluorescence enhancement of ANS and Bis-ANS was observed in the presence of h-IAPP amyloid fibrils while no such

enhancement was observed in the presence of monomers and oligomers. The concentration of ANS and Bis-ANS was 4 μM for the studies displayed in Figure 4-4B and Figure 4-4C. Bis-ANS was found to have a higher fluorescence enhancement in the presence of h-IAPP fibrils and higher sensitivity than the ANS experiments. The Bis-ANS exhibited a 9-fold fluorescence signal increase in the presence of h-IAPP fibrils relative to monomers while the ANS only exhibited a 7-fold fluorescence increase in the presence of h-IAPP fibrils relative to monomers. A blue shift is evident for both ANS and Bis-ANS in the presence of h-IAPP fibrils, from 510 nm to 485 nm for ANS and 525 nm down to 495 nm for Bis-ANS, relative to dye by itself. Nile Red, DCVJ, and DAPI were also tested and the dyes did not show any increase in fluorescence intensity in the presence of h-IAPP monomers, oligomers, or amyloid fibrils (Figures 4-4D – 4-4F). The maximum emission for Nile Red and DAPI are also unchanged in the presence of h-IAPP monomers, oligomers, or amyloid fibrils. The emission maxima for Nile Red, and DAPI was 650 nm and 455 nm respectively. The max emission of DCVJ in the presence of h-IAPP fibrils was blue shifted from 610 nm to 595 nm in relation to max emission of the dye itself.

4.3.3 DAPI is Sensitive to Experimental Conditions

DAPI is typically applied directly to tissue samples in the form of a saturated stain in order to visualize DNA in cell nuclei. In order to determine if buffer conditions were quenching the dye, we measured the fluorescence of DAPI in the presence of increasing amounts of DMSO. At low concentrations of DMSO, the fluorescence of the dye is minor. However, as the concentration of DMSO increases, the overall fluorescence intensity does as well (Figure 4-6). When the concentration of DMSO is increased from 10 % to 100% we observe a 30-fold increase in fluorescence quantum yield. The chemical structure of DAPI is similar to thioflavin-T (Figure 4-2). It contains a flexible bond between its two moieties similar to the bond between the

benzothiazole and aminobenzene ring of thioflavin-T. DMSO is more viscous than water. This would cause that bond to become fixed in a more rigid position relative to the bond's flexibility in buffer solution and result in an increased fluorescence quantum yield (Figure 4-2). Thioflavin-T is mildly sensitive to polarity. Its absorption maxima is affected by polarity [31]. Since the chemical structure of DAPI is similar to the chemical structure of thioflavin-T, DAPI may also be sensitive to polarity and so polarity effects may also play a role in its behavior in the different solvent. These results likely indicate that the dye is not binding to amyloid fibrils, or that it is being quenched by the buffer solutions, or both.

4.3.4 YOYO-1 Exhibits Different Behavior at Different Concentrations

We recorded emission scans of the YOYO-1 dye in the presence of h-IAPP monomers, oligomers, and fibrils. These studies were conducted using 16 μM h-IAPP, in monomer units. Two concentrations of the YOYO-1 dye were used: 0.53 μM, which is 30-fold less than h-IAPP monomer concentration, and 32 μM which is twice the concentration of h-IAPP monomers. The lower concentration was selected because previous work with the Aβ(1-42) peptide indicated that when the dye was added at concentrations much lower than Aβ(1-42), it resulted in greater signal enhancement. 32 μM was chosen because it the concentration used for thioflavin-T assays and also to determine the effects of using a higher concentration of the dye than h-IAPP. No significant increase in fluorescence intensity of the YOYO-1 dye was observed when h-IAPP, monomers, oligomers, or amyloid fibrils were present at both concentrations used (Figure 4-7). However, the emission maxima at each concentration are different. The emission maximum at the higher concentration of YOYO-1 was about 550 nm in the presence of h-IAPP monomers, oligomers, and fibrils (Figure 4-7A). At the lower concentration of the dye, the emission maximum was about 515 nm in the presence of h-IAPP monomers, oligomers, and fibrils (Figure

4-7B). Interestingly, the emission maximum of the dye alone at both 32 μM and 0.53 μM was 550 nm indicating that a blue shift is occurring when smaller amounts of the dye are in the presence of h-IAPP monomers, oligomers, and amyloid fibrils. Though there is no fluorescence enhancement, YOYO-1 may be binding to h-IAPP.

4.3.5 SYPRO Orange, ANS, and Bis-ANS Can Be Used to Follow the Time Course of h-IAPP Amyloid Formation While Nile Red Can Not

The observation that SYPRO-orange, ANS, and Bis-ANS experience a large increase in fluorescence intensity in the presence of h-IAPP amyloid fibrils, but not in the presence of prefibrillar species, suggest that these dyes could be used to follow the time course of amyloid formation by h-IAPP in a fashion similar to thioflavin-T assays. Two basic requirements need to be met if an extrinsic agent is to be used to follow amyloid formation: First, the dye should not exhibit a significant signal enhancement in the presence of monomers or pre-fibril oligomers and secondly, the dye should not perturb the kinetics of amyloid formation. We conducted side by side assays of amyloid formation by h-IAPP using thioflavin-T, SYPRO-orange, ANS, and Bis-ANS. Nile Red was also examined though it did not show an increase in fluorescence intensity in the presence of h-IAPP monomers, oligomers, or amyloid fibrils. The experiments were conducted using 16 μM h-IAPP and 32 uM thioflavin-T or a 4000-fold dilution of the commercially supplied solution of SYPRO-orange, or 4 μM ANS, or 4 μM Bis ANS, or 4 μM Nile Red. Thioflavin-T is known to not perturb the kinetics of h-IAPP amyloid formation when added at this concentration [32]. A typical thioflavin-T time course is observed for the h-IAPP; a lag phase followed by a growth phase leading to a final plateau (Figure-3A). Similar results are observed when SYPRO-orange, ANS, and Bis-ANS are used. No detectable change in fluorescence is observed during the lag phase, but an increase in fluorescence is detected in the

growth phase which displays the same time course as that detected in the thioflavin-T assay (Figure 4-8A). No change in Nile Red fluorescence was observed over the entire course of the experiment. The SYPRO-orange, ANS, and Bis-ANS fluorescence reach a plateau at the same time as the thioflavin-T fluorescence. T_{50}, the time required to achieve 50 % of the fluorescence change in an assay is often used to characterize the time frame of amyloid formation. The t_{50} for the thioflavin-T assay is 53 ± 3.3 hours, 53 ± 2.9 hours for the SYPRO-orange assay, 49 ± 3.5 hours for the ANS assay, and 49 ± 1.2 hours for the Bis-ANS assay under the conditions of these experiments. There was no change in fluorescence of the Nile Red assays during the course of the experiment. To within the experimental precision, the values of T_{50} are identical, indicating that SYPRO-orange, ANS, and Bis-ANS do not perturb the kinetics of h-IAPP amyloid formation under these conditions. We also recorded transmission electron microscopy (TEM) of the products of the reactions. In both cases, dense mats of amyloid fibrils were observed (Figure 4-8B). No detectable differences were observed in the images of the SYPRO-orange, ANS, Bis-ANS and thioflavin-T containing samples. These experiments indicate that SYPRO-orange, ANS, and Bis-ANS can be used to monitor the kinetics of h-IAPP amyloid formation and demonstrates that these dyed do not perturb the morphology of the resulting fibrils, at least at the level that can be detected by TEM. However, Nile Red cannot be used to monitor the kinetics of h-IAPP.

4.3.6 SYPRO Orange is Specific to h-IAPP Amyloid

As a further test of the specificity of the dye for amyloid, we examined the fluorescence of SYPRO-orange in the presence of r-IAPP (Figure 4-9A). Rats and mice do not form islet amyloid *in vivo* and the rat/mouse IAPP polypeptide is non-amyloidogenic in solution although it can form low order oligomers [33]. The different behavior of the hormone is due to the six

substitutions in the rat sequence relative to the human sequence (Figure 4-1). These include three prolines in the rat/mouse sequence and a His-18 to Arg replacement; collectively these substitutions reduce the ability of r-IAPP to form amyloid [30, 34-36]. Thus, the rat polypeptide provides a useful negative control. No change in SYPRO-orange fluorescence is observed when r-IAPP is incubated with the dye and TEM confirms the absence of amyloid fibrils (Figure 4-9B). The experiment provides excellent additional evidence that SYPRO-orange does not bind to non-amyloidogenic forms of IAPP.

4.3.7 Rifampicin Interferes with SYPRO Orange, ANS, and Bis ANS Assay of Amyloid Formation by h-IAPP Amyloid Fibrils and Quenches Fluorescence

Thioflavin-T assays are widely employed to search for inhibitors of amyloid formation, but can be compromised by inner filter effects due to the putative inhibitor and because the compound of interest may displace thioflavin-T from the amyloid fibrils. Inner filter effects depend on the fluorescence properties of the compounds being screened.[37] The dyes used here have different excitation and emission maxima (Table 4-1). These differences indicate that SYPRO-orange, ANS, or Bis-ANS may be useful when thioflavin-T assays suffer from inner filter effects. The excitation maxima of ANS and Bis-ANS (370 and 385 nm respectively) significantly different from thioflavin-T and SYPRO-orange while the emission maxima of ANS and Bis-ANS (500 and 495 nm respectively are relatively close to thioflavin-T while the emission maximum for SYPRO-orange is substantially different (Table 4-1). The different characteristics of each dye could be useful when the absorbance spectrum of a putative inhibitor overlaps the emission of thioflavin-T. An absorbance spectrum was collected of SYPRO-orange which indicates that this dye absorbs strongly at 450 nm (Figure 4-10). However, the question still remains if SYPRO-orange, ANS, or Bis-ANS can be used in inhibitor assays when false

negatives are a concern because the compounds being tested either displace bound thioflavin-T from amyloid fibrils or quench the fluorescence of the bound thioflavin-T. Consequently, we examined the effect of a compound which is known to interfere with thioflavin-T assays. Early work, based on thioflavin-T assays, lead to the conclusion that rifampicin is an inhibitor of amyloid formation by h-IAPP. However, subsequent studies showed that it was not and instead showed that rifampicin interferes with thioflavin-T assays [3].

We conducted side by side assays using thioflavin-T, SYPRO-orange, ANS, and Bis-ANS. The experiments were conducted using 16 μM h-IAPP, 32 μM thioflavin-T, or a 4000-fold dilution of the SYPRO-orange, or 4 μM ANS, or 4 μM Bis ANS. A typical sigmoidal curve was observed indicating that formation of amyloid fibrils had occurred. After 90 hours, rifampicin was then added to a final concentration of 8 μM (Figure 4-11A). After addition, a rapid and drastic decrease in the fluorescence of the thioflavin-T dye was observed. A similar effect was observed with the SYPRO-orange, ANS, and Bis-ANS assays (Figure 4-11A). We also recorded TEM images before and after the addition of the rifampicin (Figure 4-11B and 4-11C). Dense mats of h-IAPP amyloid fibrils were evident for both samples before and after addition of rifampicin and no detectable differences in the fibril morphology were apparent after addition of rifampicin. These experiments indicate that SYPRO-orange, ANS, and Bis-ANS are subject to the same complications as thioflavin-T. The exact reason for the loss of fluorescence in each of the assays in the presence of rifampicin is not known. It is possible that rifampicin binds competitively with thioflavin-T, SYPRO-orange, ANS, and Bis-ANS. If true, this would suggest that the all of the dyes bind to amyloid fibrils in a similar fashion. It is also possible that rifampicin quenches the fluorescence of these dyes. Irrespective of the mechanism, the key

observation is that caution should be employed when conducting inhibitor assays with thioflavin-T, SYPRO-orange, ANS, Bis-ANS, or any other dye.

4.4 Conclusions

The data presented here demonstrates that SYPRO-orange, ANS, and Bis-ANS can bind to IAPP amyloid fibrils. The ability to bind to IAPP amyloid fibrils while not binding to monomers or oligomers or non-amyloidogenic forms of IAPP indicates that all three of these dyes can be used as an alternative to thioflavin-T. The fact that these dyes do not bind to h-IAPP lag phase intermediates also provides biophysical information on the h-IAPP oligomers. SYPRO-orange, ANS, and Bis-ANS are all polarity-sensitive dyes and the lack of fluorescence during the lag phase indicates that oligomers do not have the necessary characteristics, i.e. suitable persistent hydrophobic patches, to bind to these dyes. These results are consistent with previous studies performed with ANS and Bis-ANS [12]. ANS has previously been shown to bind to pre-amyloid oligomers formed by a wide variety of proteins but not to those formed by h-IAPP.[11, 38-40] ANS does however, bind to h-IAPP amyloid fibrils. The results here are in agreement with previous findings [12, 41].

The ability of SYPRO-orange to bind to h-IAPP amyloid fibrils is a potential factor to consider when interpreting thermal shift assays or when using the dye to screen stability of libraries of mutant proteins. In most cases, the dye is assumed to bind to relatively unordered aggregates that can be populated upon thermal denaturation; the data presented here shows that the dye can also bind to ordered cross-β structures. In most cases this effect should not diminish the utility of the dye in other applications, but it may impact the analysis if the structure of the unfolded aggregate is of interest. Though DCVJ is a molecular rotor, similar to thioflavin-T, it

was not able to bind to h-IAPP monomer, oligomers, or amyloid fibrils. Nile Red and DAPI were also found to not be suitable for monitoring h-IAPP amyloid fibril formation. DAPI was sensitive to experimental conditions, exhibiting low fluorescence in buffer, but very high fluorescence in DMSO. DAPI is commonly used as a concentrated stain that is directly applied to tissues in order to bind to DNA in cell nuclei, it is possible the concentrations used in this study are not sufficient to appreciably bind to amyloid fibrils and exhibit an increased fluorescence signal. The results here indicate that this dye is not suitable for use in buffer conditions where toxicity and perturbation of the kinetics is a concern. Fluorescence emission scans did not show any enhancement when YOYO-1 was in the presence of h-IAPP amyloid fibrils. However in the presence of h-IAPP amyloid fibrils, the dye showed a blue shift at low concentrations relative to measurements taken at higher concentrations as well as low concentrations of the dye alone. This indicates that the dye may be binding to h-IAPP amyloid fibrils. In the presence of h-IAPP amyloid fibrils, the dye at the lower concentration has a similar emission maximum as it does when bound to Aβ(1-42)[28]. This blue shift was also evident in the presence of h-IAPP monomers and oligomers. The dye exhibited the highest fluorescence in the presence of h-IAPP monomers; however the difference was negligible across all h-IAPP species tested.

All the dyes tested showed an immediate drop in fluorescence upon the addition of rifampicin. The differences in excitation and emission maxima are substantial enough that the lower fluorescence is likely not a result of inner filter effects. It is possible that the inhibitor displaces the dye resulting in a loss of fluorescence quantum yield. These results provide a cautionary tale when working with small molecules. A secondary method should always be used to confirm fibril formation.

4.5 Figures

Figure 4-1: Sequence of human and rat IAPP. Residues in rat IAPP which differ from human IAPP are colored red.

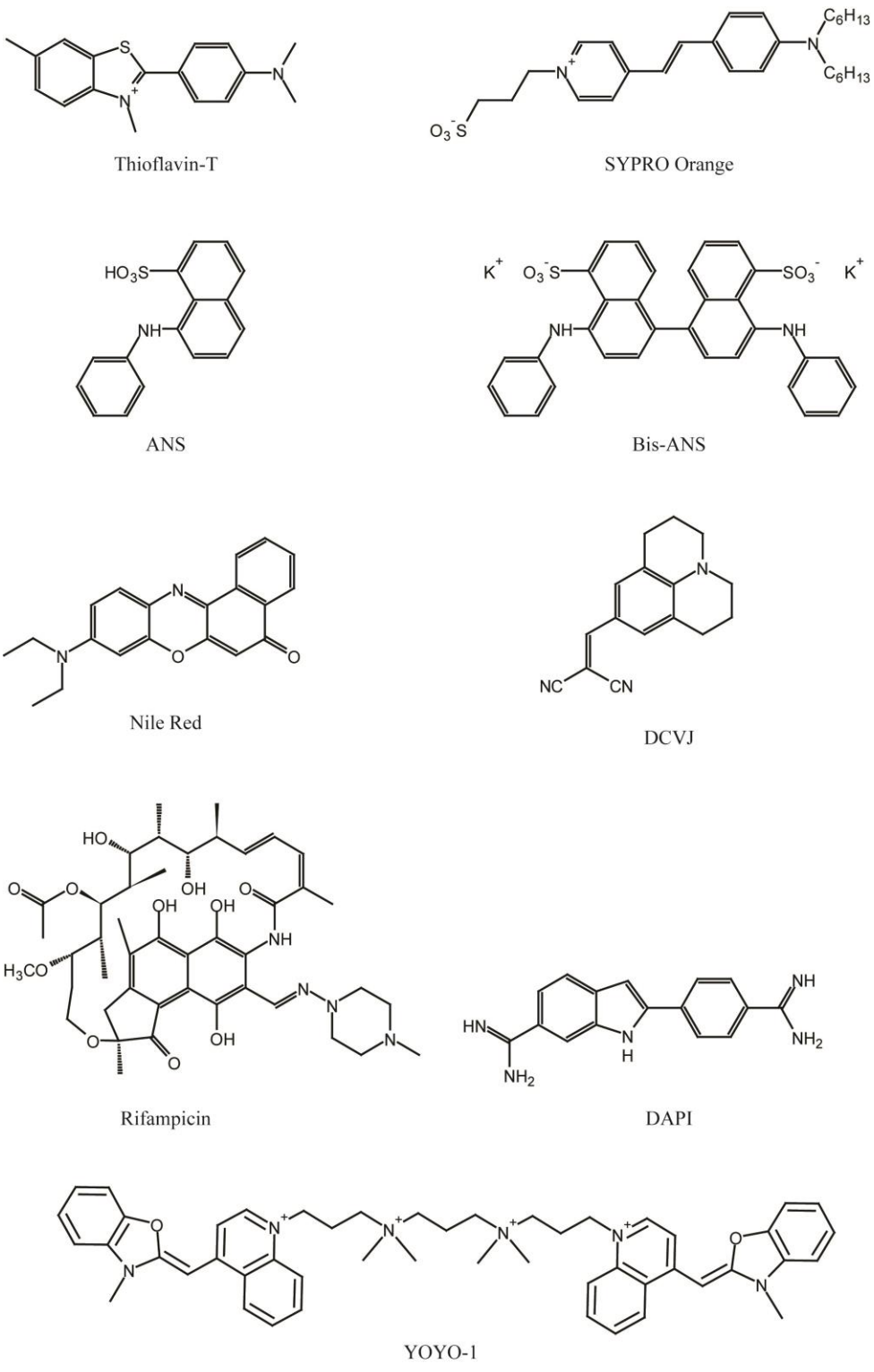

Figure 4-2: Chemical structures of the dyes used, rifampicin and the proposed chemical structure of SYPRO-orange. This structure best agrees with the patent and the LC-MS data.

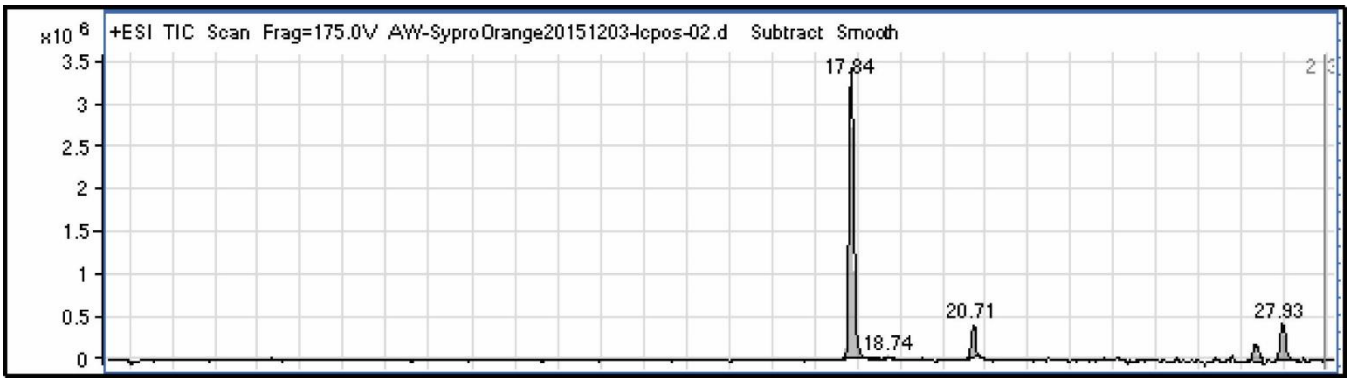

Figure 4-3: LC-MS of SYPRO-orange. The LC trace is shown. A 50-95% buffer B gradient was used over a period of 22.5 minutes immediately followed by a 95-97% buffer B gradient over a period of 4.5 minutes where Buffer A was H_2O and Buffer B was 100% methanol. The SYPRO-orange had a retention time corresponding to 17.84 minutes (83.7% B) and an m/z of 486.3.

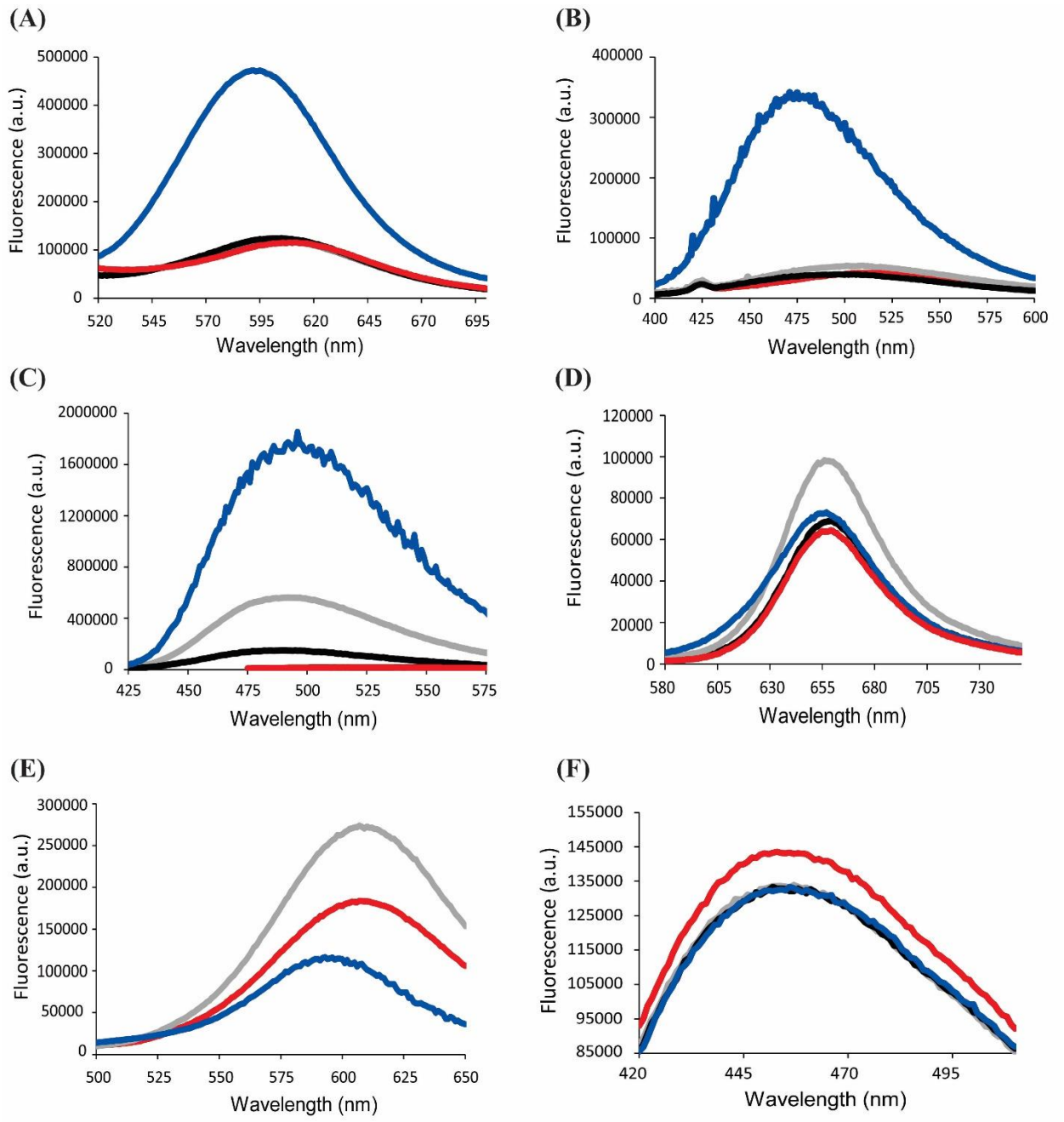

Figure 4-4: Emission spectra of the dyes in the presence of h-IAPP monomers (grey), oligomers (black), fibrils (blue) and the dye alone (red). (A) Emission spectra of SYPRO Orange. (B) Emission spectra of ANS. (C) Emission spectra of Bis-ANS. (D) Emission spectra of Nile Red. (E) Emission spectra of DCVJ. (F) Emission spectra of DAPI. Experiments were conducted with 16 µM human IAPP, SYPRO-orange diluted 4000-fold from the supplied stock solution or 16

μM ANS, or 4 μM Bis-ANS, or 4 μM Nile Red, or 16 μM DCVJ, or 32 μM DAPI at 25 °C in 20 mM tris-HCl at pH 7.4.

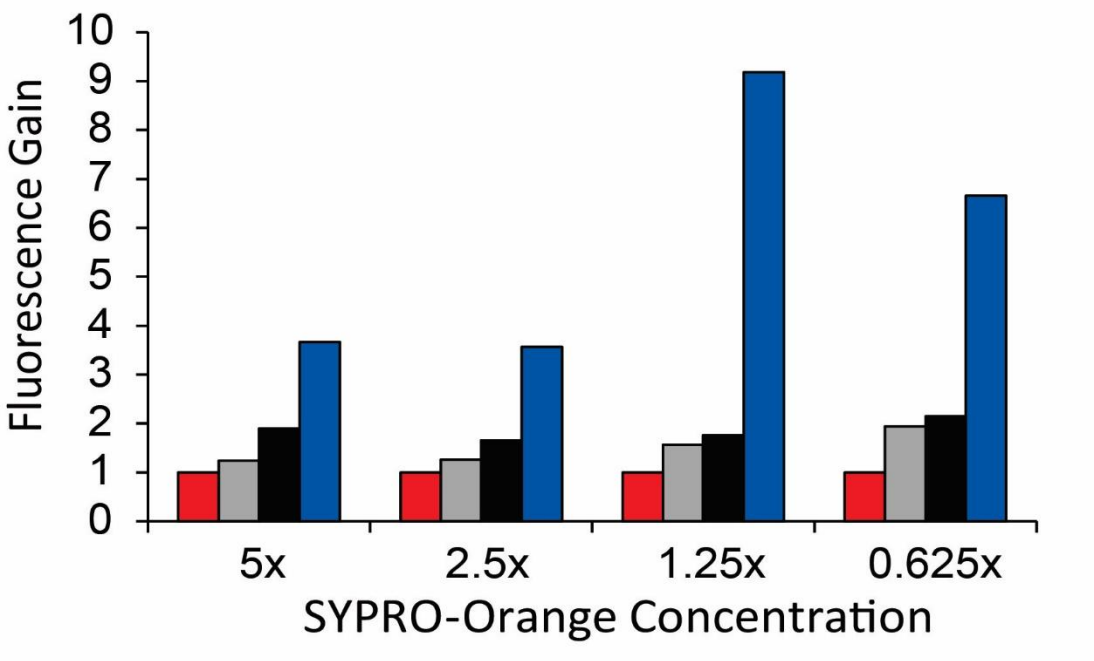

Figure 4-5: Plot of the absolute fluorescence intensity of different concentrations of SYPRO-orange in the presence of h-IAPP monomers (grey), oligomers (black), fibrils (blue) and the dye alone (red). SYPRO Orange is commercially supplied as a "5000x" concentrated solution in DMSO. Fluorescence was measured for samples containing the dye at concentrations ranging from a 1,000-fold dilution (a "5x" solution) to an 80,000-fold dilution (a "0.625x" solution) in the presence of h-IAPP fibrils (16 μM in monomer units). Experiments were conducted at pH 7.4 in 20 mM Tris, 25 ^{o}C.

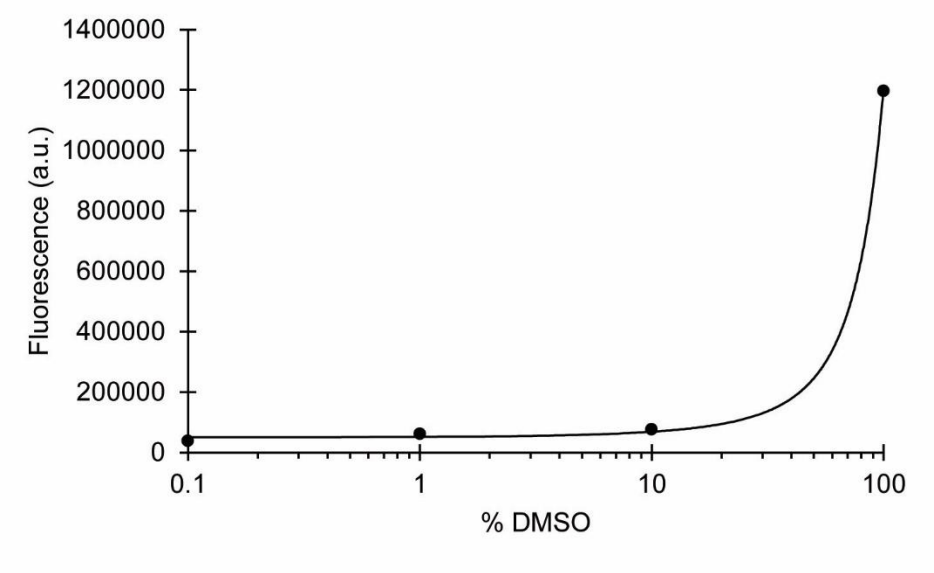

Figure 4-6: Plot of the fluorescence intensity of DAPI in the presence of increasing amounts of DMSO. Fluorescence was measured for samples containing the dye at concentrations at 8 µM concentration. Experiments were conducted at pH 7.4 in 20 mM Tris, 25 ^{o}C. Percent DMSO is plotted in log scale.

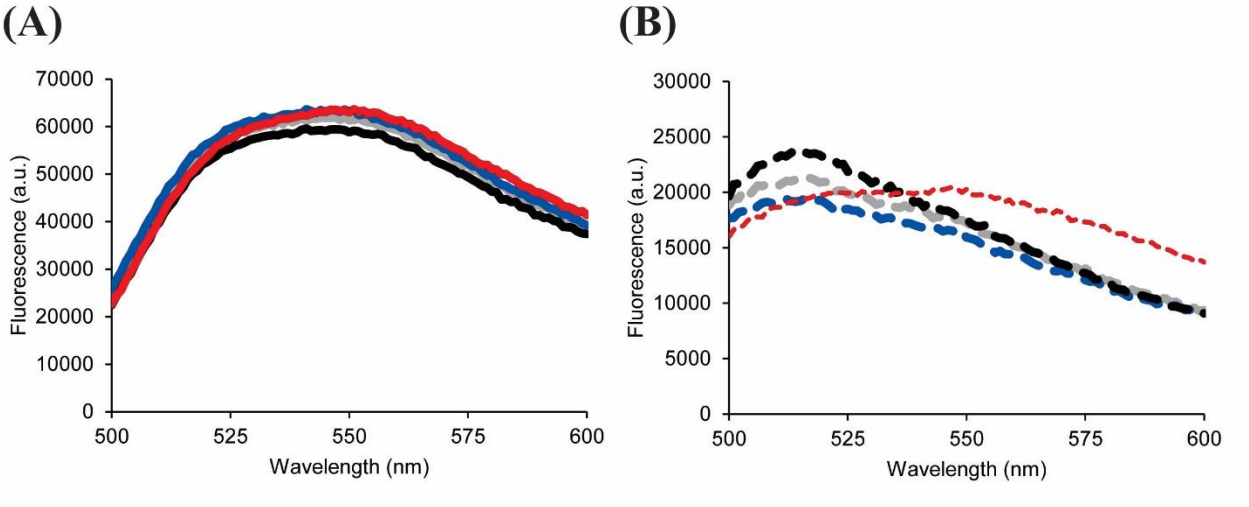

Figure 4-7: Emission spectra of the dye YOYO-1 in the presence of h-IAPP monomers (grey), oligomers (black), fibrils (blue) and the dye alone (red). (A) Emission spectra of 32 µM YOYO-1. (B) Emission spectra of 0.53 µM YOYO-1.

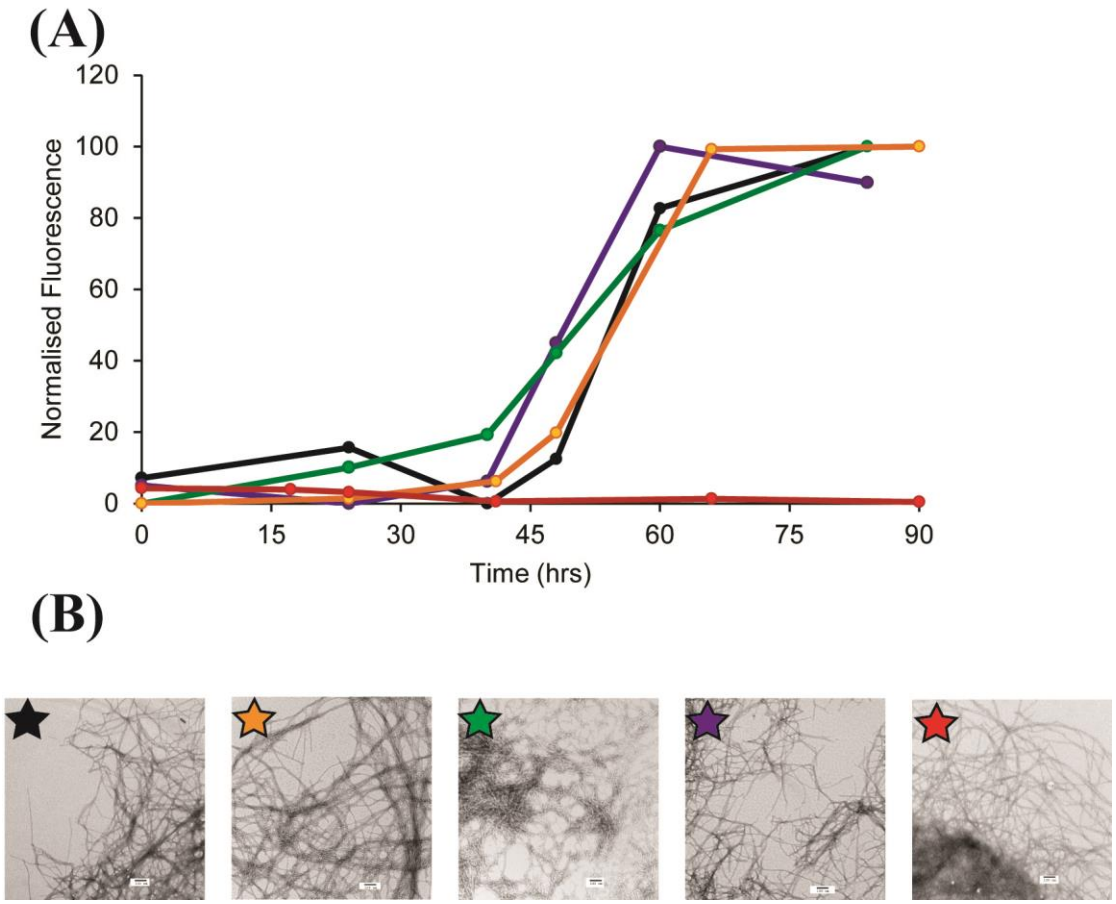

Figure 4-8: (A) Analysis of amyloid formation by human IAPP using thioflavin-T (black), SYPRO-orange (orange), ANS (green), Bis-ANS (purple), and Nile Red (red) as the fluorescent dye. (B) TEM images of samples of human IAPP amyloid fibrils formed in the presence of thioflavin-T (black), SYPRO-orange (orange), ANS (green), Bis-ANS (purple), and Nile Red (red). Scale bars represent 100 nm. Experiments were conducted with 16 μM h-IAPP, 32 μM thioflavin-T, or SYPRO-orange diluted 4000-fold from the supplied stock solution, or 4 μM ANS, or 4 μM Bis ANS, or 4 μM Nile Red at 25 °C in 20 mM tris-HCl at pH 7.4.

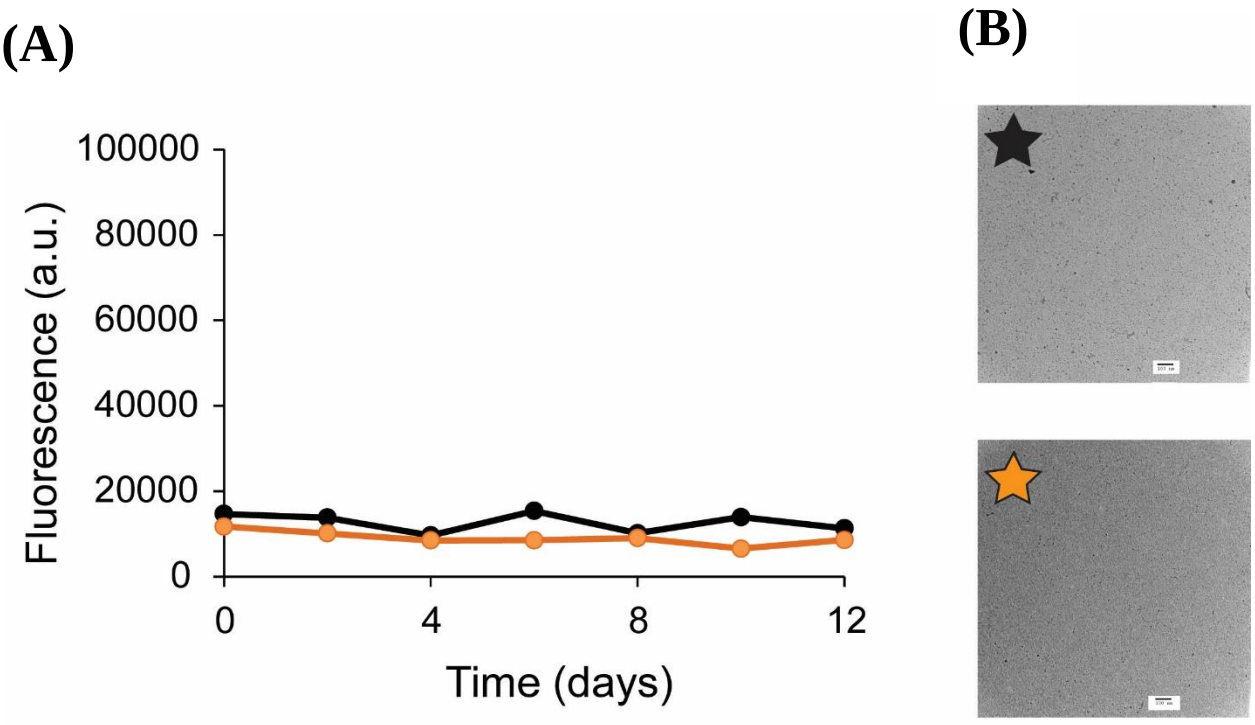

Figure 4-9: (A) Analysis of r-IAPP using thioflavin-T (black) and SYPRO-orange (orange) as the fluorescent dye. (B) TEM images of samples of rat IAPP in the presence of thioflavin-T (black) and SYPRO-orange (orange). Scale bars represent 100 nm. Experiments were conducted with 16 µM rat IAPP, 32 µM thioflavin-T, SYPRO-orange diluted 4000-fold from the supplied stock solution at 25 °C in 20 mM tris-HCl at pH 7.4. Samples were collected for TEM after sample had incubated on the bench for 12 days.

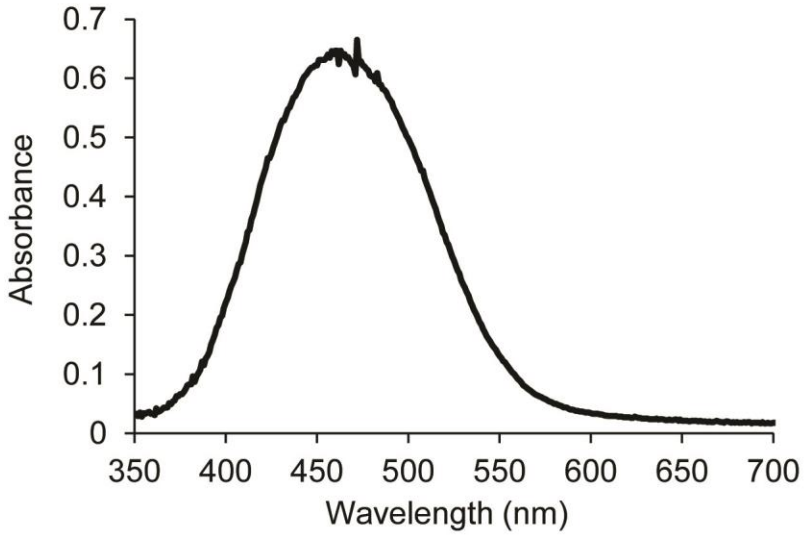

Figure 4-10: Absorbance spectrum of SYPRO-orange. Experiment were conducted with SYPRO-orange diluted 400-fold from the supplied stock solution at 25 °C in 20 mM tris-HCl at pH 7.4.

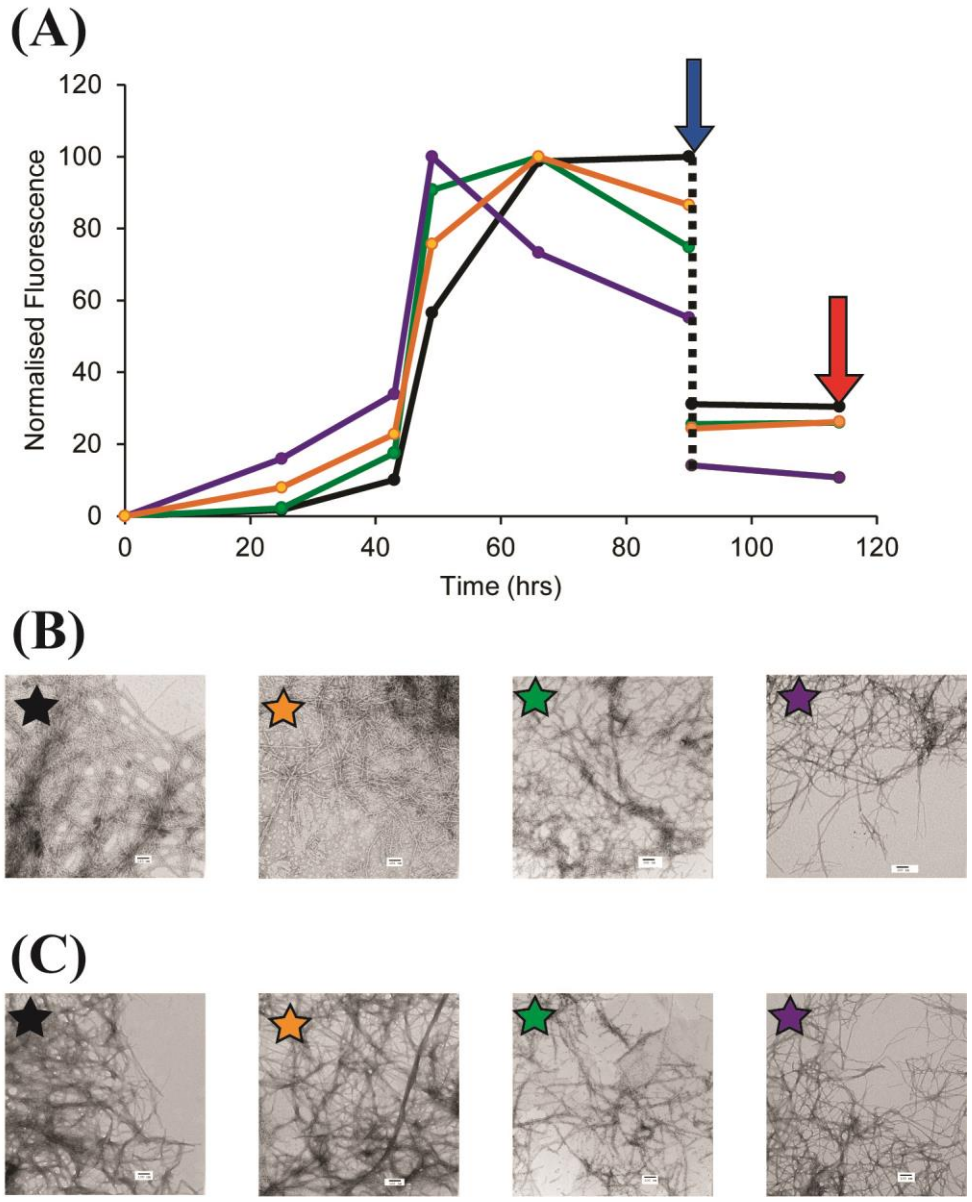

Figure 4-11: (A) Analysis of thioflavin-T (black), SYPRO-orange (orange), ANS (green) and Bis-ANS (purple) fluorescence in the presence of h-IAPP and rifampicin. (B) TEM images of human IAPP samples in the presence of thioflavin-T (black), SYPRO-orange (orange), ANS (green), and Bis-ANS (purple) before the addition of rifampicin. Aliquots for TEM were removed at 90 hours, denoted by the blue arrow. (C) TEM images of human IAPP samples in the presence of thioflavin-T (black), SYPRO-orange (orange), ANS (brown) and Bis-ANS (purple) after the addition of rifampicin. Scale bars represent 100 nm. Aliquots for TEM were removed at

114 hours denoted by the red arrow. Experiments were conducted with 16 μM human IAPP, 32 μM thioflavin-T, SYPRO-orange diluted 4000-fold from the supplied stock solution, or 4 μM ANS, or 4 μM Bis ANS at 25 °C in 20 mM tris-HCl at pH 7.4. After 90 hours, rifampicin was added for a final concentration of 8 μM rifampicin and 1 % DMSO.

4.6 Tables

Fluorescent Dye	Excitation Wavelength (nm)	Emission Wavelength (nm)
Thioflavin-T	450	485
SYPRO Orange	490	594
ANS	370	500
Bis-ANS	385	495
Nile Red	552	650
DCVJ	450	595
DAPI	350	455
YOYO-1	400	515 (low) / 550 (high)

Table 4-1: Excitation and emission maxima of all dyes examined. The two emission maxima for YOYO-1 correspond to 0.53 μM (low concentration) and 32 μM (high concentration).

4.7 References

1. Wong, A. G., Wu, C., Hannaberry, E., Watson, M. D., Shea, J. E., and Raleigh, D. P. Analysis of the Amyloidogenic Potential of Pufferfish (Takifugu rubripes) Islet Amyloid Polypeptide Highlights the Limitations of Thioflavin-T Assays and the Difficulties in Defining Amyloidogenicity, *Biochemistry*, 2016, *55*,510-518.

2. Cloe, A. L., Orgel, J. P. R. O., Sachleben, J. R., Tycko, R., and Meredith, S. C. The Japanese Mutant Abeta (DeltaE22-Abeta(1-39)) Forms Fibrils Instantaneously, with Low-Thioflavin T Fluorescence: Seeding of Wild-Type Abeta(1-40) Into Atypical Fibrils by DeltaE22-Abeta(1-39), *Biochemistry*, 2011, *50*,2026-2039.

3. Meng, F. L., Marek, P., Potter, K. J., Verchere, C. B., and Raleigh, D. P. Rifampicin Does Not Prevent Amyloid Fibril Formation by Human Islet Amyloid Polypeptide But Does Inhibit Fibril Thioflavin-T Interactions: Implications For Mechanistic Studies Beta-Cell Death, *Biochemistry*, 2008, *47*,6016-6024.

4. Hudson, S. A., Ecroyd, H., Kee, T. W., and Carver, J. A. The Thioflavin T Fluorescence Assay For Amyloid Fibril Detection Can Be Biased by The Presence of Exogenous Compounds, *FEBS J.*, 2009, *276*,5960-5972.

5. Lavinder, J. J., Hari, S. B., Sullivan, B. J., and Magliery, T. J. High-Throughput Thermal Scanning: A General, Rapid Dye-Binding Thermal Shift Screen For Protein Engineering, *J. Am. Chem. Soc.*, 2009, *131*,3794-3795.

6. Steinberg, T. H., Haugland, R. P., and Singer, V. L. Applications of SYPRO Orange and SYPRO Red Protein Gel Stains, *Anal. Biochem.*, 1996, *239*,238-245.

7. Haugland, R. P., Jones, L. J., Singer, V. L., and Steinberg, T. H. (1997) Merocyanine Dye Protein Stains, Google Patents.

8. Binkowski, T. A., Jiang, W., Roux, B., Anderson, W. F., and Joachimiak, A. Virtual High-Throughput Ligand Screening, *Methods Mol. Biol.*, 2014, *1140*,251-261.

9. Lo, M. C., Aulabaugh, A., Jin, G., Cowling, R., Bard, J., Malamas, M., and Ellestad, G. Evaluation of Fluorescence-Based Thermal Shift Assays For Hit Identification in Drug Discovery, *Anal. Biochem.*, 2004, *332*,153-159.

10. Nashine, V. C., Kroetsch, A. M., Sahin, E., Zhou, R., and Adams, M. L. Orthogonal High-Throughput Thermal Scanning Method for Rank Ordering Protein Formulations, *AAPS PharmSciTech*, 2013, *14*,1360-1366.

11. Bolognesi, B., Kumita, J. R., Barros, T. P., Esbjorner, E. K., Luheshi, L. M., Crowther, D. C., Wilson, M. R., Dobson, C. M., Favrin, G., and Yerbury, J. J. ANS Binding Reveals Common Features of Cytotoxic Amyloid Species, *ACS Chem Biol*, 2010, *5*,735-740.

12. Younan, N. D., and Viles, J. H. A Comparison of Three Fluorophores for the Detection of Amyloid Fibers and Prefibrillar Oligomeric Assemblies. ThT (Thioflavin T); ANS (1-Anilinonaphthalene-8-sulfonic Acid); and bisANS (4,4 '-Dianilino-1,1 '-binaphthyl-5,5 '-disulfonic Acid), *Biochemistry*, 2015, *54*,4297-4306.

13. Hawe, A., Sutter, M., and Jiskoot, W. Extrinsic Fluorescent Dyes as Tools for Protein Characterization, *Pharm. Res.*, 2008, *25*,1487-1499.

14. Rosen, C. G., and Weber, G. Dimer Formation from 1-Amino-8-Naphthalenesulfonate Catalyzed by Bovine Serum Albumin. A New Fluorescent Molecule with Exceptional Binding Properties, *Biochemistry*, 1969, *8*,3915-3920.

15. Gao, F., Mei, E., Lim, M., and Hochstrasser, R. M. Probing Lipid Vesicles by Bimolecular Association and Dissociation Trajectories of Single Molecules, *J. Am. Chem. Soc.*, 2006, *128*,4814-4822.

16. Mukherjee, S., Raghuraman, H., and Chattopadhyay, A. Membrane Localization and Dynamics of Nile Red: Effect of Cholesterol, *Biochim. Biophys. Acta*, 2007, *1768*,59-66.

17. Greenspan, P., Mayer, E. P., and Fowler, S. D. Nile Red: A Selective Fluorescent Stain for Intracellular Lipid Droplets, *J. Cell Biol.*, 1985, *100*,965-973.

18. Mishra, R., Sjolander, D., and Hammarstrom, P. Spectroscopic Characterization of Diverse Amyloid Fibrils in vitro By the Fluorescent Dye Nile Red, *Mol. Biosyst.*, 2011, *7*,1232-1240.

19. Sackett, D. L., and Wolff, J. Nile Red as a Polarity-Sensitive Fluorescent Probe of Hydrophobic Protein Surfaces, *Anal. Biochem.*, 1987, *167*,228-234.

20. Mishra, R., Sorgjerd, K., Nystrom, S., Nordigarden, A., Yu, Y. C., and Hammarstrom, P. Lysozyme Amyloidogenesis is Accelerated by Specific Nicking and Fragmentation But Decelerated by Intact Protein Binding and Conversion, *J. Mol. Biol.*, 2007, *366*,1029-1044.

21. Haidekker, M. A., and Theodorakis, E. A. Molecular Rotors - Fluorescent Biosensors for Viscosity and Flow, *Org. Biomol. Chem.*, 2007, *5*,1669-1678.

22. Kung, C. E., and Reed, J. K. Fluorescent Molecular Rotors: A New Class of Probes for Tubulin Structure and Assembly, *Biochemistry*, 1989, *28*,6678-6686.

23. Lindgren, M., Sorgjerd, K., and Hammarstrom, P. Detection and Characterization of Aggregates, Prefibrillar Amyloidogenic Oligomers, and Protofibrils Using Fluorescence Spectroscopy, *Biophys. J.*, 2005, *88*,4200-4212.

24. Wallberg, F., Tenev, T., and Meier, P. Analysis of Apoptosis and Necroptosis by Fluorescence-Activated Cell Sorting, *Cold Spring Harb. Protoc.*, 2016, *2016*,pdb prot087387.

25. Telford, W. G., King, L. E., and Fraker, P. J. Comparative Evaluation of Several DNA Binding Dyes in the Detection of Apoptosis-Associated Chromatin Degradation by Flow Cytometry, *Cytometry*, 1992, *13*,137-143.

26. Larsen, T. A., Goodsell, D. S., Cascio, D., Grzeskowiak, K., and Dickerson, R. E. The Structure of DAPI Bound to DNA, *J. Biomol. Struct. Dyn.*, 1989, *7*,477-491.

27. Bennink, M. L., Scharer, O. D., Kanaar, R., Sakata-Sogawa, K., Schins, J. M., Kanger, J. S., de Grooth, B. G., and Greve, J. Single-Molecule Manipulation of Double-Stranded DNA Using OpticalTtweezers: Interaction Studies of DNA with RecA and YOYO-1, *Cytometry*, 1999, *36*,200-208.

28. Lindberg, D. J., and Esbjorner, E. K. Detection of Amyloid-Beta Fibrils Using the DNA-Intercalating Dye YOYO-1: Binding Mode and Fibril Formation Kinetics, *Biochem. Biophys. Res. Commun.*, 2016, *469*,313-318.

29. Marek, P., Woys, A. M., Sutton, K., Zanni, M. T., and Raleigh, D. P. Efficient Microwave Assisted Synthesis of Human Islet Amyloid Polypeptide Designed to Facilitate The Specific Incorporation of Labeled Amino Acids, *Org. Lett.*, 2010, *12*,4848-4851.

30. Abedini, A., and Raleigh, D. P. Incorporation of Pseudoproline Derivatives Allows the Facile Synthesis of Human IAPP, A Highly Amyloidogenic and Aggregation-Prone Polypeptide, *Org. Lett.*, 2005, *7*,693-696.

31. Maskevich, A. A., Stsiapura, V. I., Kuzmitsky, V. A., Kuznetsova, I. M., Povarova, O. I., Uversky, V. N., and Turoverov, K. K. Spectral Properties of Thioflavin T in Solvents with Different Dielectric Properties and in a Fibril-Incorporated Form, *J. Proteome Res.*, 2007, *6*,1392-1401.

32. Tu, L.-H., and Raleigh, D. P. Role of Aromatic Interactions in Amyloid Formation by Islet Amyloid Polypeptide, *Biochemistry*, 2013, *52*,333-342.

33. Young, L. M., Saunders, J. C., Mahood, R. A., Revill, C. H., Foster, R. J., Tu, L. H., Raleigh, D. P., Radford, S. E., and Ashcroft, A. E. Screening and Classifying Small-Molecule Inhibitors of Amyloid Formation Using Ion Mobility Spectrometry-Mass Spectrometry, *Nat. Chem.*, 2015, *7*,73-81.

34. Westermark, P., Engstrom, U., Johnson, K. H., Westermark, G. T., and Betsholtz, C. Islet Amyloid Polypeptide Pinpointing Amino Acid Residues Linked to Amyloid Fibril Formation, *PNAS*, 1990, *87*,5036-5040.

35. Green, J., Goldsbury, C., Min, T., Sunderji, S., Frey, P., Kistler, J., Cooper, G., and Aebi, U. Full-Length Rat Amylin Forms Fibrils Following Substitution of Single Residues From Human Amylin, *J. Mol. Biol.*, 2003, *326*,1147-1156.

36. Jha, S., Snell, J. M., Sheftic, S. R., Patil, S. M., Daniels, S. B., Kolling, F. W., and Alexandrescu, A. T. pH Dependence of Amylin Fibrillization, *Biochemistry*, 2014, *53*,300-310.

37. Jameson, D. M., Croney, J. C., and Moens, P. D. Fluorescence: Basic Concepts, Practical Aspects, and Some Anecdotes, *Methods Enzymol.*, 2003, *360*,1-43.

38. Mannini, B., Mulvihill, E., Sgromo, C., Cascella, R., Khodarahmi, R., Ramazzotti, M., Dobson, C. M., Cecchi, C., and Chiti, F. Toxicity of Protein Oligomers is Rationalized by a Function Combining Size and Surface Hydrophobicity, *Acs Chemical Biology*, 2014, *9*,2309-2317.

39. Frare, E., Mossuto, M. F., de Laureto, P. P., Tolin, S., Menzer, L., Dumoulin, M., Dobson, C. M., and Fontana, A. Characterization of Oligomeric Species on the Aggregation Pathway of Human Lysozyme, *J. Mol. Biol.*, 2009, *387*,17-27.

40. Bhattacharya, M., Jain, N., and Mukhopadhyay, S. Insights into the Mechanism of Aggregation and Fibril Formation from Bovine Serum Albumin, *J. Phys. Chem. B*, 2011, *115*,4195-4205.

41. Abedini, A., Plesner, A., Cao, P., Ridgway, Z., Zhang, J., Tu, L. H., Middleton, C. T., Chao, B., Sartori, D. J., Meng, F., Wang, H., Wong, A. G., Zanni, M. T., Verchere, C. B., Raleigh, D. P., and Schmidt, A. M. Time-Resolved Studies Define the Nature of Toxic IAPP Intermediates, Providing Insight for Anti-Amyloidosis Therapeutics, *eLife*, 2016, *5*.

Chapter 5. Analysis of the Amyloidogenicity and Cytotoxicity of Baboon Islet Amyloid Polypeptide Provides Insight into Amyloid Formation by Human Islet Amyloid Polypeptide and Reveals the Importance of Lys-1 and Ala-25 in Modulating Amyloidogenicity

Abstract

Islet amyloid polypeptide (IAPP) is responsible for islet amyloid deposition in type-2 diabetes. The sequence of IAPP is well conserved, but not all species form islet amyloid and the ability to do so correlates with the primary sequence. Humans form islet amyloid, but baboon IAPP has not been studied. The baboon peptide differs from human IAPP at three positions containing K1I, H18R, and A25T substitutions. The K1I substitution is a rare example of a replacement in the N-terminal region of IAPP and is the only known substitution of the Lys residue normally found at position-1. The effect of the K1I mutation on amyloid formation has not been studied, but it reduces the net charge, and amyloid prediction programs suggest that it should increase amyloidogenicity. The A25T replacement involves a non-conservative substitution in a region of IAPP that is believed to be important in the early stages of aggregation. The H18R point mutant has been previously shown to reduce human IAPP toxicity in cell culture and to reduce aggregation. Baboon IAPP forms amyloid more slowly than human IAPP *in vitro*. The K1I replacement in human IAPP leads to a similar rate of amyloid formation, while the A25T substitution substantially accelerates amyloid formation. Photochemical cross-linking studies reveal that the baboon IAPP, like human IAPP, forms low order oligomers in the lag phase of amyloid formation. The baboon peptide is toxic to cultured INS-1 β-cells. The

toxicity of baboon IAPP is consistent with the hypothesis that pre-amyloid oligomers are the most toxic species produced during IAPP amyloid formation.

NOTE: The material presented in this chapter has been submitted for publication to Biochemistry (Amy. G Wong, Andisheh Abedini, Zachary Ridgeway, Eleni Hannaberry, Ann Marie Schmidt, and Daniel P. Raleigh "Analysis of the Amyloidogenicity and Cytotoxicity of Baboon Islet Amyloid Polypeptide Provides Insight into Amyloid Formation by Human Islet Amyloid Polypeptide and Reveals the Importance of Lys-1 and Ala-25 in Modulating Amyloidogenicity") This chapter contains direct excerpts from the manuscript, which was written by me with suggestions and revisions from Professor Daniel P. Raleigh. The cytotoxicity experiments were performed by Dr. Andisheh Abedini in the Ann Marie Schmidt group at NYU. PICUP experiments were performed by group member Zachary Ridgway.

5.1 Introduction

Amyloid formation plays a central role in a number of devastating human diseases including Alzheimer's disease, the systemic amyloidosis and type-2 diabetes (T2D). Islet amyloid polypeptide, (IAPP also known as amylin) is a 37 residue neuropancreatic polypeptide hormone, which helps regulate satiety, controls gastric emptying, suppresses glucagon release from α-cells and helps to maintain glucose homeostasis [1, 2]. In T2D, IAPP aggregates to form islet amyloid in the islet of Langerhans [3, 4]. The process of islet amyloid formation by human IAPP (h-IAPP) contributes to β-cell dysfunction in T2D and to islet transplant failure [3-7].

IAPP contains an amidated C-terminus and a disulfide bridged loop between residues 2 and 7. However, not all species form islet amyloid and the ability to form amyloid *in vivo* and *in vitro* correlates with the sequence of the polypeptide. Notably mice and rats do not form amyloid

in vivo and the mouse/rat polypeptide is non-amyloidogenic *in vitro* under standard conditions [8]. Comparison of the rat/mouse sequence to the sequence of h-IAPP, together with early *in vitro* experiments, led to the hypothesis that the ability to form amyloid is controlled by the identity of the 20-29 segment [8, 9]. h-IAPP and rat IAPP (r-IAPP) differ at six positions, with five of the substitutions located between residues 23-29, including three Pro residues at positions 25, 28 and 29 of r-IAPP (Figure 5-1). The region lying between residues 20 to 29 of IAPP is important for amyloid formation, but it is clear that the sequence in this region is not the sole factor dictating amyloidogencity [8-10]. For example, His-18 in h-IAPP is replaced by Arg in r-IAPP and the H18R point mutant is known to slow amyloid formation by h-IAPP and to moderate toxicity towards cultured cells [11-15]. Other substitutions outside of the 20-29 segment also influence amyloid formation, but the role of residues located within the N-terminal disulfide bridged loop is not known [15-17]. Deducing the sequence determinants of IAPP amyloidogencity is important for the development of next generation soluble analogs for use as adjuncts to insulin therapy and for the potential development of xenobiotic islet transplantation [18-21]. The sequence of baboon IAPP (b-IAPP) is known, but its ability to form amyloid has not been examined, nor has its potential toxicity towards β-cells been assessed. The baboon polypeptide contains the H18R substitution found in rat IAPP, but also includes two other replacements relative to the human polypeptide; a K1I and an A25T replacement. The K1I substitution is particularly interesting since it is the only reported substitution at position-1 in IAPP (Figure 5-1). The effect of these substitutions on amyloid formation have not been examined.

Here we examine the ability of b-IAPP to form amyloid, compare its amyloidogencity to the human polypeptide, test the role of the individual residue differences between baboon and human IAPP, and examine the effects of the aggregation of baboon IAPP on the viability of INS-1 β-cells. The results provide information about regions of the polypeptide which are important for controlling amyloidogencity and support the hypothesis that pre-amyloid oligomers are the most toxic species produced during IAPP amyloid formation.

5.2 Materials and Methods

5.2.1 Computational Analysis of Amyloidogenicity

The predicted amyloidogencity of the various sequences was calculated using several web based amyloid prediction programs: AGGRESCAN, (http://bioinf.uab.es/aggrescan/); FoldAmyloid, (http://bioinfo.protres.ru/fold-amyloid/; Zygreggator, (http://www-mvsoftware.ch.cam.ac.uk/index.php/zyggregator); and TANGO, (http://www.switchlab.org/bioinformatics/tango).

5.2.2 Peptide Synthesis

Human and baboon IAPP were prepared via solid phase peptide synthesis using standard Fmoc (9-fluorenylemethoxy carbonyl) solid phase peptide synthesis methods. Syntheses were conducted on a 0.1 mmol scale, using a CEM Liberty automated microwave peptide synthesizer. Fmoc-PAL-PEG-PS resin was used to obtain the naturally occurring amidated C-terminus. Fmoc protected pseudoproline (Oxazolidine) dipeptide derivatives were used as previously described [22, 23]. The first amino acid attached to the resin, pseudoproline dipeptide derivatives, and all β-branched amino acids were double coupled. Peptides were cleaved from the resin and

sidechain protecting groups removed using standard trifluoroacetic acid (TFA) protocols as previously described.[22] All solvents were ACS grade. Fmoc-Pal-PEG-PS resin was purchased from Applied Biosystems. Fmoc protected amino acids and all other reagents were purchased from AAPPTec, Novabiochem, Sigma-Aldrich, VWR and Fisher Scientific.

5.2.3 Disulfide Bond and Purification

Crude peptides were dissolved in 15% acetic acid (v/v) and freeze dried to increase the solubility of the peptide. The DMSO based oxidation method of Tam and coworkers were used to promote disulfide bond formation [24, 25]. Reversed phase HPLC was used to purify the crude peptides. Hydrochloric acid was used as an ion pairing agent instead of TFA, as TFA can influence IAPP aggregation kinetics and cell toxicity assays. A 25-65 % buffer B gradient was used over a period of 40 minutes where buffer A corresponded to 100% H_2O, 0.045% HCl and buffer B corresponded to 80% acetonitrile, 0.045% HCl. The retention times of h-IAPP, b-IAPP, K1I, H18R, and A25T were 26 minutes (51 % B), 28 minutes (53 % B), 21 minutes (46 % B), 27 minutes (52 % B), and 25 minutes (50 % B) respectively. Residual scavengers were removed by dissolving the dried peptides in in 1, 1, 1, 3, 3, 3-Hexafluoro-2-propanol (HFIP) to extract trace amounts of scavengers and then re-purified with reversed-phase HPLC. The purity of the peptides was checked by reverse-phase HPLC using a C18 analytic column. The molecular weights of the purified peptides were confirmed by mass spectrometry via matrix assisted laser desorption ionization time of flight mass spectrometry instrument: human IAPP expected, 3903.30; observed, 3902.6; baboon IAPP, expected, 3937.3 observed, 3938.1; K1I h-IAPP expected, 3885.9 observed, 3885.0; A25T h-IAPP expected, 3933.3; observed, 3932.9.

5.2.4 Sample Preparation

Dry peptides were dissolved in 100 % HFIP to prepare a 1.6 mM stock solution. Aliquots were filtered through a 0.22 μm Millex syringe-driven filter and the concentration determined by measuring the absorbance at 280 nm. Measured amounts of aliquots were freeze dried to remove HFIP.

5.2.5 Thioflavin-T Fluorescence Assay

Thioflavin-T binding assays were employed to monitor amyloid formation as a function of time using a Beckman Coulter DTX 880 Multimode Detector plate reader. Fluorescence was measured using a 430 nm excitation wavelength with a filter bandwidth of 35 nm and emission at 485 nm with a filter bandwidth of 20 nm. Corning 96-well non-binding surface black plates with lids were used for all assays. Plates were sealed with polyethylene sealing tape. Freeze dried peptides were dissolved in buffer and thioflavin-T solution immediately before measurements. All the experiments used: 16 μM IAPP, 32 μM thioflavin-T, 25 °C, PBS pH 7.4 and no agitation.

5.2.6 Photochemical Cross-linking

NOTE: The photochemical cross-linking assays were performed by group member Zachary Ridgway. The methods here have been included here for completeness.

Samples were cross-linked using tris (bipyridyl) Ru (II), in the presence of ammonium persulfate (APS). The ratios of Ru(bpy), APS, and peptide were 3.5 : 70 : 1. Samples were dissolved in buffer (PBS, pH 7.4), and were centrifuged for 10 minutes at 15,000g before the reaction. In a typical reaction, 2.5 μL of Ru(bpy) and APS were added to a 15 uL aliquot of 40 or 16 μM peptide, and irradiated for 10 s with a 140W incandescent bulb. After reaction, solutions

were quenched with 10 uL of Tricine sample buffer containing 5 % β-mercaptoethanol. Samples were then heated for 5 minutes at 85 °C prior to loading on the gel. Gels were visualized by silver staining, and gel densitometry was performed using GelAnalyzer version 2010a. The relative intensity of each band was calculated by first correcting the baseline, then integrating the area under each peak.

5.2.7 Transmission Electron Microscopy

TEM images were recorded with a FEI Bio TwinG^2 Transmission Electron Microscope. Samples were blotted on a carbon-coated formvar 300-mesh copper grid for 1 min and then negatively stained with 2% uranyl acetate for 1 min. Images were taken at a 68,000X magnification and 100 nm under focus.

5.2.8 Cytotoxicity Assays

NOTE: The cytotoxicity assays were performed by Dr. Andisheh Abedini in the Ann Marie Schmidt group at NYU. The methods have been included here for completeness.

Rat INS-1 β-cells were seeded in 96-well plates at a density of 40,000 cells per well 24 hours prior to start of experiments. Peptides were dissolved in complete RPMI, and incubated on cells for 24, 48 and 84 hours prior to cell viability measurements, which was assessed by AlamarBlue reduction assays. AlamarBlue was diluted ten-fold in culture media and incubated on cells for 5 hours at 37 °C. Fluorescence (excitation 530 nm; emission 590 nm) was measured with a Beckman Coulter DTX880 plate reader. Values are reported relative to untreated control cells.

5.3 Results and Discussion

5.3.1 Amyloid Prediction Algorithms Give Conflicting Results for the Relative Amyloidogenicity of baboon IAPP, K1I, H18R, and A25T Variants

The primary sequence of baboon and human IAPP are shown in Figure 5-1 which displays an alignment of the known IAPP sequences. The three substitutions in b-IAPP relative to h-IAPP are predicted to have different effects on amyloidogenicity and it is not known if b-IAPP has a different propensity to form amyloid than h-IAPP (Table 5-1). The Lys-1 to Ile replacement is the only known substitution at residue-1 found to date in IAPP; this position is otherwise strictly conserved (Figure 5-1). In fact, very few substitutions are found within the first seven residues of IAPP (Figure 5-1) and the K1I replacement is one of only three substitutions, relative to h-IAPP, that removes a charged residue into this region. The effect of sequence substitutions within this region on the amyloidogenicity of h-IAPP has not been examined. The K1I substitution reduces the net charge on IAPP at all relevant pH values and hence should influence solubility and amyloidogencity. Standard amyloid prediction algorithms predict that the Ile substitution will enhance amyloidogenicity or will have no effect [26-30]. AGGRESCAN, FoldAmyloid, and Zygreggator all predict an enhancement in amyloidogenicity, while TANGO predicts that the replacement will have very little effect. The replacement of His-18 in h-IAPP with an Arg is a common substitution (Figure 5-1). Arg is found at position-18 in monkey and macaque IAPP, both of which are amyloidogenic, but is also found in the non-amyloidogenic rat IAPP. Substitution of His-18 with Arg in h-IAPP has been reported to reduce its amyloidogenicity as does reducing the pH to ensure that His-18 is fully charged [11-14]. The AGGRESCAN, TANGO, and Zygreggator programs predict that the His to Arg replacement reduces amyloidogenicity while FoldAmyloid predicts only a modest impact. The final

substitution in b-IAPP relative to h-IAPP is the replacement of Ala-25 in h-IAPP with Thr in b-IAPP. Position-25 lies in the region initially proposed to be the critical amyloidogenic determinant of IAPP [8]. More recent work indicates that h-IAPP formation *in vitro* may involve the formation of an obligatory intermolecular β-sheet in this region which is then disrupted as the polypeptides rearrange to form the final amyloid fibril structure [10]. Thr is a relatively non-conservative mutation for Ala. The change significantly decreases α-helical propensity, increases β-sheet propensity and introduces hydrogen bonding functionality into the side chain. The AGGRESCAN, Zygreggator, and TANGO programs all predict that this substitution reduces amyloidogenicity while FoldAmyloid predicts no significant effect. The complete b-IAPP sequence is predicted to be less amyloidogenic by TANGO and Zyggregator, while AGGRESCAN predicts that b-IAPP is more amyloidogenic than h-IAPP and FoldAmyloid predicts that both peptides have similar core amyloidogenic regions (Table 5-1).

5.3.2 Baboon IAPP Forms Amyloid More Slowly Than Human IAPP

We first examined amyloid formation by b-IAPP and compared it to h-IAPP using fluorescence detected thioflavin-T binding assays together with transmission electron microscopy (TEM). Thioflavin-T is a small dye that experiences an increase in quantum yield upon binding to amyloid fibrils [31-33]. The dye is an extrinsic probe, but it has been shown to report accurately on the kinetics of h-IAPP amyloid formation under the conditions used here. However, there are cases where fluorescence of the dye does not noticeably increase in the presence of amyloid [34]. In addition, the relationship between the intensity of thioflavin-T fluorescence and the amount of amyloid formed is not clear. Thus, we used TEM to confirm the results of the thioflavin-T assays.

Amyloid formation by h-IAPP is composed of three phenomenological phases; an initial lag phase which does not generate any significant thioflavin-T response, followed by a growth phase in which amyloid fibrils elongate and a final plateau stage in which fibrils are in equilibrium with soluble peptide. This sequence of events gives rise to a sigmoidal plot of thioflavin-T fluorescence vs time. We studied amyloid formation in phosphate buffered saline (PBS, 10 mM phosphate, 140 mM KCl). Both the human and baboon peptides exhibit sigmodal thioflavin-T fluorescence curves, as expected for an amyloidogenic IAPP (Figure 5-2A). T_{50}, the time required to achieve 50 % of the total fluorescence gain in a thioflavin-T assay, is 40 ± 0.6 hrs for h-IAPP in PBS .The baboon polypeptide forms amyloid more slowly than h-IAPP in PBS with a t_{50} that is 3-fold longer than the value for h-IAPP. Aliquots were removed from each kinetic experiment after 24 hours, a time sufficient for both peptides to reach the thioflavin-T fluorescence plateau, and TEM images were recorded (Figure 5-2B and 5-2C). Dense mats of amyloid fibrils were observed in the images of both peptides and both exhibited the typical morphology associated with *in vitro* h-IAPP amyloid.

5.3.3 Baboon IAPP Populates Low Order Oligomers During the Lag Phase of Amyloid Formation

Amyloid formation by h-IAPP is believed to proceed through formation of low order oligomers [35-38]. We conducted comparative photochemical cross-linking studies to test if this is also the case for b-IAPP. Peptides were dissolved in solution and the photo-induced cross-linking of unmodified proteins (PICUP) *in situ* photochemical cross-linking method of Teplow and coworkers was used to probe the distribution of oligomers [39]. A distribution of oligomeric species ranging from monomers to hexamers is observed for the baboon polypeptide with noticeably higher populations of monomer, dimer, and trimer than of higher order species

(Figure 5-3A). Quantitative analysis of the silver stained gels reveals that the distribution of oligomers populated by baboon and human IAPP are broadly similar. There are some differences in the relative intensities; the relative population of pentamers and hexamers is higher for h-IAPP compared to b-IAPP, while the relative population of lower order oligomers is higher for b-IAPP (Figure 5-3B). However, we are hesitant to draw any conclusions from these differences as they could arise from a small, but genuine difference in oligomeric distributions or from intrinsic differences in cross-linking efficiency, or both. PICUP targets multiple amino acids, but particularly Trp, Tyr, Met, Cys, and to a lesser extent Phe and His. The difference in primary sequence (particularly the H18R mutation) may thus contribute to the observed differences [39]. The key point is both polypeptides form low order oligomers during the lag phase.

5.3.4 Mutational Analysis of Amyloid Formation by IAPP

We next examined the effect of individually substituting the baboon residues into h-IAPP. The results of the H18R substitution have been reported to lead to a reduction in amyloidogenicity at pH 7.4, but the effects of the substitutions at Lys-1 and at Ala-25 have not been studied [12]. We synthesized the peptides and tested their ability to form amyloid in PBS (Figure 5-4A). We first examined the effect of the H18R replacement under the conditions of our assays. Consistent with previous results, the mutation leads to a three-fold increase in the value of t_{50}. K1I forms amyloid at a similar rate relative to h-IAPP, even though several amyloid prediction programs predict that the mutant should be more amyloidogenic than h-IAPP. The t_{50} for K1I was found to be 4.9 ± 0.6 hrs in PBS, compared to 4.0 ± 0.6 hrs for h-IAPP. The A25T replacement was found to form amyloid more than twice as fast as h-IAPP, though amyloid

prediction programs all predicted that this mutant should be less amyloidogenic than h-IAPP. The t_{50} for A25T was 1.5 ± 0.4 hrs in PBS.

5.3.5 Baboon IAPP is Toxic to Cultured β-Cells

Having established that b-IAPP forms amyloid we next examined its effect on the viability of cultured β-cells using the rat INS-1 β-cell line. Treatment with h-IAPP for 24, 48, and 84 hours led to time-dependent and dose-dependent decreases in β-cell viability (Figure 5-5, Figure 5-6). Incubation with 30 μM h-IAPP for 24 hours led to a 49% reduction in β-cell viability compared to control cells. In contrast, 24 hours incubation of the baboon polypeptide led to an 83 % decrease in β-cell viability (Figure 5-5). Longer incubation of h-IAPP on β-cells led to further reduction in β-cell viability; a 62 % decrease was observed after 48 hours and a 70 % reduction was measured at 84 hours. The effects of b-IAPP are even more pronounced; incubation with 30 μM peptide reduced β-cell viability by 88 % after 48 hours of incubation and by 93 % after 84 hours of incubation. Both human and baboon IAPP were tested at different concentrations, but the baboon peptide was always more toxic than h-IAPP. At 20 μM concentration, b-IAPP induced a 63 % decrease in cell viability after 24 hours incubation, and 92 % decrease in cell viability at 40 μM concentration. Incubation with 20 μM concentration h-IAPP for 24 hours led only a 15 % decrease in cell viability while 40 μM concentration lead to a decrease in cell viability of 74 %. At 15 μM concentration, both h-IAPP and b-IAPP had a lower toxicity relative to untreated cells, but b-IAPP is more toxic (Figure 5-6).

5.4 Conclusions

The data presented here shows b-IAPP is similar to IAPP's derived from other primates in the sense that it forms amyloid, although it does so more slowly than h-IAPP. Both baboon

and human IAPP form low order oligomers in the lag phase of amyloid formation with broadly similar distributions. It is difficult to interpret the small differences in the observed distributions given the difference in primary sequence, but we believe the key point is that both polypeptides form low order oligomer species. This is consistent with the hypothesis that low order soluble pre-amyloid oligomers are the most toxic species produced during IAPP amyloid formation.

The analysis of the point variants K1I and A25T together with earlier work on the H18R mutant provides insight into the factors which help control IAPP's ability to form amyloid and provides examples of the difficulty in defining amyloidogencity. Prior work has shown that the H18R substitution leads to slower aggregation. The K1I replacement in h-IAPP is a unique example, to date, of a replacement at position-1 and is only one of six sequence changes in the first 16 residues of IAPP that alters the net charge (Figure 1-9). The N-terminal disulfide bridge is not part of the cross-β core structure in models of h-IAPP amyloid fibrils.[40, 41] Trp triplet quenching studies have shown that the disulfide makes transient contacts with other regions of the polypeptide chain [42]. Previous studies have reported that removal of the first 7 residues of h-IAPP had modest effects on the t_{50} for amyloid formation, but the data presented here shows that mutations in this region can significantly slow the rate of amyloid formation [43]. This suggests that the role of the N-terminal region in aggregation is more complex than originally thought. It is interesting to note that the K1I mutation did not affect the rate of amyloid formation even though the net charge of the polypeptide is reduced. This is surprising since the rate of h-IAPP amyloid formation is sensitive to the ionic strength of the experimental conditions. Phosphate accelerates h-IAPP amyloid formation and we would expect to see a less dramatic

effect on the rate of amyloid formation by K1I relative to wild-type h-IAPP since there would be a weakened interaction with phosphate due to the decreased positive charge of the variant.

The results with the A25T substitution highlight the importance of this region of the polypeptide, and also highlight the difficulties with current methods to predict amyloidogenicity. The mutant forms amyloid faster than wild-type even though it is predicted to be less amyloidogenic. The molecular basis for the more rapid aggregation is not understood, but the replacement may alter the stability of the transient β-sheet intermediate which has been recently identified by time-resolved 2D-IR.[10] Replacement of Ala with Thr leads to an increased β-sheet propensity, a decreased α-helical propensity, and also introduces a hydrogen bonding functionality into the sidechain which could contribute to stabilizing intermolecular sidechain-sidechain interactions. Along these lines, it is interesting to examine cross strand pairing propensities in parallel β-sheets. Statistical analysis of pairing preferences between adjacent strands in parallel β-sheets in globular proteins indicates that Thr:Thr pairs occur more frequently than expected based on the relative abundance of Thr in parallel β-sheets whereas Ala:Ala pairs occur less frequently than expected based on the relative abundance of Ala in parallel β-sheets [44, 45]. The differences in cross-strand pairing frequencies reflect the packing across the strands; an Ala:Ala pair is considerably smaller than a Thr:Thr pair and may introducing an instability in the β-sheet by creating a gap and thus be less favored than the Thr:Thr pair.

In summary, the data presented here highlights the difficulties in predicting amyloidogenicity from sequence and reveals that there is no simple relationship between net

charge on a polypeptide and its rate of amyloid formation. The work also demonstrates that the identity of residues in the N-terminal region of hIAPP make important contributions to the rate of amyloid formation, suggesting that they may offer additional sites to target during efforts to redesign hIAPP to produce more soluble less aggregation prone variants of hIAPP.

5.5 Figures

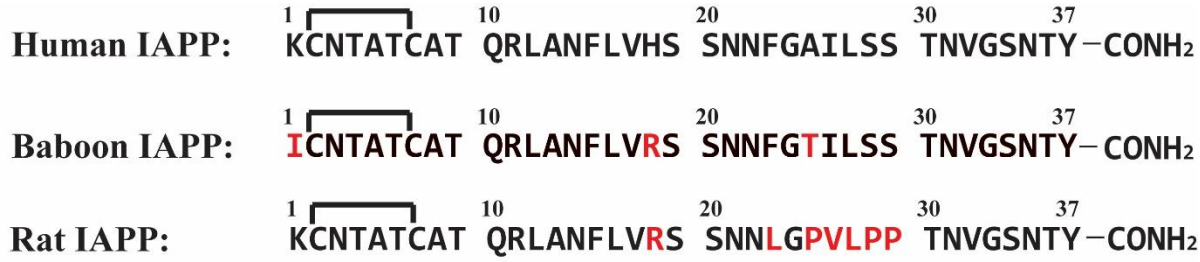

Figure 5-1: Comparison of sequences of human, baboon, and rat IAPP. Residues that differ from human IAPP are colored red. All variants contain a disulfide bond between cysteines 2 and 7 and an amidated C-terminus

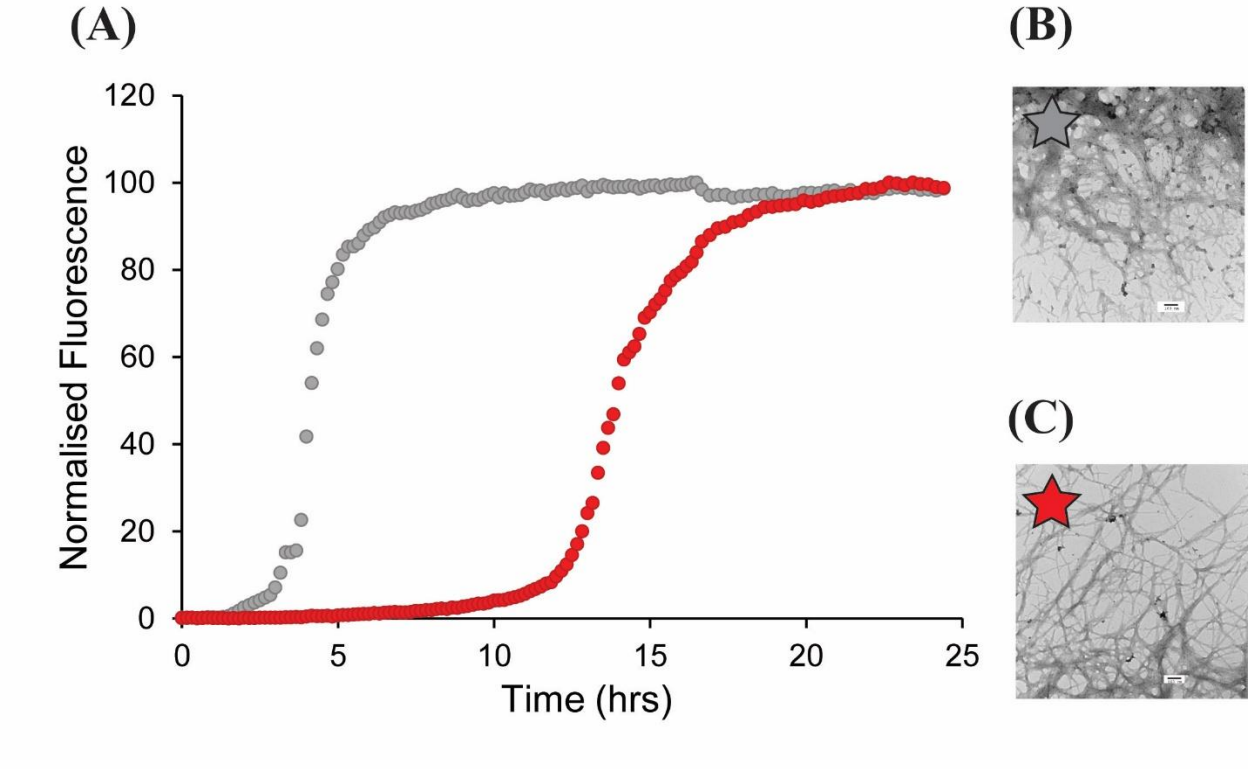

Figure-5-2: Baboon IAPP forms amyloid at a reduced rate relative to human IAPP. (A) Thioflavin-T fluorescence assays of amyloid formation by human IAPP (grey) and baboon IAPP (red) (B) TEM image of amyloid fibrils formed by h-IAPP. (C) TEM image of fibrils formed by b-IAPP. Aliquots were removed from the kinetic experiments after 24 hrs. Experiments were conducted at 25 °C pH 7.4 PBS with 16 μM IAPP. Scale bars in the TEM images are 100 nm.

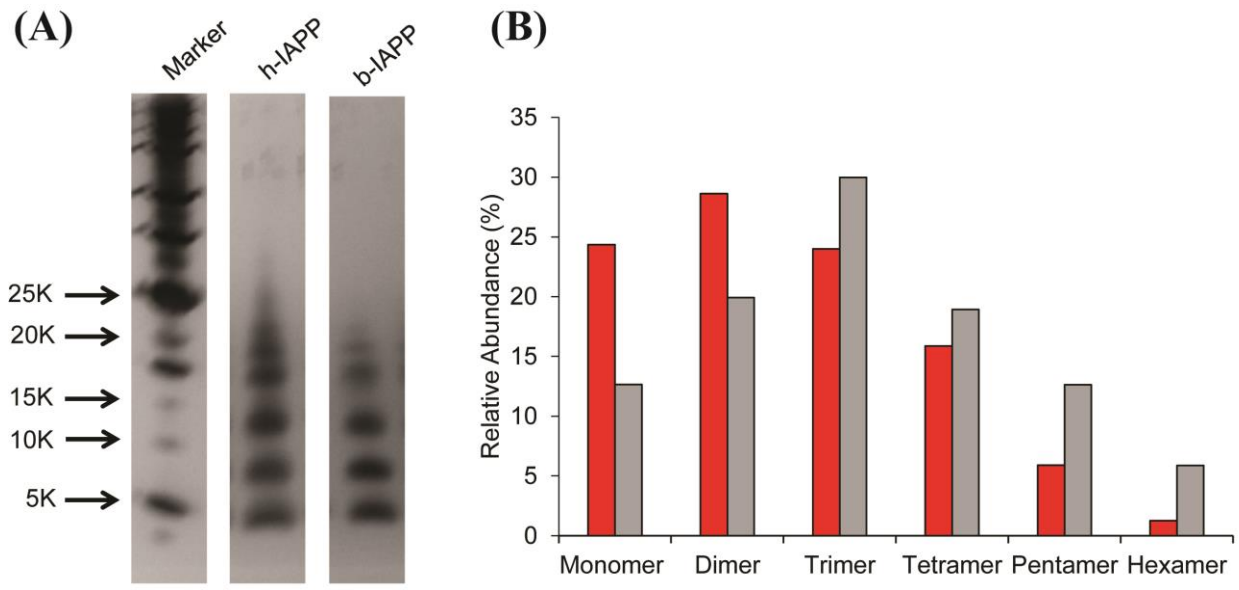

Figure 5-3: Both human and baboon IAPP form oligomers. (A) Silver stained gel showing the distribution of oligomer species populated by human and baboon IAPP at 40 µM. (B) Relative populations of the cross-linked species detected via the PICUP experiments of h-IAPP (grey) and b-IAPP (red). Intensity was derived from the silver stained gel at left.

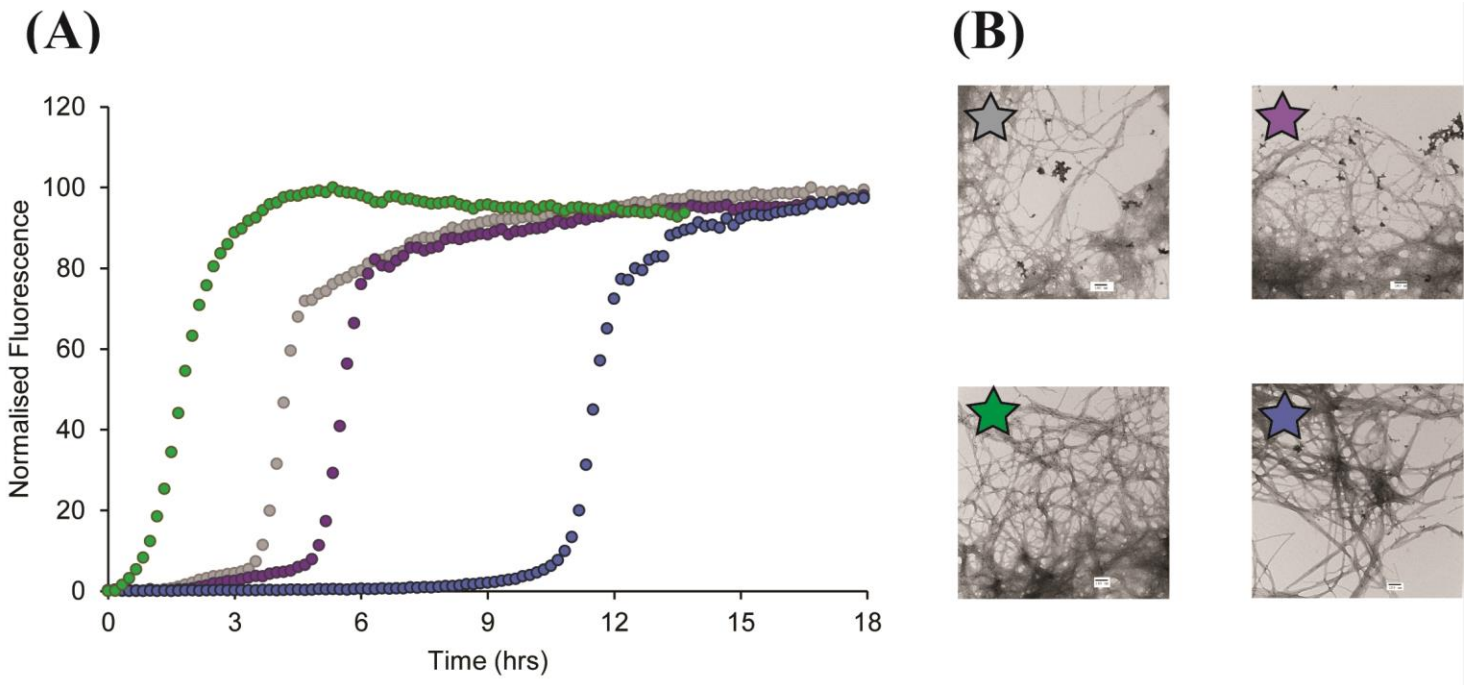

Figure 5-4: Kinetic analysis of wild-type h-IAPP, K1I, H18R, and A25T. (A) Thioflavin-T fluorescence assays of amyloid formation by human IAPP (grey), K1I (purple), A25T (green) and H18R (blue). (B) TEM image of amyloid fibrils formed by human IAPP. (C) TEM image of fibrils formed by human IAPP (grey), K1I (purple), A25T (green) and H18R (blue). Aliquots were removed from the kinetic experiments after 24 hrs. Experiments were conducted at 25 °C pH 7.4 PBS with 16 μM IAPP. Scale bars in the TEM images are 100 nm.

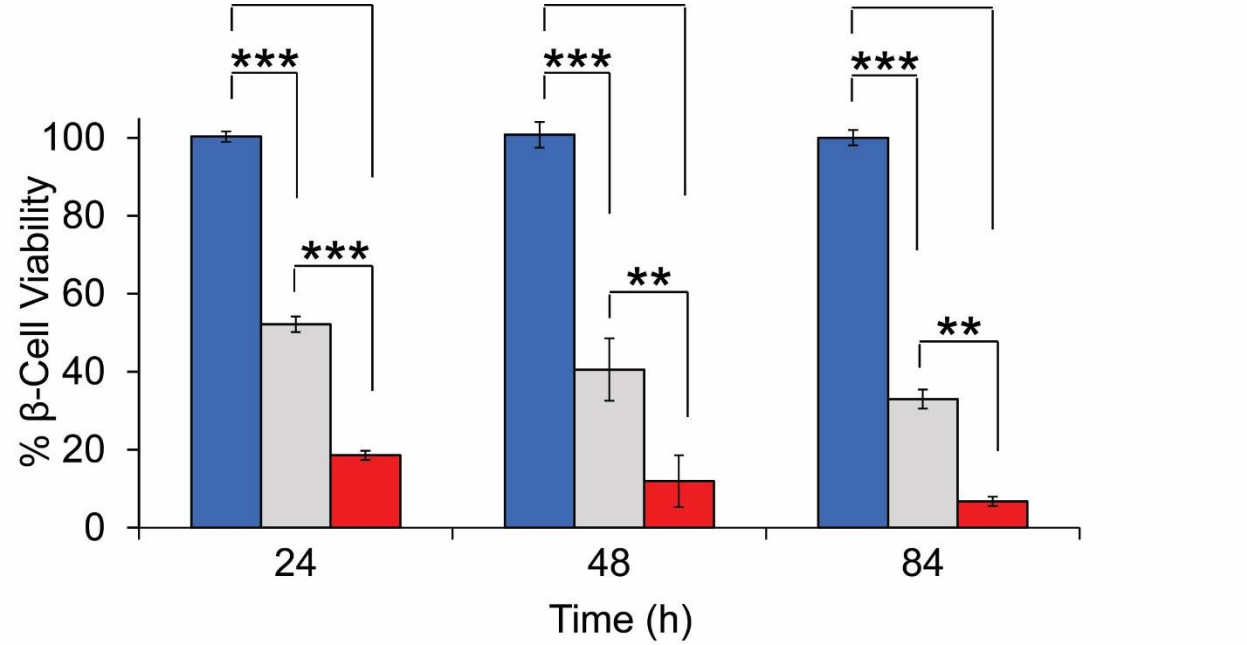

Figure 5-5: Baboon IAPP is more toxic to cultured INS-1 β-cells than Human IAPP. Cell toxicity studies using Alamar Blue reduction assays which measure loss in metabolic function, are plotted. Peptides were dissolved directly in culture medium and incubated on rat INS-1 β-cells for 24, 48 and 84 hours. Cell viability data for h-IAPP (grey) and b-IAPP (red) were normalized to untreated cells (blue). Final peptide concentration in β-cell assays was 30 μM. Data represent mean ± SD of three to six replicates per condition and a minimum of three experiments. **P<0.001, ***P<0.0001.

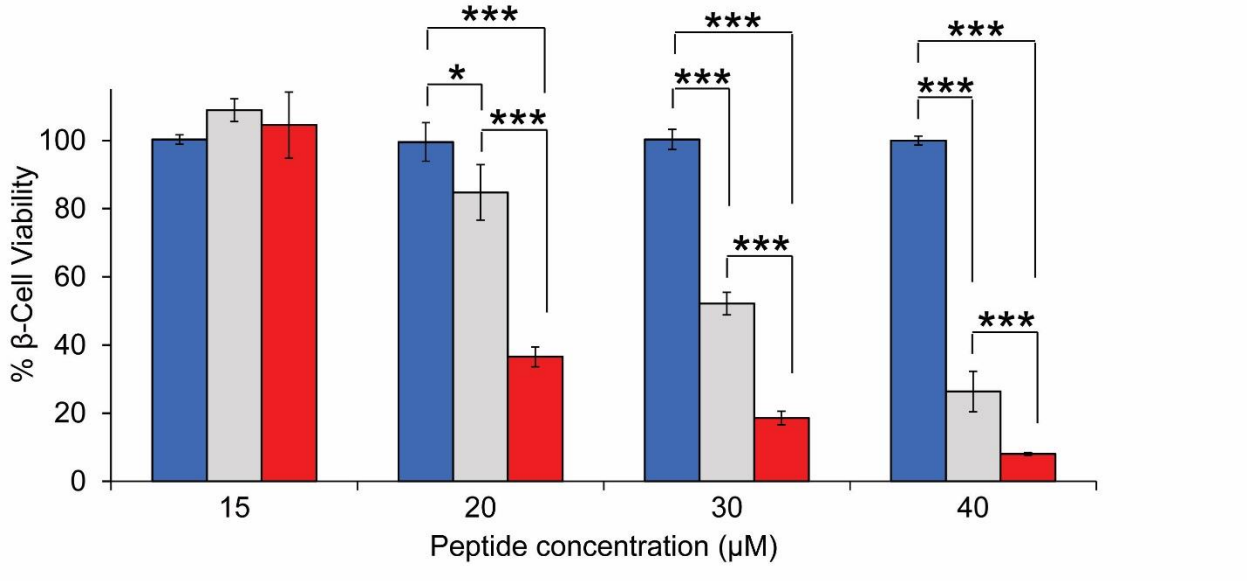

Figure 5-6: The toxicity of b-IAPP and h-IAPP is dose-dependent, but b-IAPP is more toxic than hIAPP under the same condition. β-Cell toxicity of b-IAPP and h-IAPP was assessed using Alamar Blue reduction assays. Peptides were dissolved directly in culture medium to produce 15, 20, 30, and 40 μM final peptide concentration, and incubated on rat INS-1 β-cells for 24 hrs. Cell viability data for h-IAPP (grey) and b-IAPP (red) were normalized to untreated cells (blue). Data represent mean ± SD of three to six replicates per condition and a minimum of three experiments. *P<0.01, ***P<0.0001

5.6 Tables

Name of Program	Relative Amyloidogenicity Of Baboon IAPP	Of K1I	Of H18R	Of A25T
AGGRESCAN	▲	▲	▼	▼
FoldAmyloid	-	▲	▲	-
Zyggregator	▼	▲	▼	▼
TANGO	▼	-	▼	▼

Table 5-1: Summary of the results of amyloid prediction algorithms. The program name is given as well as the predicted effect on the relative amyloidogenicity of b-IAPP, K1I, H18R, and A25T. (▲) The program predicts higher amyloidogenicity for the variant. (▼) The program predicts lower amyloidogenicity for the variant. (-) The program predicts no change in amyloidogenicity.

.

5.7 References

1. Westermark, P., Andersson, A., and Westermark, G. T. Islet Amyloid Polypeptide, Islet Amyloid, and Diabetes Mellitus, *Physiol. Rev.*, **2011**, *91*,795-826.

2. Lutz, T. A. The Role of Amylin in the Control of Energy Homeostasis, *Am. J. Physiol. - Regul. Integ, Comp Physiol.*, **2010**, *298*,R1475-R1484.

3. Westermark, P., Wernstedt, C., Wilander, E., Hayden, D. W., O'Brien, T. D., and Johnson, K. H. Amyloid Fibrils in Human Insulinoma and Islets of Langerhans of the Diabetic Cat Are Derived from a Neuropeptide-Like Protein Also Present in Normal Islet Cells, *PNAS*, **1987**, *84*,3881-3885.

4. Abedini, A., and Schmidt, A. M. Mechanisms of Islet Amyloidosis Toxicity in Type 2 Diabetes, *FEBS Lett.*, **2013**, *587*,1119-1127.

5. Cooper, G. J. S., Willis, A. C., Clark, A., Turner, R. C., Sim, R. B., and Reid, K. B. M. Purification and Characterization of a Peptide from Amyloid-Rich Pancreases of Type 2 Diabetic Patients, *PNAS*, **1987**, *84*,8628-8632.

6. Westermark, G. T., Westermark, P., Berne, C., and Korsgren, O. Widespread Amyloid Deposition in Transplanted Human Pancreatic Islets, *N. Engl. J. Med.*, **2008**, *359*,977-979.

7. Potter, K. J., Abedini, A., Marek, P., Klimek, A. M., Butterworth, S., Driscoll, M., Baker, R., Nilsson, M. R., Warnock, G. L., Oberholzer, J., Bertera, S., Trucco, M., Korbutt, G. S., Fraser, P. E., Raleigh, D. P., and Verchere, C. B. Islet Amyloid Deposition Limits the Viability of Human Islet Grafts But Not Porcine Islet Grafts, *PNAS*, **2010**, *107*,4305-4310.

8. Westermark, P., Engstrom, U., Johnson, K. H., Westermark, G. T., and Betsholtz, C. Islet Amyloid Polypeptide Pinpointing Amino Acid Residues Linked to Amyloid Fibril Formation, *PNAS*, **1990**, *87*,5036-5040.

9. Betsholtz, C., Christmansson, L., Engstrom, U., Rorsman, F., Svensson, V., Johnson, K. H., and Westermark, P. Sequence Divergence in a Specific Region of Islet Amyloid Polypeptide (Iapp) Explains Differences in Islet Amyloid Formation between Species, *FEBS Lett.*, **1989**, *251*,261-264.

10. Buchanan, L. E., Dunkelberger, E. B., Tran, H. Q., Cheng, P.-N., Chiu, C.-C., Cao, P., Raleigh, D. P., de Pablo, J. J., Nowick, J. S., and Zanni, M. T. Mechanism of IAPP Amyloid Fibril Formation Involves an Intermediate with a Transient Beta-Sheet, *PNAS*, **2013**, *110*,19285-19290.

11. Green, J., Goldsbury, C., Min, T., Sunderji, S., Frey, P., Kistler, J., Cooper, G., and Aebi, U. Full-Length Rat Amylin Forms Fibrils Following Substitution of Single Residues From Human Amylin, *J. Mol. Biol.*, **2003**, *326*,1147-1156.

12. Jha, S., Snell, J. M., Sheftic, S. R., Patil, S. M., Daniels, S. B., Kolling, F. W., and Alexandrescu, A. T. pH Dependence of Amylin Fibrillization, *Biochemistry*, **2014**, *53*,300-310.

13. Charge, S. B. P., De Koning, E. J. P., and Clark, A. Effect of pH and Insulin on Fibrillogenesis of Islet Amyloid Polypeptide In Vitro, *Biochemistry*, **1995**, *34*,14588-14593.

14. Abedini, A., and Raleigh, D. P. The Role of His-18 in Amyloid Formation By Human Islet Amyloid Polypeptide, *Biochemistry*, **2005**, *44*,16284-16291.

15. Knight, J. D., Hebda, J. A., and Miranker, A. D. Conserved and Cooperative Assembly of Membrane-Bound Alpha-Helical States of Islet Amyloid Polypeptide, *Biochemistry*, **2006**, *45*,9496-9508.

16. Abedini, A., and Raleigh, D. P. Destabilization of Human IAPP Amyloid Fibrils By Proline Mutations Outside of The Putative Amyloidogenic Domain: Is There A Critical Amyloidogenic Domain in Human IAPP?, *J. Mol. Biol.*, **2006**, *355*,274-281.

17. Koo, B. W., Hebda, J. A., and Miranker, A. D. Amide Inequivalence in The Fibrillar Assembly of Islet Amyloid Polypeptide, *Protein Eng., Des. Sel.*, **2008**, *21*,147-154.

18. Ratner, R. E., Dickey, R., Fineman, M., Maggs, D. G., Shen, L., Strobel, S. A., Weyer, C., and Kolterman, O. G. Amylin Replacement With Pramlintide As An Adjunct to Insulin Therapy Improves Long-Term Glycaemic And Weight Control in Type 1 Diabetes Mellitus: a 1-Year, Randomized Controlled Trial, *Diabetic Med.*, **2004**, *21*,1204-1212.

19. Kruger, D. F., and Gloster, M. A. Pramlintide For The Treatment of Insulin-Requiring Diabetes Mellitus: Rationale And Review of Clinical Data, *Drugs*, **2004**, *64*,1419-1432.

20. Wang, H., Abedini, A., Ruzsicska, B., and Raleigh, D. P. Rationally Designed, Nontoxic, Nonamyloidogenic Analogues of Human Islet Amyloid Polypeptide with Improved Solubility, *Biochemistry*, **2014**, *53*,5876-5884.

21. Nguyen, T. M., Wright, J. R., Jr., Nielsen, P. F., and Conlon, J. M. Characterization of the Pancreatic Hormones From The Brockmann Body of The Tilapia: Implications for Islet Xenograft Studies, *Comp. Biochem. Physiol. C: Pharmacol. Toxicol.*, **1995**, *111*,33-44.

22. Marek, P., Woys, A. M., Sutton, K., Zanni, M. T., and Raleigh, D. P. Efficient microwave-assisted synthesis of human islet amyloid polypeptide designed to facilitate the specific incorporation of labeled amino acids, *Organic letters*, **2010**, *12*,4848-4851.

23. Abedini, A., and Raleigh, D. P. Incorporation of Pseudoproline Derivatives Allows the Facile Synthesis of Human IAPP, A Highly Amyloidogenic and Aggregation-Prone Polypeptide, *Org. Lett.*, **2005**, *7*,693-696.

24. Tam, J. P., Wu, C. R., Liu, W., and Zhang, J. W. Disulfide Bond Formation in Peptides by Dmso Scope and Applications, *J Am Chem Soc*, **1991**, *113*,6657-6662.

25. Abedini, A., Singh, G., and Raleigh, D. P. Recovery and Purification of Highly Aggregation-Prone Disulfide-Containing Peptides: Application to Islet Amyloid Polypeptide, *Anal. Biochem.*, **2006**, *351*,181-186.

26. Thompson, M. J., Sievers, S. A., Karanicolas, J., Ivanova, M. I., Baker, D., and Eisenberg, D. The 3D Profile Method for Identifying Fibril-Forming Segments of Proteins, *PNAS*, **2006**, *103*,4074-4078.

27. Chakraborty, S., Chatterjee, B., and Basu, S. A Mechanistic Insight into the Amyloidogenic Structure of hIAPP Peptide Revealed From Sequence Analysis and Molecular Dynamics Simulation, *Biophys. Chem.*, **2012**, *168*,1-9.

28. Tartaglia, G. G., and Vendruscolo, M. The Zyggregator Method For Pedicting Potein Agregation Propensities, *Chem. Soc. Rev.*, **2008**, *37*,1395-1401.

29. Garbuzynskiy, S. O., Lobanov, M. Y., and Galzitskaya, O. V. FoldAmyloid: A Method of Prediction of Amyloidogenic Regions From Protein Sequence, *Bioinformatics*, **2010**, *26*,326-332.

30. Fernandez-Escamilla, A.-M., Rousseau, F., Schymkowitz, J., and Serrano, L. Prediction of Sequence-Dependent And Mutational Effects on the Aggregation of Peptides and Proteins, *Nat. Biotechnol.*, **2004**, *22*,1302-1306.

31. Hobbs, J. R., and Morgan, A. D. Fluorescence Microscopy with Thioflavine-T in Diagnosis of Amyloid, *J. Pathol. Bacteriol.*, **1963**, *86*,437-&.

32. Levine, H. Thioflavine-T Interaction with Synthetic Alzheimers-Disease Beta-Amyloid Peptides - Detection of Amyloid Aggregation in Solution, *Protein Sci.*, **1993**, *2*,404-410.

33. Sulatskaya, A. I., Maskevich, A. A., Kuznetsova, I. M., Uversky, V. N., and Turoverov, K. K. Fluorescence Quantum Yield of Thioflavin T in Rigid Isotropic Solution and Incorporated Into The Amyloid Fibrils, *PLoS One*, **2010**, *5*,e15385.

34. Cloe, A. L., Orgel, J. P. R. O., Sachleben, J. R., Tycko, R., and Meredith, S. C. The Japanese Mutant Abeta (DeltaE22-Abeta(1-39)) Forms Fibrils Instantaneously, with Low-Thioflavin T Fluorescence: Seeding of Wild-Type Abeta(1-40) Into Atypical Fibrils by DeltaE22-Abeta(1-39), *Biochemistry*, **2011**, *50*,2026-2039.

35. Young, L. M., Cao, P., Raleigh, D. P., Ashcroft, A. E., and Radford, S. E. Ion Mobility Spectrometry-Mass Spectrometry Defines the Oligomeric Intermediates in Amylin Amyloid Formation and the Mode of Action of Inhibitors, *J. Am. Chem. Soc.*, **2014**, *136*,660-670.

36. Bram, Y., Frydman-Marom, A., Yanai, I., Gilead, S., Shaltiel-Karyo, R., Amdursky, N., and Gazit, E. Apoptosis Induced by Islet Amyloid Polypeptide Soluble Oligomers is Neutralized by Diabetes-Associated Specific Antibodies, *Sci. Rep.*, **2014**, *4*.

37. Weise, K., Radovan, D., Gohlke, A., Opitz, N., and Winter, R. Interaction of hIAPP with Model Raft Membranes and Pancreatic beta-Cells: Cytotoxicity of hIAPP Oligomers, *Chem. Bio. Chem.*, **2010**, *11*,1280-1290.

38. Chen, M.-S., Zhao, D.-S., Yu, Y.-P., Li, W.-W., Chen, Y.-X., Zhao, Y.-F., and Li, Y.-M. Characterizing the Assembly Behaviors of Human Amylin: A Perspective Derived from C-Terminal Variants, *Chem. Commun.*, **2013**, *49*,1799-1801.

39. Bitan, G., and Teplow, D. B. Rapid Photochemical Cross-Linking--A New Tool For Studies of Metastable, Amyloidogenic Protein Assemblies, *Acc. Chem. Res.*, **2004**, *37*,357-364.

40. Luca, S., Yau, W. M., Leapman, R., and Tycko, R. Peptide Conformation and Supramolecular Organization in Amylin Fibrils: Constraints From Solid-State NMR, *Biochemistry*, **2007**, *46*,13505-13522.

41. Wiltzius, J. J. W., Sievers, S. A., Sawaya, M. R., Cascio, D., Popov, D., Riekel, C., and Eisenberg, D. Atomic Structure of The Cross-Beta Spine of Islet Amyloid Polypeptide (Amylin), *Protein Sci.*, **2008**, *17*,1467-1474.

42. Vaiana, S. M., Best, R. B., Yau, W. M., Eaton, W. A., and Hofrichter, J. Evidence for a Partially Structured State of the Amylin Monomer, *Biophys. J.*, **2009**, *97*,2948-2957.

43. Koo, B. W., and Miranker, A. D. Contribution of the Intrinsic Disulfide to the Assembly Mechanism of Islet Amyloid, *Protein Sci.*, **2005**, *14*,231-239.

44. Fooks, H. M., Martin, A. C., Woolfson, D. N., Sessions, R. B., and Hutchinson, E. G. Amino Acid Pairing Preferences in Parallel Beta-Sheets in Proteins, *J. Mol. Biol.*, **2006**, *356*,32-44.

45. Zhang, N., Ruan, J., Duan, G., Gao, S., and Zhang, T. The Interstrand Amino Acid Pairs Play a Significant Role in Determining the Parallel or Antiparallel Orientation of Beta-Strands, *Biochem. Biophys. Res. Commun.*, **2009**, *386*,537-543.

Chapter 6. Exploration of the Role of the Disulfide Bond in Amyloid Formation by Islet Amyloid Polypeptide

Abstract

The disulfide bond in islet amyloid polypeptide (IAPP) located between Cys-2 and Cys-7 is strictly conserved and has been found in all higher organisms examined regardless of the amyloidogenicity of the primary sequence. The role of the disulfide bond has not been elucidated, although it has more recently been shown to reduce the amyloidogenicity and increase the bioactivity of IAPP. To study the role of the disulfide, several peptides were generated lacking the disulfide bond. Two truncated versions, an 8-37 fragment of IAPP ($IAPP_{8-37}$) and an acetylated variant of $IAPP_{8-37}$ (Ac_{8-37}) were synthesized. In addition, a double cysteine to serine replacement (C2S, C7S) and protected cysteine variant ($IAPP_{CAM}$) were also examined. All the variants form amyloid fibrils faster than human IAPP *in vitro*, as judged by thioflavin-T fluorescence assays and transmission electron microscopy. The C2S, C7S double replacement is less toxic to INS-1 β-cells than the human IAPP. Testing the binding to the amylin ($AMY_{1(a))}$ receptor showed a reduction in potency for all the variants relative to human IAPP but the efficacy of Ac_{8-37} and $IAPP_{CAM}$ were markedly better than $IAPP_{8-37}$ and C2S, C7S relative to h-IAPP.

NOTE: The cytotoxicity assays were performed by Dr. Andisheh Abedini in the Ann Marie Schmidt group at NYU. Amylin and calcitonin receptor activity studies were performed by Rebekah Bower in the Debbie Hay group at the University of Auckland.

6.1 Introduction

Disulfide bonds are a common structural feature of proteins and are present in 65 % of secreted proteins and in over half of proteins associated with amyloidosis [1]. Removal of this bond has been shown to change the morphology of fibrils, the rate of aggregation, or change the toxicity of the fibrils [2-4]. The disulfide bond located between Cys-2 and Cys-7 in islet amyloid polypeptide (IAPP, amylin) is highly conserved and it is found in all higher organisms examined. Additionally as shown in Chapter 1, the first seven residues, of IAPP are also highly conserved with substitutions in this region only in baboon, cow, pig, and horse [5]. The cyclical rigidity of the 1-7 segment of human IAPP (h-IAPP) led to the initial hypothesis that this region did not participate in amyloid formation. Current models of the IAPP fibril all show the 1-7 region of the peptide outside of the β-sheet core fibril [6-8]. However, removal of the first seven residues and the disulfide bond result in an elimination of the lag phase and an increased rate of aggregation, indicating that the bond may play a role in amyloid formation by IAPP [9, 10]. The role of the disulfide bond is currently not known though it appears to be necessary for bioactivity and may play a protective role in preventing h-IAPP amyloid formation [11-14]. The bond may play a role in the early events of amyloid formation by stabilizing the monomer and preventing formation of oligomers or by increasing number of prefibrillar oligomer species [15, 16]. It has been proposed that this region may interact with the 20-29 amyloidogenic core region of the peptide and thus prohibit this region from interacting with other amyloidogenic regions of IAPP monomers [17].

Herein, we examine two truncated variants, an 8-37 fragment of IAPP ($IAPP_{8-37}$) and an acetylated variant of $IAPP_{8-37}$ (Ac_{8-37}). Both truncated peptides lack the first seven residues and the disulfide bond and Ac_{8-37} lacks the charged N-terminus resulting in a reduced net charge compared to h-IAPP. Cysteines will form intramolecular bonds provided the structure is comparable with the geometric constraints unless reducing agents are used, which may perturb the kinetics of IAPP. To avoid this, two variants designed to mimic the reduced form of h-IAPP were designed and examined. The C2S, C7S double replacement was chosen because serine is a conservative replacement for cysteine since the OH group on the serine sidechain has many of the same chemical properties as the SH group on the cysteine sidechain while not having the ability to form disulfide bonds. In addition, a protected variant of h-IAPP was synthesized by blocking the thiol group of each cysteine with a carboxyamidomethy protecting group ($IAPP_{CAM}$). Of these, the $IAPP_{CAM}$ is particularly interesting as it is a more accurate model of the reduced form of IAPP. The results provide insight into role of the disulfide bond in amyloid formation by h-IAPP. Additionally, testing binding to the human amylin ($AMY_{1(a)}$) receptor also provides information on the regions of IAPP that are important for bioactivity.

6.2 Materials and Methods

6.2.1 Peptide Synthesis and Purification

Peptides were synthesized with a CEM microwave peptide synthesizer on a 0.10 mmol scale utilizing 9-fluorenylmethoxycarbonyl (Fmoc) chemistry. 5-(4’-Fmoc-aminomethyl-3’,5-dimethoxyphenol) valeric acid (PAL-PEG) resin was used to provide an amidated C-terminus. Fmoc-protected pseudoproline (oxazolidine) dipeptide derivatives were utilized as previously described [18, 19]. Solvents used were ACS-grade. β-branched residues, the first residue

attached to the resin, pseudoproline dipeptide derivatives and the residues following the pseudoproline dipeptide derivatives were double-coupled. A capping solution composed of acetic anhydride, diisopropylethylamine, and DMF with the ratios 0.5 : 0.2 : 9.3 (v/v%) was made. Hydroxybenzotriazole was added to this solution to a final concentration of 18 mM. The peptide was microwaved in the capping solution for two minutes. Peptides were cleaved from the resin via standard trifluoroacetic acid (TFA) methods and triisopropyl silane (TIPS) as the scavenger. The cleaved crude peptides were dissolved into 15% (v/v) acetic acid and lyophilized. The disulfide bond was formed in 100% dimethyl sulfoxide at room temperature for three days. Peptides were purified via reverse-phase high-performance liquid chromatography (RP-HPLC) using a Higgins Analytical Proto 300 C18 preparative column (10 mm x 250 mm). A 20 – 60 % gradient was used over 40 minutes where buffer A was 100 % H_2O, 0.045 % HCl and buffer B was 80 % acetonitrile, 0.045 % HCl. h-IAPP had a retention time of 31 minutes (51 % B). $IAPP_{8-37}$ had a retention time of 20 minutes (40%). Ac_{8-37} had a retention time of 26 minutes (46%). C2S, C7S, had a retention time of 25 minutes (45%). The purity of the peptides was tested using analytical HPLC. The masses of the pure peptides were confirmed with MALDI time-of-flight mass spectrometry. h-IAPP, expected 3903.6, observed 3902.9; $IAPP_{8-37}$, expected 3183.4, observed 3184.0, Ac_{8-37} expected 3225.5, observed 3226.1, C2S, C7S, expected 3873.2, observed, 3874.1.

6.2.2 Preparation of $IAPP_{CAM}$

$IAPP_{CAM}$ was synthesized as previously described [20]. Pure h-IAPP at a concentration of 0.25 mg/mL was incubated in the presence of 13 mM DTT, 6 M GdnHCl, 0.19 M Tris HCl, 10% DMSO, pH 8.0 for 4 hours at 4 °C under nitrogen gas in order to fully reduce the peptide. Iodoacetamide was added to the cocktail to a final concetration of 8 mM. The reaction was then

allowed to proceed for another 4 hours at 4 °C in the dark. The reaction was quenched with 80 mM of 2-mercaptoethanol. $IAPP_{CAM}$ was purified by RP-HPLC using a Higgins Analytical Proto 300 C18 preparative column. A 20 – 60 % gradient was used over 40 minutes where buffer A was 100 % H2O, 0.045 % HCl and buffer B was 80 % acetonitrile, 0.045 % HCl. $IAPP_{CAM}$ had a retention time of 28 minutes (48 % B). The purity of the peptide was tested using analytical HPLC. The masses of the pure peptides was confirmed with MALDI time-of-flight mass spectrometry. $IAPP_{CAM}$, expected 4019.6, observed 4019.0.

6.2.3 Sample Preparation and Fluorescence Assays

Stock solutions were prepared by dissolving peptide into 100% hexafluoroisopropanol (HFIP) at 1.6 mM. Solutions were filtered with 0.45 μM Acrodisc syringe filters and the required amount was lyophilized overnight to remove HFIP. Dry peptide was then dissolved into tris buffer or PBS for the fluorescence assays. The kinetics of amyloid formation were monitored using thioflavin-T binding assays conducted at 25 °C. Fluorescence measurements were performed using a Beckman Coulter DTX 880 plate reader with a multimode detector using an excitation wavelength of 430 nm and an emission wavelength of 485 nm.

6.2.4 Transmission Electron Microscopy

TEM images were collected at the Life Science Microscopy Center at the State University of New York at Stony Brook. At the end of each experiment, 15 μL aliquots of the samples used for the kinetic studies were removed, blotted on a carbon-coated 300-mesh copper grid for 1 min and then negatively stained with saturated uranyl acetate for 1 min.

6.2.5 Cytotoxicity Assays

NOTE: The cytotoxicity assays were performed by Dr. Andisheh Abedini in the Anne Marie Schmidt group at NYU. The methods have been included here for completeness.

Rat INS-1 β-cells were seeded in 96-well plates at a density of 35,000-40,000 cells per well 15-24 hrs prior to start of experiments. Peptides were dissolved in complete RPMI (20, 30 or 40 μM final concentration), and incubated on cells for 24 hours prior to cell viability measurements which was assessed by Alamar Blue reduction assays. Alamar Blue solution was diluted ten-fold in culture medium and incubated on cells for 5 hrs at 37 °C. Fluorescence (excitation 530 nm; emission 590 nm) was measured with a Beckman Coulter DTX880 plate reader. Toxicity data was normalized with respect to untreated control cells and reported as percent β-cell viability.

6.3 Results and Discussion

6.3.1 Modification of the Disulfide Bond Shortens the Lag Phase and Increases the Rate of Aggregation

We compared the time course of amyloid formation by h-IAPP, $IAPP_{8-37}$, Ac_{8-37}, C2S, C7S, and $IAPP_{CAM}$ using thioflavin-T fluorescence assays and transmission electron microscopy (TEM). We conducted initial experiments in 20 mM tris at pH 7.4, chosen because this buffer has been used extensively in studies of amyloid formation by IAPP. The concentration of each of the peptides was 16 μM and was chosen because this is a typical concentration used for biophysical studies with the peptide. Amyloid formation by IAPP follows a sigmoidal curve consisting of a lag phase, an elongation phase and a final plateau where amyloid fibrils and monomers are in equilibrium. For each of the variants, this sigmoidal thioflavin-T fluorescence response is observed for each of the variants (Figure 6-2A). Both truncated variants formed amyloid significantly faster than the full length peptides with a t_{50} of 1.83 ± 0.63 for $IAPP_{8-37}$ and

1.45 ± 0.40 for Ac_{8-37} relative to 7.73 ± 1.6 for h-IAPP where t_{50} is defined as the time required to reach half maximum fluorescence intensity in a thioflavin-T assay (Table 6-1). The full length variants, C2S, C7S and $IAPP_{CAM}$, also formed amyloid fibrils faster than h-IAPP with t_{50}s that were roughly half that of h-IAPP. TEM was used as a secondary method to confirm the formation of fibrils. Aliquots were removed at the end of each kinetic experiment after 24 hours, a time sufficient for all the peptides to reach the thioflavin-T fluorescence plateau, and TEM images were recorded (Figure 6-2B). Dense mats of amyloid fibrils were observed in the images of all of the peptides and all exhibited the typical morphology of amyloid fibrils associated with *in vitro* h-IAPP amyloid formation.

We also examined the behavior of h-IAPP and each of the variants in a more physiological buffer, phosphate buffered saline (PBS) [10 mM sodium phosphate, 140 mM KCl, pH 7.4] Again, we observe a shortening in the lag phase for each of the variants examined (Figure 6-3A). The shorter lag phase is consistent with the known effects of salts on IAPP amyloid formation [21]. C2S, C7S and $IAPP_{CAM}$ have t_{50}s that are roughly half that of h-IAPP (Table 6-1). Under these conditions, the truncated variants, $IAPP_{8-37}$ and Ac_{8-37} form amyloid faster than h-IAPP but the lag phase is not as short as we would expect. In tris buffer, the t_{50} was roughly a quarter of the t_{50} of h-IAPP whereas in PBS it is roughly half. In fact, the t_{50} values for $IAPP_{8-37}$ and Ac_{8-37} are similar in both buffer conditions examined here. The t_{50} of $IAPP_{8-37}$ was 1.93 ± 0.26 and was 2.32 ± 0.92 for Ac_{8-37} relative to 3.35 ± 0.30 for h-IAPP. Due to the removal of the lysine of both variants, and the removal of the charged N-terminus of the Ac_{8-37}, these truncated peptides have a reduced net charge compared to h-IAPP. Therefore, it is likely that the phosphate anions in PBS are not accelerating these two variants to the same extent as the full length peptides examined here. The key point is that the disulfide bond plays a role in amyloid

formation by IAPP and the 1-7 region of the peptide may also have a role in amyloid formation. TEM images were collected at the conclusion of each experiment. The fibrils for each variant exhibited a typical morphology similar to h-IAPP (Figure 6-3B).

6.3.2 The C2S, C7S Double Replacement is Less Toxic Relative to h-IAPP

Having established that C2S, C7S forms amyloid, we next examined its effect on the viability of cultured β-cells using the rat INS-1 β-cell line. Treatment with h-IAPP for 24 hours led to a dose-dependent decrease in β-cell viability (Figure 6-4). Incubation with 20 μM h-IAPP for 24 hours led to a 35% reduction in β-cell viability compared to control cells. Incubation with the C2S, C7S peptide led to a 28% decrease in β-cell viability (Figure 6-4). Higher concentrations of h-IAPP on β-cells led to further reductions in β-cell viability; a 73% decrease was observed at 30 μM concentration and an 81% reduction was observed at 40 μM. The effects of C2S, C7S were also dose dependent; incubation of 30 μM peptide reduced β-cell viability by 59% and incubation of 40 μM concentration saw a reduction of 83% compared to untreated cells. Both human and C2S, C7S were less toxic at lower peptide concentrations, but the h-IAPP consistently remained more toxic. We hesitate to draw conclusions without further experiments at different time points but it would appear that C2S, C7S may be less toxic to β-cells than h-IAPP. This trend has commonly been observed in peptides with shorter lag phases relative to h-IAPP.

6.3.3 The Disulfide Variants Relative to h-IAPP Have Reduced Activity Towards the Human Amylin and Calcitonin Receptors

NOTE: The receptor activity studies were performed by Rebekah Bower in the Debbie Hay group at the University of Auckland.

h-IAPP is a ligand of the calcitonin (CT) receptor. There are two isoforms of the calcitonin receptor which are known as $CT_{(a)}$ and $CT_{(b)}$. These two isoforms can heterodimerize with accessory proteins known as receptor activity-modifying proteins (RAMPS). There are three ramps that can combine with the two isoforms of CT in order to create six amylin (AMY) receptors of which amylin has an increased affinity to relative to the unmodified CT receptor. The $AMY_{1(a)}$ and $AMY_{3(a)}$ receptors are the best characterized of the amylin receptors, the former of which is used for these studies [22]. In order, to develop new therapeutics for the treatment of T2D, its activity to amylin receptors must be considered. Thus, receptor activity studies are a useful tool in determining structure-function relationships of h-IAPP.

Each of the variants was tested at $AMY_{1(a)}$ and were directly compared to h-IAPP activity in each experiment (Figure 6-5) . Activity was determined by cAMP production and compared to h-IAPP in each experiment. The activity of $IAPP_{8-37}$ was greatly reduced with an efficacy that was roughly half that of h-IAPP (Table 6-2). The potency of $IAPP_{8-37}$ was also greatly reduced with a 400-fold reduction compared to h-IAPP. In contrast, the Ac_{8-37} was much better tolerated than $IAPP_{8-37}$. The activity was only mildly reduced with an efficacy of 82.8 ± 10.4 relative to h-IAPP. The potency of Ac_{8-37} was also much higher than that of $IAPP_{8-37}$ as it only had a 32-fold reduction.

C2S, C7S resulted in an approximately 300-fold reduction in potency compared to h-IAPP. The activity was also greatly decreased with max efficacy of only half that of h-IAPP. In contrast, the activity of $IAPP_{CAM}$ was virtually unchanged compared to the h-IAPP control. The potency of $IAPP_{CAM}$ was also only mildly changed compared to C2S, C7S with a 71-fold reduction.

Ac_{8-37}, and $IAPP_{CAM}$ were tested at $CT_{(a)}$ and were directly compared to h-IAPP activity in each experiment (Figure 6-6). Activity was again determined by cAMP production. Ac_{8-37} had a mild loss in activity with an efficacy of 80.2 ± 6.13 relative to h-IAPP (Table 6-3). $IAPP_{CAM}$ had a very similar activity as Ac_{8-37} with an efficacy of 81.2 ± 4.70 relative to h-IAPP. $IAPP_{CAM}$ and Ac_{8-37} had similar potency with 56-fold and 42-fold loss in potency respectively relative to h-IAPP.

6.4 Conclusions

The data presented here demonstrates that the disulfide bond and the 1-7 region of IAPP play a role in forming amyloid fibrils. Removal of the disulfide bond and/or the first seven residues resulted in an elimination of the lag phase and an increase in the rate of amyloid formation by each of the variants. This region was previously believed to not participate in amyloid formation and thus the results shown here have clear implications for studies which use truncated constructs and fragments in order to study the structure of the mature fibrils or the prefibrillar oligomers. Both of the full length variants of IAPP, C2S, C7S and $IAPP_{CAM}$, were slower to form amyloid than the truncated variants, $IAPP_{8-37}$ and Ac_{8-37} though all the variants were faster than h-IAPP. These results indicate that removal of the first seven residues has an effect on amyloid formation by IAPP and the shortening of the lag phase is not just due to removal of the disulfide bond. This region may have a role in blocking the formation of pre-fibrillar oligomers. Mild differences arose between experiments conducted in tris buffer and PBS. These differences may be because the truncated variants have a reduced net charge relative to h-IAPP, C2S, C7S, and $IAPP_{CAM}$. Analysis of the effects of anions on h-IAPP amyloid formation have revealed that the rate of aggregation is incredibly sensitive to the concentration of

salt, the identity of the anion, and to the overall charge of the sequence [21]. The Ac_{8-37} variant formed amyloid fibrils the fastest of the variants when examined in tris buffer, but was the slowest of the variants in PBS although it was still able to form amyloid fibrils faster than h-IAPP. The Ac_{8-37} peptide has the lowest charge of all as both Lys-1 and the charged N-terminus have been removed and thus this variant may have a lower affinity to phosphate and therefore, not be accelerated to the same extent as the other peptides examined here. The $IAPP_{CAM}$ variant has been previously examined and was observed to form amyloid slower than h-IAPP [20]. However, the previous experiments were done in the presence of 2.5% HFIP. As was described in Chapter 2, the presence of HFIP changed the behavior of the variants by potentially changing electrostatic and hydrophobic interactions and by leading to phase separation of the solvent. The use of the organic solvent may account for the differences between our observations and previous results. Regardless of the differences between buffer conditions, the results indicate that the disulfide bond and the first seven residues are important for stabilizing IAPP and preventing the formation of amyloid fibrils.

The C2S, C7S double replacement was less toxic to INS-1 β-cells relative to h-IAPP. This is not surprising since its lag phase is less than that of h-IAPP and is in agreement with the hypothesis that pre-fibrillar oligomers are more toxic to INS-1 β-cells than mature fibrils [23, 24]. However, we are hesitant to draw any definite conclusions without a longer time course for experiments. It would be interesting to see what effects the truncated variants and $IAPP_{CAM}$ have on the toxicity to INS-1 β-cells.

The receptor activity at $AMY_{1(a)}$ was relatively unchanged upon the addition of Ac_{8-37} and $IAPP_{CAM}$ while the activity was greatly reduced upon the addition of $IAPP_{8-37}$ and C2S, C7S. Surprisingly, these results indicate that the carboxyamidomethyl protecting groups is a more

conservative change than the serines as $IAPP_{CAM}$ was better tolerated to the receptor relative to C2S, C7S making it a full agonist as opposed to a partial agonist. The polar OH functional groups on the serine sidechains may have a more detrimental interaction with the $AMY_{1(a)}$ receptor than the carboxyamidomethyl groups on $IAPP_{CAM}$. While the mechanism of receptor binding interaction of the $AMY_{1(a)}$ receptor by h-IAPP is not fully known, a two domain model of binding has been proposed. In this model, the C-terminus initiates binding to the receptor then the N-terminal region interacts with the receptor in order to activate it [25]. Fragments of IAPP lacking the N-terminus have been shown to be antagonists of the receptor with poor efficacy and potency and have lent support to this model. $IAPP_{8-37}$ has previously been shown to be an antagonist of the amylin receptor and that is what is observed here [26, 27]. Ac_{8-37} was better able to activate the receptor relative to $IAPP_{8-37}$. This is surprising since the sole difference between these peptides is the acetylated N-terminus of Ac_{8-37} which is a feature that is lacking on h-IAPP. It would appear that the acetylated N-terminus is able to restore some of the activity that is lost when removing the first seven residues. It could be due in part to the larger size of the acetyl group on the N-terminus is better able to activate the receptor than the typical N-terminus. Alternatively, removal of the charge could enhance binding to the receptor relative to $IAPP_{8-37}$. The charged N-terminus in $IAPP_{8-37}$ could be in a different location in the receptor binding site than the N-terminus in full-length IAPP. Both Ac_{8-37} and $IAPP_{CAM}$ had similar activity to $CT_{(a)}$ receptor. The potency for both variants was also similar relative to h-IAPP.

We believe this work shows that the disulfide bond and the first seven residues of IAPP play a role in stabilizing the non-amyloid forms of the peptide. In addition, the disulfide bond and the 1-7 segment play a role in the bioactivity of IAPP. The significant change in the rate of amyloid formation when the disulfide bond and the first seven residues are removed should be

taken into consideration when using fragments or constructs of IAPP for simulations, structural studies, or analysis of prefibrillar species of the peptide. It is also worth noting that the sequences of baboon, cow, and horse have substitutions within the first seven residues of the peptide. Further examination of these three primary sequences will undoubtedly yield more information about the N-terminal region of IAPP.

6.5 Figures

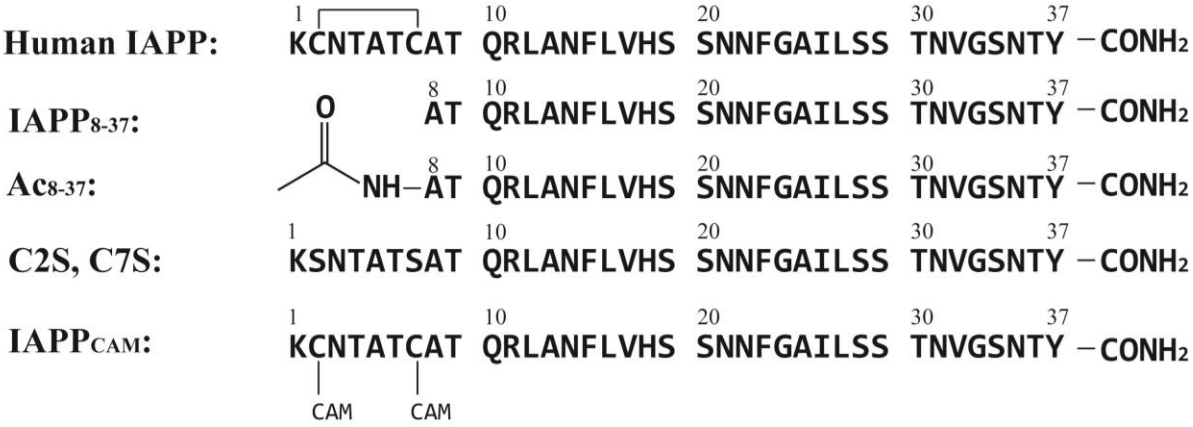

Figure 6-1: Comparison of the primary sequence of human IAPP, $IAPP_{8-37}$, Ac_{8-37}, C2S, C7S, and $IAPP_{CAM}$. Each of the cysteines of $IAPP_{CAM}$ is blocked by a carboxyamidomethy (CAM) protecting group.

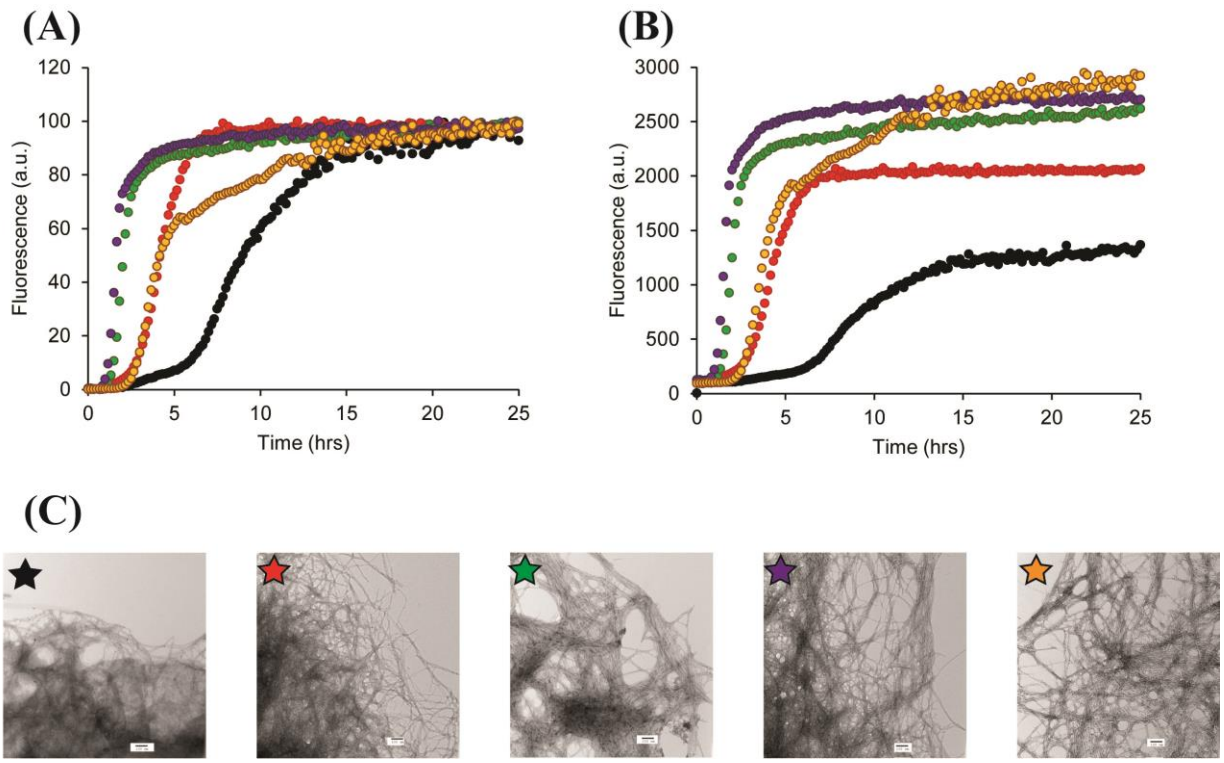

Figure 6-2: Analysis of amyloid formation of the disulfide variants in tris-HCl at pH 7.4 (A) Normalised fluorescence monitored thioflavin-T assays of amyloid formation by h-IAPP (black), $IAPP_{8-37}$ (green), Ac_{8-37} (purple), C2S, C7S (yellow), and $IAPP_{CAM}$ (red) in 20 mM tris-HCl at pH 7.4. (B) Non-normalised fluorescence monitored thioflavin-T assays of amyloid formation by h-IAPP (black), $IAPP_{8-37}$ (green), Ac_{8-37} (purple), C2S, C7S (yellow), and $IAPP_{CAM}$ (red) in 20 mM tris-HCl at pH 7.4. (C) TEM images of samples of h-IAPP (black), $IAPP_{8-37}$ (green), Ac_{8-37} (purple), C2S, C7S (yellow), and $IAPP_{CAM}$ (red) collected at the end of each experiment. Aliquots were removed after 24 hours, a time sufficient for amyloid formation to go to completion for all the peptides examined. Experiments were conducted with 16 µM peptide, 32 µM thioflavin-T at 25 °C in 20 mM tris-HCl at pH 7.4. Scale bars in TEM images represent 100 nm.

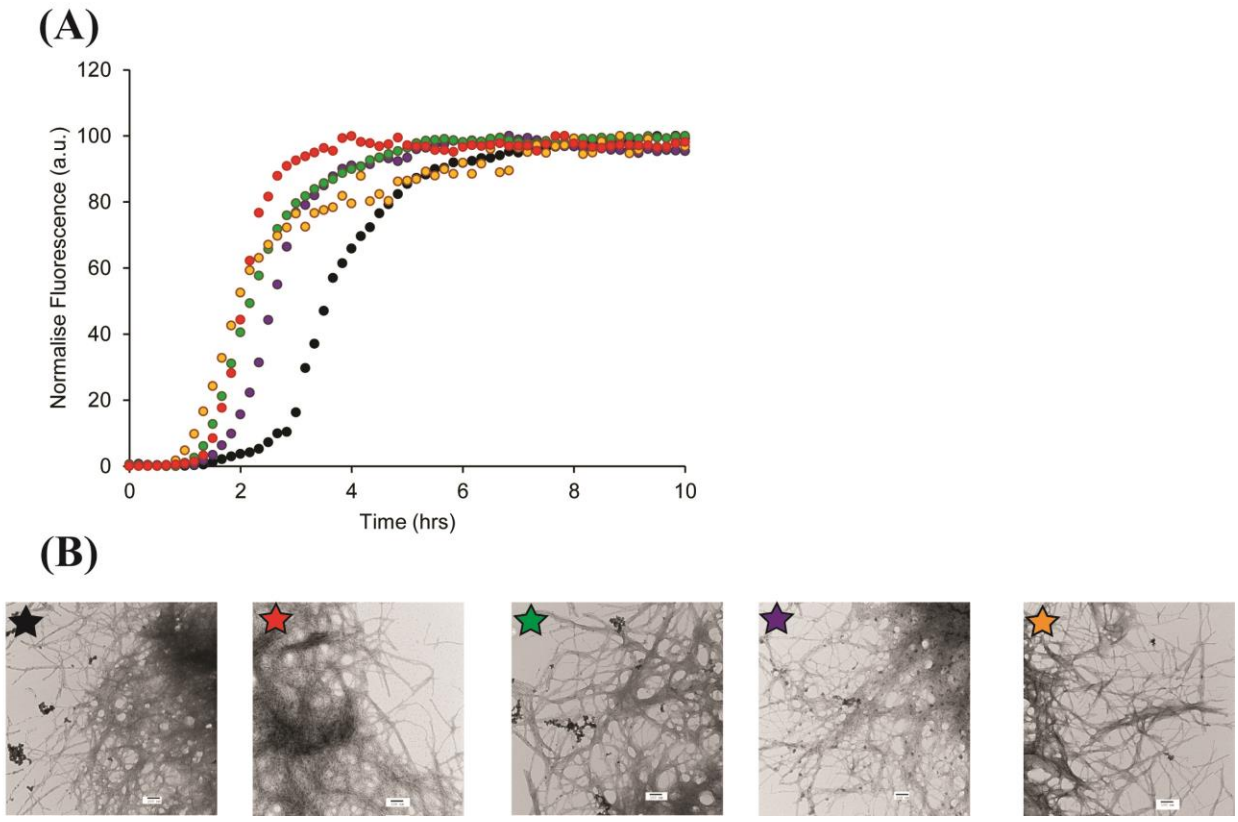

Figure 6-3: Analysis of amyloid formation of the disulfide variants in PBS [10 mM sodium phosphate, 140 mM potassium chloride pH 7.4]. (A) Fluorescence monitored thioflavin-T assays of amyloid formation by h-IAPP (black), $IAPP_{8-37}$ (green), Ac_{8-37} (purple), C2S, C7S (yellow), and $IAPP_{CAM}$ (red) in PBS at pH 7.4. (B) TEM images of samples of h-IAPP (black), $IAPP_{8-37}$ (green), Ac_{8-37} (purple), C2S, C7S (yellow), and $IAPP_{CAM}$ (red) collected at the end of each experiment. Aliquots were removed after 24 hours, a time sufficient for amyloid formation to go to completion for all the peptides examined. Experiments were conducted with 16 µM peptide, 32 µM thioflavin-T at 25 °C in PBS at pH 7.4. Scale bars in TEM images represent 100 nm.

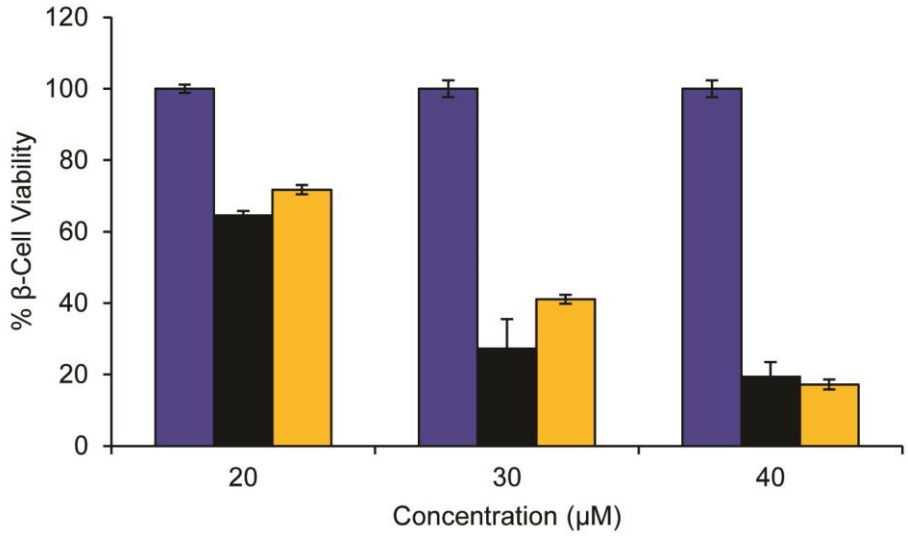

Figure 6-4: C2S, C7S is less toxic to INS-1 β-cells as human IAPP. The results of cell viability studies, based on Alamar blue reduction assays, are plotted. Peptide was added to cultured INS-1 β-cells and incubated for 24 hours. Cell viability was determined for human IAPP (black), and C2S, C7S (yellow) and the untreated cells (blue) at 20, 30, and 40 μM concentrations.

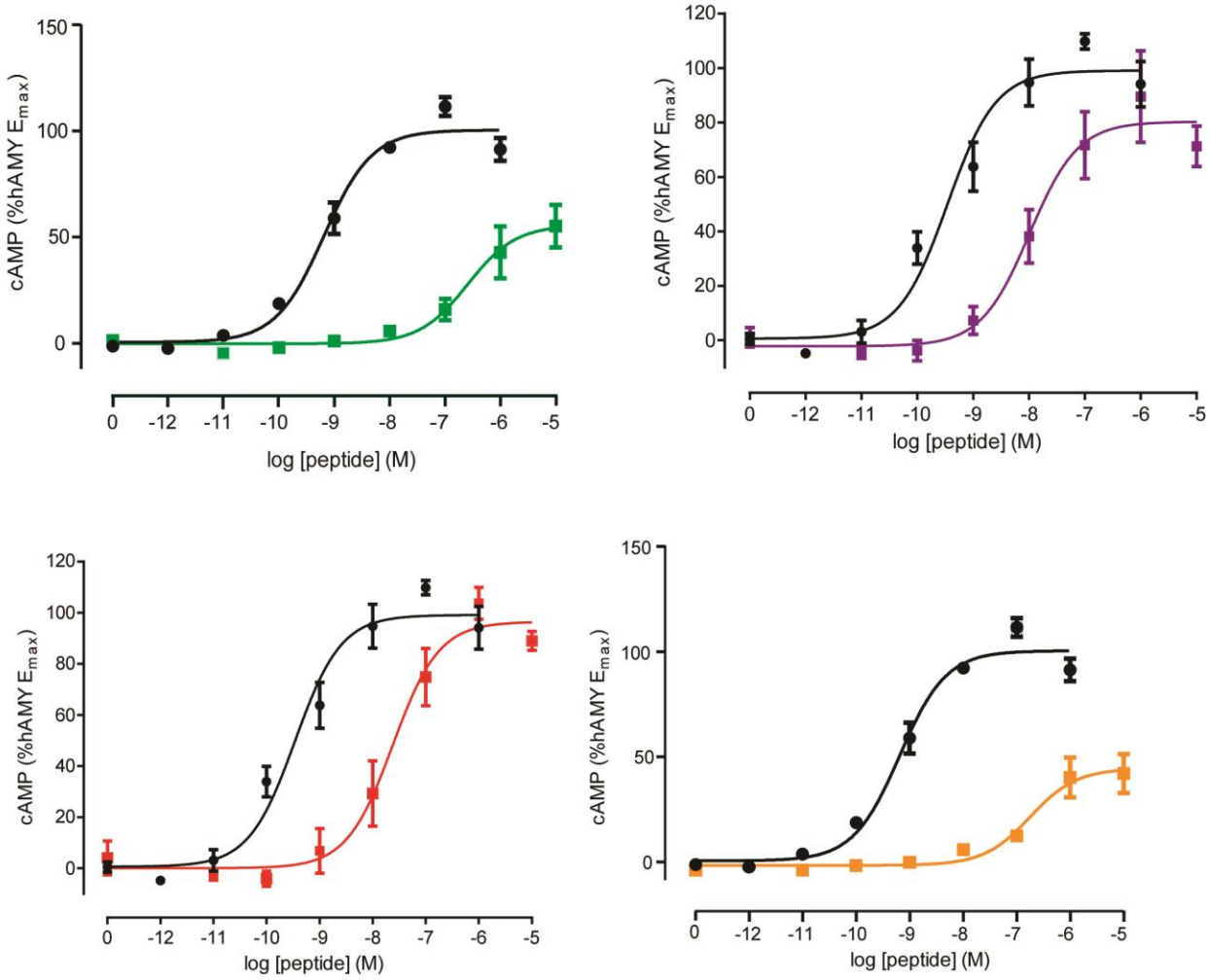

Figure 6-5: Activity of h-IAPP (black), $IAPP_{8-37}$ (green), Ac_{8-37} (purple), C2S, C7S (yellow), and $IAPP_{CAM}$ (red) at the $AMY_{1(a)}$ receptor.

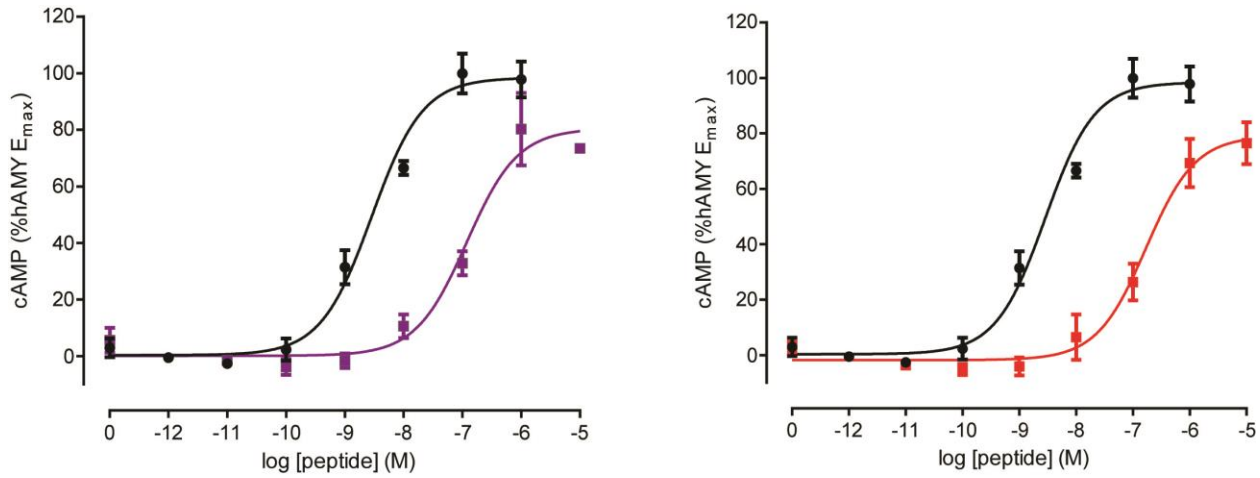

Figure 6-6: Activity of h-IAPP (black), $Ac_{8\text{-}37}$ (purple), and $IAPP_{CAM}$ (red) at the $CT_{(a)}$ receptor.

6.6 Tables

	t_{50} (hrs) in tris buffer pH 7.4	t_{50} (hrs) in PBS pH 7.4
h-IAPP	7.73 ± 1.60	3.35 ± 0.30
$IAPP_{8-37}$	1.69 ± 0.63	1.93 ± 0.26
Ac_{8-37}	1.45 ± 0.40	2.32 ± 0.92
C2S, C7S	4.1 ± 1.77	1.68 ± 0.43
$IAPP_{CAM}$	3.62 ± 0.44	1.68 ± 1.28

Table 6-1: Summary of t_{50}s of all variants in both buffer conditions tested.

	pEC_{50} ([nM])	pEC_{50} Control ([nM])	E_{max}	E_{max} Control	Fold-Change
$IAPP_{8-37}$	6.81 ± 0.19	9.21 ± 0.13	53.5 ± 12.3	100	394
Ac_{8-37}	7.97 ± 0.09	9.47 ± 0.24	82.8 ± 10.4	100	32
C2S, C7S	6.61 ± 0.32	9.21 ± 0.13	49.5 ± 9.09	100	274
$IAPP_{CAM}$	7.62 ± 0.31	9.47 ± 0.24	99.6 ± 1.42	100	71

Table 6-2: Summary of potency (pEC_{50}), and efficacy (E_{max}) of h-IAPP and disulfide variants at the $AMY_{1(a)}$ receptor. The potency and efficacy of each variant was compared directly to an h-IAPP control.

	pEC_{50} ([nM])	pEC_{50} Control ([nM])	E_{max}	E_{max} Control	Fold-Change
Ac_{8-37}	6.93 ± 0.06	8.55 ± 0.18	80.2 ± 6.13	100	42
$IAPP_{CAM}$	6.80 ± 0.08	8.55 ± 0.18	81.2 ± 4.70	100	56

Table 6-3: Summary of potency (pEC_{50}), and efficacy (E_{max}) of h-IAPP, Ac_{8-37}, and $IAPP_{CAM}$ at the $CT_{(a)}$ receptor. The potency and efficacy of each variant was compared directly to an h-IAPP control.

6.7 References

1. Li, Y., Yan, J., Zhang, X., and Huang, K. Disulfide Bonds in Amyloidogenesis Diseases Related Proteins, *Proteins*, **2013**, *81*,1862-1873.

2. Mossuto, M. F., Bolognesi, B., Guixer, B., Dhulesia, A., Agostini, F., Kumita, J. R., Tartaglia, G. G., Dumoulin, M., Dobson, C. M., and Salvatella, X. Disulfide Bonds Reduce the Toxicity of the Amyloid Fibrils Formed by an Extracellular Protein, *Angew. Chem. Int. Ed. Engl.*, **2011**, *50*,7048-7051.

3. Wang, S. S., Liu, K. N., and Wang, B. W. Effects of Dithiothreitol on the Amyloid Fibrillogenesis of Hen Egg-White Lysozyme, *Eur. Biophys. J.*, **2010**, *39*,1229-1242.

4. Sarkar, N., Kumar, M., and Dubey, V. K. Effect of Sodium Tetrathionate on Amyloid Fibril: Insight into the Role of Disulfide Bond in Amyloid Progression, *Biochimie*, **2011**, *93*,962-968.

5. Wu, C., and Shea, J. E. Structural Similarities and Differences Between Amyloidogenic and Non-Amyloidogenic Islet Amyloid Polypeptide (IAPP) Sequences and Implications for the Dual Physiological and Pathological Activities of These Peptides, *PLoS Comput. Biol.*, **2013**, *9*,e1003211.

6. Kajava, A. V., Aebi, U., and Steven, A. C. The Parallel Superpleated Beta-Structure as a Model for Amyloid Fibrils of Human Amylin, *J. Mol. Biol.*, **2005**, *348*,247-252.

7. Luca, S., Yau, W. M., Leapman, R., and Tycko, R. Peptide Conformation and Supramolecular Organization in Amylin Fibrils: Constraints From Solid-State NMR, *Biochemistry*, **2007**, *46*,13505-13522.

8. Wiltzius, J. J. W., Sievers, S. A., Sawaya, M. R., Cascio, D., Popov, D., Riekel, C., and Eisenberg, D. Atomic Structure of The Cross-Beta Spine of Islet Amyloid Polypeptide (Amylin), *Protein Sci.*, **2008**, *17*,1467-1474.

9. Goldsbury, C., Goldie, K., Pellaud, J., Seelig, J., Frey, P., Muller, S. A., Kistler, J., Cooper, G. J., and Aebi, U. Amyloid Fibril Formation from Full-Length and Fragments of Amylin, *J. Struct. Biol.*, **2000**, *130*,352-362.

10. Tu, L. H., Young, L. M., Wong, A. G., Ashcroft, A. E., Radford, S. E., and Raleigh, D. P. Mutational Analysis of the Ability of Resveratrol to Inhibit Amyloid Formation by Islet Amyloid Polypeptide: Critical Evaluation of the Importance of Aromatic-Inhibitor and Histidine-Inhibitor Interactions, *Biochemistry*, **2015**, *54*,666-676.

11. Westermark, P., Andersson, A., and Westermark, G. T. Islet Amyloid Polypeptide, Islet Amyloid, and Diabetes Mellitus, *Physiol. Rev.*, **2011**, *91*,795-826.

12. Barwell, J., Gingell, J. J., Watkins, H. A., Archbold, J. K., Poyner, D. R., and Hay, D. L. Calcitonin and Calcitonin Receptor-Like Receptors: Common Themes with Family B GPCRs?, *Br. J. Pharmacol.*, **2012**, *166*,51-65.

13. Roberts, A. N., Leighton, B., Todd, J. A., Cockburn, D., Schofield, P. N., Sutton, R., Holt, S., Boyd, Y., Day, A. J., Foot, E. A., and et al. Molecular and Functional Characterization of Amylin, a Peptide Associated with Type 2 Diabetes Mellitus, *PNAS*, **1989**, *86*,9662-9666.

14. Tartaglia, G. G., Pawar, A. P., Campioni, S., Dobson, C. M., Chiti, F., and Vendruscolo, M. Prediction of Aggregation-Prone Regions in Structured Proteins, *J. Mol. Biol.*, **2008**, *380*,425-436.

15. Wineman-Fisher, V., Tudorachi, L., Nissim, E., and Miller, Y. The Removal of Disulfide Bonds in Amylin Oligomers Leads to the Conformational Change of the 'Native' Amylin Oligomers, *Phys. Chem. Chem. Phys.*, **2016**, *18*,12438-12442.

16. Laghaei, R., Mousseau, N., and Wei, G. Structure and Thermodynamics of Amylin Dimer Studied by Hamiltonian-Temperature Replica Exchange Molecular Dynamics Simulations, *J. Phys. Chem. B*, **2011**, *115*,3146-3154.

17. Vaiana, S. M., Best, R. B., Yau, W. M., Eaton, W. A., and Hofrichter, J. Evidence for a Partially Structured State of the Amylin Monomer, *Biophys. J.*, **2009**, *97*,2948-2957.

18. Marek, P., Woys, A. M., Sutton, K., Zanni, M. T., and Raleigh, D. P. Efficient Microwave Assisted Synthesis of Human Islet Amyloid Polypeptide Designed to Facilitate The Specific Incorporation of Labeled Amino Acids, *Org. Lett.*, **2010**, *12*,4848-4851.

19. Abedini, A., and Raleigh, D. P. Incorporation of Pseudoproline Derivatives Allows the Facile Synthesis of Human IAPP, A Highly Amyloidogenic and Aggregation-Prone Polypeptide, *Org. Lett.*, **2005**, *7*,693-696.

20. Koo, B. W., and Miranker, A. D. Contribution of the Intrinsic Disulfide to the Assembly Mechanism of Islet Amyloid, *Protein Sci.*, **2005**, *14*,231-239.

21. Marek, P. J., Patsalo, V., Green, D. F., and Raleigh, D. P. Ionic Strength Effects on Amyloid Formation by Amylin Are a Complicated Interplay among Debye Screening, Ion Selectivity, and Hofmeister Effects, *Biochemistry*, **2012**, *51*,8478-8490.

22. Bower, R. L., and Hay, D. L. Amylin Structure-Function Relationships and Receptor Pharmacology: Implications for Amylin Mimetic Drug Development, *Br. J. Pharmacol.*, **2016**, *173*,1883-1898.

23. Abedini, A., Plesner, A., Cao, P., Ridgway, Z., Zhang, J., Tu, L. H., Middleton, C. T., Chao, B., Sartori, D. J., Meng, F., Wang, H., Wong, A. G., Zanni, M. T., Verchere, C. B., Raleigh, D. P., and Schmidt, A. M. Time-Resolved Studies Define the Nature of Toxic IAPP Intermediates, Providing Insight for Anti-Amyloidosis Therapeutics, *eLife*, **2016**, *5*.

24. Bram, Y., Frydman-Marom, A., Yanai, I., Gilead, S., Shaltiel-Karyo, R., Amdursky, N., and Gazit, E. Apoptosis Induced by Islet Amyloid Polypeptide Soluble Oligomers is Neutralized by Diabetes-Associated Specific Antibodies, *Sci. Rep.*, **2014**, *4*.

25. Hoare, S. R. Mechanisms of Peptide and Nonpeptide Ligand Binding to Class B G-Protein-Coupled Receptors, *Drug Discov Today*, **2005**, *10*,417-427.

26. Wang, Z. L., Bennet, W. M., Ghatei, M. A., Byfield, P. G., Smith, D. M., and Bloom, S. R. Influence of Islet Amyloid Polypeptide and the 8-37 Fragment of islet Amyloid Polypeptide on Insulin Release from Perifused Rat Islets, *Diabetes*, **1993**, *42*,330-335.

27. Ye, J.-M., Lim-Fraser, M., Cooney, G. J., Cooper, G. J. S., Iglesias, M. A., Watson, D. G., Choong, B., and Kraegen, E. W. Evidence that Amylin Stimulates Lipolysis in Vivo: A Possible Mediator of Induced Insulin Resistance, *Am. J. Physiol. - Endocrin. Metabol.*, **2001**, *280*,E562-E569.

Chapter 7. Concluding Remarks

The deposition of amyloid plaques in the islets of Langerhans in the pancreas is a hallmark feature in type-2 diabetes. This dissertation focuses on the aggregation process of IAPP and methods to detect them. In this final chapter, the implications of this work will be discussed as well as future directions.

In Chapter 2, the role of helical intermediates in amyloid formation by IAPP was investigated, by making multiple substitution at residue-17. By analyzing how each substitution affects the rates of amyloid formation, we can make deductions about the mechanism of amyloid formation by IAPP. The helical model of IAPP proposes that an α-helix is present in the 8-18 region of the IAPP peptide. The latter part of the peptide composes the amyloidogenic core region and will convert to β-sheet after the helices have associated via helix-helix interactions.

There was a mild correlation between the helical propensity of the residue at position-17 and the rate of amyloid formation by human IAPP, however this correlation was weaker than what was observed at position-15 [1].The V17A replacement was found to form amyloid at a much slower rate than human IAPP and was contrary to what we expected. This was especially surprising since alanine had one of the highest helical propensities of the substitutions made and a much higher helical propensity than Val (-0.27 vs -0.74 as judged by the free energy for helix formation of each amino acid relative to glycine) [2].

The size of alanine and its reduced hydrophobicity relative to Val may have a greater effect on amyloid formation by IAPP than its α-helical propensity. The mature IAPP amyloid fibril is a parallel β-sheet meaning that the sidechains in each layer are aligned. Though alanine

has a higher helical propensity, because of its size the packing in the mature IAPP fibril may not be ideal. Additionally, it is not known which residues are important for self-assembling with the helices from other IAPP monomers. It is possible that the small size makes it difficult for helix-helix interactions to occur. Along these lines, work from the Eisenberg lab on structural models of IAPP fused to maltose binding protein highlight residues 15 to 17 of IAPP as possible dimer contacts, while peptide mapping studies from the Gazit lab implicated the region between residues 13 and 17 as being critical for IAPP interactions [3, 4]. These results may indicate that not just the helical propensity of the residues within the putative helical region are important but the size, shape and hydrophobicity may be important as well and that Val-17 may be important for making contacts with other IAPP monomers.

PICUP on the V17A could reveal interesting information on the distribution of oligomers as could ion-mobility mass spectrometry [5]. If Val-17 is necessary for making helix-helix interactions we might expect to see a different distribution of oligomers during the lag phase. The observation of a similar distribution of oligomers would be less informative because the cross-linking methods can not reveal structural details. Unfortunately no good methods have been developed to trap specific oligomers in concertations suitable for biophysical studies so it is currently not possible to directly determine the impact of replacements such as V17A on their structure.

In Chapter 3, the pufferfish IAPP variant was shown to be amyloidogenic yet not capable of binding to the thioflavin-T dye. Additionally, in Chapter 4, it was demonstrated that the thioflavin-T assay was compromised by rifampicin. These findings both highlight shortcomings in the thioflavin-T fluorescence assay and have implications in monitoring not just IAPP but other types of amyloids as well. There has been a great deal of interest in developing new dyes

to monitor amyloid formation, but no notable successes have been reported. The work described in Chapter 4 showed that SYPRO-orange, ANS, and Bis-ANS can be used to monitor IAPP amyloid formation especially when inner filter effects may be a concern in inhibition studies. However, these dyes were also compromised by the addition of rifampicin. One of the interesting implications of this work relates to the properties of intermediates formed during amyloid formation by IAPP. Previous work has shown that ANS binds to pre-amyloid intermediates and this has been interpreted to mean that they have solvent exposed hydrophobic patches which are sufficient to confirm ANS binding, but this is not the case with IAPP.

It would be interesting to determine how specific SYPRO-orange, ANS, and Bis-ANS are to IAPP amyloid by testing them in the presence of other amyloidogenic proteins such as Aβ, or α-synuclein. However, without reliable high resolution structures of the IAPP amyloid fibril it would be challenging to develop a more universal dye for monitoring amyloid formation.

In Chapter 3, PBS was shown to be capable of intensifying the fluorescence intensity of pufferfish IAPP so that the rate of amyloid formation could be determined. In fact, it is a common observation that the fluorescence intensity of the thioflavin-T assay is markedly higher than when the assay is performed in tris buffer. The reason for this is not entirely known. Due to the sensitivity of IAPP to ionic strength and it's affinity to phosphate, it is possible that the quantity of amyloid fibrils is increased as well as the rate of amyloid formation. This could be deduced by centrifuging the fibrils and measuring the monomer concentration of IAPP at the end of a kinetic experiment or by conducting experiments with a quartz crystal microbalance. However, the fluorescence intensity of thioflavin-T may not have any bearing on the quantity of amyloid fibrils, but might reflect subtle changes in the structure of the fibers or the packing of fibers.

Amyloid fibers have a tendency to associate with each other. It is possible that this effect could differ between tris and PBS. Differing degrees of lateral association could occlude the surface binding sites for thioflavin-T. The binding of thioflavin-T to the grooves of β-sheets may be improved in PBS buffer than in tris buffer. It would be interesting to see how the fluorescence intensity of thioflavin-T is affected by salt concentration. If the binding of thioflavin-T to the IAPP amyloid fibril is truly improved, then perhaps rifampicin will not immediately quench fluorescence when it is added to solution. Additionally, this experiment would also be worthwhile performing in the presence of ANS, Bis-ANS, and SYPRO-orange since ionic strength may also have an effect on these dyes.

Amyloid prediction programs were used in order to predict the amyloidogenicity of several sequences in both Chapters 3 and 5. In both cases, the programs gave conflicting results or were inaccurate. One reason for this is that IAPP contains an amidated C-terminus and a disulfide bond between Cys-2 and Cys-7. Amyloid prediction programs do not take this into account. Another reason that programs gave conflicting results may be due to the fact that some of the programs were not designed to compare the relative rates of amyloid formation but can only predict the regions of amyloidogenicity in a given sequence and though the sequence may have a higher percentage of amyloidogenicity this may not have any affect on the rate of amyloid formation. Amyloid prediction programs are continuously being refined. The Trovato group has since developed PASTA 2.0 server in order to better predict amyloidogenicity [6]. Perhaps in the future, amyloid predictions programs will better able to predict relative amyloidogenicity. Human IAPP also has an unusual sequence, rich in polar but uncharged sidechains, 6 Asn, 5 Thr, 5 Ser, and 1 Gln. Perhaps the unusual sequence confounds amyloid prediction methods which were derived from other types of sequences.

Lastly, in Chapter 6, several disulfide variants were investigated in order to determine the effect the first seven residues and the disulfide bond have on amyloid formation by IAPP. It was found that all the variants were able to form amyloid fibrils at a faster rate than human IAPP. These results indicate that the disulfide bond and first seven residues may play a protective role by limiting the aggregation propensity of the peptide. The disulfide variants were less active towards the amylin receptor than human IAPP and this is likely the major reason the disulfide is conversed. The C2S, C7S variant was found to be less toxic when added to INS-1 β-cells. It would be interesting to see how these variants behave in the presence of membranes and if they can induce leakage to the same extent that human IAPP can since membrane leakage has been proposed to be a mechanism of toxicity, although this has been questioned [7]. Additionally, in Chapter 3, a K1I replacement was examined. This variant was found to form amyloid at a similar rate relative to human IAPP. It would be interesting to determine if the Lys-1 plays a role in the biological activity of IAPP since it is so strictly conserved in the known sequences of the peptide.

The work in this dissertation has increased understanding of the early events of aggregation and may also serve as a useful benchmark when using amyloid prediction programs. The results here have also revealed pitfalls in the thioflavin-T assay which is directly applicable to the entire field of amyloid. It is the belief of the researcher that the findings here will be of interest to the amyloid community and are also a foundation for which further studies can be performed.

7-1 References

1. Tu, L.-H., and Raleigh, D. P. Role of Aromatic Interactions in Amyloid Formation by Islet Amyloid Polypeptide, *Biochemistry*, **2013**, *52*,333-342.

2. Lyu, P. C., Sherman, J. C., Chen, A., and Kallenbach, N. R. Alpha-Helix Stabilization by Natural and Unnatural Amino Acids with Alkyl Side Chains, *PNAS*, **1991**, *88*,5317-5320.

3. Wiltzius, J. J. W., Sievers, S. A., Sawaya, M. R., and Eisenberg, D. Atomic Structures of IAPP (amylin) Fusions Suggest a Mechanism for Fibrillation and the Role of Insulin in the Process, *Protein Sci.*, **2009**, *18*,1521-1530.

4. Gilead, S., Wolfenson, H., and Gazit, E. Molecular Mapping of the Recognition Interface Between the Islet Amyloid Polypeptide and Insulin, *Angew. Chem. Int. Ed. Engl.*, **2006**, *45*,6476-6480.

5. Young, L. M., Cao, P., Raleigh, D. P., Ashcroft, A. E., and Radford, S. E. Ion Mobility Spectrometry-Mass Spectrometry Defines the Oligomeric Intermediates in Amylin Amyloid Formation and the Mode of Action of Inhibitors, *J. Am. Chem. Soc.*, **2014**, *136*,660-670.

6. Walsh, I., Seno, F., Tosatto, S. C., and Trovato, A. PASTA 2.0: An Improved Server for Protein Aggregation Prediction, *Nucleic Acids Res.*, **2014**, *42*,W301-307.

7. Cao, P., Abedini, A., and Raleigh, D. P. Folding and Aggregation of Islet Amyloid Polypeptide: from Physical Chemistry to Cell Biology, *Curr. Opinion Struct. Biol.*, **2013**, *23*,82-88.

Full List of References

Abedini, A., and Raleigh, D. P. Incorporation of Pseudoproline Derivatives Allows the Facile Synthesis of Human IAPP, A Highly Amyloidogenic and Aggregation-Prone Polypeptide, *Org. Lett.*, **2005**, *7*,693-696.

Abedini, A., and Raleigh, D. P. The Role of His-18 in Amyloid Formation By Human Islet Amyloid Polypeptide, *Biochemistry*, **2005**, *44*,16284-16291.

Abedini, A., and Raleigh, D. P. Destabilization of Human IAPP Amyloid Fibrils By Proline Mutations Outside of The Putative Amyloidogenic Domain: Is There A Critical Amyloidogenic Domain in Human IAPP?, *J. Mol. Biol.*, **2006**, *355*,274-281.

Abedini, A., Singh, G., and Raleigh, D. P. Recovery and Purification of Highly Aggregation-Prone Disulfide-Containing Peptides: Application to Islet Amyloid Polypeptide, *Anal. Biochem.*, **2006**, *351*,181-186.

Abedini, A., Meng, F., and Raleigh, D. P. A Single-Point mutation Converts the Highly Amyloidogenic Human Islet Amyloid Polypeptide into a Potent Fibrillization Inhibitor, *J. Am. Chem. Soc.*, **2007**, *129*,11300-11301.

Abedini, A., and Raleigh, D. P. A Critical Assessment of the Role of Helical Intermediates in Amyloid Formation by Natively Unfolded Proteins and Polypeptides, *Protein Eng. Des. Sel.*, **2009**, *22*,453-459.

Abedini, A., and Raleigh, D. P. A Role for Helical Intermediates in Amyloid Formation by Natively Unfolded Polypeptides?, *Phys. Biol.*, **2009**, *6*,015005.

Abedini, A., and Schmidt, A. M. Mechanisms of Islet Amyloidosis Toxicity in Type 2 Diabetes, *FEBS Lett.*, **2013**, *587*,1119-1127.

Abedini, A., Plesner, A., Cao, P., Ridgway, Z., Zhang, J., Tu, L. H., Middleton, C. T., Chao, B., Sartori, D. J., Meng, F., Wang, H., Wong, A. G., Zanni, M. T., Verchere, C. B., Raleigh, D. P., and Schmidt, A. M. Time-Resolved Studies Define the Nature of Toxic IAPP Intermediates, Providing Insight for Anti-Amyloidosis Therapeutics, *eLife*, **2016**, *5*.

Ahmed, A. B., and Kajava, A. V. Breaking the Amyloidogenicity Code: Methods to Predict Amyloids from Amino Acid Sequence, *FEBS Lett.*, **2013**, *587*,1089-1095.

Andersen, N. H., Dyer, R. B., Fesinmeyer, R. M., Gai, F., Liu, Z. H., Neidigh, J. W., and Tong, H. Effect of Hexafluoroisopropanol on the Thermodynamics of Peptide Secondary Structure Formation, *J. Am. Chem. Soc.*, **1999**, *121*,9879-9880.

Ashburn, T. T., Auger, M., and Lansbury, P. T. The Structural Basis of Pancreatic Amyloid Formation: Isotope-Edited Spectroscopy in the Solid State, *J. Am. Chem. Soc.*, **1992**, *114*,790-791.

Ashburn, T. T., and Lansbury, P. T. Interspecies Sequence Variations Affect the Kinetics and Thermodynamics of Amyloid Formation - Peptide Models of Pancreatic Amyloid, *J. Am. Chem. Soc.*, **1993**, *115*,11012-11013.

Barwell, J., Gingell, J. J., Watkins, H. A., Archbold, J. K., Poyner, D. R., and Hay, D. L. Calcitonin and Calcitonin Receptor-Like Receptors: Common Themes with Family B GPCRs?, *Br. J. Pharmacol.*, **2012**, *166*,51-65.

Bedrood, S., Li, Y., Isas, J. M., Hegde, B. G., Baxa, U., Haworth, I. S., and Langen, R. Fibril Structure of Human Islet Amyloid Polypeptide, *J. Biol. Chem.*, **2012**, *287*,5235-5241.

Bennink, M. L., Scharer, O. D., Kanaar, R., Sakata-Sogawa, K., Schins, J. M., Kanger, J. S., de Grooth, B. G., and Greve, J. Single-Molecule Manipulation of Double-Stranded DNA Using OpticalTtweezers: Interaction Studies of DNA with RecA and YOYO-1, *Cytometry*, **1999**, *36*,200-208.

Benoni, R., Pertinhez, T. A., Spyrakis, F., Davalli, S., Pellegrino, S., Paredi, G., Pezzotti, A., Bettati, S., Campanini, B., and Mozzarelli, A. Structural Insight into the Interaction of O-Acetylserine Sulfhydrylase with Competitive, Peptidic Inhibitors by Saturation Transfer Difference-NMR, *FEBS Lett.*, **2016**, *590*,943-953.

Betsholtz, C., Christmansson, L., Engstrom, U., Rorsman, F., Svensson, V., Johnson, K. H., and Westermark, P. Sequence Divergence in a Specific Region of Islet Amyloid Polypeptide (Iapp) Explains Differences in Islet Amyloid Formation between Species, *FEBS Lett.*, **1989**, *251*,261-264.

Bhattacharya, M., Jain, N., and Mukhopadhyay, S. Insights into the Mechanism of Aggregation and Fibril Formation from Bovine Serum Albumin, *J. Phys. Chem. B*, **2011**, *115*,4195-4205.

Biancalana, M., and Koide, S. Molecular Mechanism of Thioflavin-T Binding to Amyloid Fibrils, *Biochim. Biophys. Acta, Proteins Proteomics*, **2010**, *1804*,1405-1412.

Binkowski, T. A., Jiang, W., Roux, B., Anderson, W. F., and Joachimiak, A. Virtual High-Throughput Ligand Screening, *Methods Mol. Biol.*, **2014**, *1140*,251-261.

Bitan, G., and Teplow, D. B. Rapid Photochemical Cross-Linking--A New Tool For Studies of Metastable, Amyloidogenic Protein Assemblies, *Acc. Chem. Res.*, **2004**, *37*,357-364.

Bolognesi, B., Kumita, J. R., Barros, T. P., Esbjorner, E. K., Luheshi, L. M., Crowther, D. C., Wilson, M. R., Dobson, C. M., Favrin, G., and Yerbury, J. J. ANS Binding Reveals Common Features of Cytotoxic Amyloid Species, *ACS Chem Biol*, **2010**, *5*,735-740.

Bram, Y., Frydman-Marom, A., Yanai, I., Gilead, S., Shaltiel-Karyo, R., Amdursky, N., and Gazit, E. Apoptosis Induced by Islet Amyloid Polypeptide Soluble Oligomers is Neutralized by Diabetes-Associated Specific Antibodies, *Sci. Rep.*, **2014**, *4*.

Brunham, L. R., Kruit, J. K., Hayden, M. R., and Verchere, C. B. Cholesterol in Beta-Cell Dysfunction: The Emerging Connection Between HDL Cholesterol and Type 2 Diabetes, *Curr. Diab. Rep.*, **2010**, *10*,55-60.

Buchanan, L. E., Dunkelberger, E. B., Tran, H. Q., Cheng, P.-N., Chiu, C.-C., Cao, P., Raleigh, D. P., de Pablo, J. J., Nowick, J. S., and Zanni, M. T. Mechanism of IAPP Amyloid Fibril Formation Involves an Intermediate with a Transient Beta-Sheet, *PNAS*, **2013**, *110*,19285-19290.

Cabaleiro-Lago, C., Lynch, I., Dawson, K. A., and Linse, S. Inhibition of IAPP and IAPP(20-29) Fibrillation by Polymeric Nanoparticles, *Langmuir*, **2010**, *26*,3453-3461.

Cao, P., Meng, F., Abedini, A., and Raleigh, D. P. The Ability of Rodent Islet Amyloid Polypeptide to Inhibit Amyloid Formation by Human Islet Amyloid Polypeptide Has Important Implications for the Mechanism of Amyloid Formation and the Design of Inhibitors, *Biochemistry*, **2010**, *49*,872-881.

Cao, P., Abedini, A., and Raleigh, D. P. Folding and Aggregation of Islet Amyloid Polypeptide: from Physical Chemistry to Cell Biology, *Curr. Opinion Struct. Biol.*, **2013**, *23*,82-88.

Chakraborty, S., Chatterjee, B., and Basu, S. A Mechanistic Insight into the Amyloidogenic Structure of hIAPP Peptide Revealed From Sequence Analysis and Molecular Dynamics Simulation, *Biophys. Chem.*, **2012**, *168*,1-9.

Chapman, M. R., Robinson, L. S., Pinkner, J. S., Roth, R., Heuser, J., Hammar, M., Normark, S., and Hultgren, S. J. Role of Escherichia coli Curli Operons in Directing Amyloid Fiber Formation, *Science*, **2002**, *295*,851-855.

Charge, S. B. P., De Koning, E. J. P., and Clark, A. Effect of pH and Insulin on Fibrillogenesis of Islet Amyloid Polypeptide In Vitro, *Biochemistry*, **1995**, *34*,14588-14593.

Chen, A. Y., Deng, Z., Billings, A. N., Seker, U. O., Lu, M. Y., Citorik, R. J., Zakeri, B., and Lu, T. K. Synthesis and Patterning of Tunable Multiscale Materials with Engineered Cells, *Nat. Mater.*, **2014**, *13*,515-523.

Chen, M.-S., Zhao, D.-S., Yu, Y.-P., Li, W.-W., Chen, Y.-X., Zhao, Y.-F., and Li, Y.-M. Characterizing the Assembly Behaviors of Human Amylin: A Perspective Derived from C-Terminal Variants, *Chem. Commun.*, **2013**, *49*,1799-1801.

Chen, S., Berthelier, V., Hamilton, J. B., O'Nuallain, B., and Wetzel, R. Amyloid-Like Features of Polyglutamine Aggregates and Their Assembly Kinetics, *Biochemistry*, **2002**, *41*,7391-7399.

Chiti, F., and Dobson, C. M. Protein Misfolding, Functional Amyloid, and Human Disease, *Annu. Rev. Biochem*, **2006**, *75*,333-366.

Chiu, S. W., Clark, M., Subramaniam, S., and Jakobsson, E. Collective Motion Artifacts Arising in Long-Duration Molecular Dynamics Simulations, *J. Comput. Chem.*, **2000**, *21*,121-131.

Cloe, A. L., Orgel, J. P. R. O., Sachleben, J. R., Tycko, R., and Meredith, S. C. The Japanese Mutant Abeta (DeltaE22-Abeta(1-39)) Forms Fibrils Instantaneously, with Low-Thioflavin T Fluorescence: Seeding of Wild-Type Abeta(1-40) Into Atypical Fibrils by DeltaE22-Abeta(1-39), *Biochemistry*, **2011**, *50*,2026-2039.

Conchillo-Sole, O., de Groot, N. S., Aviles, F. X., Vendrell, J., Daura, X., and Ventura, S. AGGRESCAN: a server for the prediction and evaluation of "hot spots" of aggregation in polypeptides, *BMC Bioinf.*, **2007**, *8*,65.

Cooper, G. J. S., Willis, A. C., Clark, A., Turner, R. C., Sim, R. B., and Reid, K. B. M. Purification and Characterization of a Peptide from Amyloid-Rich Pancreases of Type 2 Diabetic Patients, *PNAS*, **1987**, *84*,8628-8632.

Cope, S. M., Shinde, S., Best, R. B., Ghirlanda, G., and Vaiana, S. M. Cyclic N-terminal Loop of Amylin Forms Non Amyloid Fibers, *Biophys. J.*, **2013**, *105*,1661-1669.

Crowther, D. C., Kinghorn, K. J., Miranda, E., Page, R., Curry, J. A., Duthie, F. A., Gubb, D. C., and Lomas, D. A. Intraneuronal Abeta, Non-Amyloid Aggregates and Neurodegeneration in a Drosophila Model of Alzheimer's Disease, *Neuroscience*, **2005**, *132*,123-135.

Duan, Y., Wu, C., Chowdhury, S., Lee, M. C., Xiong, G., Zhang, W., Yang, R., Cieplak, P., Luo, R., Lee, T., Caldwell, J., Wang, J., and Kollman, P. A Point-Charge Force Field for Molecular Mechanics Simulations of Proteins Based on Condensed-Phase Quantum Mechanical Calculations, *J. Comput. Chem.*, **2003**, *24*,1999-2012.

Dupuis, N. F., Wu, C., Shea, J. E., and Bowers, M. T. The Amyloid Formation Mechanism in Human IAPP: Dimers Have Beta-Strand Monomer-Monomer Interfaces, *J. Am. Chem. Soc.*, **2011**, *133*,7240-7243.

Ehses, J. A., Perren, A., Eppler, E., Ribaux, P., Pospisilik, J. A., Maor-Cahn, R., Gueripel, X., Ellingsgaard, H., Schneider, M. K., Biollaz, G., Fontana, A., Reinecke, M., Homo-Delarche, F., and Donath, M. Y. Increased Number of Islet-Associated Macrophages in Type 2 Diabetes, *Diabetes*, **2007**, *56*,2356-2370.

Eichner, T., and Radford, S. E. A Diversity of Assembly Mechanisms of a Generic Amyloid Fold, *Mol. Cell*, **2011**, *43*,8-18.

Essmann, U., Perera, L., Berkowitz, M. L., Darden, T., Lee, H., and Pedersen, L. G. A Smooth Particle Mesh Ewald Method, *J. Chem. Phys.*, **1995**, *103*,8577-8593.

Fandrich, M. Oligomeric Intermediates in Amyloid Formation: Structure Determination and Mechanisms of Toxicity, *J. Mol. Biol.*, **2012**, *421*,427-440.

Fauchere, J. L., Charton, M., Kier, L. B., Verloop, A., and Pliska, V. Amino Acid Side Chain Parameters for Correlation Studies in Biology and Pharmacology, *Int. J. Pept. Protein Res.*, **1988**, *32*,269-278.

Fernandez-Escamilla, A.-M., Rousseau, F., Schymkowitz, J., and Serrano, L. Prediction of Sequence-Dependent And Mutational Effects on the Aggregation of Peptides and Proteins, *Nat. Biotechnol.*, **2004**, *22*,1302-1306.

Fooks, H. M., Martin, A. C., Woolfson, D. N., Sessions, R. B., and Hutchinson, E. G. Amino Acid Pairing Preferences in Parallel Beta-Sheets in Proteins, *J. Mol. Biol.*, **2006**, *356*,32-44.

Fortin, J. S., Santamaria-Bouvier, A., Lair, S., Dallaire, A. D., and Benoit-Biancamano, M. O. Anatomic and Molecular Characterization of the Endocrine Pancreas of a Teleostean Fish: Atlantic Wolffish (Anarhichas lupus), *Zool. Stud.*, **2015**, *54*.

Frare, E., Mossuto, M. F., de Laureto, P. P., Tolin, S., Menzer, L., Dumoulin, M., Dobson, C. M., and Fontana, A. Characterization of Oligomeric Species on the Aggregation Pathway of Human Lysozyme, *J. Mol. Biol.*, **2009**, *387*,17-27.

Gao, F., Mei, E., Lim, M., and Hochstrasser, R. M. Probing Lipid Vesicles by Bimolecular Association and Dissociation Trajectories of Single Molecules, *J. Am. Chem. Soc.*, **2006**, *128*,4814-4822.

Garbuzynskiy, S. O., Lobanov, M. Y., and Galzitskaya, O. V. FoldAmyloid: A Method of Prediction of Amyloidogenic Regions From Protein Sequence, *Bioinformatics*, **2010**, *26*,326-332.

Gebre-Medhin, S., Mulder, H., Pekny, M., Westermark, G., Tornell, J., Westermark, P., Sundler, F., Ahren, B., and Betsholtz, C. Increased Insulin Secretion and Glucose Tolerance in Mice Lacking Islet Amyloid Polypeptide (Amylin), *Biochem. Biophys. Res. Commun.*, **1998**, *250*,271-277.

Gessel, M. M., Wu, C., Li, H., Bitan, G., Shea, J. E., and Bowers, M. T. Abeta(39-42) Modulates Abeta Oligomerization but not Fibril Formation, *Biochemistry*, **2012**, *51*,108-117.

Gilead, S., Wolfenson, H., and Gazit, E. Molecular Mapping of the Recognition Interface Between the Islet Amyloid Polypeptide and Insulin, *Angew. Chem. Int. Ed. Engl.*, **2006**, *45*,6476-6480.

Glabe, C. G., and Kayed, R. Common Structure and Toxic Function of Amyloid Oligomers Implies a Common Mechanism of Pathogenesis, *Neurology*, **2006**, *66*,S74-78.

Glenner, G. G. Reprint of "Alzheimer's Disease: Initial Report of the Purification and Characterization of a Novel Cerebrovascular Amyloid Protein", *Biochem. Biophys. Res. Commun.*, **2012**, *425*,534-539.

Goldsbury, C., Goldie, K., Pellaud, J., Seelig, J., Frey, P., Muller, S. A., Kistler, J., Cooper, G. J., and Aebi, U. Amyloid Fibril Formation from Full-Length and Fragments of Amylin, *J. Struct. Biol.*, **2000**, *130*,352-362.

Graw, J. The Crystallins: Genes, Proteins and Diseases, *Biol. Chem.*, **1997**, *378*,1331-1348.

Green, J., Goldsbury, C., Min, T., Sunderji, S., Frey, P., Kistler, J., Cooper, G., and Aebi, U. Full-Length Rat Amylin Forms Fibrils Following Substitution of Single Residues From Human Amylin, *J. Mol. Biol.*, **2003**, *326*,1147-1156.

Greenspan, P., Mayer, E. P., and Fowler, S. D. Nile Red: A Selective Fluorescent Stain for Intracellular Lipid Droplets, *J. Cell Biol.*, **1985**, *100*,965-973.

Haidekker, M. A., and Theodorakis, E. A. Molecular Rotors - Fluorescent Biosensors for Viscosity and Flow, *Org. Biomol. Chem.*, **2007**, *5*,1669-1678.

Hamodrakas, S. J., Liappa, C., and Iconomidou, V. A. Consensus Prediction of Amyloidogenic Determinants in Amyloid Fibril-Forming Proteins, *Int. J. Biol. Macromol.*, **2007**, *41*,295-300.

Harvey, S. C., Tan, R. K. Z., and Cheatham, T. E. The Flying Ice Cube: Velocity Rescaling in Molecular Dynamics Leads to Violation of Energy Equipartition, *J. Comput. Chem.*, **1998**, *19*,726-740.

Haugland, R. P., Jones, L. J., Singer, V. L., and Steinberg, T. H. (1997) Merocyanine Dye Protein Stains, Google Patents.

Hawe, A., Sutter, M., and Jiskoot, W. Extrinsic Fluorescent Dyes as Tools for Protein Characterization, *Pharm. Res.*, **2008**, *25*,1487-1499.

Hebda, J. A., Saraogi, I., Magzoub, M., Hamilton, A. D., and Miranker, A. D. A Peptidomimetic Approach to Targeting Pre-Amyloidogenic States in Type II Diabetes, *Chem. Biol.*, **2009**, *16*,943-950.

Hobbs, J. R., and Morgan, A. D. Fluorescence Microscopy with Thioflavine-T in Diagnosis of Amyloid, *J. Pathol. Bacteriol.*, **1963**, *86*,437-&.

Höppener, J. W. M., Ahrén, B., and Lips, C. J. M. Islet Amyloid and Type 2 Diabetes Mellitus, *N. Engl. J. Med.*, **2000**, *343*,411-419.

Hudson, S. A., Ecroyd, H., Kee, T. W., and Carver, J. A. The Thioflavin T Fluorescence Assay For Amyloid Fibril Detection Can Be Biased by The Presence of Exogenous Compounds, *FEBS J.*, **2009**, *276*,5960-5972.

Iijima-Ando, K., and Iijima, K. Transgenic Drosophila Models of Alzheimer's Disease and Tauopathies, *Brain. Struct. Funct.*, **2010**, *214*,245-262.

Ilitchev, A. I., Giammona, M. J., Do, T. D., Wong, A. G., Buratto, S. K., Shea, J. E., Raleigh, D. P., and Bowers, M. T. Human Islet Amyloid Polypeptide N-Terminus Fragment Self-Assembly: Effect of Conserved Disulfide Bond on Aggregation Propensity, *J. Am. Soc. Mass. Spectrom.*, **2016**, *27*,1010-1018.

Invernizzi, G., Papaleo, E., Sabate, R., and Ventura, S. Protein Aggregation: Mechanisms and Functional Consequences, *Int. J. Bio. Cell Biol.*, **2012**, *44*,1541-1554.

Jameson, D. M., Croney, J. C., and Moens, P. D. Fluorescence: Basic Concepts, Practical Aspects, and Some Anecdotes, *Methods Enzymol.*, **2003**, *360*,1-43.

Jha, S., Snell, J. M., Sheftic, S. R., Patil, S. M., Daniels, S. B., Kolling, F. W., and Alexandrescu, A. T. pH Dependence of Amylin Fibrillization, *Biochemistry*, **2014**, *53*,300-310.

Jorgensen, W. L., Chandrasekhar, J., Madura, J. D., Impey, R. W., and Klein, M. L. Comparison of Simple Potential Functions for Simulating Liquid Water, *J. Chem. Phys.*, **1983**, *79*,926-935.

Kajava, A. V., Aebi, U., and Steven, A. C. The Parallel Superpleated Beta-Structure as a Model for Amyloid Fibrils of Human Amylin, *J. Mol. Biol.*, **2005**, *348*,247-252.

Kenney, J. M., Knight, D., Wise, M. J., and Vollrath, F. Amyloidogenic Nature of Spider Silk, *Eur. J. Biochem.*, **2002**, *269*,4159-4163.

Khurana, R., Uversky, V. N., Nielsen, L., and Fink, A. L. Is Congo Red an Amyloid-Specific Dye?, *J. Biol. Chem.*, **2001**, *276*,22715-22721.

Kitada, T., Asakawa, S., Hattori, N., Matsumine, H., Yamamura, Y., Minoshima, S., Yokochi, M., Mizuno, Y., and Shimizu, N. Mutations in the Parkin Gene Cause Autosomal Recessive Juvenile Parkinsonism, *Nature*, **1998**, *392*,605-608.

Knight, J. D., Hebda, J. A., and Miranker, A. D. Conserved and Cooperative Assembly of Membrane-Bound Alpha-Helical States of Islet Amyloid Polypeptide, *Biochemistry*, **2006**, *45*,9496-9508.

Kodali, R., Williams, A. D., Chemuru, S., and Wetzel, R. A Beta(1-40) Forms Five Distinct Amyloid Structures Whose Beta-Sheet Contents and Fibril Stabilities Are Correlated, *J. Mol. Biol.*, **2010**, *401*,503-517.

Koo, B. W., and Miranker, A. D. Contribution of the Intrinsic Disulfide to the Assembly Mechanism of Islet Amyloid, *Protein Sci.*, **2005**, *14*,231-239.

Koo, B. W., Hebda, J. A., and Miranker, A. D. Amide Inequivalence in The Fibrillar Assembly of Islet Amyloid Polypeptide, *Protein Eng., Des. Sel.*, **2008**, *21*,147-154.

Krebs, M. R., Morozova-Roche, L. A., Daniel, K., Robinson, C. V., and Dobson, C. M. Observation of sequence specificity in the seeding of protein amyloid fibrils, *Protein Sci.*, **2004**, *13*,1933-1938.

Krebs, M. R., Bromley, E. H., and Donald, A. M. The Binding of Thioflavin-T to Amyloid Fibrils: Localisation and Implications, *J. Struct. Biol.*, **2005**, *149*,30-37.

Kruger, D. F., and Gloster, M. A. Pramlintide For The Treatment of Insulin-Requiring Diabetes Mellitus: Rationale And Review of Clinical Data, *Drugs*, **2004**, *64*,1419-1432.

Kumar, S., and Walter, J. Phosphorylation of Amyloid Beta (Abeta) Peptides - A Trigger for Formation of Toxic Aggregates in Alzheimer's Disease, *Aging*, **2011**, *3*,803-812.

Kung, C. E., and Reed, J. K. Fluorescent Molecular Rotors: A New Class of Probes for Tubulin Structure and Assembly, *Biochemistry*, **1989**, *28*,6678-6686.

Larsen, T. A., Goodsell, D. S., Cascio, D., Grzeskowiak, K., and Dickerson, R. E. The Structure of DAPI Bound to DNA, *J. Biomol. Struct. Dyn.*, **1989**, *7*,477-491.

Lavinder, J. J., Hari, S. B., Sullivan, B. J., and Magliery, T. J. High-Throughput Thermal Scanning: A General, Rapid Dye-Binding Thermal Shift Screen For Protein Engineering, *J. Am. Chem. Soc.*, **2009**, *131*,3794-3795.

Levine, H. Thioflavine-T Interaction with Synthetic Alzheimers-Disease Beta-Amyloid Peptides - Detection of Amyloid Aggregation in Solution, *Protein Sci.*, **1993**, *2*,404-410.

Levine, H., 3rd. Quantification of Beta-Sheet Amyloid Fibril Structures with Thioflavin T, *Methods Enzymol.*, **1999**, *309*,274-284.

Li, Y., Yan, J., Zhang, X., and Huang, K. Disulfide Bonds in Amyloidogenesis Diseases Related Proteins, *Proteins*, **2013**, *81*,1862-1873.

Lindberg, D. J., Wranne, M. S., Gatty, M. G., Westerlund, F., and Esbjorner, E. K. Steady-State and Time-Resolved Thioflavin-T Fluorescence Can Report on Morphological Differences in Amyloid Fibrils Formed by A Beta(1-40) and A Beta(1-42), *Biochem. Biophys. Res. Commun.*, **2015**, *458*,418-423.

Lindberg, D. J., and Esbjorner, E. K. Detection of Amyloid-Beta Fibrils Using the DNA-Intercalating Dye YOYO-1: Binding Mode and Fibril Formation Kinetics, *Biochem. Biophys. Res. Commun.*, **2016**, *469*,313-318.

Lindgren, M., Sorgjerd, K., and Hammarstrom, P. Detection and Characterization of Aggregates, Prefibrillar Amyloidogenic Oligomers, and Protofibrils Using Fluorescence Spectroscopy, *Biophys. J.*, **2005**, *88*,4200-4212.

Lo, M. C., Aulabaugh, A., Jin, G., Cowling, R., Bard, J., Malamas, M., and Ellestad, G. Evaluation of Fluorescence-Based Thermal Shift Assays For Hit Identification in Drug Discovery, *Anal. Biochem.*, **2004**, *332*,153-159.

Lorenzo, A., Razzaboni, B., Weir, G. C., and Yankner, B. A. Pancreatic Islet Cell Toxicity of Amylin Associated with Type-2 Diabetes Mellitus, *Nature*, **1994**, *368*,756-760.

Luca, S., Yau, W. M., Leapman, R., and Tycko, R. Peptide Conformation and Supramolecular Organization in Amylin Fibrils: Constraints From Solid-State NMR, *Biochemistry*, **2007**, *46*,13505-13522.

Lundmark, K., Westermark, G. T., Olsen, A., and Westermark, P. Protein Fibrils in Nature Can Enhance Amyloid Protein A Amyloidosis in Mice: Cross-Seeding As a Disease Mechanism, *PNAS*, **2005**, *102*,6098-6102.

Lutz, T. A. The Role of Amylin in the Control of Energy Homeostasis, *Am. J. Physiol. - Regul. Integ, Comp Physiol.*, **2010**, *298*,R1475-R1484.

Lyu, P. C., Sherman, J. C., Chen, A., and Kallenbach, N. R. Alpha-Helix Stabilization by Natural and Unnatural Amino Acids with Alkyl Side Chains, *PNAS*, **1991**, *88*,5317-5320.

Makin, O. S., and Serpell, L. C. Structures for Amyloid Fibrils, *The FEBS journal*, **2005**, *272*,5950-5961.

Mannini, B., Mulvihill, E., Sgromo, C., Cascella, R., Khodarahmi, R., Ramazzotti, M., Dobson, C. M., Cecchi, C., and Chiti, F. Toxicity of Protein Oligomers is Rationalized by a Function Combining Size and Surface Hydrophobicity, *ACS Chem. Biol.*, **2014**, *9*,2309-2317.

Marek, P., Woys, A. M., Sutton, K., Zanni, M. T., and Raleigh, D. P. Efficient Microwave Assisted Synthesis of Human Islet Amyloid Polypeptide Designed to Facilitate The Specific Incorporation of Labeled Amino Acids, *Org. Lett.*, **2010**, *12*,4848-4851.

Marek, P., Mukherjee, S., Zanni, M. T., and Raleigh, D. P. Residue-Specific, Real-Time Characterization of Lag-Phase Species and Fibril Growth During Amyloid Formation: A Combined Fluorescence and IR Study of p-Cyanophenylalanine Analogs of Islet Amyloid Polypeptide, *J. Mol. Bio.*, **2010**, *400*, 878-888.

Marek, P., Patsalo, V., Green, D. F., and Raleigh, D. P. Ionic Strength Effects on Amyloid Formation by Amylin Are a Complicated Interplay among Debye Screening, Ion Selectivity, and Hofmeister Effects, *Biochemistry*, **2012**, *51*, 8478-8490.

Martinez-Alvarez, R. M., Volkoff, H., Cueto, J. A. M., and Delgado, M. J. Molecular Characterization of Calcitonin Gene-Related Peptide (CGRP) Related Peptides (CGRP, Amylin, Adrenomedullin And Adrenomedullin-2/Intermedin) in Goldfish (Carassius auratus): Cloning And Distribution, *Peptides*, **2008**, *29*,1534-1543.

Maskevich, A. A., Stsiapura, V. I., Kuzmitsky, V. A., Kuznetsova, I. M., Povarova, O. I., Uversky, V. N., and Turoverov, K. K. Spectral Properties of Thioflavin T in Solvents with Different Dielectric Properties and in a Fibril-Incorporated Form, *J. Proteome Res.*, **2007**, *6*,1392-1401.

Masliah, E., Rockenstein, E., Veinbergs, I., Mallory, M., Hashimoto, M., Takeda, A., Sagara, Y., Sisk, A., and Mucke, L. Dopaminergic Loss and Inclusion Body Formation in Alpha-Synuclein Mice: Implications for Neurodegenerative Disorders, *Science*, **2000**, *287*,1265-1269.

Masters, S. L., Dunne, A., Subramanian, S. L., Hull, R. L., Tannahill, G. M., Sharp, F. A., Becker, C., Franchi, L., Yoshihara, E., Chen, Z., Mullooly, N., Mielke, L. A., Harris, J., Coll, R. C., Mills, K. H., Mok, K. H., Newsholme, P., Nunez, G., Yodoi, J., Kahn, S. E., Lavelle, E. C., and O'Neill, L. A. Activation of the NLRP3 Inflammasome by Islet Amyloid Polypeptide Provides a Mechanism for Enhanced IL-1Beta in Type 2 Diabetes, *Nat. Immunol.*, **2010**, *11*,897-904.

Matveyenko, A. V., and Butler, P. C. Beta-Cell Deficit Due to Increased Apoptosis in the Human Islet Amyloid Polypeptide Transgenic (HIP) Rat Recapitulates the Metabolic Defects Present in Type 2 Diabetes, *Diabetes*, **2006**, *55*,2106-2114.

Maurer-Stroh, S., Debulpaep, M., Kuemmerer, N., Lopez de la Paz, M., Martins, I. C., Reumers, J., Morris, K. L., Copland, A., Serpell, L., Serrano, L., Schymkowitz, J. W., and Rousseau, F. Exploring the Sequence Determinants of Amyloid Structure Using Position-Specific Scoring Matrices, *Nat. Methods*, **2010**, *7*,237-242.

Meng, F., Abedini, A., Song, B., and Raleigh, D. P. Amyloid Formation by Pro-Islet Amyloid Polypeptide Processing Intermediates: Examination of the Role of Protein Heparan Sulfate Interactions and Implications for Islet Amyloid Formation in Type 2 Diabetes, *Biochemistry*, **2007**, *46*,12091-12099.

Meng, F. L., Marek, P., Potter, K. J., Verchere, C. B., and Raleigh, D. P. Rifampicin Does Not Prevent Amyloid Fibril Formation by Human Islet Amyloid Polypeptide But Does Inhibit Fibril Thioflavin-T Interactions: Implications For Mechanistic Studies Beta-Cell Death, *Biochemistry*, **2008**, *47*,6016-6024.

Meng, F., Raleigh, D. P., and Abedini, A. Combination of Kinetically Selected Inhibitors in trans Leads to Highly Effective Inhibition of Amyloid Formation, *J. Am. Chem. Soc.*, **2010**, *132*,14340-14342.

Mishra, R., Sorgjerd, K., Nystrom, S., Nordigarden, A., Yu, Y. C., and Hammarstrom, P. Lysozyme Amyloidogenesis is Accelerated by Specific Nicking and Fragmentation But Decelerated by Intact Protein Binding and Conversion, *J. Mol. Biol.*, **2007**, *366*,1029-1044.

Mishra, R., Sjolander, D., and Hammarstrom, P. Spectroscopic Characterization of Diverse Amyloid Fibrils in vitro By the Fluorescent Dye Nile Red, *Mol. Biosyst.*, **2011**, *7*,1232-1240.

Moran, S. D., and Zanni, M. T. How to Get Insight into Amyloid Structure and Formation from Infrared Spectroscopy, *J. Phys. Chem. Lett.*, **2014**, *5*,1984-1993.

Moreno-Gonzalez, I., and Soto, C. Misfolded Protein Aggregates: Mechanisms, Structures and Potential for Disease Transmission, *Semin. Cell. Dev. Biol.*, **2011**, *22*,482-487.

Moriarty, D. F., and Raleigh, D. P. Effects of Sequential Proline Substitutions on Amyloid Formation by Human Amylin 20-29, *Biochemistry*, **1999**, *38*,1811-1818.

Mossuto, M. F., Bolognesi, B., Guixer, B., Dhulesia, A., Agostini, F., Kumita, J. R., Tartaglia, G. G., Dumoulin, M., Dobson, C. M., and Salvatella, X. Disulfide Bonds Reduce the Toxicity of the Amyloid Fibrils Formed by an Extracellular Protein, *Angew. Chem. Int. Ed. Engl.*, **2011**, *50*,7048-7051.

Mukherjee, S., Raghuraman, H., and Chattopadhyay, A. Membrane Localization and Dynamics of Nile Red: Effect of Cholesterol, *Biochim. Biophys. Acta*, **2007**, *1768*,59-66.

Nanga, R. P., Brender, J. R., Xu, J., Veglia, G., and Ramamoorthy, A. Structures of Rat and Human Islet Amyloid Polypeptide IAPP(1-19) in Micelles by NMR Spectroscopy, *Biochemistry*, **2008**, *47*,12689-12697.

Nanga, R. P., Brender, J. R., Xu, J., Hartman, K., Subramanian, V., and Ramamoorthy, A. Three-Dimensional Structure and Orientation of Rat Islet Amyloid Polypeptide Protein in a Membrane Environment by Solution NMR Spectroscopy, *J. Am. Chem. Soc.*, **2009**, *131*,8252-8261.

Nanga, R. P., Brender, J. R., Vivekanandan, S., and Ramamoorthy, A. Structure and Membrane Orientation of IAPP in Its Natively Amidated Form at Physiological pH in a Membrane Environment, *Biochim. Biophys. Acta*, **2011**, *1808*,2337-2342.

Nashine, V. C., Kroetsch, A. M., Sahin, E., Zhou, R., and Adams, M. L. Orthogonal High-Throughput Thermal Scanning Method for Rank Ordering Protein Formulations, *AAPS PharmSciTech*, **2013**, *14*,1360-1366.

Nguyen, T. M., Wright, J. R., Jr., Nielsen, P. F., and Conlon, J. M. Characterization of the Pancreatic Hormones From The Brockmann Body of The Tilapia: Implications for Islet Xenograft Studies, *Comp. Biochem. Physiol. C: Pharmacol. Toxicol.*, **1995**, *111*,33-44.

Obrien, T. D., Hellman, U., Westermark, P., Wernstedt, C., Rathbun, W. B., and Johnson, K. H. Pancreatic-Islet Amyloid in the Degu Is Derived from Insulin, *Amyloid and Amyloidosis 1990*, **1991**,462-465.

O'Nuallain, B., Williams, A. D., Westermark, P., and Wetzel, R. Seeding Specificity in Amyloid Growth Induced by Heterologous Fibrils, *J. Biol. Chem.*, **2004**, *279*,17490-17499.

Opie, E. L. Pathological Changes Affecting the Islands of Langerhans of the Pancreas, *J. Boston Soc. Med. Sci.*, **1900**, *4*,251-260.

Pace, C. N., and Scholtz, J. M. A Helix Propensity Scale Based on Experimental Studies of Peptides and Proteins, *Biophys. J.*, **1998**, *75*,422-427.

Poitout, V., and Robertson, R. P. Minireview: Secondary Beta-Cell Failure in Type 2 Diabetes--A Convergence of Glucotoxicity and Lipotoxicity, *Endocrinology*, **2002**, *143*,339-342.

Potter, K. J., Abedini, A., Marek, P., Klimek, A. M., Butterworth, S., Driscoll, M., Baker, R., Nilsson, M. R., Warnock, G. L., Oberholzer, J., Bertera, S., Trucco, M., Korbutt, G. S., Fraser, P. E., Raleigh, D. P., and Verchere, C. B. Islet Amyloid Deposition Limits the Viability of Human Islet Grafts But Not Porcine Islet Grafts, *PNAS*, **2010**, *107*,4305-4310.

Procacci, P., and Berne, B. J. Multiple Time-Scale Methods for Constant-Pressure Molecular-Dynamics Simulations of Molecular-Systems, *Mol. Phys.*, **1994**, *83*,255-272.

Puchtler, H., Sweat, F., and Levine, M. On The Binding of Congo Red by Amyloid, *J. Histochem. Cytochem.*, **1962**, *10*,355-364.

Ratner, R. E., Dickey, R., Fineman, M., Maggs, D. G., Shen, L., Strobel, S. A., Weyer, C., and Kolterman, O. G. Amylin Replacement With Pramlintide As An Adjunct to Insulin Therapy Improves Long-Term Glycaemic And Weight Control in Type 1 Diabetes Mellitus: a 1-Year, Randomized Controlled Trial, *Diabetic Med.*, **2004**, *21*,1204-1212.

Reddy, A. S., Wang, L., Singh, S., Ling, Y. L., Buchanan, L., Zanni, M. T., Skinner, J. L., and de Pablo, J. J. Stable and Metastable States of Human Amylin in Solution, *Biophys. J.*, **2010**, *99*,2208-2216.

Rising, A., Widhe, M., Johansson, J., and Hedhammar, M. Spider Silk Proteins: Recent Advances in Recombinant Production, Structure-Function Relationships and Biomedical Applications, *Cell Mol. Life Sci.*, **2011**, *68*,169-184.

Rivera, J. F., Gurlo, T., Daval, M., Huang, C. J., Matveyenko, A. V., Butler, P. C., and Costes, S. Human-IAPP disrupts the Autophagy/Lysosomal Pathway in Pancreatic Beta-Cells: Protective Role of p62-Positive Cytoplasmic Inclusions, *Cell Death Differ.*, **2011**, *18*,415-426.

Roberts, A. N., Leighton, B., Todd, J. A., Cockburn, D., Schofield, P. N., Sutton, R., Holt, S., Boyd, Y., Day, A. J., Foot, E. A., and et al. Molecular and Functional Characterization of Amylin, a Peptide Associated with Type 2 Diabetes Mellitus, *PNAS*, **1989**, *86*,9662-9666.

Roland, B. P., Kodali, R., Mishra, R., and Wetzel, R. A Serendipitous Survey of Prediction Algorithms for Amyloidogenicity, *Biopolymers*, **2013**, *100*,780-789.

Romero, D., Aguilar, C., Losick, R., and Kolter, R. Amyloid Fibers Provide Structural Integrity to Bacillus subtilis Biofilms, *PNAS*, **2010**, *107*,2230-2234.

Rosen, C. G., and Weber, G. Dimer Formation from 1-Amino-8-Naphthalenesulfonate Catalyzed by Bovine Serum Albumin. A New Fluorescent Molecule with Exceptional Binding Properties, *Biochemistry*, **1969**, *8*,3915-3920.

Ryan, E. A., Paty, B. W., Senior, P. A., Bigam, D., Alfadhli, E., Kneteman, N. M., Lakey, J. R., and Shapiro, A. M. Five-Year Follow-Up After Clinical Islet Transplantation, *Diabetes*, **2005**, *54*,2060-2069.

Ryckaert, J. P., Ciccotti, G., and Berendsen, H. J. C. Numerical-Integration of Cartesian Equations of Motion of a System with Constraints - Molecular-Dynamics of N-Alkanes, *J. Comput. Phys.*, **1977**, *23*,327-341.

Sackett, D. L., and Wolff, J. Nile Red as a Polarity-Sensitive Fluorescent Probe of Hydrophobic Protein Surfaces, *Anal. Biochem.*, **1987**, *167*,228-234.

Sakagashira, S., Sanke, T., Hanabusa, T., Shimomura, H., Ohagi, S., Kumagaye, K. Y., Nakajima, K., and Nanjo, K. Missense Mutation of Amylin Gene (S20G) in Japanese NIDDM Patients, *Diabetes*, **1996**, *45*,1279-1281.

Sanke, T., Bell, G. I., Sample, C., Rubenstein, A. H., and Steiner, D. F. An Islet Amyloid Peptide Is Derived from an 89-Amino Acid Precursor by Proteolytic Processing, *J. Biol. Chem.*, **1988**, *263*,17243-17246.

Sanke, T., and Sakagashira, S. S20G Mutation of Amylin Gene--Amyloid Diabetes Due to S20G Amylin Gene Mutation, *Nihon Rinsho*, **2005**, *63 Suppl 2*,160-165.

Sarkar, N., Kumar, M., and Dubey, V. K. Effect of Sodium Tetrathionate on Amyloid Fibril: Insight into the Role of Disulfide Bond in Amyloid Progression, *Biochimie*, **2011**, *93*,962-968.

Sawaya, M. R., Sambashivan, S., Nelson, R., Ivanova, M. I., Sievers, S. A., Apostol, M. I., Thompson, M. J., Balbirnie, M., Wiltzius, J. J., McFarlane, H. T., Madsen, A. O., Riekel, C., and Eisenberg, D. Atomic Structures of Amyloid Cross-Beta Spines Reveal Varied Steric Zippers, *Nature*, **2007**, *447*,453-457.

Selkoe, D. J. Cell Biology of Protein Misfolding: The Examples of Alzheimer's and Parkinson's Diseases, *Nat. Cell Biol.*, **2004**, *6*,1054-1061.

Serpell, L. C., Sunde, M., Benson, M. D., Tennent, G. A., Pepys, M. B., and Fraser, P. E. The Protofilament Substructure of Amyloid Fibrils, *J. Mol. Biol.*, **2000**, *300*,1033-1039.

Sipe, J. D., Benson, M. D., Buxbaum, J. N., Ikeda, S., Merlini, G., Saraiva, M. J., Westermark, P., and Nomenclature Committee of the International Society of, A. Amyloid Fibril Protein Nomenclature: 2012 Recommendations from the Nomenclature Committee of the International Society of Amyloidosis, *Amyloid*, **2012**, *19*,167-170.

Sparks, S., Liu, G., Robbins, K. J., and Lazo, N. D. Curcumin Modulates the Self-Assembly of the Islet Amyloid Polypeptide by Disassembling Alpha-Helix, *Biochem. Biophys. Res. Commun.*, **2012**, *422*,551-555.

Sparr, E., Engel, M. F. M., Sakharov, D. V., Sprong, M., Jacobs, J., de Kruijff, B., Höppener, J. W. M., and Antoinette Killian, J. Islet Amyloid Polypeptide-Induced Membrane Leakage Involves Uptake of Lipids by Forming Amyloid Fibers, *FEBS Lett.*, **2004**, *577*,117-120.

Stefani, M. Generic Cell Dysfunction in Neurodegenerative Disorders: Role of Surfaces in Early Protein Misfolding, Aggregation, and Aggregate Cytotoxicity, *Neuroscientist*, **2007**, *13*,519-531.

Steinberg, T. H., Haugland, R. P., and Singer, V. L. Applications of SYPRO Orange and SYPRO Red Protein Gel Stains, *Anal. Biochem.*, **1996**, *239*,238-245.

Street, A. G., and Mayo, S. L. Intrinsic Beta-Sheet Propensities Result From Van der Waals Interactions Between Side Chains and the Local Backbone, *PNAS*, **1999**, *96*,9074-9076.

Stryer, L. The Interaction of a Naphthalene Dye with Apomyoglobin and Apohemoglobin. A Fluorescent Probe of Non-Polar Binding Sites, *J. Mol. Biol.*, **1965**, *13*,482-495.

Sulatskaya, A. I., Maskevich, A. A., Kuznetsova, I. M., Uversky, V. N., and Turoverov, K. K. Fluorescence Quantum Yield of Thioflavin T in Rigid Isotropic Solution and Incorporated Into The Amyloid Fibrils, *PLoS One*, **2010**, *5*,e15385.

Sunde, M., Serpell, L. C., Bartlam, M., Fraser, P. E., Pepys, M. B., and Blake, C. C. Common Core Structure of Amyloid Fibrils by Synchrotron X-ray Diffraction, *J. Mol. Biol.*, **1997**, *273*,729-739.

Swift, S. M., Clayton, H. A., London, N. J., and James, R. F. The Potential Contribution of Rejection to Survival of Transplanted Human Islets, *Cell Transplant.*, **1998**, *7*,599-606.

Tam, J. P., Wu, C. R., Liu, W., and Zhang, J. W. Disulfide Bond Formation in Peptides by Dmso Scope and Applications, *J Am Chem Soc*, **1991**, *113*,6657-6662.

Tartaglia, G. G., and Vendruscolo, M. The Zyggregator Method For Pedicting Potein Agregation Propensities, *Chem. Soc. Rev.*, **2008**, *37*,1395-1401.

Tartaglia, G. G., Pawar, A. P., Campioni, S., Dobson, C. M., Chiti, F., and Vendruscolo, M. Prediction of Aggregation-Prone Regions in Structured Proteins, *J. Mol. Biol.*, **2008**, *380*,425-436.

Telford, W. G., King, L. E., and Fraker, P. J. Comparative Evaluation of Several DNA Binding Dyes in the Detection of Apoptosis-Associated Chromatin Degradation by Flow Cytometry, *Cytometry*, **1992**, *13*,137-143.

Tenidis, K., Waldner, M., Bernhagen, J., Fischle, W., Bergmann, M., Weber, M., Merkle, M. L., Voelter, W., Brunner, H., and Kapurniotu, A. Identification of a Penta- and Hexapeptide of Islet Amyloid Polypeptide (IAPP) with Amyloidogenic and Cytotoxic Properties, *J. Mol. Biol.*, **2000**, *295*,1055-1071.

Thompson, M. J., Sievers, S. A., Karanicolas, J., Ivanova, M. I., Baker, D., and Eisenberg, D. The 3D Profile Method for Identifying Fibril-Forming Segments of Proteins, *PNAS*, **2006**, *103*,4074-4078.

Trovato, A., Chiti, F., Maritan, A., and Seno, F. Insight into the Structure of Amyloid Fibrils from the Analysis of Globular Proteins, *PLoS Comput. Biol.*, **2006**, *2*,e170.

Tu, L.-H., and Raleigh, D. P. Role of Aromatic Interactions in Amyloid Formation by Islet Amyloid Polypeptide, *Biochemistry*, **2013**, *52*,333-342.

Tu, L. H., Young, L. M., Wong, A. G., Ashcroft, A. E., Radford, S. E., and Raleigh, D. P. Mutational Analysis of the Ability of Resveratrol to Inhibit Amyloid Formation by Islet Amyloid Polypeptide: Critical Evaluation of the Importance of Aromatic-Inhibitor and Histidine-Inhibitor Interactions, *Biochemistry*, **2015**, *54*,666-676.

Tukel, C., Wilson, R. P., Nishimori, J. H., Pezeshki, M., Chromy, B. A., and Baumler, A. J. Responses to Amyloids of Microbial and Host Origin are Mediated Through Toll-Like Receptor 2, *Cell Host Microbe*, **2009**, *6*,45-53.

Vaiana, S. M., Best, R. B., Yau, W. M., Eaton, W. A., and Hofrichter, J. Evidence for a Partially Structured State of the Amylin Monomer, *Biophys. J.*, **2009**, *97*,2948-2957.

Wallberg, F., Tenev, T., and Meier, P. Analysis of Apoptosis and Necroptosis by Fluorescence-Activated Cell Sorting, *Cold Spring Harb. Protoc.*, **2016**, *2016*,pdb prot087387.

Wang, H., Abedini, A., Ruzsicska, B., and Raleigh, D. P. Rationally Designed, Nontoxic, Nonamyloidogenic Analogues of Human Islet Amyloid Polypeptide with Improved Solubility, *Biochemistry*, **2014**, *53*,5876-5884.

Wang, J. M., Wolf, R. M., Caldwell, J. W., Kollman, P. A., and Case, D. A. Development and Testing of a General AMBER Force Field, *J. Comput. Chem.*, **2004**, *25*,1157-1174.

Wang, M., Yang, J. P., Wang, J. Y., and Wang, X. J. Structural Effects of L16Q, S20G, and L16Q-S20G Mutations on hIAPP: A Comparative Molecular Dynamics Study, *Chin. J. Chem* . **2012**, *30*,241-248.

Wang, S. S., Liu, K. N., and Wang, B. W. Effects of Dithiothreitol on the Amyloid Fibrillogenesis of Hen Egg-White Lysozyme, *Eur. Biophys. J.*, **2010**, *39*,1229-1242.

Wang, X., Smith, D. R., Jones, J. W., and Chapman, M. R. In vitro Polymerization of a Functional Escherichia coli Amyloid Protein, *J. Biol. Chem.*, **2007**, *282*,3713-3719.

Wei, L., Jiang, P., Xu, W., Li, H., Zhang, H., Yan, L., Chan-Park, M. B., Liu, X. W., Tang, K., Mu, Y., and Pervushin, K. The Molecular Basis of Distinct Aggregation Pathways of Islet Amyloid Polypeptide, *J. Biol. Chem.*, **2011**, *286*,6291-6300.

Weise, K., Radovan, D., Gohlke, A., Opitz, N., and Winter, R. Interaction of hIAPP with Model Raft Membranes and Pancreatic beta-Cells: Cytotoxicity of hIAPP Oligomers, *Chem. Bio. Chem.*, **2010**, *11*,1280-1290.

Westermark, G. T., Johnson, K. H., and Westermark, P. Staining Methods for Identification of Amyloid in Tissue, *Methods Enzymol.*, **1999**, *309*,3-25.

Westermark, G. T., Falkmer, S., Steiner, D. F., Chan, S. J., Engstrom, U., and Westermark, P. Islet Amyloid Polypeptide is Expressed in The Pancreatic Islet Parenchyma of the Teleostean Fish, Myoxocephalus (Cottus) Scorpius, *Comp. Biochem. Physiol., Part B: Biochem. Mol. Biol.*, **2002**, *133*,119-125.

Westermark, G. T., Westermark, P., Berne, C., and Korsgren, O. Widespread Amyloid Deposition in Transplanted Human Pancreatic Islets, *N. Engl. J. Med.*, **2008**, *359*,977-979.

Westermark, P., Wernstedt, C., Wilander, E., Hayden, D. W., O'Brien, T. D., and Johnson, K. H. Amyloid Fibrils in Human Insulinoma and Islets of Langerhans of the Diabetic Cat Are Derived from a Neuropeptide-Like Protein Also Present in Normal Islet Cells, *PNAS*, **1987**, *84*,3881-3885.

Westermark, P., Engstrom, U., Johnson, K. H., Westermark, G. T., and Betsholtz, C. Islet Amyloid Polypeptide Pinpointing Amino Acid Residues Linked to Amyloid Fibril Formation, *PNAS*, **1990**, *87*,5036-5040.

Westermark, P., Benson, M. D., Buxbaum, J. N., Cohen, A. S., Frangione, B., Ikeda, S., Masters, C. L., Merlini, G., Saraiva, M. J., Sipe, J. D., and Nomenclature Committee of the International Society of, A. Amyloid: Toward Terminology Clarification. Report from the Nomenclature Committee of the International Society of Amyloidosis, *Amyloid*, **2005**, *12*,1-4.

Westermark, P. Amyloid in the Islets of Langerhans: Thoughts and Some Historical Aspects, *Ups. J. Med. Sci.*, **2011**, *116*,81-89.

Westermark, P., Andersson, A., and Westermark, G. T. Islet Amyloid Polypeptide, Islet Amyloid, and Diabetes Mellitus, *Physiol. Rev.*, **2011**, *91*,795-826.

Westwell-Roper, C., Dai, D. L., Soukhatcheva, G., Potter, K. J., van Rooijen, N., Ehses, J. A., and Verchere, C. B. IL-1 Blockade Attenuates Islet Amyloid Polypeptide-Induced Proinflammatory Cytokine Release and Pancreatic Islet Graft Dysfunction, *J. Immunol.*, **2011**, *187*,2755-2765.

Wetzel, R. Kinetics and Thermodynamics of Amyloid Fibril Assembly, *Acc. Chem. Res.*, **2006**, *39*,671-679.

Williamson, J. A., and Miranker, A. D. Direct Detection of Transient Alpha-Helical States in Islet Amyloid Polypeptide, *Protein Sci.*, **2007**, *16*,110-117.

Williamson, J. A., Loria, J. P., and Miranker, A. D. Helix Stabilization Precedes Aqueous And Bilayer-Catalyzed Fiber Formation in Islet Amyloid Polypeptide, *J. Mol. Biol.*, **2009**, *393*,383-396.

Wiltzius, J. J. W., Sievers, S. A., Sawaya, M. R., Cascio, D., Popov, D., Riekel, C., and Eisenberg, D. Atomic Structure of The Cross-Beta Spine of Islet Amyloid Polypeptide (Amylin), *Protein Sci.*, **2008**, *17*,1467-1474.

Wiltzius, J. J. W., Sievers, S. A., Sawaya, M. R., and Eisenberg, D. Atomic Structures of IAPP (amylin) Fusions Suggest a Mechanism for Fibrillation and the Role of Insulin in the Process, *Protein Sci.*, **2009**, *18*,1521-1530.

Winner, B., Jappelli, R., Maji, S. K., Desplats, P. A., Boyer, L., Aigner, S., Hetzer, C., Loher, T., Vilar, M., Campioni, S., Tzitzilonis, C., Soragni, A., Jessberger, S., Mira, H., Consiglio, A., Pham, E., Masliah, E., Gage, F. H., and Riek, R. In vivo Demonstration That Alpha-Synuclein Oligomers Are Toxic, *PNAS*, **2011**, *108*,4194-4199.

Wong, A. G., Wu, C., Hannaberry, E., Watson, M. D., Shea, J. E., and Raleigh, D. P. Analysis of the Amyloidogenic Potential of Pufferfish (Takifugu rubripes) Islet Amyloid Polypeptide Highlights the Limitations of Thioflavin-T Assays and the Difficulties in Defining Amyloidogenicity, *Biochemistry*, **2016**, *55*,510-518.

Wookey, P. J., Xuereb, L., Tikellis, C., and Cooper, M. E. Amylin in the Periphery, *Sci. World J.*, **2003**, *3*,163-175.

Wu, C., Wang, Z., Lei, H., Zhang, W., and Duan, Y. Dual Binding Modes of Congo Red to Amyloid Protofibril Surface Observed in Molecular Dynamics Simulations, *J. Am. Chem. Soc.*, **2007**, *129*,1225-1232.

Wu, C., Wang, Z., Lei, H., Duan, Y., Bowers, M. T., and Shea, J. E. The Binding of Thioflavin T and its Neutral Analog BTA-1 to Protofibrils of the Alzheimer's Disease Abeta(16-22) Peptide Probed by Molecular Dynamics Simulations, *J. Mol. Biol.*, **2008**, *384*,718-729.

Wu, C., Biancalana, M., Koide, S., and Shea, J.-E. Binding Modes of Thioflavin-T to the Single-Layer beta-Sheet of the Peptide Self-Assembly Mimics, *J. Mol. Biol.*, **2009**, *394*,627-633.

Wu, C., Bowers, M. T., and Shea, J. E. Molecular Structures of Quiescently Grown and Brain-Derived Polymorphic Fibrils of the Alzheimer Amyloid Abeta9-40 Peptide: A Comparison to Agitated Fibrils, *PLoS Comput. Biol.*, **2010**, *6*,e1000693.

Wu, C., Bowers, M. T., and Shea, J.-E. On the Origin of the Stronger Binding of PIB over Thioflavin T to Protofibrils of the Alzheimer Amyloid-beta Peptide: A Molecular Dynamics Study, *Biophys. J.*, **2011**, *100*,1316-1324.

Wu, C., and Shea, J. E. Structural Similarities and Differences Between Amyloidogenic and Non-Amyloidogenic Islet Amyloid Polypeptide (IAPP) Sequences and Implications for the Dual Physiological and Pathological Activities of These Peptides, *PLoS Comput. Biol.*, **2013**, *9*,e1003211.

Yanagi, K., Ashizaki, M., Yagi, H., Sakurai, K., Lee, Y. H., and Goto, Y. Hexafluoroisopropanol Induces Amyloid Fibrils of Islet Amyloid Polypeptide by Enhancing Both Hydrophobic and Electrostatic Interactions, *J. Biol. Chem.*, **2011**, *286*,23959-23966.

Yang, H., Dickson, B. C., O'Hali, W., Kearns, H., and Wright, J. R., Jr. Functional Comparison of Mouse, Rat, and Fish Islet Grafts Transplanted Into Diabetic Nude Mice, *Gen. Comp. Endocrinol.*, **1997**, *106*,384-388.

Younan, N. D., and Viles, J. H. A Comparison of Three Fluorophores for the Detection of Amyloid Fibers and Prefibrillar Oligomeric Assemblies. ThT (Thioflavin T); ANS (1-Anilinonaphthalene-8-sulfonic Acid); and bisANS (4,4 '-Dianilino-1,1 '-binaphthyl-5,5 '-disulfonic Acid), *Biochemistry*, **2015**, *54*,4297-4306.

Young, L. M., Cao, P., Raleigh, D. P., Ashcroft, A. E., and Radford, S. E. Ion Mobility Spectrometry-Mass Spectrometry Defines the Oligomeric Intermediates in Amylin Amyloid Formation and the Mode of Action of Inhibitors, *J. Am. Chem. Soc.*, **2014**, *136*,660-670.

Young, L. M., Saunders, J. C., Mahood, R. A., Revill, C. H., Foster, R. J., Tu, L. H., Raleigh, D. P., Radford, S. E., and Ashcroft, A. E. Screening and Classifying Small-Molecule Inhibitors of Amyloid Formation Using Ion Mobility Spectrometry-Mass Spectrometry, *Nat. Chem.*, **2015**, *7*,73-81.

Zhang, N., Ruan, J., Duan, G., Gao, S., and Zhang, T. The Interstrand Amino Acid Pairs Play a Significant Role in Determining the Parallel or Antiparallel Orientation of Beta-Strands, *Biochem. Biophys. Res. Commun.*, **2009**, *386*,537-543.